Chapter 1

Introduction

General Introduction:

1.1: Characteristic features of 2,6-pyridinedicarboxylic acid (or Dipicolinic acid)

Pyridinedicarboxylic acids in the form of different isomers such as 2,3-, 2,4-, 2,5-, 2,6-, 3,4- and 3,5-pyridinedicarboxylic acid (Fig 1.1) are widely used as ligands and also used in supramolecular chemistry for guest binding. Among these isomers of pyridinedicarboxylic acids; the 2,6-substituted isomer commonly dipicolinic acid has a nitrogen atom flanked by two carboxylic acid groups that makes it more symmetric than the other isomers and is a good substrate to bind a guest molecule or a metal ion [1]. Further, the advantage in dealing with 2,6-substituted pyridinedicarboxylic acid over the other isomers are (i) it is fairly soluble in common protic solvents such as water, methanol or ethanol, and (ii) it forms metal complexes as well as host-guest complexes in the form of supramolecular assemblies which have some potential applications. In contrast to this, the other isomers form generally relatively less-soluble coordination polymers with metal ions. The present study in the thesis, we deal with the supramolecular and coordination chemistry of dipicolinate complexes and the relevant literature related to our work is presented in this chapter.

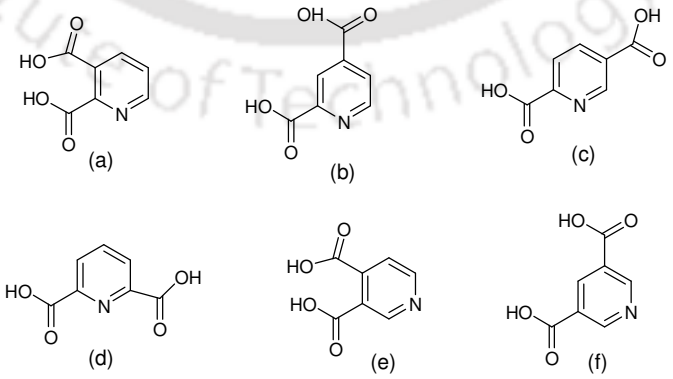

Fig. 1.1

1.2: General features of dipicolinic acid

The dipicolinic acid has attracted attention of chemist in the year 1953, when J. F. Powell discovered that dipicolinic acid exist as 5 to 15% of the dry weight of bacterial spores [2]. The role of dipicolinic acid is to assist in the heat resistance of the endospores of bacteria by creating a highly impenetrable barrier [3]. Other than being a constituent of bacterial spores, [4-7], it also participates in a variety of processes such as enzyme inhibitors [8-10], in plant preservatives [11] and as food sanitizers [12]. Biosynthesis of dipicolinic acid by bacteria from α,ε–diketopimelic acid was carried out by Powell (Scheme 1.1) [13]. It is formed through cyclization of the α,ε–diketopimelic acid followed by dehydrogenative aromatization of the intermediate dicarboxylic acid.

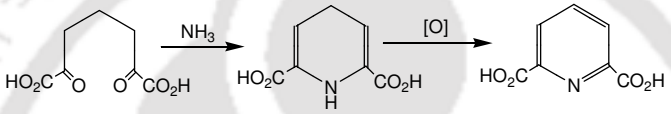

Scheme 1.1

It also can be prepared by incubating extracts of sporulating cultures of *Bacillus megaterium* with pyruvate and aspartic semialdehyde [14]. The accumulation of dipicolinic acid in culture filtrates of the mold of penicillium citreo-viride was studied in surface and submerged cultures [15]. Shymanska and coworkers synthesized dipicolinic acid by arial oxidation of 2,6-dimethylpyridine in the presence of *tert*-BuOK with 18-crown-6 as phase-transfer catalyst (Scheme 1.2) [16].

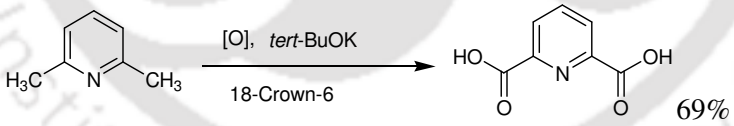

Scheme 1.2

Dipicolinic acid does not adopt conventional dimeric form observed in carboxylic acids because of its geometrical constrains. It forms an aqua bridged hydrogen bonded assembly when crystallized from water (Fig. 1.2) [17-18].

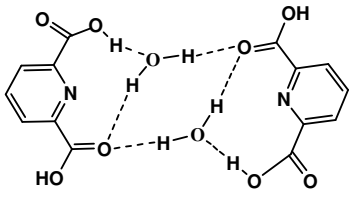

Fig. 1.2: Hydrogen bonded aqua bridged assembly

The IR spectrum of dipicolinic acid is often used to understand its complex formation and host-guest complexes. The most intense IR frequencies for dipicolinic acid correspond to the O-H stretching appears at about 3479 cm^{-1}, the C=O stretch appears near 1700 cm^{-1}, the C-H bending mode is observed near 1275 cm^{-1}, while it shows intense Raman absorptions at 3115 and 1710 cm^{-1} respectively [19].

It is typically a weak acid and dissociates in aqueous solution. It has three types of protonated and deprotonated states as illustrated in Fig. 1.3. The pKa value of dipicolinic acid in the protonated form, H_3L^+ is pK_{a1} <<0.4, mono-deprotonated form with pK_{a2} = 2.10 ± 0.01 and di-deprotonated form with pK_{a3} = 4.383 ± 0.004 at 25 ℃ in aqueous NaCl (0.6 M) solution respectively [20].

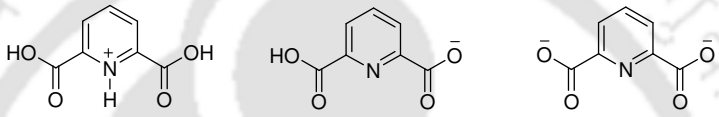

Fig. 1.3

It acts as a proton donor for nitrogen containing bases such as pyridine 2,6-diamine, melamine, guanidine, piperazine, 1,10-phenanthroline, 2,2´-bipyridine etc. leading to the formation of organic salts [21-23]. Recently co-crystals of dipicolinic acid with some active pharmaceutical ingredients such as caffeine, theophylline, nicotinamide and isonicotinamide are synthesized [17-18]. It has been widely used to construct large number metal complexes that find applications in the field of drugs, catalysis, biochemistry, luminescence materials, magnetic materials, in bleaching and bactericidal actions etc. [24-36].

1.3: Dipicolinic acid as ligand

Dipicolinic acid possesses a rigid 120° angle between the pyridine ring and two carboxylate groups. This directional property of the carboxylic acid functional groups controls the formation of different coordination complexes with metal ions. Thus, dipicolinate ligand adopts diverse binding modes such as monodentate, bidentate or tridentate as illustrated in Fig. 1.4. It generally forms chelate with one metal center, or it acts as a bridging ligand. Such binding modes may occur in multiple numbers in the same compound [37]. It has been observed that the tridentate chelating and carboxylate bridging modes are common in metal dipicolinate complexes, the other coordination modes (Fig 1.4, vi-ix) are observed in relatively less occasions [38-39].

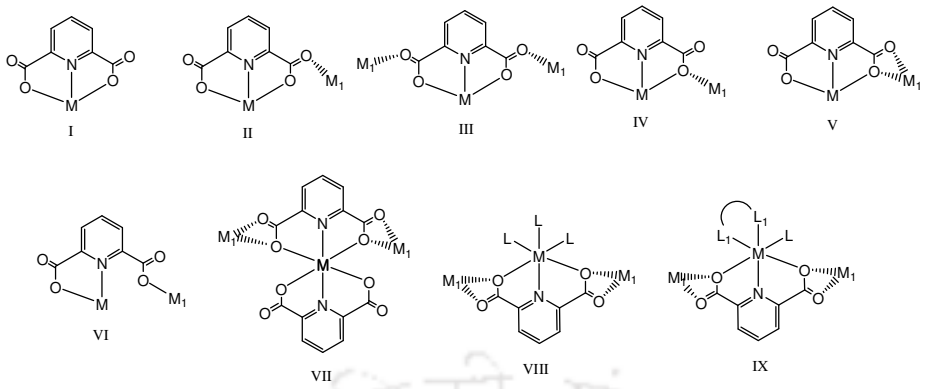

Fig. 1.4: Different coordination modes in dipicolinate complexes

1.4: Coordination complexes of dipicolinic acid

1.4.1: Mononuclear metal dipicolinate complexes

There are large numbers of mono, bis or tris chelated dipicolinate complexes available in literature. In mononuclear complexes tridentate chelating mode of dipicolinates are commonly observed. Examples of selective complexes are given here. Mononuclear vanadium and cobalt dipicolinate complexes are known to exhibit insulin mimic properties [40-41]. Oral administration of $NH_4[VO_2(dipic)]$, $K[VO_2(dipic\text{-}OH)]$ or $[Co(dipic)_2]$ (where dipic = dipicolinate) are found to be effective to lower the hyperglycemia and hyperlipidemia of diabetes [27].

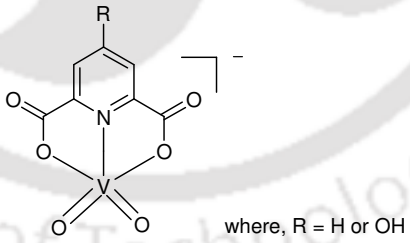

Fig. 1.5: Structure of vanadium dipicolinate complexes

Mononuclear complexes $[(dipic)Fe^{II}(OH_2)_3]$, $[H_2Cu(dipic)_2]\cdot H_2O$ and $[H_2Zn(dipic)_2]\cdot 3H_2O$ have been reported (Fig. 1.6) [42-43]. Among these the iron(II) complex is a hexa-coordinated complex with one dipicolinate anion and three water molecules. The copper(II) complex contains two different ligand molecules, one is neutral and other is doubly ionized. In contrast, the zinc(II) complex contains two identical singly ionized ligand molecules.

These three complexes are primary dipicolinate units of the iron(II), copper(II) and zinc(II) dipicolinate complexes on which various structural modifications have been reported [42-43].

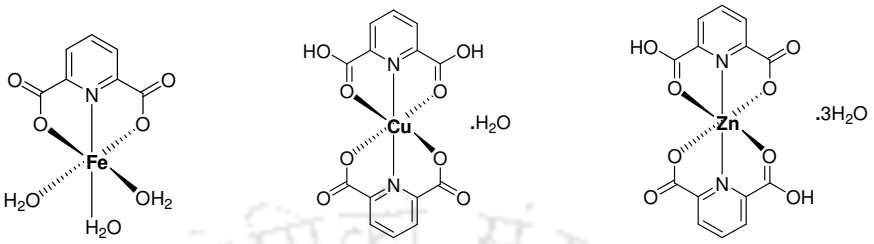

Fig. 1.6

Reaction of dipicolinic acid with $[Ru^{III}X_3(EPh_3)_3]$ gives mononuclear Ru(III) complexes with the composition of $[Ru(dipic)(EPh_3)_2X]$ (where X = Cl, Br ; E = P, As) (Fig.1.7) [44]. In these complexes the coordination polyhedrons of Ru(III) consist of NO_2P_2Cl octahedrons with dipicolinate ligand occupying the equatorial plane. These complexes with N-methyl morpholine-N-oxide as co-oxidant catalyze the oxidation of alcohols to aldehydes.

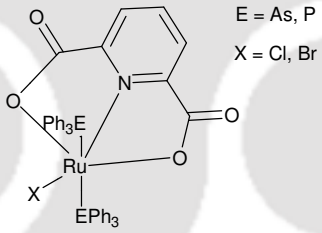

Fig. 1.7

1.4.2: Dinuclear dipicolinate complexes

Homo or hetero dinuclar dipicolinate complexes are well studied. In these dinuclear complexes, carboxylate bridging modes of dipicolinates are commonly observed. The combination of dipicolinate ligand and metal aqua ligands lead to homo or heterodimetallic aqua complexes of general composition $[M_2(H_2O)_5M_1(dipic)_2]\cdot mH_2O$ and $[M(H_2O)_6][M(dipic)_2]\cdot mH_2O$ ($M_1 = M_2$ = Fe [28], Co [25, 27, 30, 31, 32, 33], Ni [34], Cu [35] or Zn [45]; $M_1 \neq M_2$ [36].

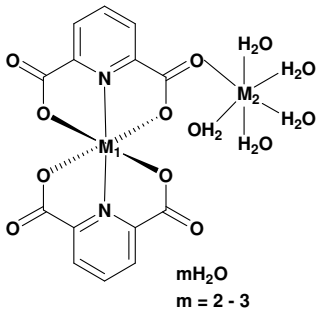

Fig. 1.8

The complexes with the composition $[M(dipicH_2)(OH_2)_3][Ce^{IV}(dipic)_3]\cdot 3H_2O$, (where M = Ni, Cu, Zn at 2+ oxidation state) crystallizes as a pair of complex ions (Fig. 1.9) [46]. The cations $[M(dipicH_2)(OH_2)_3]^{2+}$ derived from transition metal ions have hexa-coordinated polyhedra where the equatorial plane contains the nitrogen atom of neutral $dipicH_2$ and the oxygen atoms of the three water molecules, while the axial positions are occupied by the carboxylate oxygen atoms. In the anion, Ce(IV) exhibit tri-capped trigonal prismatic geometry which is also the case in Ce(IV)-alkaline earth-dipicolinate complexes [47].

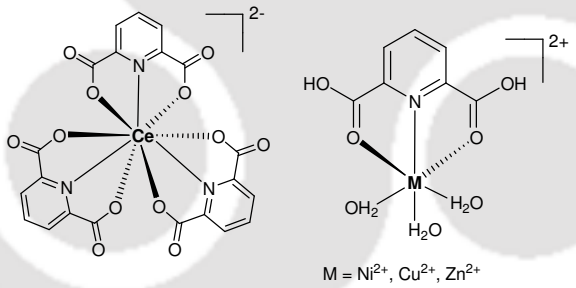

Fig. 1.9

Reaction of dipicolinic acid with $(NH_4)_2Ce(NO_3)_6$ and $BaCl_2$ led to following coordination complexes with similar stoichoimetry but with different network structures [48]. The complex $[Ba(dipicH_2)(OH_2)_4][Ce(dipic)_3]\cdot 4.6H_2O$ exhibits 1D alternating chains of nine-coordinate cerium and barium polyhedra, each having tricapped trigonal prismatic geometry. Complex $[Ba(OH_2)_6][Ce(dipic)_3]$ shows a chain of nine-coordinate aquo-barium polyhedra, which is threaded through the channel formed by a trigonal arrangement of the $[Ce(dipic)_3]^{2-}$ anions (Fig. 1.10). It exhibits a layered network in which cerium and barium coordination polyhedra are joined by dipicolinate ligands to form a corrugated sheet structure.

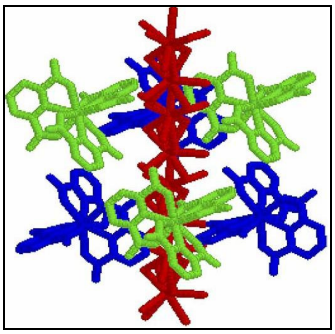

Fig. 1.10: A view showing the polymeric chain of $[Ba(OH_2)_6]^{2+}$ (red) passing through the trigonal channels of $[Ce(dipic)_3]^{2-}$ (green and blue) in the complex $[Ba(OH_2)_6][Ce(dipic)_3]$.

1.5: Coordination polymers of dipicolinates with alkali/alkaline, transition and lanthanide metals

1.5.1: Polymeric complexes of dipicolinates with alkali and alkaline earth metals

Calcium dipicolinate is a constituent of resting spores of *Bacillus* species and is excreted during spore germination. In this complex, dipicolinate cross-links with Ca^{2+} ions embedded in the spore coat of bacteria. Actually this cross linkage is responsible to the extreme resistance capabilities of the endospores of bacteria because it creates a highly impenetrable barrier. Recently, calcium-dipicolinate complex has been synthesized under hydrothermal conditions using $Ca(OH)_2$, $dipicH_2$, DMF, HNO_3 and H_2O as reagents [49]. The structure is a uni-dimensional helical chain that consists of CaO_6N polyhedra. The Ca^{2+} cation is linked to four oxygen and a nitrogen atoms in the equatorial positions and two oxygen atoms in the axial positions. Thus, Ca^{2+} cation occupies seven-coordinate pentagonal bipyramidal geometry. The interesting feature of the complex is that it transforms to a new complex on heating by loss of H_2O (Fig. 1.11).

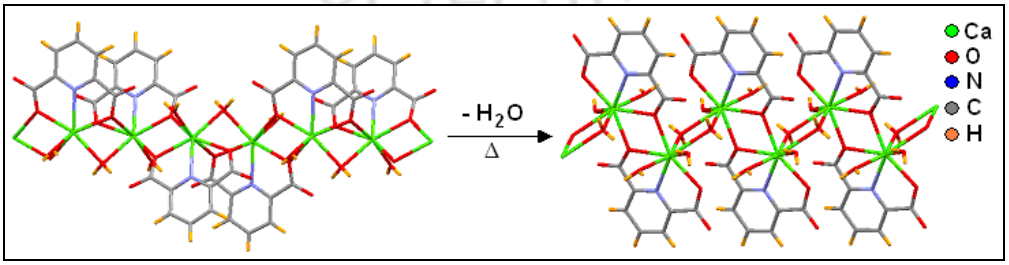

Fig. 1.11: Transformation of 1D helical chain

Magnesium-dipicolinate complex $[Mg(dipic)(H_2O)_3]\cdot 2H_2O$ was synthesized from a salt of piperazine-dipicolinate and magnesium(II) nitrate hexahydrate in aqueous solution [50]. Strontium(II) forms polymeric complex with stoichiometry $[Sr_5(dipic)_6\ 2(H_2O)_2]_n$ that exhibits interesting structural diversities [51]. The two Sr1 and Sr5 atoms are nine-coordinated and possess distorted tricapped trigonal-prismatic and capped square-antiprismatic geometries respectively (Fig. 1.12). The remaining Sr atoms have eight coordination numbers. Sr2 and Sr3 atoms are bridged by two water molecules, Sr5 is chelated by two $(dipic)^{2-}$ ligands. The dipicolinate units of adjacent Sr atoms has π-π stacking interactions between pyridine rings of dipicolinate fragments with distances of 3.41 Å and 3.60 Å respectively.

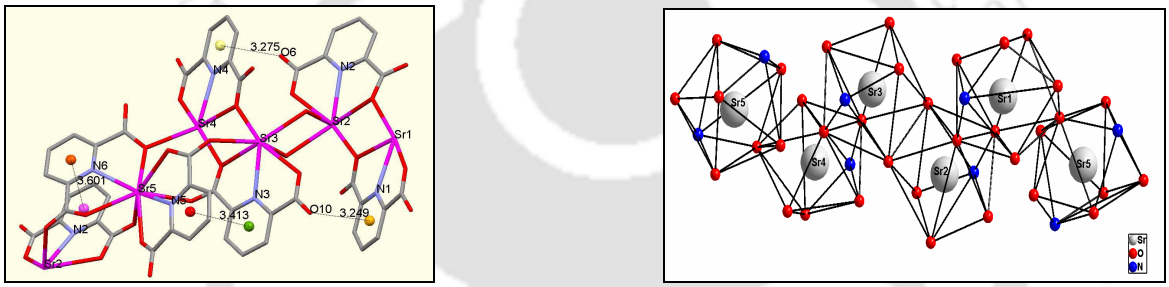

(a) (b)

Fig. 1.12**:** (a) Anion-π and π-π interactions in Sr(II) dipicolinate complex, (b) Different coordination numbers around Sr(II) in the lattice.

Alkali metal complexes with general formula $[M(dipicH)(dipicH_2)(H_2O)_m]_n\cdot xH_2O$ {$m = 2$, 3; $n = 1$, 2, n, and $x = 0$, 0, 0.5; M = Na, K and Cs} are reported [52]. Sodium complex is hepta-coordinated mononuclear complex where the geometry around the sodium ion can be described as a distorted pentagonal bipyramid; potassium complex is octa-coordinated

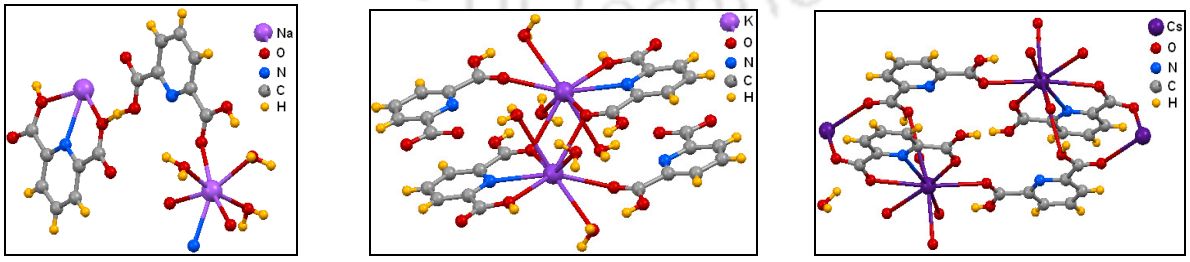

(a) (b) (c)

Fig. 1.13: Dipicolinate complexes of (a) Na, (b) K and (c) Cs.

dinuclear complex with dinuclear K_2O_2 type of carboxylate core, whereas the cesium complex is nona-coordinate polymeric complex (Fig. 1.13). These mono, di and polynuclear alkali metal complexes form extensive hydrogen-bonded self-assemblies in the lattice.

1.5.2: Monomeric, Dimeric and Polymeric complexes of first row transition metals with dipicolinic acid and nitrogen containing ancillary ligands

The coordination complexes of Cu(II) dipicolinates and nitrogen containing ancillary ligands are important in chemical biology [53-54]. Reaction of dipicolinic acid with Cu(II) salts followed by treatment with 2,2′-bipyridine (bpy) or 1,10-phenantroline (phen) led to the formation of the complexes $[Cu(dipicH_2)(bpy)(OH_2)][Cu(dipic)_2]\cdot 3H_2O$ and $[Cu_2(dipicH)_2(dipic)(phen)]\cdot 5.5H_2O$ respectively [55]. These complexes exhibit wide range of coordination geometries, nuclearity, chirality and polymeric architectures. The complex $[Cu(dipicH_2)(bpy)(OH_2)][Cu(dipic)_2]\cdot 3H_2O$ has two distinct ionic complexes. In the cation $[Cu(dipicH_2)(bpy)(OH_2)]^{2+}$, the Cu(II) is coordinated to a neutral dipicolinic acid, bpy and an aqua group and the anion $[Cu(dipic)_2]^{2-}$ consists of an octahedral Cu(II) centre with two meridionally coordinated dipicolinate ligands (Fig. 1.14a). The phen complex $[Cu_2(dipicH)_2(dipic)(phen)]\cdot 5.5H_2O$ can be described as two distinct octahedral complexes, $[Cu(dipicH)(phen)]^+$ and $[Cu(dipicH)(dipic)]^-$, bridged by a carboxylate group (Fig. 1.14b). The two adjacent complexes form a one-dimensional polymer *via* hydrogen bonds, which propagates along the crystallographic *b* axis. Each chain is linked by a number of hydrogen bond interactions resulting in a three-dimensional network.

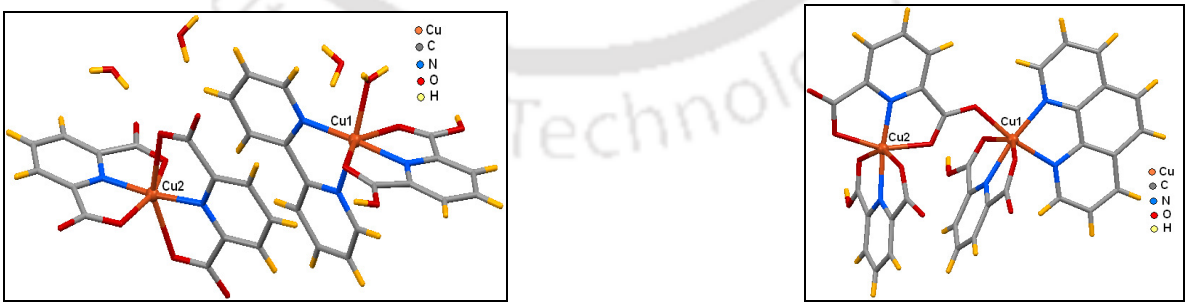

(a) (b)

Fig. 1.14: Structure of the complexes, (a) $[Cu(dipicH_2)(bpy)(OH_2)][Cu(dipic)_2]\cdot 3H_2O$ and (b) $[Cu_2(dipicH)_2(dipic)(phen)]\cdot 5.5H_2O$

In general, first row transition metals prefer to form monomeric or dimeric dipicolinate complexes *via* tridentate chelating mode followed by carboxylate bridging mode. In a recent study, transition metal dipicolinates in association with ancillary ligands such as 4,4´-bipyridine (4,4´-bpy) and trans-4,4´-azobis(pyridine) (azpy) results in coordination polymers [56]. For example, Co(II) or Ni(II) dipicolinates with 4,4´-bipyridine affords coordination complexes comprising of [M(dipic)] : 4,4´-bpy with different molar ratios. In the complex, $\{[\{Ni(\mu\text{-dipic})\}(\mu\text{-4,4´-bpy})]\cdot n(solvent)\}_{\infty}$, Ni(II) coordination geometry is completed by two N-donor bridges and an oxygen atom of a bridging dipicolinate anion (Fig. 1.15a).. In the complex, $\{[\{Co(dipic)(OH_2)_2\}_2\{\mu\text{-4,4´-bpy}\}]\cdot nH_2O\}_{\infty}$, the coordination geometry around Co(II) is completed by one N-donor bridge and two water molecules along with dipicolinate ligand (Fig. 1.15b).

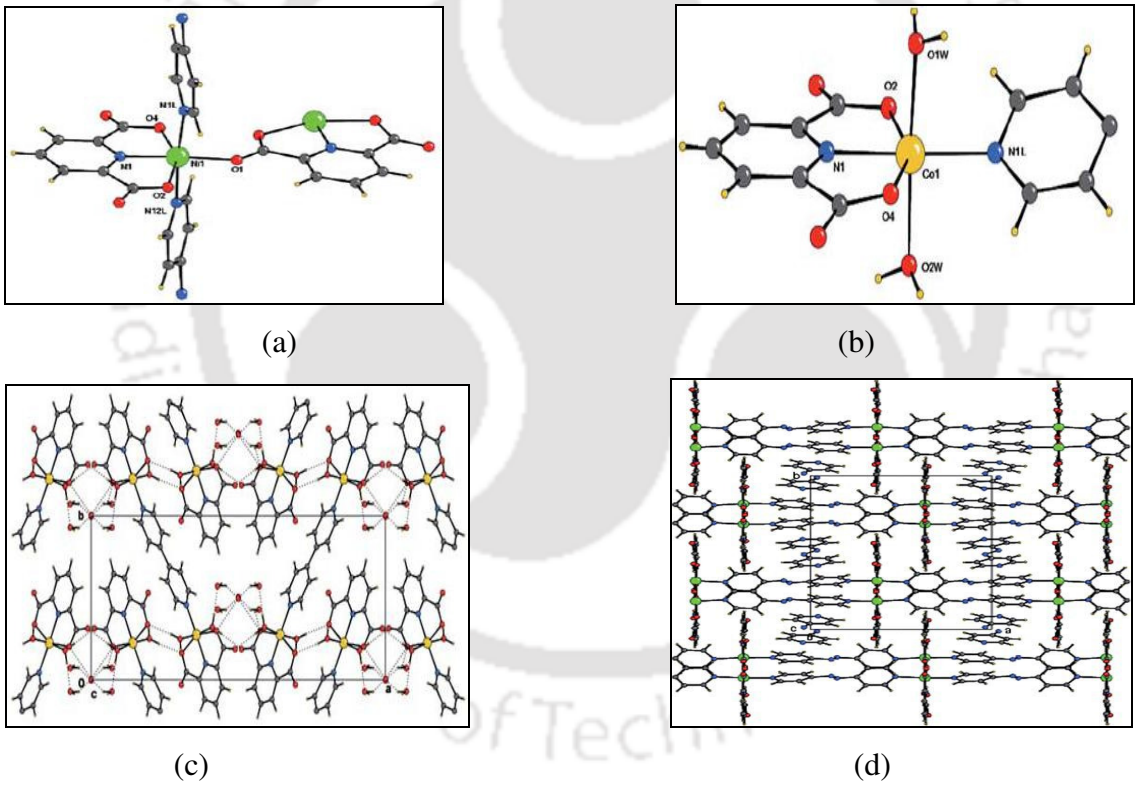

Fig. 1.15: (a) $\{[\{Ni(\mu\text{-dipic})\}(\mu\text{-4,4´-bpy})]\cdot n(solvent)\}_{\infty}$, (b) $\{[\{Co(dipic)(OH_2)_2\}_2\{\mu\text{-4,4´-bpy}\}]\cdot nH_2O\}_{\infty}$ (c) Packing diagram showing hydrogen bonded $[Co(dipic)(OH_2)_2]$ moieties linked through bridging bpy molecules, and (d) π-π stacking interactions between adjacent $Ni(dipic)^{2-}$ anions.

The use of trans-4,4´-azobis(pyridine) as ancillary ligand resulted in the formation of $\{[\{Ni(\mu\text{-dipic})\}(\mu\text{-azpy})]\cdot H_2O.azpy\}_{\infty}$. This complex shows inclusion of a non-coordinated

azpy molecule. In lattice, it comprises a series of $[Co(dipic)]_\infty$ chains bridged by 4,4´-bipyridine molecules to give a 2D structure (Fig. 1.15c).

1.5.3: Heterometallic polymeric complexes of dipicolinic acid with transition metals and lanthanides

High coordination number of lanthanide ions enables them to form a variety of polymeric dipicolinate complexes. Such complexes can be easily connected through carboxylate bridges to transition metal ions to form mixed metal complexes. One dimensional heterometallic coordination polymers are reported with dipicolinic acid and alternating Ce(IV) and Zn(II)/Cd(II) coordination polyhedra [57]. Structural studies reveal that the tricapped trigonal prismatic polyhedra of $[Ce(dipic)_3]^{2-}$ are linked to its adjacent M(II) ions in the ...Ce-M-Ce… infinite chain (where M(II) = Zn(II)/Cd(II)). In the complex $[Zn(H_2O)_4Ce(dipic)_3]\cdot 8H_2O$, the polymeric chain made of alternating units of $[Ce(dipic)_3]^{2-}$ and $[Zn(H_2O)_4]^{2+}$ groups, is situated on inversion centers and is linked on either side by carboxylate bridge (Fig. 1.16a). Ce(IV) ions are nine coordinated with distorted tricapped trigonal prismatic geometries and Zn(II) ions have distorted octahedral geometries. The lattice water molecules available in the complex occupy 24% of the unit cell volume. The key feature of the complex is that it reversibly gains or loses water molecules on heating. Such reversible hydration process was monitored by PXRD and the changes observed with temperature are shown in Fig 1.16b.

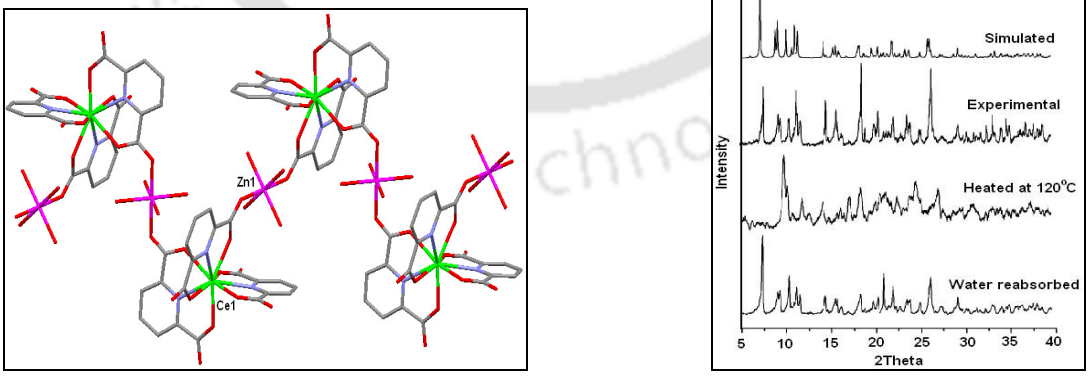

(a) (b)

Fig. 1.16: (a) Complex $[Zn(H_2O)_4Ce(dipic)_3]\cdot 8H_2O$, (b) X-ray powder patterns showing the crystalline transformations on dehydration–rehydration of the complex.

Three dimensional polymeric heterometallic dipicolinate complexes $\{[Ln(dipic)_3 Fe_{1.5}(H_2O)_3]\cdot 1.5H_2O\}_n$ (where Ln = Eu, Gd, Tb at +3 oxidation state), with high-spin Fe(II) shows high thermal stability and posses porous 1D channels [58]. In the complex, Ln(III) is coordinated to three tridentate dipicolinate ligand and establishes a nine-coordinated environment. The octahedral geometry of Fe(II) is completed by four carboxylate O atoms and two water molecules (Fig. 1.17a). The adjacent Ln(III) and Fe(II) are bridged by carboxylate group, forming a Ln-OCO-Fe unit, and the units are further connected by carboxylate groups to form a 3D heterometallic organic frameworks.

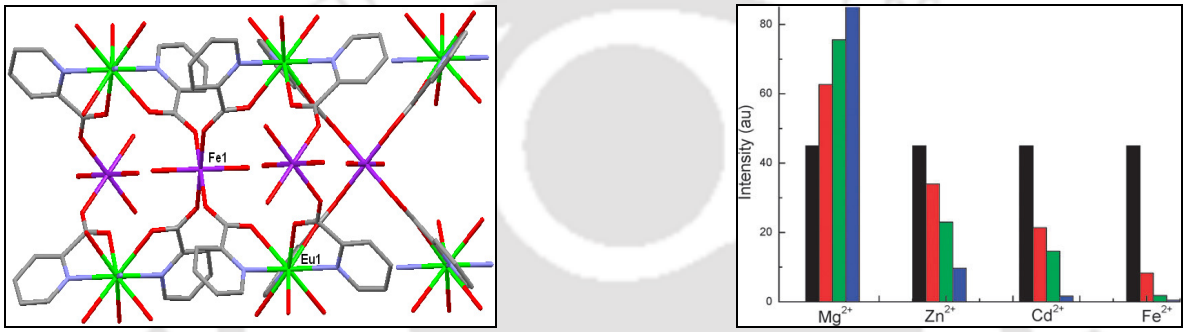

(a) (b)

Fig. 1.17: (a) Polymeric complex $\{[Eu(dipic)_3Fe_{1.5}(H_2O)_3]\cdot 1.5H_2O\}_n$, (b) Change in luminescent intensity upon addition of different metal salts (black, control; red, 1 eqv.; green, 2 eqv.; blue, 3 eqv.)

One of the complex in this series, $\{[Eu(dipic)_3Fe_{1.5}(H_2O)_3]\cdot 1.5H_2O\}_n$ shows enhancement of emission intensity by 1.9 times upon addition of 1-3 equivalent of Mg(II) ion at 613 nm (Fig. 1.17b). Addition of Cd(II) and Zn(II) into the system shows weakening of the luminescent intensities. The introduction of some other metal ions like Zn(II), Fe(II), Cu(II) and Ni(II) either quenches or weakens the luminescence. Thus, high selectivity for Mg(II) implies that it can be used as luminescent probes for magnesium.

1.5.4: Water clusters in Lanthanum-dipicolinates

In an attempt to provide insight into the structure and anomalous properties of liquid water and ice, formations of hydrogen bonded water clusters within the metal-organic frameworks (MOFs) have been widely studied [59-64]. Due to hydrophillic nature, water clusters have often been observed in dipicolinate complexes of transition or lanthanide elements.

Stabilization of a hydrogen-bonded octameric water cluster in the crystal lattice of cerium-dipicolinate complex $Ce(dipic)_2(H_2O)_3 \cdot 4H_2O$ was reported by Rajasekharan and coworkers [65]. The four lattice water molecules available in the asymmetric unit are assembled into a centrosymmetric octamer (Fig. 1.18b). The cluster is stabilized by hydrogen bonding with the $[Ce(dipic)_2]^{2-}$ unit lining the cavity in the host crystal. On heating the water clusters can be removed but they reassembles upon exposure to moisture.

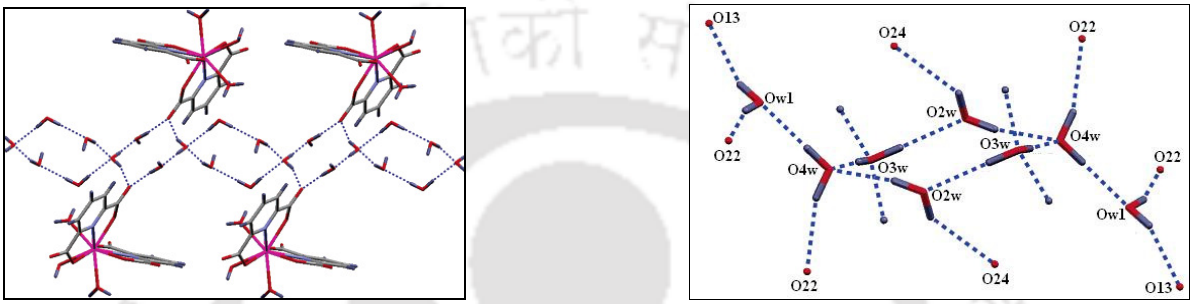

(a) (b)

Fig. 1.18: (a) 1D infinite chair network of octameric water cluster stabilized by cerium dipicolinates, and (b) Close view of hydrogen bonded octameric cluster

They have also synthesized four different types of Ce(IV) and Ln(III) mixed dipicolinate complexes depending on the reaction conditions [66]. One of the representative example of type I complex is $[La(dipicH)(H_2O)_4][Ce(dipic)_3] \cdot 7H_2O$. The 1D coordination polymers are made up of alternating $[La(dipicH)(H_2O)_4]^{2+}$ and $[Ce(dipic)_3]^{2-}$ units. The $[Ce(dipic)_3]^{2-}$ are coordinated to adjacent $[La(dipicH)(H_2O)_4]^{2+}$ unit through carboxylate bridging mode leading to the formation of a 1D chain (Fig. 1.19a). Out of seven, three lattice water molecules and their symmetry related partner aggregates to form hydrogen bonded planar water hexamer (Fig. 1.19d). Type-II complex, for example, $[Nd(dipicH)(H_2O)_6][Ce(dipic)_3] \cdot 7H_2O$ showed the formation of a $(H_2O)_{14}$ water cluster (Fig. 1.19c). The $(H_2O)_{14}$ cluster consists of a tetramer core, and two lattice water molecules are again hydrogen-bonded to two sides of the tetramer, which acts as a bridge between two corners of the tetramer. Two branched chain water tetramers are hydrogen bonded to two opposite corners of the tetramer core. The donor-acceptor distances between the oxygen atoms in the cluster are typically in the range of 2.51(2)-2.97(2) Å, and the corresponding distances between the cluster and complex ions are in the range of 2.52(2)-3.02(2) Å. Type-III

complexes consist of octanuclear cluster incorporating a six-membered coordination ring, $[La(H_2O)_7Ln(dipic)(H_2O)_4(Ce(dipic)_3)_2]_2 \cdot 24H_2O$. Complex $[(Ln(H_2O)_5)_2(Ce(dipic)_3)_4(2H^+)] \cdot 34H_2O$ that represents the type-IV complex has a hexanuclear cluster with a four-membered ring at its core.

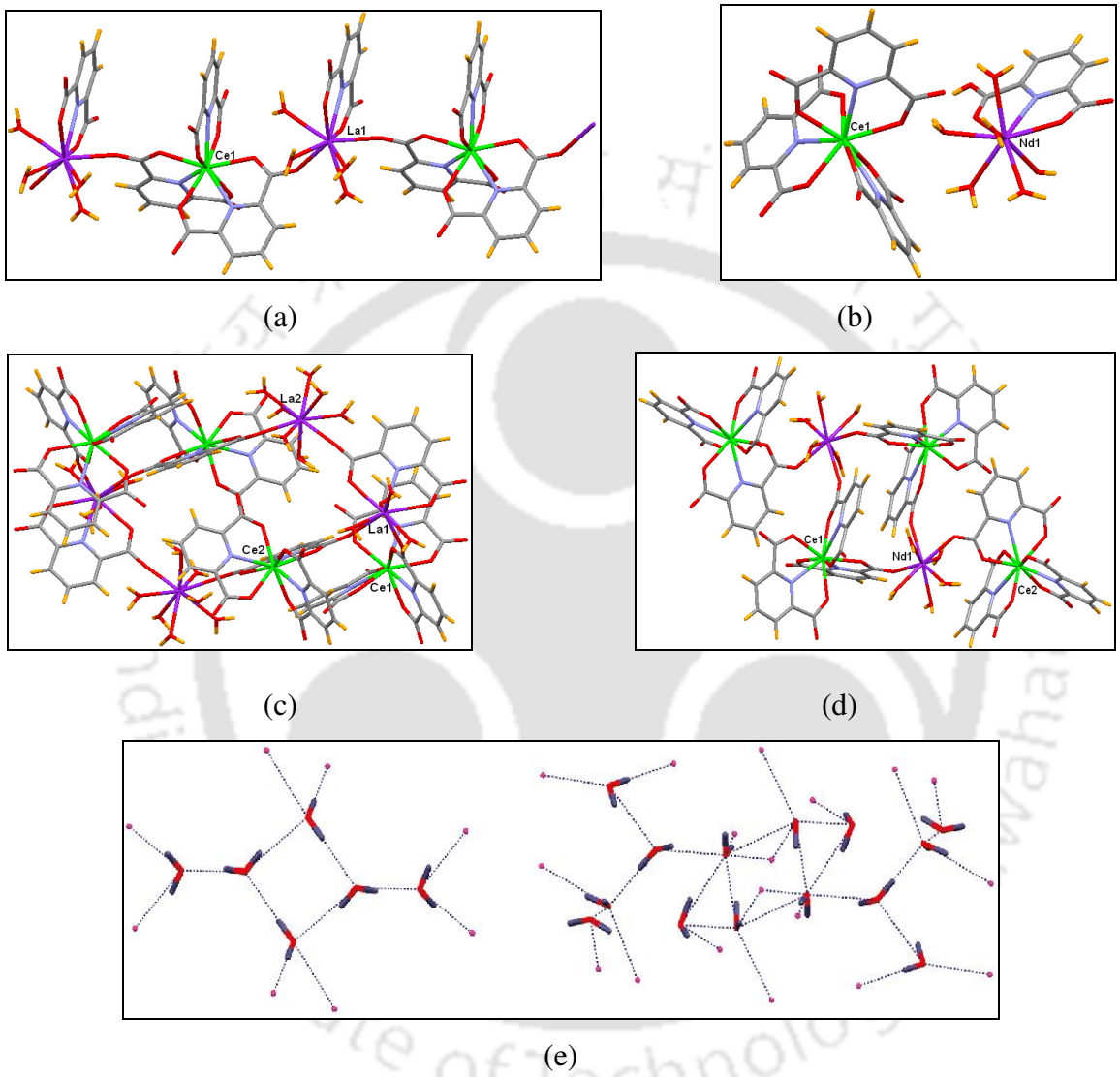

Fig. 1.19: Representative examples of (a) Type I complex, $[La(dipicH)(H_2O)_4][Ce(dipic)_3] \cdot 7H_2O$, (b) Type II complex, $[Nd(dipicH)(H_2O)_6][Ce(dipic)_3] \cdot 7H_2O$, (c) Type III complex, $[La(H_2O)_7La(dipic)(H_2O)_4(Ce(dipic)_3)_2]_2 \cdot 24H_2O$, (d) Type IV complex, $[(Nd(H_2O)_5)_2(Ce(dipic)_3)_4(2H^+)] \cdot 34H_2O$, (e) Water clusters: hexamer (left) and $(H_2O)_{14}$ cluster (right) in type I and II complexes.

Reaction of dipicolinic acid with $LaCl_3 \cdot 7H_2O/La(NO_3)_3 \cdot 7H_2O$ under hydrothermal condition resulted in tubular metal organic framework structure $[La(dipic)(H_2O)_4] \cdot Cl$ or

$[La(dipic)(H_2O)_4]\cdot NO_3$ in the form of infinitely long bunched nanotubes [67]. In the polymeric structure, the six La(III) ions are arranged in a circular fashion bridging *via* carboxylate oxygen atoms (Fig. 1.20a). The chloride or nitrate ions and water molecules occupy the tubular as well as the inter-tubular spaces. When the chloride or nitrate ions are replaced by BF_4^- the tubular structure breaks down, and a new 3D MOF structure, $[La(dipic)(dipicH)(H_2O)_2]\cdot 4H_2O$, is formed where the cavities are occupied by dimeric and hexameric water clusters.

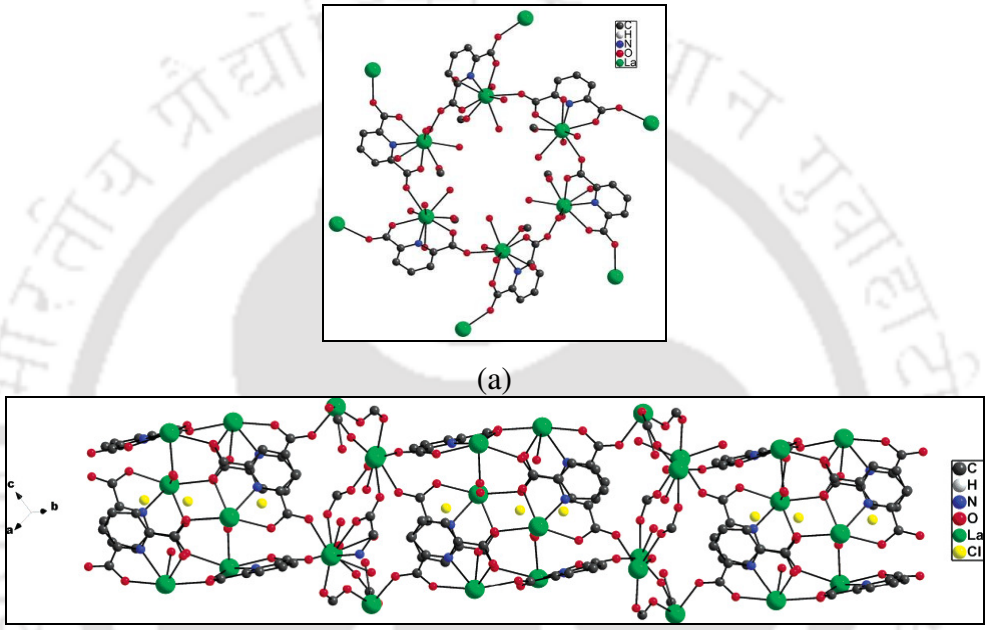

(a)

(b)

Fig. 1.20: (a) Complex $[La(dipic)(H_2O)_4].Cl$ (anions not shown), (b) Packing view of nanotubular complex $[La(dipic)(H_2O)_4]\cdot Cl$ (Cl^- ions inside the tube as a solid circle).

Praseodymium (III) also forms 2D and 3D dipicolinate coordination polymers similar to La(III) [68]. Complex $\{[Pr_3(dipic)_4(dipicH)(H_2O)_8]\cdot 8H_2O\}_n$, shows an nanosized square motif as a building block constructed by eight Pr(III) ions, that further assembles into a highly ordered 2D grid compound. The repeat unit of decanuclear Pr metal-based complex $\{[Pr_2(dipic)_3(H_2O)_3]\cdot H_2O\}_n$, is a novel 3D coordination polymer (Fig. 1.21a). Complex $\{[Pr(dipic)(H_2O)_4]\cdot ClO_4\}_n$ is a 3D network polymer fabricated through a hexanuclear Pr(III) ring as a building block, where ClO_4^- anions are trapped in the cavity. In the complex $\{[Pr_2(dipic)_2(H_2O)_5SO_4]\cdot 2H_2O\}_n$, six Pr(III) atoms, two SO_4^{2-} anions, and carboxylate

oxygen of dipicolinic acid form a 2D grid where the unique bi-bidentate coordination mode of SO_4^{2-} anion have been observed (Fig. 1.21b).

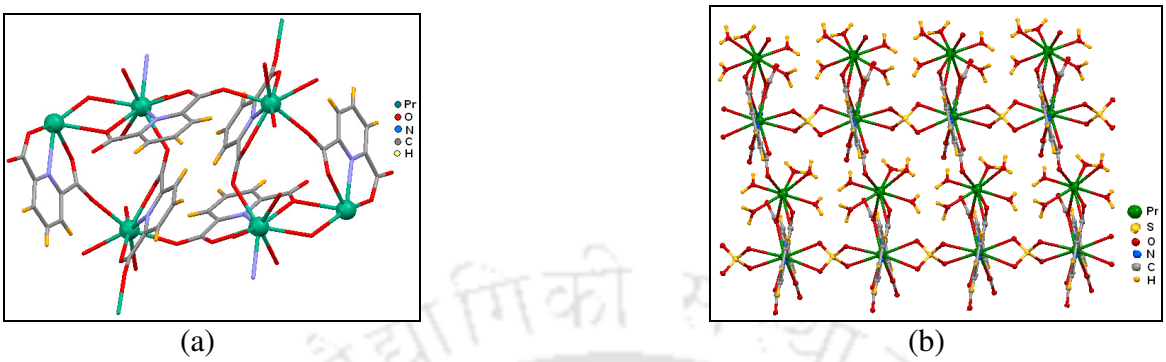

(a) (b)

Fig. 1.21: (a) Polymeric structure of $\{[Pr_2(dipic)_3(H_2O)_3]\cdot H_2O\}_n$, (b) Grid motif structure of $\{[Pr_2(dipic)_2(H_2O)_5SO_4]\cdot 2H_2O\}_n$ showing the repeat unit consisting of six Pr(III) atoms and the bi-bidentate coordinated mode of SO_4^{2-} anion.

Some higher ordered water clusters are also observed in lanthanide-dipicolinate complexes. For example, complex $[In(dipic)(dipicH)(H_2O)_2]\cdot 5H_2O$ and $[In_2SO_4(dipic)_2(phen)_2(H_2O)_2]\cdot 5.5H_2O$, shows the formation of infinite water cluster, $(H_2O)_\infty$ and 16-water cluster, $(H_2O)_{16}$ in the respective complexes [69-70]. In $(H_2O)_\infty$, the oxygen atoms are not coplanar, rather involves in formation of a side arm wave pattern, whereas the $(H_2O)_{16}$ is also a non coplanar single branched chain cluster (Fig. 1.22). Stabilization of a branched-cage 15-water cluster $(H_2O)_{15}$ has been reported in complex $(pipzH_2)_3[Nd(dipic)_3]_2\cdot 15H_2O$ [71].

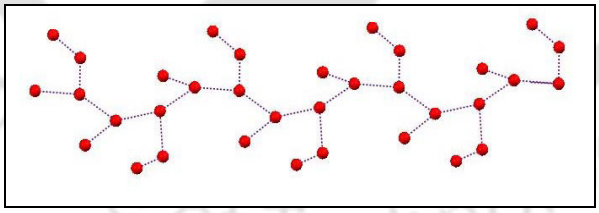

(a)

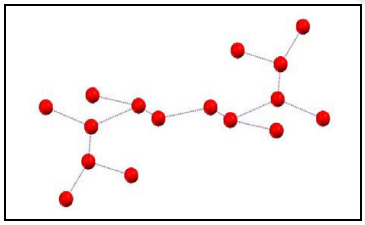

(b)

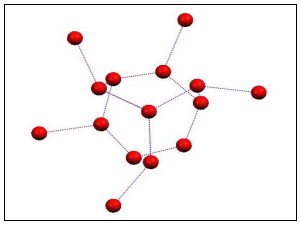

(c)

Fig. 1.22: Some water clusters obtained in dipicolinate complexes are (a) Infinite cluster, $(H_2O)_\infty$, (b) $(H_2O)_{16}$, and (c) $(H_2O)_{15}$

1.6: Supramolecular chemistry metal dipicolinate complexes

The dipicolinic acid exhibits proton transfer behavior and the mono-nuclear metal complex, $H_2[ML_2]$ derived from dipicolinic acid can be considered as a primary motif for transferring protons. So interesting host molecule to form supramolecular assemblies of inorganic-organic hybrid complexes with suitable nitrogen containing bases such as imidazole, 2-methyl imidazole, 2,6-pyridinediamine, 1,10-phenanthroline, guanidine, ethylene guanidine, melamine, creatinine, piperazine, 1,3-propanediamine, 2,2´-bipyridine, 4,4´-bipyridine and 2-aminopyridine are possible. Some of such ionic complexes are discussed below.

1.6.1: Inorganic-organic hybrid materials of $[M(dipic)_2]$ complex with imidazolium or 2-methylimidazolium cation

In recent years, inorganic-organic hybrid compounds are considered as superior class of materials due to their tremendous potentials for targeted delivery of drugs and biomolecules in controlled manner, as luminescent and fluorescent materials and sensors for selective monitoring devices [72-80]. Metal complexes synthesized from dipicolinic acid, transition metal salts and imidazole base, $[imidazolium]_2\ [M(II)(dipic)_2]\cdot xH_2O$ (where M(II) = Mn, Co, Ni, Cu, or Zn) serve as supramolecular building blocks that form a well-defined inorganic-organic layered structure in the solid state [81]. In these structures, the organic cation serves as structural component, which governs the packing arrangement and the metal serves as an interchangeable component. The layers pack to form a robust host lattice that accommodates different types of metal ions without significantly altering the packing arrangement. But presence of lattice hydrates makes them thermally unstable and hence unsuitable as materials for applications. Introducing a methyl substituent at C2 of imidazole results in the steric displacement of water in the new crystal lattice that overcomes the disadvantage without much altering the molecular packing [82].

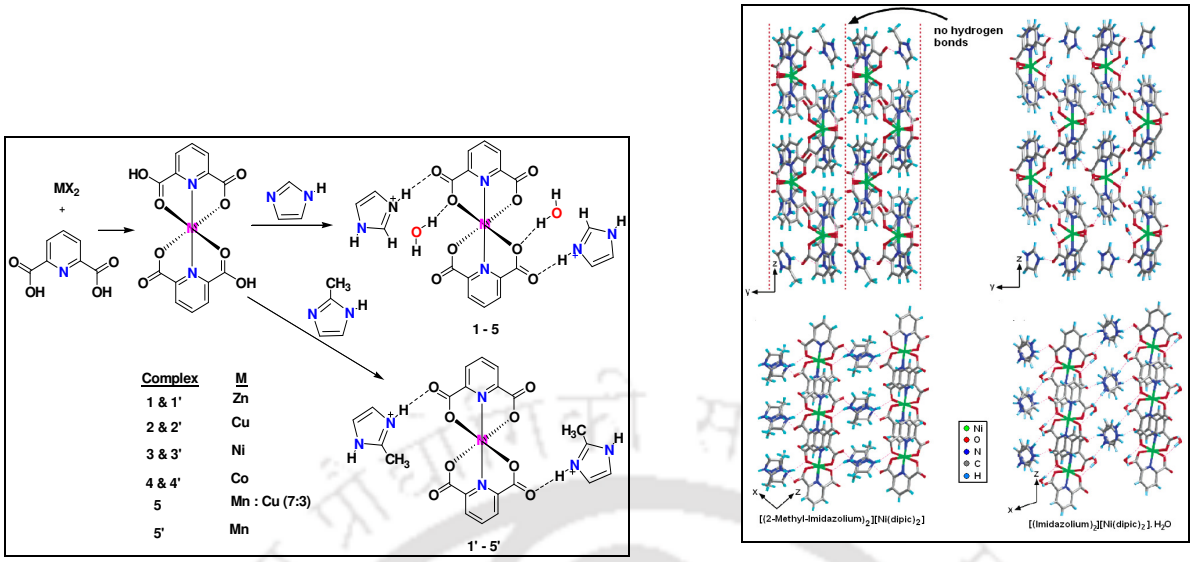

(a) (b)

Fig. 1.23: (a) Synthetic scheme of M(II) dipicolinate imidazole/2-methylimidazole complexes, (b) Crystal packing, layered structure and hydrogen bonds for [(2-methylimidazolium)$_2$][Ni(dipic)$_2$] (left) and [(imidazolium)$_2$][Ni(dipic)$_2$] (right).

Crystal packing is mainly dominated by charge-assisted H-bonding, which allow strength and provide flexibility between imidazolium or 2-methylimidazolium cations and the complex anion (Fig.1.23b). Each anionic metal complex is linked to four different cations by N^+-H$^{\cdots}O^-$ hydrogen bonds that form hydrogen-bonded chains of alternating cations and anions. The cations and anions occupy similar positions within the lattices of the two structures. The primary difference arises in packing and hydrogen-bonded connectivity because the 2-methylimidazolium and imidazolium cations pack in different orientations. The methyl group on the 2-methylimidazolium cations occupies sites of water molecules in the crystal lattices of dihydrates. Hydrogen bonds present along the *y*-axis in imidazole complex are absent in 2-methylimidazole. As a consequence of this change, the re-orientation of the cations takes place.

1.6.2: Inorganic-organic hybrid materials of [M(dipic)$_2$] complex with pyridine-2,6-diammonium cation (pyda)

The (pydaH)$_2$[Co(dipic)$_2$]·H$_2$O, (pydaH)$_2$[Ni(dipic)$_2$]·H$_2$O (Fig. 1.24a) and (pydaH)$_2$ [Cu(dipic)$_2$]·H$_2$O, [83-85] are some of the interesting examples in which the central metal

ions are meridionally coordinated by two tridentate dipicolinate ligands and the cations are involved in extensive supramolecular interactions.

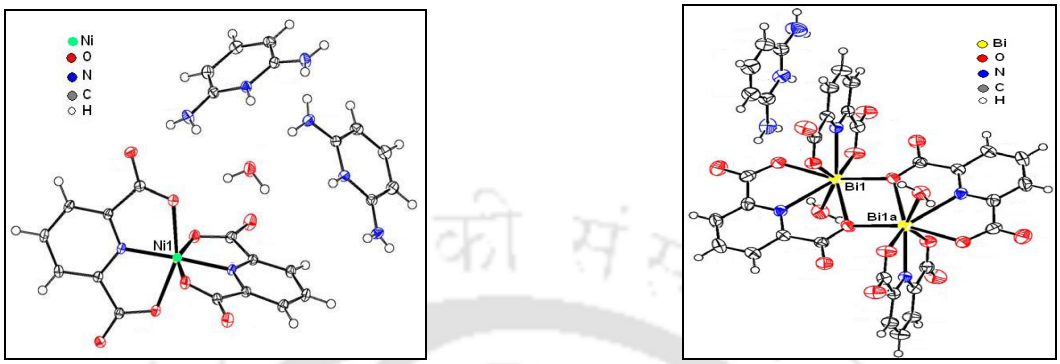

(a) (b)

Fig. 1.24: Structure of complex (a) $(pydaH)_2[Ni(dipic)_2]\cdot H_2O$, (b) $(pydaH)_2[Bi_2(dipic)_4(H_2O)_2]\cdot 4H_2O$ (drawn with 50% thermal ellipsoids).

Dimeric complex $(pydaH)_2$ $[Bi_2(dipic)_4(H_2O)_2]\cdot 4H_2O$ (Fig. 1.24b) and $(pydaH)_2$ $[La_2(dipic)_4(H_2O)_4]\cdot 2H_2O$ shows two metal fragments linked *via* a central four-membered M_2O_2 ring [86-87]. Protonation of the nitrogenous base occurs at the pyridine nitrogen atom of 2,6-pyridinediamine. The intermolecular forces result in the formation of supramolecular coordination compounds possessing ion pair, hydrogen bond and π-π stacking interactions. In yet another example, the complex $(pydaH)_2[Zr(dipic)_3]\cdot 5H_2O$ has the coordination polyhedron of Zr(IV) as distorted tricapped antiprism which is formed by three $(dipic)^{2-}$ ligands [88]. On the other hand the antimony complex, $(pydaH)[Sb(dipic)_2]\cdot 3H_2O \cdot 0.5CHCl_3$, dipicolinate ligand coordinates as a bidentate ligand *via* one oxygen and one nitrogen atom [89], whereas in most of the other complexes, it adopts tridentate chelating mode. The Cr(III) complex has a complicated crystal structure consisting of two crystallographic independent pairs of ions in the unit cell along with lattice water molecules and neutral dipicolinic acid molecules [90]. In $(pydaH)[VO_2(dipic)]$, the oppositely charged cationic and anionic fragments, $(pydaH)^+$ and $[VO_2(dipic))]^-$ are held together by electrostatic forces and other weak interactions [91].

1.6.3: Inorganic-organic hybrid materials of $[M(dipic)_2]$ complex with cations of guanidine (G) and creatinine (creat)

Transition or lanthanide metal dipicolinate complexes with guanidine or creatinine guest molecules are reported in literature. In the complex $(GH)_3[Ce(dipic)_3]\cdot 3H_2O$, Ce(III) shows an usual coordination number of nine attached with three $(dipic)^{2-}$ ligands [92]. The complex shows formation of a trimeric water cluster that interacts with the anion as well as with planar guanidinium cation. Co(II) guanidine complex, $(GH)_2[Co(H_2O)_6][Co(dipic)_2]_2$, exhibits simultaneous formation of anionic $[Co(pydc)_2]^{2-}$ and two cationic $[Co(H_2O)_6]^{2+}$ and $(GH)^+$ moieties in the structure leading to a three component complex (Fig. 1.25a) [93]. The complex $(GH)[Zn(dipic)(dipicH)]\cdot(dipicH_2)\cdot 4H_2O$ shows the presence of doubly ionized, $(dipic)^{2-}$ and singly ionized $(dipicH)^-$ as well as neutral dipicolinic acid molecule in the crystal structure [94].

Bi(III) forms carboxylate bridged dimeric complex with dipicolinic acid and creatinine as guest organic molecule, $(creatH)_2[Bi(dipic)_2]_2\cdot 4H_2O$ (Fig. 1.25b) [95]. The complex exhibits centroid to centroid π-π stacking measured as 3.69 Å between adjacent $(dipic)^{2-}$ fragments and also N-H···π stacking with distance of 3.46 Å between N-H group of creatinine and pyridine ring of $(dipic)^{2-}$ fragments.

(a) (b)

Fig. 1.25: Structure of complex (a) $(GH)_2[Co(H_2O)_6][Co(dipic)_2]_2$ and (b) $(creatH)_2[Bi(dipic)_2]_2\cdot 4H_2O$ (drawn with 50% thermal ellipsoids).

1.6.4: Inorganic-organic hybrid materials of [M(dipic)$_2$] complex with cations of 1,3,5-triazine 2,4,6-triamine (tata) or melamine

Zn(II) and Cd(II) form isostructural complexes (tataH)$_2$[Zn(dipic)$_2$]·10H$_2$O and (tataH)$_2$ [Cd(dipic)$_2$]·10H$_2$O, where the metallic center binds to dipicolinate ligand using its usual tridentate chelating mode [96-97]. Lead dipicolinate-melamine complex (tataH$_2$)$_2$ [Pb(dipic)$_2$]$_2$·(tata)$_2$·4H$_2$O, derived from (tataH)$_2$(dipic), has two metal fragments linked *via* a central ten-membered ring [98]. In the complex, the arrangement of two $(dipic)^{2-}$ as ligands leave a free space around the Pb(II), which is attributed to lone pair of electrons on the Pb(II) atom. Bi(III) forms a polymeric complex with these proton donor and acceptor ligands {(tataH)[Bi(dipic)$_2$(H$_2$O)]}$_n$ [99]. The melaminium ions and complex anions are connected *via* electrostatic, hydrogen bond and π-π stacking interactions between the parallel aromatic rings.

1.6.5: Inorganic-organic hybrid materials of [M(dipic)$_2$] complex with piperazinium cations (pipzH$_2$)

A series of complexes with the general composition of (pipzH$_2$) [M(dipic)$_2$]·xH$_2$O, where M = Mn, Ni, Cu, Zn, Cd, Hg, Pb (at +2 oxidation state) has been reported [100-104]. Except the metal in the anionic complex, they differ by the number of lattice water molecules, supramolecular interactions and its strengths. For example, Ni(II), Cu(II) and Zn(II) shows considerable face to face π-π stacking with distances (centroid to centroid) of 3.47-3.50 Å between the pyridine rings of dipicolinate unit, whereas Pb(II) shows π-π stacking distances in the range of 3.35-3.95 Å. Co(II) forms a three component complex with the composition (pipzH$_2$)[Co(H$_2$O)$_6$][Co(dipic)$_2$]$_2$·8H$_2$O that contains an anion $[Co(dipic)_2]^{2-}$ and two cations, $[Co(H_2O)_6]^{2+}$ and $(pipzH_2)^{2+}$ in the crystal structure [105]. In complex (pipzH$_2$)$_{1/2}$ [Al(H$_2$O)$_6$](SO$_4$)$_2$·4H$_2$O, Al(III) is coordinated to six water molecules together with the tetrahedral sulfate, piperazinium cation and lattice water molecules held by electrostatic and other weak interactions [106].

In dinuclear complex (pipzH$_2$)[Sb$_2$(dipic)$_4$]·2H$_2$O, Sb(III) atoms are penta-coordinated and the coordination polyhedra reflect distortion from a regular trigonal bipyramid due to lone

pair on metallic centers (Fig. 1.26a). The four dipicolinate ligands of the formula unit behave differently against metallic centers, *i.e.* two act as tridentate and the other two as bidentate ligands [107]. In the isostructural complexes, $(pipzH_2)[Zr(pydc)_3]\cdot 8H_2O$ and $(pipzH_2)[Ce(dipic)_3]\cdot 8H_2O$, Zr(IV)/Ce(IV) is coordinated to three dipicolinates in a regular tridentate fashion, one piperazinium as counter ion along with eight lattice water molecules. In both the structures, each M(IV) exhibits distorted tricapped trigonal prism geometry by three nitrogen and six oxygen atoms of carboxylate groups of three $(dipic)^{2-}$ fragments [108-109]. Extensive O-H···O, N-H···O and C-H···O hydrogen bonds as well as ion pairing and π-π interactions play important role in stabilizing the structures and formation of three-dimensional supramolecular networks.

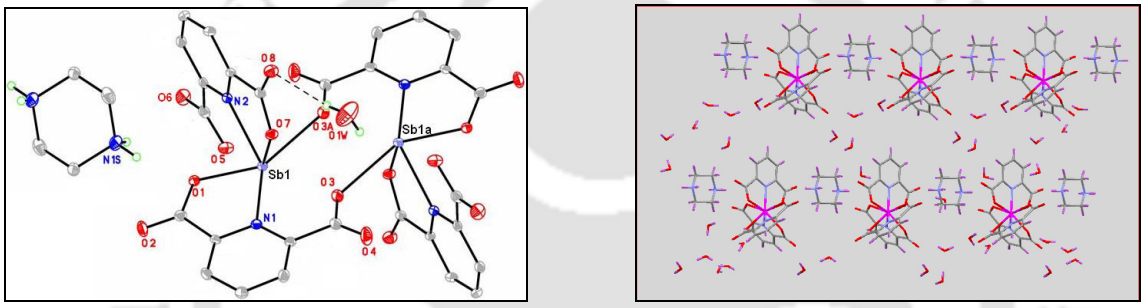

(a) (b)

Fig. 1.26: (a) Structure of complex $(pipzH_2)[Sb_2(dipic)_4]\cdot 2H_2O$ (drawn with 50% thermal ellipsoids), (b) Layered packing diagram of complex $(pipzH_2)[Zr(dipic)_3]\cdot 8H_2O$.

1.6.6: Inorganic-organic hybrid materials of $M(dipic)_2]$ complex with cation of 1,3-propanediamine (pn)

In the $(pnH_2)[M(dipic)_2]\cdot xH_2O$ (where M = Co(II), Cu(II) and Cd(II)), each $[M(dipic)_2]^{2-}$ anionic complex are accompanied by one $(pnH_2)^{2+}$ as counter ion and lattice water molecules [110]. In the lattice, the oppositely charged ribbons and lattice water molecules form several O-H···O, N-H···O and C-H···O hydrogen bonds and π-π stacking led to construct a supramolecular network. In the Co(II) and Cu(II) complexes, π-π stacking is observed between two pyridine rings with distance of 3.42 Å and 3.512 Å respectively. In addition to ionic interactions, the complex $(pnH_2)_2[Ce(dipic)_3](NO_3)\cdot 3.5H_2O$ has a variety of intermolecular O-H···O, N-H···O and C-H···O hydrogen bonds and π-π stacking which connect the various components into a supramolecular network [111]. Further, metal

dipicolinate complexes derived from other ligands such as 4,4′-bipyridine (bpy), benzene-1,3-diamine (bda), 2-aminopyridine (2-apy) and pyridine-4-carboxamide (pyc) are also reported in literature [112-113].

1.7: Scope of the present work

Design of crystalline hybrid materials, based on the organic and inorganic compound is an important and rapidly growing area of interest. The foregoing introductory discussion has shown the potential of coordination complexes derived from dipicolinic acid. In addition, the proton transfer to suitable nitrogen containing organic bases by the dihydro-metal dipicolinate complex; makes it interesting building unit to study supramolecular host-guest complexes. The key feature of these host-guest complexes is that the organic and inorganic moieties self-assemble to generate layers. Although some interesting layered structures have been reported in recent years, the goal of achieving functional materials from organic components in layers of inorganic complex has not yet been fully explored. Due to low thermal and mechanical stability, pure organic components have often been observed as ineffective materials for devices. Coordination compounds have an edge over organic compounds as building blocks because metals exhibit different coordination geometries and a wide range of physical properties. The disadvantage of coordination polymers is that greater strength of metal-ligand bonds often makes them very rigid and fast nucleation led to insoluble microcrystalline powders. Advantage of inorganic-organic hybrid materials over the pure organic or coordination polymer is that due to the possibility of combining the different characteristic of the components, it leads to achieve unusual structures, properties or applications.

For example, hybrid materials based on layered double hydroxides (LDHs) exhibits diverse properties in optic devices, as drug delivery systems, catalysis and also as nano- and macro-fillers in polymer nanocomposites etc. depending on the shape and function of interlayer organic anions [114-117]. The LDH interlayer gap supplies an interesting, constrained environment arising from the anisotropic accommodation of the guest molecule at the nanoscale. Bio-nanocomposites are also an emerging group of hybrid materials derived from natural polymers and inorganic solids interacting at the nanometric scale. These nanostructured organic–inorganic materials could be designed and prepared using a different

type of biopolymers and also inorganic solids with different compositions and topologies [118-120].

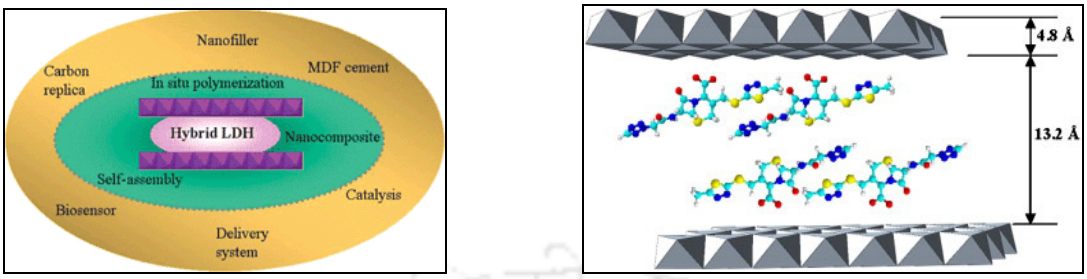

(a) (b)

Fig. 1.26: (a) Overview inorganic–organic hybrid assemblies based on LDH, and (b) Schematic structure of cefazolin (antibiotics) in the interlayer of LDH as a drug delivery system.

Looking at the potential of these hybrid materials, we set our objective to design and explore a strategy to generate layer structures using transition metal dipicolinate complex as supramolecular motif and incorporating wide range of basic organic cations within the layers. Although similar study to construct layered structures by dipicolinate was undertaken earlier, there is no systematic approach to understand the nature of the layers controlled by anions or cations. Thus, there is necessity for a systematic study to discern the type of layered structures formed by dipicolinate complexes *via* intercalation under different conditions. Such study would enlarge domain of guest selectivity and would help to generate layers with different space as required for specific function. Since the dipicolinate metal complexes are basically constituted by three different complimentary components, a complex anion, a basic organic cation and lattice hydrates, the structural role of these moieties from crystal engineering standpoint is essential. For example, (i) the influence of complex anions to control the crystal structures, (ii) the role of cations and its size / geometry to control the layer structure, and (iii) the role of lattice water molecules to stabilize these highly ordered crystal structures. Besides these, the studies on the role of different cations would help to understand the ion-exchange processes. There are also examples of dipicolinate complexes, which are used as insulin mimic; the stability of those complexes under various conditions would provide structural aspects of intermediate species. However, all these processes are guided by the stability and ability of ligand exchange reactions of dipicolinate metal complexes. The stability factors are controlled by

the oxidation state and the nature of the central metal ions. Thus, there is definite need to study cation binding to make supramolecular assemblies as well as to use the complex anions as a ligand to make multinuclear species. Advantage from different binding modes of dipicolinate ligand in free or metal bound state can be taken to prepare multinuclear species. With this background the supramolecular aspects of metal dipicolinate anionic frameworks are being investigated in this present work.

References:

[1] A.A. Holder, L.C. Lewis-Alleyne, D.V. Derveer, Dipicolinic acid, Its Analogues and Derivatives: Aspects of Their Coordination Chemistry; Nova Science Publishers Inc: NY, USA, 2011.

[2] J.F. Powell, Biochem. J. 54 (1953) 210.

[3] T.A. Sliemandagger, W.L. Nicholson, Appl. Environ. Microbiol. 67 (2001) 1274.

[4] T. Douki, B. Setlow, P. Setlow, Photochem. Photobiol. Sci. 4 (2005) 591.

[5] J. Errington, Microbiol. Rev. 57 (1993) 1.

[6] F.W. Janssen, A.J. Lund, L.E. Anderson, Science 127 (1958) 26.

[7] B. Setlow, P. Setlow, Appl. Environ. Microbiol. 59 (1993) 640.

[8] D.L. Griggs, P. Hedden, K.E. Templesmith, W. Rademacher, Phytochemistry 30 (1991) 2513.

[9] L. Couper, J.E. Mckendrick, D.J. Robins, E.J.T. Chrystal, Bioorg. Med. Chem. Lett. 4 (1994) 2267.

[10] K. Murakami, Y. Tanemura, M. Yoshino, J. Nutr. Biochem. 14 (2003) 99.

[11] Y. Kazuhiro, Y. Noriko, F. Tadayasu, Europ. Patent. EP0603165, 1994.

[12] G.A. Burdock, Encyclopedia of Food and Color Additives, vol. 3, CRC Press, 1996.

[13] J.F. Powel, R.E. Strange, Nature 184 (1959) 878.

[14] M.L. Bach, C. Gilvarg, J. Biol. Chem. 241 (1966) 4563.

[15] P.H. Hodson, J.W. Foster. J. Bacteriol. 91 (1966) 562.

[16] I. Iovel, M. Shymanska, Synth. Commun. 22 (1992) 2691.

[17] B. Das, J.B. Baruah, Cryst. Growth Des. 11 (2011) 278.

[18] B. Das, J.B. Baruah, Cryst. Growth Des. 11 (2011) 5522.

[19] P. Carmona, Spectrochim. Acta 36 (1979) 705.

[20] G.G. Bombi, R. Aikebaier, A. Dean, V.B. Di Marco, D. Marton, A. Tapparo, Polyhedron 28 (2009) 327.

[21] A. Moghimi, M. Ranjbar, H. Aghabozorg, F. Jalali, M. Shamsipur, G.P.A. Yap, H. Rahbarnoohi, J. Mol. Struct. 605 (2002) 133.

[22] A. Moghimi, S. Sheshmani, A. Shokrollahi, M. Shamsipur, G. Kickelbick, H. Aghabozorg, Z. Anorg. Allg. Chem. 631 (2005) 160.

[23] A. Moghimi, M.A. Sharif, H. Aghabozorg, Acta Cryst. E60 (2004) o1790.

[24] M. Chatterjee, M. Maji, S. Ghosh, T.C.W. Mak, J. Chem. Soc., Dalton Trans. (1998) 3641.

[25] L.C. Nathan, T.D. Mai, J. Chem. Cryst. 30 (2000) 509.

[26] L.C. Nathan, Trends Inorg. Chem. 3 (1993) 415.

[27] L. Yang, D.C. Crans, S.M. Miller, A. la Cour, O.P. Anderson, P.M. Kaszynski, M.E. Godzala III, L.D. Austin, G.R. Willsky, Inorg. Chem. 41 (2002) 4859.

[28] P. Laine, A. Gourdon, J.-P. Launay, Inorg. Chem. 34 (1995) 5138.

[29] D.T. Richens, The Chemistry of Aqua Ions: Synthesis, Structure and Reactivity: A Tour Through the Periodic Table of the Elements, Wiley, 1997.

[30] K.-B. Shiu, C.-H. Yen, F.-L. Liao, S.-L. Wang, Acta Cryst. E60 (2004) m35.

[31] L. Xie, Y. Wei, Y. Wang, H. Hou, Y. Fan, Y. Zhu, J. Mol. Struct. 692 (2004) 201.

[32] Y. Qi, Y. Wang, H. Fan, M. Cao, L. Mao, C. Hu, E. Wang, N. Hu, H. Jia, J. Mol. Struct. 694 (2004) 73.

[33] L. Wang, L. Duan, E. Wang, D. Xiao, Y. Li, Y. Lan, L. Xu, C. Hu, Transition Met. Chem. 29 (2004) 212.

[34] Y.-H. Wen, Z.-J. Li, Y.-Y. Qin, Y. Kang, Y.-B. Chen, J.-K. Cheng, Y.-G. Yao, Acta Cryst. E58 (2002) m762.

[35] L. Wang, L. Duan, D. Xiao, E. Wang, C. Hu, J. Coord. Chem. 57 (2004) 1079.

[36] M.V. Kirillova, M.F.C. Guedes da Silva, A.M. Kirillova, J.J.R. Frausto da Silva, A.J.L. Pombeiro, Inorg. Chim. Acta 360 (2007) 506.

[37] H. Gao, L. Yi, B. Zhao, X. Zhao, P. Cheng, D. Liao, S. Yan, Inorg. Chem. 45 (2006) 5980.

[38] H. Aghabozorg, F. Manteghi, S. Sheshmani, J. Iran. Chem. Soc. 5 (2008) 184.

[39] M. Mirzaei, H. Aghabozorg, H. Eshtiagh-Hosseini, J. Iran. Chem. Soc. 8 (2011) 580.

[40] D.C. Crans, L. Yang, T. Jakusch, T. Kiss, Inorg. Chem. 39 (2000) 4409.

[41] D.C. Crans, M. Mahroof-Tahir, M. Johnson, P. Wilkins, L. Yang, K. Robbins, A. Johnson, J. Alfano, M. Godzala, L. Austin, G. Willsky, Inorg. Chim. Acta 356 (2003) 365.

[42] P. Laine, A. Gourdon, J.-P. Launay, Inorg. Chem. 34 (1995) 5129.

[43] N. Okabe, N. Oya, Acta Cryst. C56 (2000) 305.

[44] D. Sukanya, R. Prabhakaran, K. Natarajan, Polyhedron 25 (2006) 2223.

[45] K. Hakansson, M. Lindahl, G. Svensson, J. Albertsson, Acta Chem. Scand. 47 (1993) 449.

[46] T.K. Prasad, M.V. Rajasekharan, Polyhedron 26 (2007) 1364.

[47] S. Sailaja, M.V. Rajasekharan, Acta Cryst. E57 (2001) m341.

[48] T.K. Prasad, S. Sailaja, M.V. Rajasekharan, Polyhedron 24 (2005) 1487.

[49] M.K. Kim, K-L. Bae, K.M. Ok, Cryst. Growth Des. 11 (2011) 930.

[50] H. Aghabozorg, P. Ghasemikhah, M. Ghadermazi, J. Soleimannejad, H. Adams, Acta Cryst. E63 (2007) m1487.

[51] H. Aghabozorg, N. Firoozi, L. Roshan, M. Mirzaei, A. Shokrollahi, R. Aghaei, Z. Aghlamnadi, Iran. J. Chem. Chem. Eng. 30 (2011) 1.

[52] S. Santra, B. Das, J.B. Baruah, J. Chem. Crystallogr. 41 (2011) 1981.

[53] Y. Hamada, H. Ohta, N. Miyamoto, R. Yamaguchi, A. Yamani, K. Hidaka, T. Kimura, K. Saito, Y. Hayashi, S. Ishiura, Y. Kiso, Bioorg. Med. Chem. Lett. 18 (2008) 1654.

[54] B. Schmidt, J. Jiricek, A. Titz, G. Ye, K. Parang, Bioorg. Med. Chem. Lett. 14 (2004) 4203.

[55] M. Fainerman-Melnikova, J.K. Clegg, A.A.H. Pakchung, P. Jensena, R. Codd, CrystEngComm. 12 (2010) 4217.

[56] M. Felloni, A.J. Blake, P. Hubberstey, S.J. Teat, C. Wilson, M. Schroder, CrystEngComm. 12 (2010) 1576.

[57] T.K. Prasad, M.V. Rajasekharan, Crystal Growth Des. 8 (2008) 1346.

[58] B. Zhao, X.-Y. Chen, Z. Chen, W. Shi, P. Cheng, S.-P. Yan, D.-Z. Liao, Chem. Commun. (2009) 3113.

[59] R. Ludwig, Angew. Chem. Int. Ed. 40 (2001) 1808.

[60] J.M. Ugalde, I. Alkorta, J. Elguero, Angew. Chem. Int. Ed. 39 (2000) 717.

[61] X.-M. Zhang, R.-Q. Fang, H.-S. Wu, Cryst. Growth Des. 5 (2005) 1335.

[62] B-Q. Ma, H.-L. Sun, S. Gao, Chem. Commun. (2005) 2336.

[63] L.E. Cheruzel, M.S. Pometun, M.R. Cecil, M.S. Mashuta, R.J. Wittebort, R.M. Buchanan, Angew. Chem. Int. Ed. 42 (2003) 5452.

[64] R. Carballo, B. Covelo, C. Lodeiro, E.M. Vazquez-Lopez, CrystEngComm. 7 (2005) 294.

[65] T.K. Prasad, M.V. Rajasekharan, Crystal Growth Des. 6 (2006) 488.

[66] T.K. Prasad, M.V. Rajasekharan, Inorg. Chem., 48 (2009) 11543.

[67] S.K. Ghosh, P.K. Bharadwaj, Inorg. Chem. 44 (2005) 3156.

[68] B. Zhao, L. Yi, Y. Dai, X-Y. Chen, P. Cheng, D-Z. Liao, S-P. Yan, Z-H. Jiang, Inorg. Chem. 44 (2005) 911.

[69] H. Aghabozorg, F. Ramezanipour, P.D. Kheirollahi, A.A. Saei, A. Shokrollahi, M. Shamsipur, F. Manteghi, J. Soleimannejad, M.A. Sharif, Z. Anorg. Allg. Chem. 632 (2006) 147.

[70] F. Ramezanipour, H. Aghabozorg, A. Shokrollahi, M. Shamsipur, H. Stoeckli-Evans, J. Soleimannejad, S. Sheshmani, J. Mol. Struct. 779 (2005) 77.

[71] Z. Derikvand, H. Aghabozorg, A. Nemati, M. Ghadermazi, J.A. Gharamaleki, Acta Cryst. E64 (2008) m350.

[72] M.P. Suh, Y.E. Cheon, E.Y. Lee, Coord. Chem. Rev. 252 (2008) 1007.

[73] B.L. Chen, L.B. Wang, F. Zapata, G.D. Qian, E.B. Lobkovsky, J. Am. Chem. Soc. 130 (2008) 6718.

[74] B.L. Chen, L.B. Wang, Y.Q. Xiao, F.R. Fronczek, M. Xue, Y.J. Cui, G.D. Qian, Angew. Chem. Int. Ed. Engl. 48 (2009) 500.

[75] B.L. Chen, Y. Yang, F. Zapata, G.N. Lin, G.D. Qian, E.B. Lobkovsky, Adv. Mater. 19 (2007) 1693.

[76] L.G. Qiu, Z.Q. Li, Y. Wu, W. Wang, T. Xu, X. Jiang, Chem. Commun. (2008) 3642.

[77] D.B. Mitzi, In Functional Hybrid Materials; P. Gomez-Romero, C. Sanchez, Eds.; Wiley-VCH Verlag GmbH & Co. KGaA: Weinheim, Germany, 2004; pp 347-386.

[78] S. Kitagawa, R. Kitaura, S.-I. Noro, Angew. Chem. Int. Ed. 43 (2004) 2334.

[79] K.T. Holman, A.M. Pivovar, J.A. Swift, M.D. Ward, Acc. Chem. Res. 34 (2001) 107.

[80] Y.Y. Li, C.K. Lin, G.L. Zheng, Z.Y. Cheng, H. You, W.D. Wang, J. Lin, Chem. Mater. 18 (2006) 3463.

[81] J.C. MacDonald, P.C. Dorrestein, M.M. Pilley, M.M. Foote, J.L. Lundburg, R.W. Henning, A.J. Schultz, J.L. Manson, J. Am. Chem. Soc. 122 (2000) 11692.

[82] J.C. MacDonald, T-J.M. Luo, G.T.R. Palmore, Cryst. Growth Des. 4 (2004) 1203.

[83] A. Moghimi, M. Ranjbar, H. Aghabozorg, F. Jalali, M. Shamsipur, R.K. Chadha, Can. J. Chem. 80 (2002) 1687.

[84] A. Moghimi, M. Ranjbar, H. Aghabozorg, F. Jalali, M. Shamsipur, R.K. Chadha, J. Chem. Res.(M) (2002) 1047.

[85] M. Ranjbar, M. Taghavipur, H. Aghabozorg, A. Moghimi, F. Jalali, M. Shamsipur, Polish J. Chem. 76 (2002) 785.

[86] M. Ranjbar, H. Aghabozorg, A. Moghimi, Z. Kristallogr. NCS 218 (2003) 432.

[87] S. Sheshmani, P.D. Kheirollahi, H. Aghabozorg, A. Shokrollahi, G. Kickelbick, M. Shamsipur, F. Ramezanipour, A. Moghimi, Z. Anorg. Allg. Chem. 631 (2005) 3058.

[88] H. Aghabozorg, A. Moghimi, F. Manteghi, M. Ranjbar, Z. Anorg. Allg. Chem. 631 (2005) 909.

[89] H. Aghabozorg, A.A. Saei, E. Sadr-khanlou, A. Moghimi, Anal. Sci. 21 (2005) x207.

[90] M. Ranjbar, H. Aghabozorg, A. Moghimi, A. Yanovsky, Z. Kristallogr. NCS 216 (2001) 626.

[91] M. Ranjbar, Anal. Sci. 20 (2004) x135.

[92] H. Aghabozorg, F. Mohammad Panah, E. Sadr-khanlou, Acta Cryst. E62 (2006) m2509.

[93] S. Sheshmani, H. Aghabozorg, F. Mohammad Panah, R. Alizadeh, G. Kickelbick, B. Nakhjavan, A. Moghimi, F. Ramezanipour, H Aghabozorg, Z. Anorg. Allg. Chem. 632 (2006) 469.

[94] H. Aghabozorg, E. Sadr-khanlou, J. Cryst. Res. Technol. 43 (2008) 327.

[95] H. Aghabozorg, F. Ramezanipour, J. Sleimannejad, M.A. Sharif, A. Shokrollahi, M. Shamsipur, A. Moghimi, J. Attar Gharamaleki, V. Lippolis, A.J. Blake, Polish J. Chem. 82 (2008) 487.

[96] Z. Aghajani, M.A. Sharif, H. Aghabozorg, A. Naderpour, Acta Cryst. E62 (2006) m830.

[97] H. Aghabozorg, Z. Aghajani, M.A. Sharif, Acta Cryst. E62 (2006) m1930.

[98] M.A. Sharif, H. Aghabozorg, A. Shokrollahi, G. Kickelbick, A. Moghimi, M. Shamsipur, Polish J. Chem. 80 (2006) 847.

[99] M.A. Sharif, H. Aghabozorg, A. Moghimi, Acta Cryst. E63 (2007) m1599.

[100] H. Aghabozorg, J. Attar Gharamaleki, P. Ghasemikhah, M. Ghadermazi, J. Soleimannejad, Acta Cryst. E63 (2007) m1710.

[101] H. Aghabozorg, F. Zabihi, M. Ghadermazi, J. Attar Gharamaleki, S. Sheshmani, Acta Cryst. E62 (2006) m2091.

[102] H. Aghabozorg, P. Ghasemikhah, J. Soleimannejad, M. Ghadermazi, J. Attar Gharamaleki, Acta Cryst. E62 (2006) m2266.

[103] H. Aghabozorg, P. Ghasemikhah, M. Ghadermazi, S. Sheshmani, Acta Cryst. E62 (2006) m2835.

[104] H. Aghabozorg, P. Ghasemikhah, M. Ghadermazi, J. Attar Gharamaleki, S. Sheshmani, Acta Cryst. E62 (2006) m2269.

[105] H. Aghabozorg, J. Attar Gharamaleki, M. Ghadermazi, P. Ghasemikhah, J. Soleimannejad, Acta Cryst. E63 (2007) m1803.

[106] M. Ghadermazi, H. Aghabozorg, S. Sheshmani, Acta Cryst. E63 (2007) m1919.

[107] H. Aghabozorg, F. Manteghi, M. Ghadermazi, M. Mirzaei, A.R. Salimi, H. Eshtiagh-Hosseini, J. Iran. Chem. Soc.7 (2010) 500.

[108] H. Aghabozorg, M. Ghadermazi, F. Manteghi, B. Nakhjavan, Z. Anorg. Allg. Chem. 632 (2006) 2058.

[109] H. Aghabozorg, E. Moteieyan, A.R. Salimi, M. Mirzaei, F. Manteghi, A. Shokrollahi, S. Derki, M. Ghadermazi, S. Sheshmani, H. Eshtiagh-Hosseini, Polyhedron 29 (2010) 1453.

[110] H. Aghabozorg, M. Ghadermazi, B. Nakhjavan, F. Manteghi, J. Chem. Cryst. 38 (2008) 135.

[111] H. Aghabozorg, B. Nakhjavan, M. Ghadermazi, F. Ramezanipour, Acta Cryst. E62 (2006) m1527.

[112] J. Soleimannejad, H. Aghabozorg, S. Hooshmand, M. Ghanbari, F. Manteghi, M. Shamsipur, J. Iran. Chem. Soc. 7 (2010) 405.

[113] J. Soleimannejad, H. Aghabozorg, S. Hooshmand, H. Adams, Acta Cryst. E63 (2007) m3089.

[114] F. Leroux, C. Taviot-Gueho, J. Mater. Chem. 15 (2005) 3628.

[115] L. Li, J. Shi, Chem. Commun. (2008) 996.

[116] B.M. Choudary, M. Lakshmi Kantam, V. Neeraja, K.K. Rao, F. Figueras, L. Delmotte, Green Chem. 3 (2001) 257.

[117] S.-J. Ryu, H. Jung, J.-M. Oh, J.-K. Lee, J.-H. Choy, J. Phy. Chem. Solids, 71 (2010) 685.

[118] E. Ruiz-Hitzky, M. Darder, P. Aranda, J. Mater. Chem. 15 (2005) 3650.

[119] C. Sanchez, B. Julián, P. Belleville, M. Popall, J. Mater. Chem. 15 (2005) 3559.

[120] A.C.S. Alcântara, P. Aranda, M. Darder, E. Ruiz-Hitzky, J. Mater. Chem. 20 (2010) 9495.

Chapter 2

Layered inorganic–organic hybrid materials of Ni(II), Cu(II) or Zn(II) dipicolinates and organic ammonium cations

Hybrid inorganic-organic materials play a major role in the development of advanced functional materials [1]. Intimately mixed components of molecular or nano-composites of organic (or bio) and inorganic compounds with one of the component in free or assembled state having a dimension of few Å to several nanometers have specific interest. The properties of these materials are not necessarily being the sum of the individual components, but the role of their inner interfaces could also be predominant. Broadly, hybrid inorganic-organic materials are divided into two classes. In class I materials, organic and inorganic components are embedded *via* ionic bonds, hydrogen bonds and van der Waals forces. In class II materials, the components interact *via* strong chemical covalent or iono-covalent bonds. They provide varieties to create materials with new and enhanced properties that find applications in many areas such as optics, electronics, mechanics, energy, environment, biology and medicine [2]. Other applications include smart membranes and separation devices, functional smart coatings, photo catalysis, sensors, micro-electronics, innovative cosmetics, therapy and controlled release of active molecules, nanoceramic–polymer composites for the automobile and packaging industries [3-9].

The families of hybrid inorganic-organic materials having layered structures such as layered double hydroxides (LDH) are structurally and industrially important. About this an elaborated description is given in chapter **1.** There are many other examples of layered structures in which organic molecules/ions are intercalated. Among them, guanidinium-sulphonate (GS) networks and ammonium-trimesates, studied by Ward and Zaworotko group are two classic examples known for reproducible lamellar networks based on hydrogen-bonded components [10-17]. Formation of lamellar solids from metal containing dicarboxylic acids (such as 2,4-pyridine dicarboxylic acid or malonic acid) and aliphatic or aromatic amines *via* ammonium-carboxylate hydrogen bond has also been studied recently [18,19]. Lamellar organic solids derived from other dicarboxylic acids such as 3,5-

pyrazoledicarboxylic acid, 3,5-pyridinedicarboxylic acid and isophthalic acid with varieties of amines are reported as relevant to organic clay mimics [20-22].

With this background and also available information on the lamellar structures of dipicolinate complexes, we have studied the effect of interlayer spacing by varying size, shape, orientation of cations and also the assembling of cations in free or hydrated form. In a dianionic bis-chelated dipicolinate complex of metal(II) ion, the dipicolinate groups are placed approximately perpendicular to each other to complete a six coordinated environment. Such perpendicular orientation of dipicolinate ligands around a metal ion is

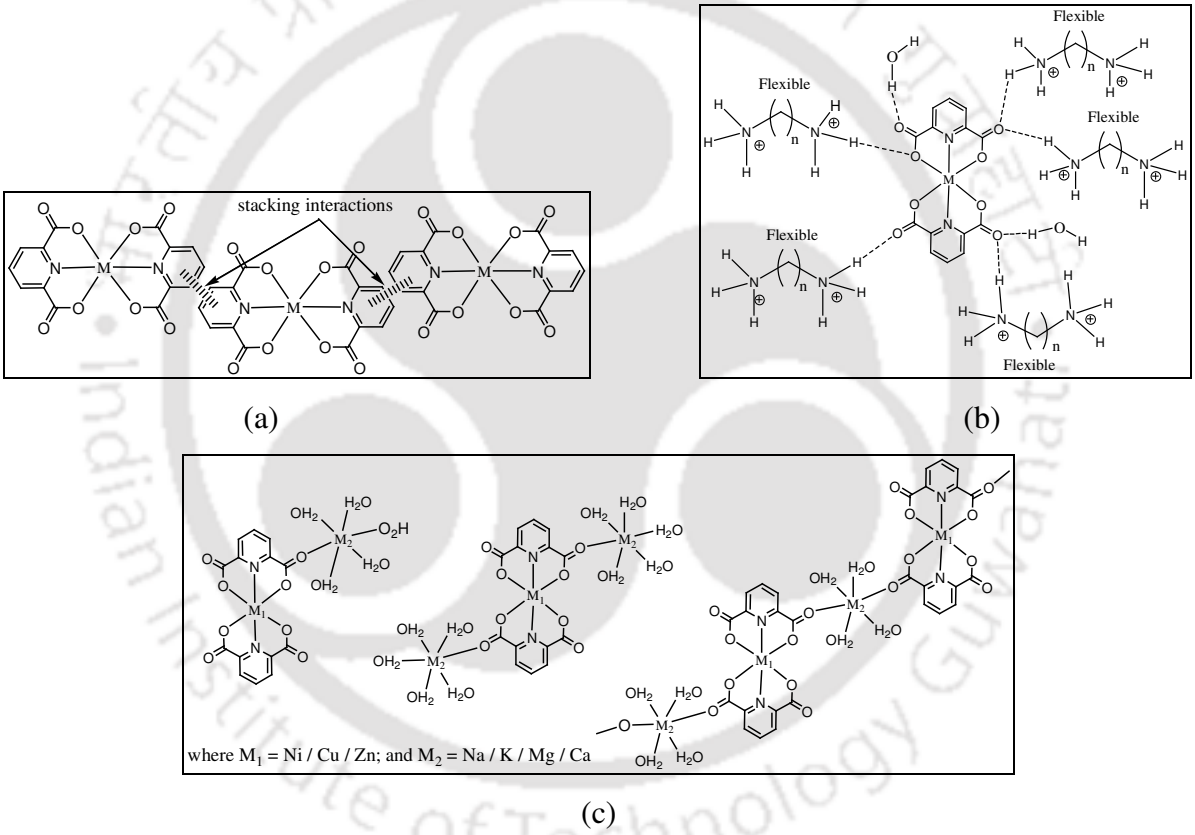

Fig. 2.1. (a) Formation of anionic layers by π-π stacking of complex anions, (b) Different $-NH_3^+$-COO^- or -COO^--lattice water interactions, (c) Possible metal dipicolinate alkali/alkaline aquated complexes after exchange of organic cation.

expected to make layered arrangement by aromatic stacking interactions as shown in Fig. 2.1a. Such layers are expected to extend in one direction through the stacking interactions. The two non-coordinating carbonyl groups of the dipicolinate should be able to act as sites

for interactions with organo-cations or aquated cations to form hydrogen bonds (Fig 2.1b). It would be also interesting to understand the folding or orientations of intervening long chain bearing diammonium cations within the layered structures. Further to understand the possibility of retention of layered structures by exchange of alkali metal cations and also the environment of encapsulated hydrated cationic species in their different forms, as per the some possibilities shown in Fig. 2.1c.

Thus, this chapter is on the synthesis and structural characterization of layered inorganic–organic hybrid materials built up of dication of aliphatic diamines and mono cation of aromatic amines sandwiched between transition metal dipicolinate frameworks (as shown in scheme 2.1). In addition, the cation exchange properties of these complexes with alkali or alkaline earth metal ions are described.

2.1: Synthesis and characterization of Ni(II), Cu(II) or Zn(II) dipicolinates with ethylenediamine, 1,5-diaminopentane, 1,8-diaminooctane or 4-aminobenzylamine

The reaction of hydrated Ni(II), Cu(II) or Zn(II) acetate salts with dipicolinic acid in methanol/water generate the dicarboxylic acid starting materials $H_2[ML_2]$, which are then allowed to react with diamines such as ethylenediamine (**en**), 1,5-diaminopentane (**pen**), 1,8-diaminooctane (**doc**) and 4-aminobenzylamine (**bam**). The protonation of the aliphatic or aromatic amines by acidic metal complex $H_2[ML_2]$ (where M =Ni(II), Cu(II), Zn(II)), led to the formation of complexes as illustrated in scheme **2.1**. In the cases of **pen** and **doc**, dicationic amines are formed as counter cations, irrespective of metal used. In the case of **bam**, mono-protonation takes place at the benzylic site resulting in the different stoichiometry than the former two diamines. The ethylenediamine is an exception; it acts both as coordinated ligand and also as dication or combination of the both. The formation of particular combination is dependent on the metal ion used. Namely, the Ni(II) and Zn(II) form dicationic complexes whereas Cu(II) complex is a combination of chelated ethylenediamine as well as a cation for $[ML_2]^{2-}$. All these complexes are characterized from their spectroscopic data, elemental and thermal analysis. Further crystal structure in each case is determined. The powder X-ray diffraction (PXRD) data of each compound is

recorded to ascertain phase purity and the experimental PXRD patterns are compared with the simulated patterns obtained from the crystallographic information files.

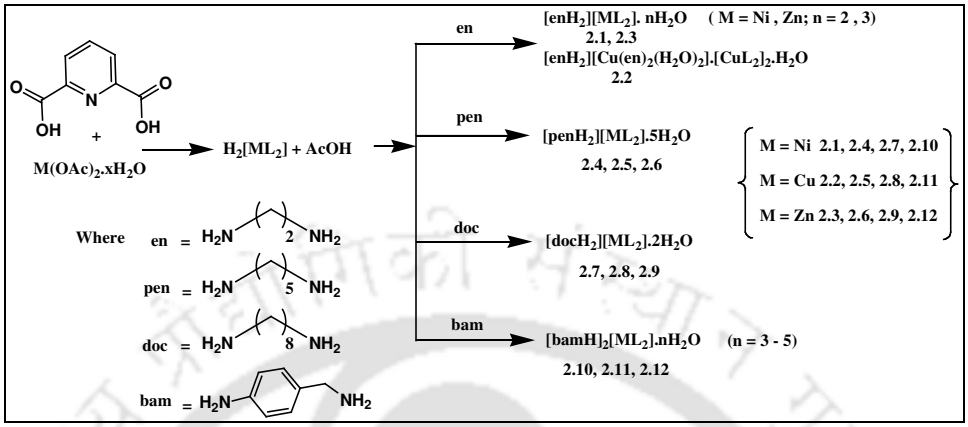

Scheme 2.1: Synthesis of dipicolinate complexes

Since each complex contains invariably ammonium cations they shows N-H stretching in the region of 3027-2611 cm^{-1}. They have characteristic IR stretching frequencies in the range of 1636-1590 cm^{-1} and 1376-1373 cm^{-1} due to the asymmetric and symmetric carboxylate stretching respectively. The asymmetric stretching for the carboxylate group spreads over a wide range, which is attributed to the effect of hydrogen bonding associated with the ammonium ions and crystallized water molecules. Some of the representative peaks are shown in table 2.1.

Table 2.1: Prominent IR stretching frequencies, Visible spectra (λ_{max}), effective magnetic moment (at 298 K) and molar conductance value of the five representative complexes

Complex	IR stretching frequencies (KBr, cm^{-1})	Vis. (H_2O) λ_{max} (ε, $M^{-1} cm^{-1}$)	μ_{eff} (BM, RT)	Molar conductance (H_2O, S cm^2 mol^{-1})
$[enH_2][NiL_2]\cdot 3H_2O$ (**2.1**)	3474(ν_{str}O-H), 3038 (ν_{str}N-H), 1636, 1592($\nu_{as}CO_2^-$), 1423(N-H_{bend}), 1371($\nu_sCO_2^-$)	622.0 nm (ε = 6.2)	2.92	246.5
$[enH_2]$ $[Cu(en)_2(H_2O)_2]\cdot[CuL_2]_2.H_2O$ (**2.2**)	3432(ν_{str}O-H), 2959 (ν_{str}N-H), 1636, 1591($\nu_{as}CO_2^-$), 1422(N-H_{bend}), 1373($\nu_sCO_2^-$)	763.0 nm (ε = 115.6)	1.65	325.7
$[penH_2][CuL_2]\cdot 5H_2O$ (**2.5**)	3419(ν_{str}O-H), 3087(ν_{str}N-H), 1634, 1621, 1590($\nu_{as}CO_2^-$), 1422(N-H_{bend}), 1373($\nu_sCO_2^-$)	774.0 nm (ε = 69.5)	1.60	237.3
$[docH_2][NiL_2]\cdot 2H_2O$ (**2.7**)	3389(ν_{str}O-H), 3072, 2932 (ν_{str}N-H), 1614, 1593($\nu_{as}CO_2^-$),	611.0 nm (ε = 6.0)	2.85	248.4

	1425($N\text{-}H_{bend}$), 1378($\nu_s CO_2^-$)			
$[bamH]_2[CuL_2]\cdot 5H_2O$ (**2.10**)	3410($\nu_{str}O\text{-}H$), 3041, 2956 ($\nu_{str}N\text{-}H$), 1633, 1620, 1590 ($\nu_{as}CO_2^-$), 1421($N\text{-}H_{bend}$), 1374($\nu_s CO_2^-$)	773.0 nm (ε = 67.3)	1.65	233.7

The 1:1 dication : dianion and 2:1 monocation : dianion containing complexes exhibit high conductance values (table 2.1) in the range of 230.0-270.0 S cm^2 mol^{-1}. This reflects the ionic nature of the complexes in aqueous solution. Conventionally such values for 1:1 divalent electrolytes should be close to 240.0 S cm^2 mol^{-1}. The complex **2.2** comprises of three different ions, namely an ethylenediammonium cation, a dication $[Cu(en)_2(H_2O)_2]^{2+}$ and two dianions of $[CuL_2]^{2-}$. Its molar conductance value 325.7 S cm^2 mol^{-1} is lower than the expected value for six ions; which is due to the larger size of the complex cation, leading to lower mobility. The higher value of conductance is related to proton conductivity.

The loss of weight of water molecules in thermogravimetry of each compound corresponds to the number of water molecules obtained from their elemental composition as well as supported by their crystal structures. Thermal decomposition of the organic cation containing complexes results in the formation of corresponding metal oxides of the central metal ion at relatively low temperatures. An illustrative thermogram of complex $[docH_2][ZnL_2]\cdot 2H_2O$ (**2.9**) is shown in Fig. 2.2. Three prominent steps of weight loss are observed. The weight loss of 5.4% (calcd. 6.2%) at the range of 60-90 ºC corresponds to the loss of two crystallized water molecules. The major weight change occurs in the temperature range of 260-325 ºC due to loss of diamines (obsd. 49.1%, calcd. 49.6%). Further to this, the decomposition of the Zn(II) dipicolinate occurs continuously in the temperature range 400-475 ºC. The final residue left 13.8% (calcd. 14.0%) is ascribed to the formation of zinc oxide.

The thermogram of complex $[bamH]_2[CuL_2]\cdot 5H_2O$ also showed three prominent steps of weight loss in the temperature range of 40-500 ºC. The first step of weight loss of 11.1% (calcd. 12.3%) at the range of 60-118 ºC corresponds to the loss of the five crystallized water molecules. The second step of 33.5% (calcd. 34.2%) weight loss in the temperature region of 225-300 ºC was due to loss of aromatic amines. The third step is the steady and continuous decomposition of Cu(II) dipicolinate complex, which takes place in the

temperature range 330-450 ºC. The final residue left 11.1% (calcd. 10.8%) shows the formation of copper oxide.

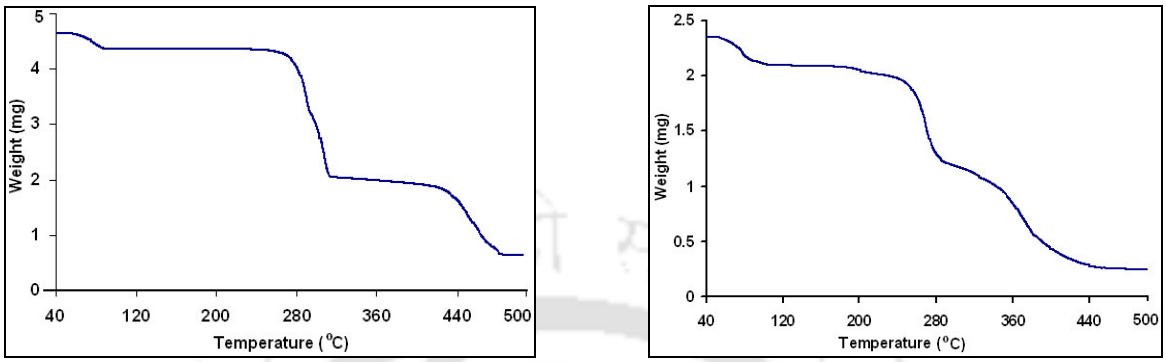

(a) (b)

Fig. 2.2: Thermograms of (a) complex **2.9** and (b) complex **2.11**

The metal dipicolinate complexes with respect to the diamine are discussed below.

2.2: Inorganic-organic hybrid materials of Ni(II), Cu(II) or Zn(II) dipicolinate complex with ethylenediammonium cation

As illustrated in scheme **2.1**, treatment of ethylenediamine with $H_2[ML_2]$ resulted in two different types of complexes with three different metal ions. For example, using nickel or zinc salt we obtained $[enH_2][ML_2]\cdot nH_2O$ (**2.1, 2.3**) (where M = Ni(II) and Zn(II)) and whereas use of copper(II) salt led to the formation of $[enH_2][Cu(en)_2(H_2O)_2]\cdot[CuL_2]_2\cdot H_2O$ (**2.2**). It is to mentioned that Ni(II)/Zn(II) easily form bis or tris chelate complexes with ethylenediamine [23-25]. These complexes have been widely studied to understand their kinetic lability, stability, electrochemical behavior and other properties. In the mixed ligand systems described in this chapter, ethylenediamine despite being a strongly basic amine, it does not coordinate with the metal ion and remain in the outside of the coordination sphere as a dication of the complex anion.

Except the number of lattice water molecules, the complexes **2.1** and **2.3** have similar compositions having a complex anion and dication of ethylenediamine. As a representative case the complex $[enH_2][NiL_2]\cdot nH_2O$ (**2.1**) is discussed in details. The anion $[NiL_2]^{2-}$ consists of a distorted octahedral Ni(II) centre with two meridionally coordinated tridentate

dipicolinate ligands. Overall it makes a MO_4N_2 coordination environment. The crystal structure shows that the ethylenediamine dication is distributed in two parts and lies in a crystallographic inversion center. Two of water molecules in the crystal structure possess 50% occupancy. Both the cation $[enH_2]^{2+}$ or anion $[NiL_2]^{2-}$ is surrounded by six oppositely charged ions in the complex (Fig. 2.2.1a). The packing of the cations and anions in its crystal lattice generates lamellar structure *via* charge-assisted ammonium-carboxylate hydrogen bond along crystallographic *a* and *b* axes. The enH_2 dications form a linear hydrogen-bonded layer in association with lattice water molecules while the inorganic layers are held together *via* π-π stacking between two adjacent $[NiL_2]^{2-}$ unit. The centroid to centroid π-π stacking distance between two such pyridine rings of adjacent dipicolinate complex is ~ 3.39 Å. The lattice water molecules act as a hydrogen bonded bridge between two nearby $[NiL_2]^{2-}$ units. It is to be mentioned that ethylenediammonium intercalated vanadyl phosphate complex was synthesized in hydrothermal conditions [26]. In that complex, $[enH_2]^{2+}$ cations occupy cavities in between the layers made up of VO_5 square pyramids and PO_4 tetrahedra.

From crystal engineering standpoint, the inter-metal distance between two adjacent $[NiL_2]^{2-}$ complex (**2.1**) that separates the organic layer is ~ 8.2 Å along *a* axis. The same distance along *b* axis is ~ 8.1 Å (Fig. 2.2.1b). The isostructural zinc complex **2.3**, shows such interlayer separation as 8.3 and 8.2 Å along *a* and *b* axis respectively. The centroid to centroid π-π stacking distance in complex **2.3** is ~ 3.47 Å. The interactions between organic and inorganic parts are reinforced further by O-H···O hydrogen bonds with the lattice water molecules and weak C-H···O interactions.

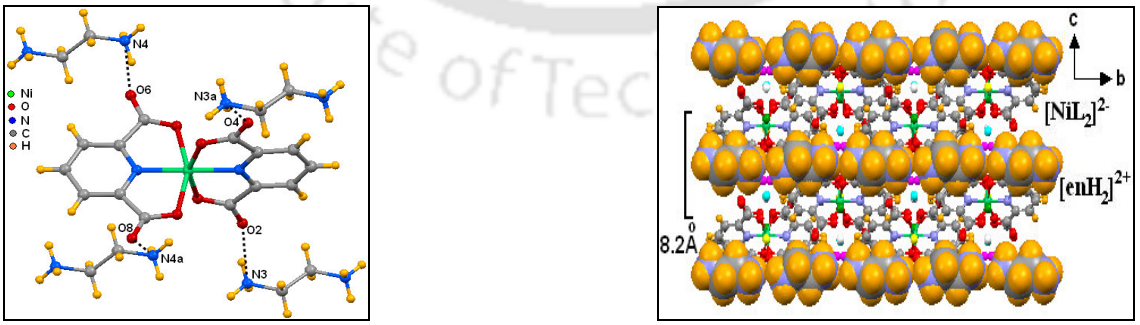

(a) (b)

Fig. 2.2.1: (a) Ammonium-carboxylate interactions in **2.1**, (b) Layered packing diagram of **2.1**, (enH_2 in space filled mode, $[NiL_2]^{2-}$ in ball and stick mode).

Copper(II) forms an interesting three-component complex with dipicolinic acid and ethylenediamine $(enH_2)[Cu(en)_2(H_2O)_2][CuL_2]_2{\cdot}H_2O$ (**2.2**). The crystal structure reveals simultaneous formation of both anionic $[CuL_2]^{2-}$ and two different cationic species, $(enH_2)^{2+}$ and $[Cu(en)_2(H_2O)_2]^{2+}$ in the complex (Fig. 2.2.2a). The complex crystallizes in monoclinic space group *C2/m*; thus, the asymmetric unit displays half of the molecule due to the presence of a 2-fold crystallographic axis. Earlier, formation of three component Co(II) dipicolinate complex with guanidinium cation, $(GH)_2[Co(H_2O)_6]$ $[CoL_2]_2$ has been observed (Ch. 1, [93]). All these complexes have the isostructural complex anion and organic cation, but the complex cations are different in each case with different stoichiometry. It should to be noted that as compared to binary complexes, ternary complexes are rarely explored [27-30]. Although formation such complexes are difficult to understand, it may be assumed that these require specific ligand environment and selective metal ion that should complement each other through weak interactions [31,32].

The oppositely charged ions generate layers in lattice. The anionic layers consists of $[CuL_2]^{2-}$, whereas in the cationic layers $(enH_2)^{2+}$ and $[Cu(en)_2(H_2O)_2]^{2+}$ occupy the alternative sites of the layer (Fig. 2.2.2b). The anionic layer exhibits weak π-π stacking (centroid to centroid distance ~ 3.70 Å). The inter-metal distance between two adjacent $[CuL_2]^{2-}$ complex sandwiching the cationic layer is ~ 9.44 Å. A larger distance is observed because of relatively larger inorganic cation $[Cu(en)_2(H_2O)_2]^{2+}$ present in the layer. The diammonium cation $(enH_2)^{2+}$ is strongly hydrogen bonded to carboxylate oxygen atom of $[CuL_2]^{2-}$ and lattice water molecules. The coordinated water molecules of $[Cu(en)_2(H_2O)_2]^{2+}$ also interact with the carboxylate oxygen atoms of $[CuL_2]^{2-}$ as a donor. Each complex cations are encapsulated by four complex anions as shown in Fig. 2.2.2c, and these encapsulated assemblies are held together by ethylenediammonium cations. The interesting feature is that these cations are held vertically. This of course is not the case in the nickel and zinc complexes **2.1** and **2.3**, which have such cations held horizontally between the layers of anions. Thus it is clear from this that the orientation of ethylenediammonium cations are largely influenced by metal ions attached to dipicolinate part and its vertical orientation assists in encapsulation of complex cations by copper(II) dipicolinate anions.

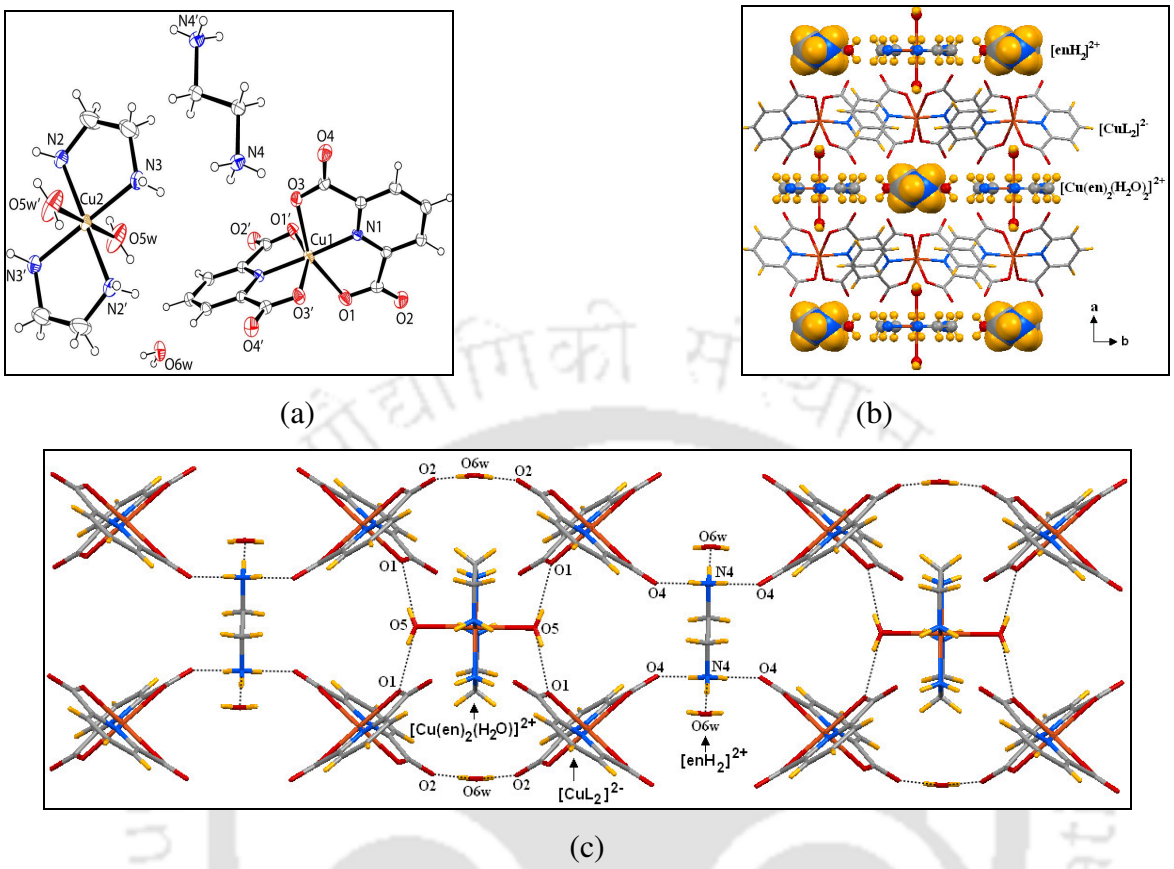

Fig. 2.2.2: (a) ORTEP of complex **2.2** (drawn with 50% thermal ellipsoids), (b) Layered packing diagram of **2.2**, (c) Hydrogen bond interactions among different components viewed along *a* axis.

The complexes derived from 1,3-propanediamine (pn) and Co(II), Cu(II) or Cd(II) dipicolinates have been studied by Aghabozorg and coworkers (Ch. 1, [110]). These complexes also exhibit layered structures through similar weak interactions. For the sake of comparison, we examined their structures and found that the interlayer separation for 1,3-propanediammonium dication in Cu(II) complex, $[pnH_2][CuL_2]\cdot nH_2O$ is ~ 10.4 Å. This interlayer separation is larger than we observed in ethylenediamine complexes. Further, we also compared with other complexes containing larger alkyl chain amines to establish the interlayer separation created by these organic cations in related metal dipicolinate complexes.

2.3: Inorganic-organic hybrid materials of Ni(II), Cu(II) or Zn(II) dipicolinate complex with dication of 1,5-diaminopentane

Cadaverine or 1,5-diaminopentane with the formula $NH_2(CH_2)_5NH_2$ is a toxic diamine. Formation and stability of this diamine complex with dicarboxylate anions such as acetate, malate, tartrate, malonate, citrate, 1,2,3-propanetricarboxylate, 1,2,3,4-butanetetra-carboxylate and glutamate are studied potentiometrically [33]. We have observed that the complexes derived from nickel, copper and zinc dipicolinate complexes with 1,5-diammoniumpentane ($penH_2$) are isostructural. They have the general composition [$penH_2$] [ML_2]·$5H_2O$ (**2.4-2.6**). As a representative example, the complex [$penH_2$] [CuL_2]·$5H_2O$ (**2.5**) is discussed in details**.** In the crystal lattice, the inorganic layer is built up of Cu(II) dipicolinate frameworks, whereas the organic layers are made up of protonated 1,5-pentanediamines. Since the Cu(II) complex is a dianion, to form neutral complex protonation of diamine takes place at both the terminal amine groups. In the complex, the conformation adopted by the dication of the 1,5-pentanediamine differs from its original form of the parent amine. In the complex, one of the terminal ammonium groups is inclined towards the complex anion to favor the ammonium–carboxylate ion pair formation. In the crystal structure, one of the carbon atoms of the dication is found to be disordered over two equivalent crystallographic positions.

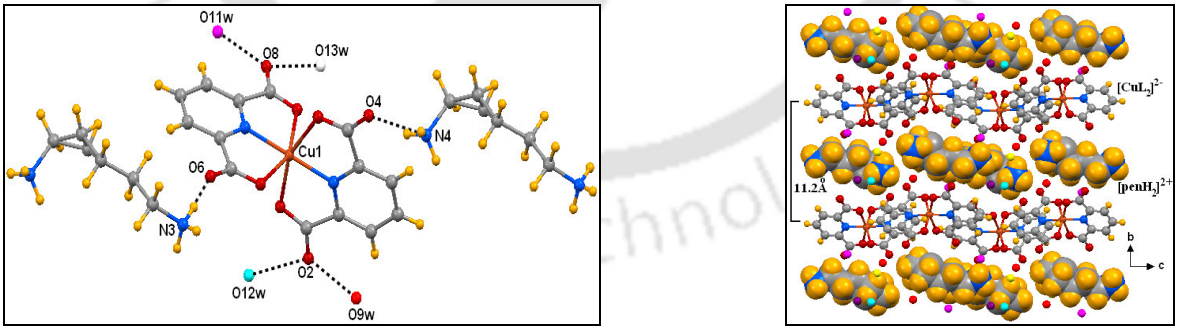

(a) (b)

Fig. 2.3.1: (a) Ammonium-carboxylate and carboxylate-lattice water interactions in **2.4**, (b) Layered packing diagram of **2.4** showing the inter-layer separation.

In the anionic layer, the adjacent pyridine ring of $[CuL_2]^{2-}$ shows very weak π-π stacking (centroid to centroid distance ~ 4.15 Å) interaction in comparison to the previous complexes obtained from ethylenediamine. The interlayer separation between the layers is ~ 11.19 Å (Fig. 2.3.1b) along *a* axis, is larger than observed in the ethylenediammonium complexes. Such separation for Ni(II) complex (**2.4**) and Zn(II) complex (**2.6**) are ~ 11.07 and ~ 11.11 Å respectively. These distances indicate that the organic cations play major role to govern the interlayer separation.

The ^{1}HNMR spectra of Zn(II) complex $[penH_2][ZnL_2]\cdot 3H_2O$ (**2.6**) is shown in Fig. 2.3.2. The signals from dipicolinate part appear at δ 8.40(d) and 8.48(t) for the two different sets of protons. The signals from dication of symmetrical 1,5-pentanediamine appears as a triplet at δ 2.9 ppm for the protons attached to the nitrogen atom and two multiplets at δ 1.6 and 1.3 ppm for the remaining two sets of protons. These chemical shift positions are found to be deshielded from the parent amine. The integration ratio shows formation of 1:1 adduct between the complex anion and the dication.

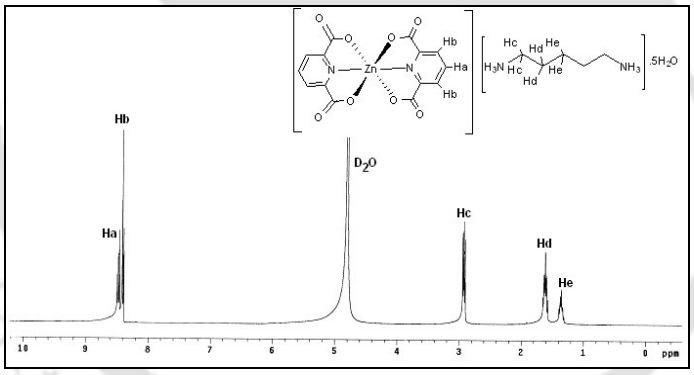

Fig. 2.3.2: ^{1}HNMR (400 MHz in D_2O) spectra of complex **2.6**

2.4: Inorganic-organic hybrid materials of Ni(II), Cu(II) or Zn(II) dipicolinate complex with dication of 1,8-diaminooctane

With the definite effect on the differences brought about by the cations of the earlier aliphatic diamines, we have studied on the interlayer spacing by increasing the chain length of the intervening flexible part by taking 1,8-diaminooctane as source for cation. In this case isostructural complexes of Ni(II), Cu(II) or Zn(II) are formed; the crystals of which belong to $P2_1/n$ space group. The structure comprises of a complex anion $[ML_2]^{2-}$, a dication of the

organic amine and two lattice water molecules. Flexible nature of the dication allows it to interact with the complex anions easily. In the lattice, each of the complex anions or dications are surrounded by five oppositely charged species *via* ammonium-carboxylate hydrogen bonds (Fig. 2.4.1a). The two lattice water molecules present in these complexes form hydrogen bonded bridge between the complex anion and the dication. The other weak interactions stabilizing the complex are face to face π-π stacking interactions (centroid to centroid distance ~ 3.55 Å in the case of $[CuL_2]^{2-}$) between the adjacent pyridine ring of $[ML_2]^{2-}$. Selected hydrogen bond parameters are listed in table 2.2.

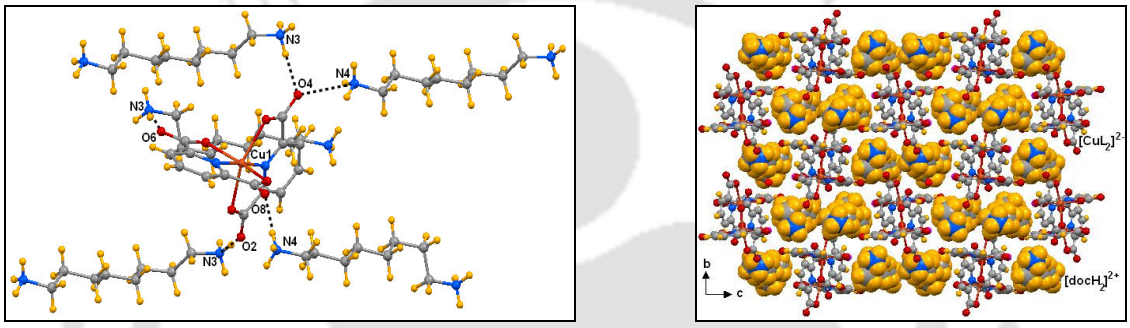

(a) (b)

Fig. 2.4.1: (a) Ammonium-carboxylate interactions in **2.8**, (b) Packing diagram of **2.8** ($docH_2$ in space filled mode, $[CuL_2]^{2-}$ in ball and stick mode).

Further, it is noticed that in this series of complexes, the cations and anions of the complexes do not form well-defined layers (Fig. 2.4.1b); an exception with the previous diamine complexes. The long chain protonated aliphatic dication fills the void created by the bulky anionic complex in the lattice. The oppositely charged species occupy the alternative space in the crystal lattice when viewed through crystallographic *a* axis (Fig. 2.4.1b). Nevertheless, we were able to synthesize inorganic-organic hybrid materials comprised of long chain diamines. In contrast, Beatty and coworkers showed that Ni(II) and Co(II) complexes with 2,4-pyridinedicarboxylic acid and octylamine resulted in the layered structures with significant interlayer separation [18]. The analogous organic systems containing 3,5-pyrazole- dicarboxylic acid and octylamine also generate lamellar structures with large interlayer separation among different amines used in this study [20].

Table 2.2: Selected hydrogen bond geometry in the representative complexes

Complex	Bond (symmetry)	$d_{D\text{-}H}$(Å)	$d_{H\cdots A}$(Å)	$d_{D\cdots A}$(Å)	< D-H···A(°)
2.1	N(3)--H(3B)···O(1) [x, y, z]	0.89	1.96	2.8433	171
	N(3)--H(3A)···O(2) [-x,y,1/2-z]	0.89	1.91	2.7691	162
	N(3)--H(3C)···O(4) [1/2-x,-1/2+y,1/2-z]	0.89	1.92	2.7665	157
	N(4)--H(4B)···O(5) [x, y, z]	0.89	2.09	2.9367	158
	N(4)--H(4A)···O(6) [1-x,y,1/2-z]	0.89	1.92	2.7650	159
	N(4)--H(4C)···O(8) [1/2-x,-1/2+y,1/2-z]	0.89	1.96	2.8161	161
	N(4)--H(4C)···O(9) [1/2+x,-1/2+y,z]	0.89	2.60	3.0426	112
	N(4)--H(4B)···O(10) [1/2-x,-1/2+y,1/2-z]	0.89	2.52	3.0227	117
2.2	N(4)--H(4A)···O(5) [x,y,1+z]	0.89	2.00	2.861(4)	162
	N(4)--H(4B)···O(2) [-x,-y,1-z]	0.89	1.91	2.794(2)	173
	N(4)--H(4C)···O(2) [-x,y,1-z]	0.89	1.93	2.794(2)	163
	O(5)--H(5O)···O(4) [1/2-x,1/2-y,-z]	0.87(4)	2.01(4)	2.851(3)	162(4)
	O(6)--H(6O)···O(3) [1/2-x,1/2-y,-z]	0.75(3)	2.17(3)	2.886(2)	160(4)
2.5	N(3)--H(3A)···O(8) [-x,1/2+y,1/2-z]	0.89	1.85	2.719(4)	164
	N(4)--H(4B)···O(2) [1-x,-1/2+y,1/2-z]	0.89	1.91	2.788(3)	167
2.8	N(3)--H(3A)···O(4) [1/2+x,1/2-y,-1/2+z]	0.89	1.93	2.819(3)	178
	N(3)--H(3B)···O(2) [1/2+x,-1/2-y,-1/2+z]	0.89	2.03	2.817(3)	147
	N(3)--H(3C)···O(6) [1-x,-y,1-z]	0.89	1.99	2.863(3)	167
	N(4)--H(4B)···O(4) [-1/2+x,1/2-y,-1/2+z]	0.89	2.42	2.972(4)	121
	N(4)--H(4C)···O(8) [x, y, z]	0.89	1.94	2.828(4)	174
2.10	N4--H4NB···O1 [x, y, z]	0.90(3)	2.10(3)	2.946(2)	155(2)
	N6--H6NC···O4 [x,y,-1+z]	0.91(3)	1.97(3)	2.846(3)	162(2)
	N3--H3NB···O2 [2-x,1-y,-z]	0.79(3)	2.25(3)	3.015(3)	162(2)
	N6--H6NB···N5 [1-x,-y,-z]	0.95(3)	2.08(3)	2.982(3)	158(2)

2.5: Inorganic-organic hybrid materials of Ni(II), Cu(II) or Zn(II) dipicolinate complex with mono cation of 4-aminobenzylamine

As the increase of flexible alkyl chain did not lead to expected results to enhance interlayer separation, we moved to aromatic diamine systems to understand the nature of layers. We have successfully crystallized the metal dipicolinate complexes with 4-aminobenzylamine.

Use of 4-aminobenzylamine (bam) led to the complexes having isostructural anionic core, cation of 4-aminobenzylamine but with different amount of water of hydration. These complexes have composition $[bamH]_2[ML_2]\cdot nH_2O$ (**2.10-2.12**) (where M = Ni(II) / Cu(II); n = 5 and for Zn(II), n = 3). Since the structure of the complexes are analogous only the crystal structure of $[bamH]_2[NiL_2]\cdot 5H_2O$ (**2.10**) is discussed. It consists of a complex anion, two symmetrically non-equivalent 4-aminobenzylamine cation and five lattice water molecules. The aryl diamine is protonated at the benzylic site. The complex anion interacts with the cation through carboxylate-ammonium and carboxylate-amine hydrogen bond interactions (Fig. 2.5.1a). The complex anion further exhibits hydrogen bond with the lattice water molecules to have a close packed structure. Out of five lattice water molecules available in the asymmetric unit, three molecules and their symmetry related partners form a planar hexameric cluster in the crystal lattice (Fig. 2.5.1c). The water cluster is stabilized by both the complex anion and the bam cation.

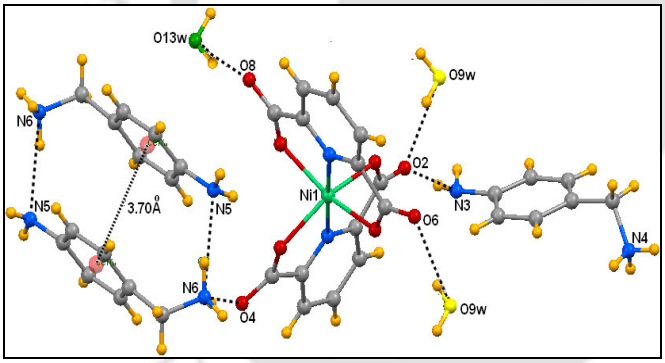

(a)

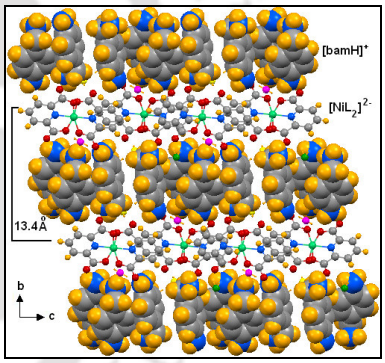

(b)

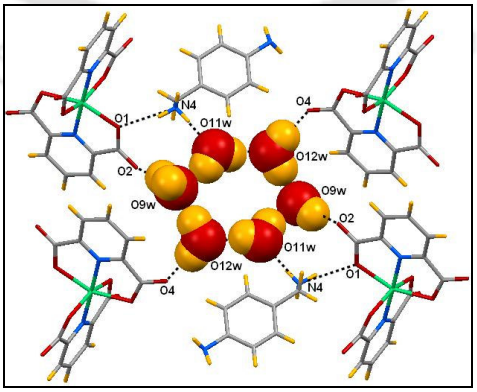

(c)

Fig. 2.5.1: (a) Weak interactions among different components of **2.10**, (b) Layered packing diagram of **2.10** showing the inter-layer separation, (c) Hexameric water cluster (space filled mode) in **2.10**.

The crystal packing pattern of the complexes can be regarded as a lamellar inorganic–organic hybrid network built up of anionic sheets by Ni(II) dipicolinate complex anion and cationic 4-aminobenzylamine among them (Fig. 2.5.1b). The anionic complexes $[NiL_2]^{2-}$ are joined by means of a weak π-π stacking (centroid to centroid distance ~ 4.01 Å) which spread out along crystallographic *a*-axis. The symmetrically non-equivalent bam cations are incorporated between the anionic layers and they lie in the alternative positions of the closely packed cationic layer. The two adjacent equivalent bam cations form pair and show π-π stacking and also hydrogen bond interactions between the $–NH_3^+$ and NH_2 group. The centroid to centroid π-π distance between two such cationic units is ~ 3.70 Å. As a consequence of these weak interactions, the bam cations lie in a perpendicular fashion resulting in a larger interlayer separation. The inter-metal distance between two adjacent $[NiL_2]^{2-}$ complex accommodating the cationic layer is measured as ~ 13.4 Å. This separation is much larger compared to the aliphatic diamines discussed so far.

The Ni(II) and Co(II) complexes with 2,4-pyridinedicarboxylic acid and benzylamine, $[benzylammonium]_2[Co(2,4\text{-}PDCA)_2(H_2O)_2]$ and $[benzylammonium]_2$ $[Ni(2,4\text{-}PDCA)_2(H_2O)_2]$ are reported as isostructural complexes [18]. These complexes also generate lamellar structures *via* ammonium-carboxylate $N\text{-}H^+\cdots O^-$ hydrogen bonds with significant interlayer separation. The benzyl substituents are interdigitated, but there is no evidence for π-π interactions (centroid to centroid distance ~ 5.1 Å). The hybrid complexes derived from Cu(II) malonates, $[Cu(mal)_2(H_2O)_2]^{2-}$ (where mal = malonate) with benzylamine and its substituents give a similar large array of interlayer interactions [19]. The interlayer separations are in the range of 11.4-11.9 Å. The aryl substituents are interdigitated and exhibit strong stacking interactions. These observations indicate that interactions between the charged species followed by arrangement of benzylammonium cations play major role to the greater interlayer separation.

All the complexes, except derived from 1,8-diaminooctane, generate two-dimensional layered structures in a reproducible fashion. Cu(II) dipicolinate ethylenediamine complex (**2.2**) is an exception, where the cationic layer is constituted by both organic and inorganic

cations sandwiched between the Cu(II) dipicolinate anionic layers. All the structures exhibit identical ammonium-carboxylate and other non-covalent interactions. As a consequence of these charge assisted hydrogen bonding, the anionic framework maintains a consistent π-π stacking arrangement that ranges from ~ 3.39 Å to 4.15 Å. The interlayer separation generated by the different amines is listed in table 2.3. Depending on the nature and size or geometry of the organic amines (small or large alkyl and aryl substituents), the cationic layer varies considerably. The distance between layers (as defined by the inter-metal distance between two adjacent complex anion) ranges from ~ 8.1 to 13.4 Å, a difference of ~ 40% from the smallest to largest interlayer separation. It is to be mentioned that the lamellar solids derived from Co(II) or Ni(II) dicarboxylic acids and mono cation of alkyl or aryl amines showed a maximum difference of ~ 33% of such separation [18].

Table 2.3: Interlayer separation generated by organic amines in the layered complexes

Complex	**Cations of**	**Interlayer separation (Å)**
$[enH_2][NiL_2]\cdot 3H_2O$	ethylenediamine	8.1
$[pnH_2][CuL_2]\cdot xH_2O$*	1,3-diaminopropane	10.4
$[penH_2][CuL_2]\cdot 5H_2O$	1,5-diaminopentane	11.2
$[bamH]_2[CuL_2]\cdot 5H_2O$	4-aminobenzylamine	13.4

(* Reported earlier)

Since the most of the complexes are isostructural with respect to the particular amine, the change in metal ion does not make any significant structural changes as well as the interlayer separation. The metal ion act as interchangeable component and the organic cation is responsible for change in dimension of the organic layer. It is also observed that the number of lattice water molecules present in the molecule depends on necessity of metal dipicolinate anion to complete a tight packed structure *via* hydrogen bond.

2.6: Cation exchange of the complexes

The complexes reported here undergo selective exchange of organic cations with alkali or alkaline earth metal ions without exchanging the ligand/s. A representative reaction scheme for preparation of such complexes through cation exchange is shown in scheme 2.6.1

Exchange of organic cation by Na^+, K^+ or Ca^{2+} ion resulted in polymeric complexes with the stoichiometry $\{[Na(H_2O)_2]_2[CuL_2]\cdot 2H_2O\}_n$, $\{[K_2(H_2O)_7][CuL_2]\}_n$ and $\{Ca(H_2O)_4][CuL_2]\cdot 2H_2O\}_n$ respectively. Formation of a dinuclear complex, $[Mg(H_2O)_5][CuL_2]\cdot 2H_2O$ was observed when bamH cations are replaced by Mg^{2+} ions in 2.11.

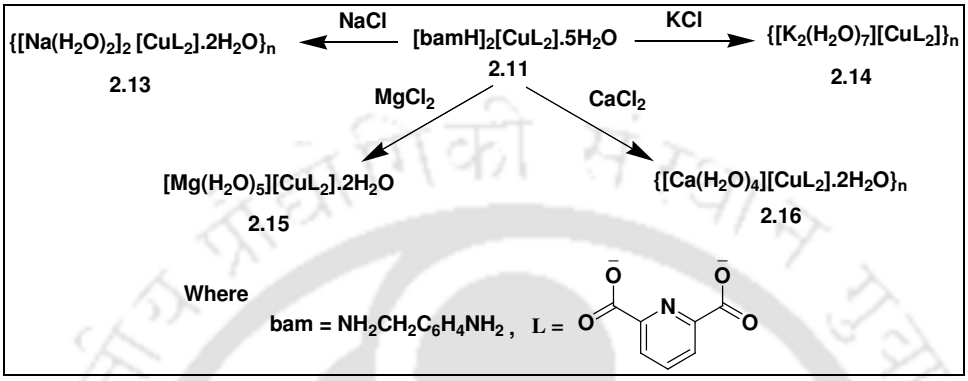

Scheme 2.6.1: Cation exchange reactions

The crystal structure of $\{[Na(H_2O)_2]_2[CuL_2]\cdot 2H_2O\}_n$ (**2.13**) is shown in Fig. **2.1.6**. A similar manganese(II) complex as the central metal ion was reported earlier; however, the synthetic procedure was different from the reported procedure in that case [34]. The structure of the polymeric complex **2.13** comprises of complex anions $[CuL_2]^{2-}$ which bridges Na^+ ions through their free oxygen of carbonyl groups. The Na^+ ions form hexa-coordinated di-aqua bridged polymeric chain like structures. Overall, each sodium ion is associated to four-bridging aqua-ligands and two carboxylate oxygen atoms of $[CuL_2]^{2-}$. The potassium ions also form similar polymeric complex $\{[K_2(H_2O)_7][CuL_2]\}_n$ (**2.14**), where the K^+ ions are linked together through singly bridged aqua ligands along with two terminal aqua ligands that makes a hepta-coordinated geometry. A comparison on the bite angles between the <M-O_{aq}-M of these two complexes **2.13** and **2.14** shows that the Na^+ containing complex has <Na-O_{aq}-Na, 84.9; 82.0º and <Na-O_{carb}-Na, 85.4º, whereas for the K^+ containing complex <K-O_{aq}-K, 91.3º and <K-O_{carb}-K, 93.6º. These differences arise from the difference in size of the cations. Such geometrical differences force the potassium complexes to have different environments around potassium in comparison to the sodium. In the lattices, the anionic complex, $[CuL_2]^{2-}$ and Na or K aquated complexes form layers. The anionic layer is stabilized by π-π staking interactions, measured as 3.58 Å, which is interestingly, identical

for both the Na or K aquated complexes. The bridging water molecules form extensive hydrogen bonded assemblies.

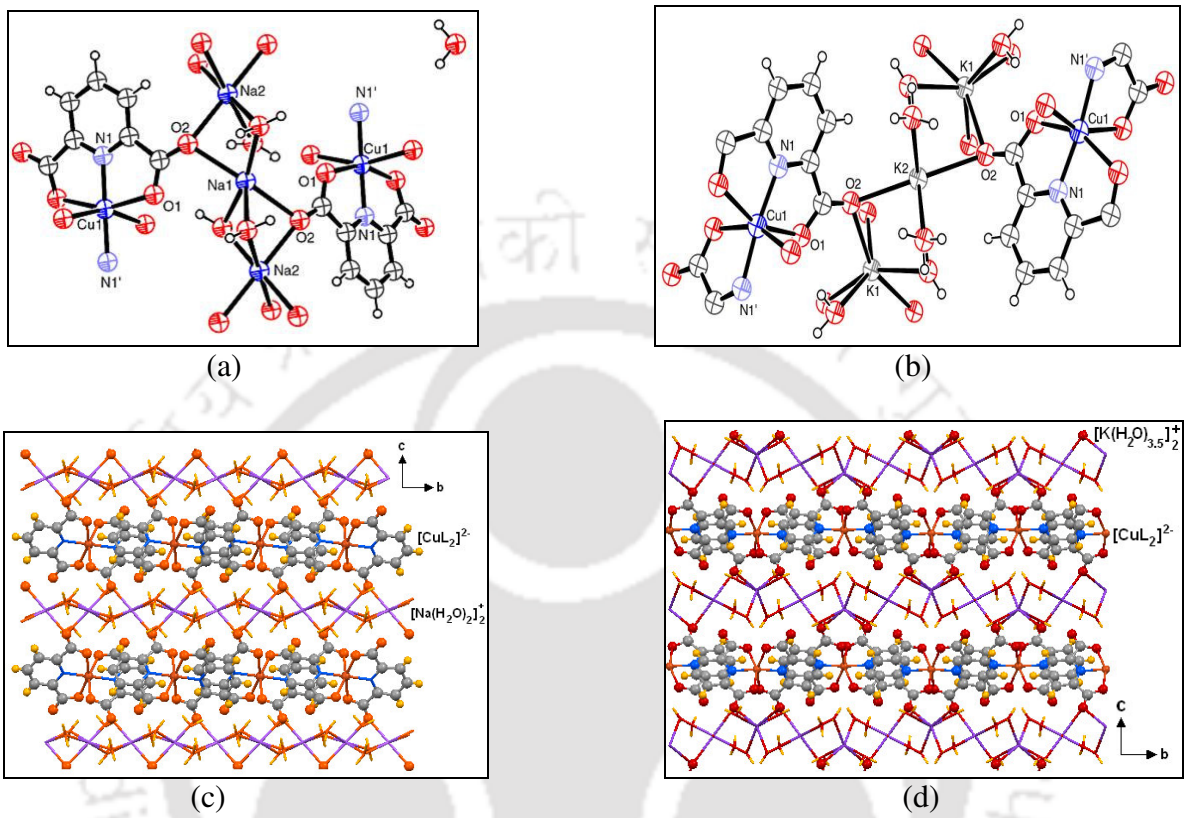

Fig. 2.6.1: ORTEP of complex (a) $\{[Na(H_2O)_2]_2[CuL_2]\cdot 2H_2O\}_n$ (**2.13**), (b) $\{[K_2(H_2O)_7][CuL_2]\}_n$ (**2.14**) (drawn with 50% thermal ellipsoids), (c-d) Packing diagram of **2.13** (view along *a* axis) and **2.14** (view along *a* axis) showing the layered structures.

The Mg^{2+} containing complex $[Mg(H_2O)_5][CuL_2]\cdot 2H_2O$ (**2.15**), has penta-aquated magnesium coordinated to the carboxylate O atoms of $[CuL_2]^{2-}$, and it results in a dinuclear complex rather than a polymeric structure (Fig. 2.6.2). The $[CuL_2]^{2-}$ part of the complex has similar structural features to its other analogues. The Ca^{2+} containing complex $\{[Ca(H_2O)_4][CuL_2]\cdot 2H_2O\}_n$ (**2.16**) has a polymeric structure in which the tetra-aqua calcium ion acts as nodes for bridge between two carbonyl oxygen of the copper(II) dipicolinate complex anion. The calcium has a distorted octahedral geometry with four aqua ligands at one plane whereas the two bridging oxygen ligands are at the axial positions trans to each other. The aqua ligands form hydrogen-bonded self-assemblies with the complex anion in

both the magnesium and calcium containing complexes. In packing, the complexes do not form well-defined layer irrespective of dinuclear or polymeric complexes. But they exhibit similar packing arrangement where a pair of cations or anions occupies the alternative position of the lattice (Fig. 2.6.2).

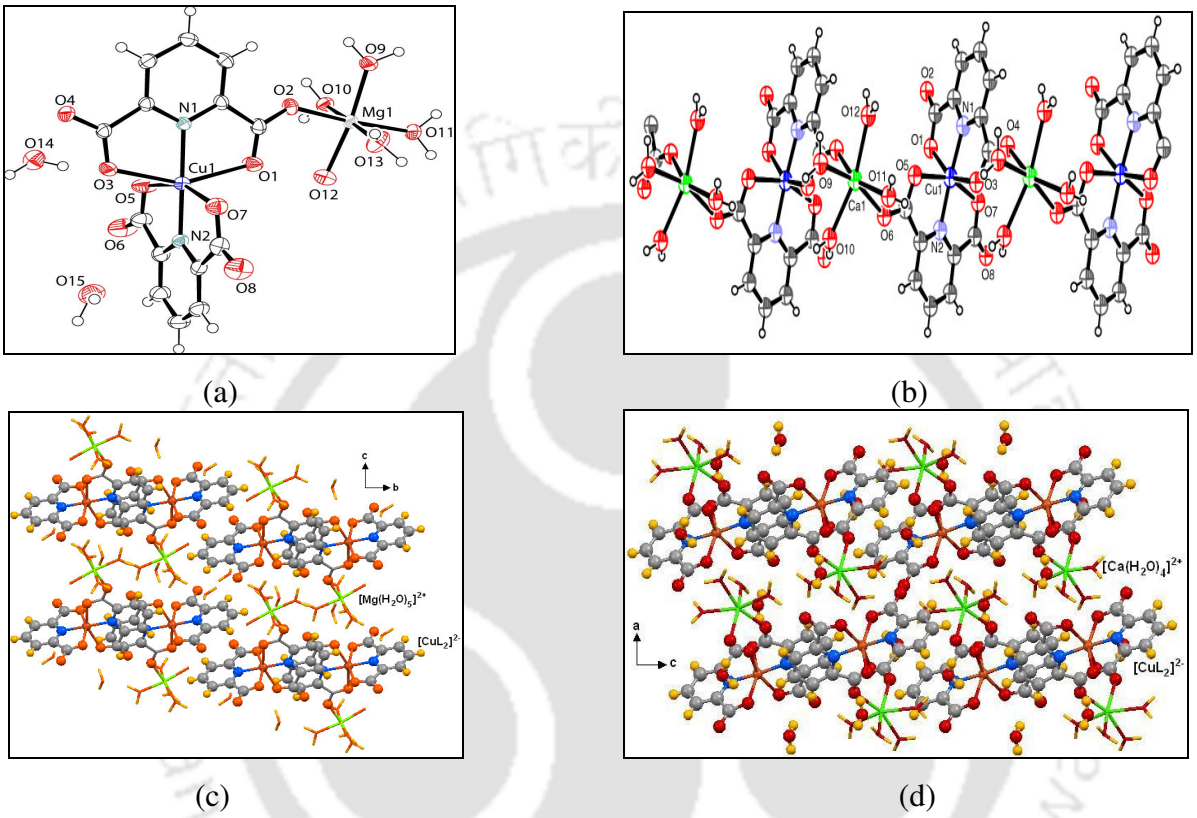

Fig. 2.6.2: ORTEP of complex (a) $[Mg(H_2O)_5][CuL_2]\cdot 2H_2O$ (**2.15**), (b) $\{[Ca(H_2O)_4][CuL_2]\cdot 2H_2O\}_n$ (**2.16**) (drawn with 50% thermal ellipsoids), (c-d) Packing diagram of **2.15** and **2.16.**

2.7: Conclusion

The results presented in this chapter demonstrate the role of the organic and inorganic cations guiding to form assembled structures and also their role in controlling the interlayer separation wherever the layered structures are formed. In the series of metal dipicolinate complexes of nickel, copper and zinc having cations of ethylenediamine, 1,5-pentanediamine and 4-aminobenzylamine respectively, the ammonium-carboxylate hydrogen bonds led to architecturally consistent lamellar solids. The inorganic-organic hybrid materials derived from 1,8-diaminooctane are not in the form of well-defined layers.

Depending on the nature of the amine substituents, the distance between the layers varies considerably. The weak interactions that guide the packing pattern in these complexes also affect the interlayer separation. There is a ~ 40% increase of inter-layer separation from ethylenediamine to 4-aminobenzylamine in the case of copper. In addition to organic substituents, the metals also act as interchangeable component in these complexes. The ethylenediamine competes to coordinate with copper ions and this leads to generate complex cation as well as free cations. The complex cations are encapsulated by the anions and such assemblies are held each other through hydrogen bond interactions and thereby making a difference in the interlayer spacing. Thus, this work can be used to make strategies for adjusting inter-metal distances in layered solids. Further, the complexes undergo selective exchange of organic cations with alkali or alkaline earth metal ions without exchanging the ligand/s. Exchange of organic cation resulted in dinuclear or polymeric complexes where carbonyl oxygen atoms of complex anion hold the aquated metal cations.

2.8: Experimental section

Detailed synthetic methodologies and analytical as well as spectroscopic data are summarized in this section. The equipment details are given in Appendix.

2.8.1: Complex $[enH_2][NiL_2]\cdot 3H_2O$ (2.1), $[enH_2][Cu(en)_2.(H_2O)_2][CuL_2]\cdot H_2O$ (2.2), and $[enH_2][ZnL_2]\cdot 2H_2O$ (2.3)

To a methanolic solution (20 mL) of dipicolinic acid (0.334 g, 2.0 mmol), nickel(II) acetate tetrahydrate (0.249 g, 1.0 mmol), copper(II) acetate monohydrate (0.199 g, 1.0 mmol) and zinc(II) acetate dihydrate (0.219 g, 1.0 mmol) was added respectively and stirred for half an hour that resulted in the formation of green, blue and white precipitates respectively. To each of these precipitates, ethylenediamine (140.0 µL, 2.0 mmol) was added dropwise at room temperature that led to dissolution of the precipitates and resulted in the formation of clear solution of the respective complex. The solutions were left for crystallization in a beaker after adding few drops of deionised water. Green, blue and colourless block shaped crystals respectively were formed in 2-3 days.

Complex **2.1**: Isolated yield: 77%. Elemental anal calcd for $C_{16}H_{22}N_4NiO_{11,}$ C, 38.02; N, 11.09; H, 4.35%; found C, 37.88; N, 10.95; H, 4.22%. IR (KBr, cm^{-1}): 3474 (b), 3038 (b), 1636 (b, s), 1592 (w), 1423 (m), 1371 (s), 1279 (m), 1182 (w), 1078 (w). Molar conductance: 246.5 S cm^2 mol^{-1} in water. Vis. (H_2O) λ_{max}: 622.0 nm; ε = 6.20 M^{-1} cm^{-1}, μ_{eff}. at 298 K: 2.92 BM. Thermal analysis: ~ 65-105 ºC (loss of three water molecules of crystallization).

Complex **2.2:** Isolated yield: 48%. Elemental anal calcd for $C_{34}H_{46}N_{10}Cu_3O_{20,}$ C, 36.91; N, 12.67; H, 4.16%; found C, 36.80; N, 12.55; H, 4.08%. IR (KBr, cm^{-1}): 3423 (b, s), 3323 (m), 2959 (w), 1636 (s), 1591 (s), 1573 (w), 1422 (m), 1373 (s), 1278 (m), 1081 (w), 1033 (m). Molar conductance: 325.7 S cm^2 mol^{-1} in water. Vis. (H_2O) λ_{max}: 763.0 nm; ε = 115.60 M^{-1} cm^{-1}. μ_{eff}. at 298 K: 1.65 BM. Thermal analysis: ~ 70-90 ºC (loss of water molecule of crystallization); further decomposition occurs at ~ 140-160 ºC (loss of two coordinated water molecules).

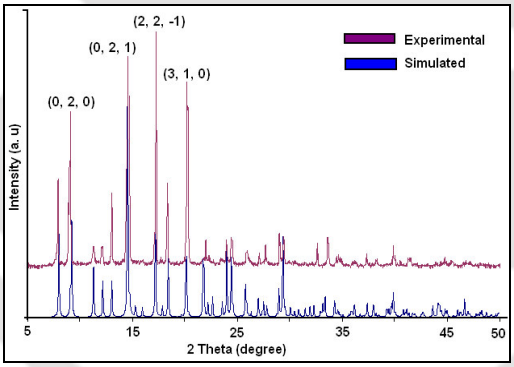

Fig. 2.8.1: PXRD pattern of complex **2.2**

Complex **2.3:** Isolated yield: 65%. Elemental anal calcd for $C_{16}H_{20}N_4O_{10}Zn_{,}$ C, 38.89; N, 11.34; H, 4.05%; found C, 38.78; N, 11.25; H, 3.95%. IR (KBr, cm^{-1}): 3430 (b, s), 3331 (m), 2964 (w), 1638 (s), 1593 (s), 1420 (m), 1372 (s), 1276 (m), 1080 (w), 1032 (m). Molar conductance: 245.0 S cm^2 mol^{-1} in water. ^{1}HNMR (D_2O, 400 MHz, ppm): 8.4 (6H, m), 3.3 (4H, t, J = 8.0 Hz). Thermal analysis: ~ 75-95 ºC (loss of two water molecules of crystallization).

2.8.2: Complex $[penH_2][NiL_2]\cdot 5H_2O$ (2.4), $[penH_2][CuL_2]\cdot 5H_2O$ (2.5) and $[penH_2][ZnL_2]\cdot 5H_2O$ (2.6)

To a solution of dipicolinic acid (0.334 g, 2.0 mmol) in methanol (20 ml), nickel (II) acetate tetrahydrate (0.249 g, 1.0 mmol), copper (II) acetate monohydrate (0.199 g, 1.0 mmol) and zinc (II) acetate dihydrate (0.219 g, 1.0 mmol) was added respectively and stirred for 30 minutes. Depending on the metal ion a green, blue or white precipitate respectively was obtained. To these precipitates, 1,5-diaminopentane (1.0 mmol) was added drop-wise in each case. A homogeneous green, light blue or colorless solution was obtained respectively on stirring at room temperature. The solution was evaporated in a rotary flash evaporator. The residue was washed with acetonitrile (10 ml) to remove unreacted amine. Recrystallization of each of the residue from deionised water yielded crystals of the corresponding complexes after 2-3 days.

Complex **2.4:** Isolated yield: 78%. Elemental anal calcd for $C_{19}H_{32}N_4NiO_{13,}$ C, 39.09; N, 9.60; H, 5.49%; found C, 39.02; N, 9.55; H, 5.42%. IR (KBr, cm^{-1}): 3399 (b), 3087 (w), 1615 (s), 1582 (w), 1594 (s), 1574 (w), 1426 (m), 1374 (s), 1280 (m), 1186 (m), 1079 (m). Molar conductance: 239.0 S cm^2 mol^{-1} in water. Vis. (H_2O) λ_{max}: 617.0 nm; $\varepsilon = 5.50$ M^{-1} cm^{-1}. $\mu_{eff.}$ at 298 K: 2.83 BM. Thermal analysis: ~ 55-140 ºC (loss of five water molecules of crystallization).

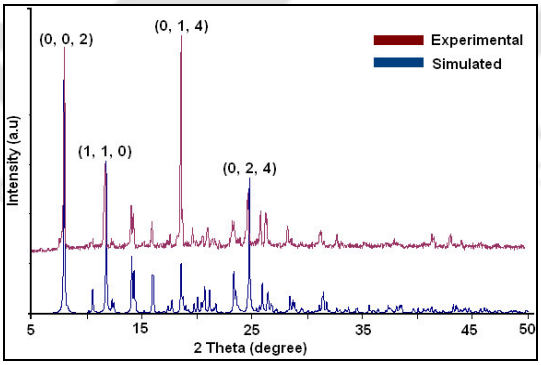

Fig. 2.8.2: PXRD pattern of complex **2.4**

Complex **2.5:** Isolated yield: 73%. Elemental anal calcd for $C_{19}H_{32}N_4CuO_{13,}$ C, 38.78; N, 9.52; H, 5.44%; found C, 38.65; N, 9.38; H, 5.28%. IR (KBr, cm^{-1}): 3419 (b), 3087 (w), 1634 (s), 1621 (s), 1590 (s), 1422 (m), 1373 (s), 1275 (m), 1186 (m), 1085 (m). Molar

conductance: 237.3 S cm^2 mol^{-1} in water. Vis. (H_2O) λ_{max}: 774.0 nm; ε = 69.50 M^{-1} cm^{-1}. μ_{eff}. at 298 K: 1.65 BM. Thermal analysis: ~ 65-145 ºC (loss of five water molecules of crystallization).

Complex **2.6:** Isolated yield: 77%. Elemental anal calcd for $C_{19}H_{32}N_4ZnO_{13,}$ C, 38.64; N, 9.49; H, 5.42%; found C, 38.58; N, 9.39; H, 5.36%. IR (KBr, cm^{-1}): 3418 (b), 3088 (w), 1634 (s), 1621 (s), 1591 (w), 1426 (m), 1378 (s), 1365 (w), 1279 (m), 1186 (w), 1080 (w), 1036 (w). ^{1}HNMR (D_2O, 400 MHz, ppm): 8.4 (6H, m), 2.9 (4H, t, J = 8.0 Hz), 1.6 (4H, m), 1.4 (2H, m). Molar conductance: 240.9 S cm^2 mol^{-1} in water. Thermal analysis: ~ 65-140 ºC (loss of five water molecule of crystallization).

2.8.3. Complex $[docH_2][NiL_2]\cdot 2H_2O$ (2.7), $[docH_2][CuL_2]\cdot 2H_2O$ (2.8) and $[docH_2][ZnL_2]\cdot 2H_2O$ (2.9)

These complexes were prepared in a similar way by reaction of dipicolinic acid (2.0 mmol) with respective metal salts (1.0 mmol) followed by treatment with 1,8-diaminooctane (0.144 g, 1.0 mmol). The different colored precipitates obtained were dried and finally crystallized from deionised water. Suitable X-ray diffraction crystals were formed in 2-3 days.

Complex **2.7**: Isolated yield: 72%. Elemental anal calcd for $C_{22}H_{32}N_4NiO_{10,}$ C, 46.21; N, 9.80; H, 5.60%; found C, 46.08; N, 9.68; H, 5.58%. IR (KBr, cm^{-1}): 3389 (b), 3072 (b), 2932 (s), 2855 (w), 1614 (b), 1593 (b), 1531 (m), 1425 (m), 1378 (m), 1365 (s), 1282 (m), 1186 (w), 1083 (w). Molar conductance: 248.4 S cm^2 mol^{-1} in water. Vis. (H_2O) λ_{max}: 611.0 nm; ε = 6.00 M^{-1} cm^{-1}. μ_{eff}. at 298 K: 2.85 BM. Thermal analysis: ~ 65-110 ºC (loss of two water molecules of crystallization).

Complex **2.8**: Isolated yield: 72%. Elemental anal calcd for $C_{22}H_{32}N_4CuO_{10,}$ C, 45.83; N, 9.72; H, 5.56%; found C, 45.72; N, 9.64; H, 5.46%. IR (KBr, cm^{-1}): 3377 (b), 3082 (w), 2927 (b), 2855 (w), 2145 (w), 1617 (b), 1423 (s), 1363 (s), 1275 (m), 1219 (m), 1188 (w), 1083 (s), 1038 (w). Molar conductance: 255.3 S cm^2 mol^{-1} in water. Vis. (H_2O) λ_{max}: 776.0 nm; ε = 67.30 M^{-1} cm^{-1}. μ_{eff}. at 298 K: 1.60 BM. Thermal analysis: ~ 70-105 ºC (loss of two water molecules of crystallization).

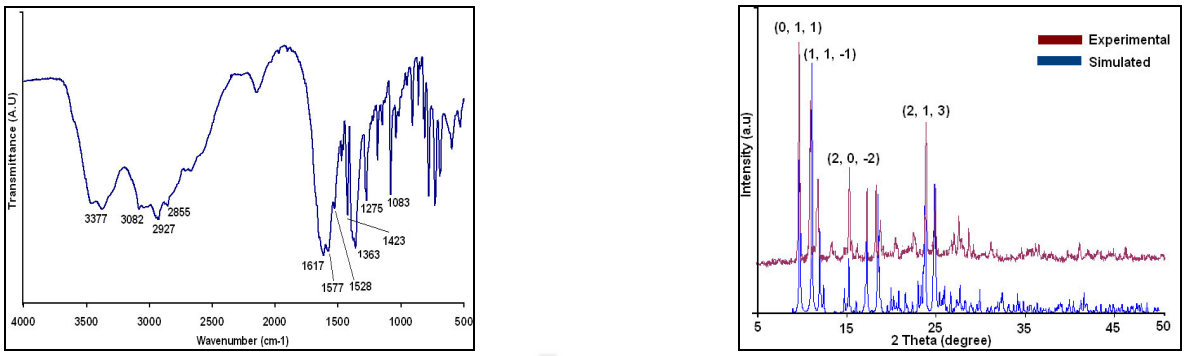

Fig. 2.8.3: FTIR spectra (left) and PXRD pattern (right) of complex **2.8**

Complex **2.9**: Isolated yield: 79%. Elemental anal calcd for $C_{22}H_{32}N_4O_{10}Zn$, C, 45.68; N, 9.69; H, 5.54%; found C, 45.62; N, 9.65; H, 5.55%. IR (KBr, cm^{-1}): 3388 (b), 3300 (w), 3220 (w), 3037 (b), 2956 (w), 2655 (w), 2611 (w), 1633 (s), 1621 (b), 1574 (w), 1519 (m), 1428 (s), 1374 (s), 1281 (s), 1186 (m), 1079 (m). ^{1}HNMR (D_2O, 400 MHz, ppm): 8.4 (6H, m), 2.9 (4H, t, J = 7.2 Hz), 1.5 (4H, m), 1.2 (8H, m). Molar conductance: 232.8 S cm^2 mol^{-1} in water. Thermal analysis: ~ 60-100 ºC (loss of two water molecules of crystallization).

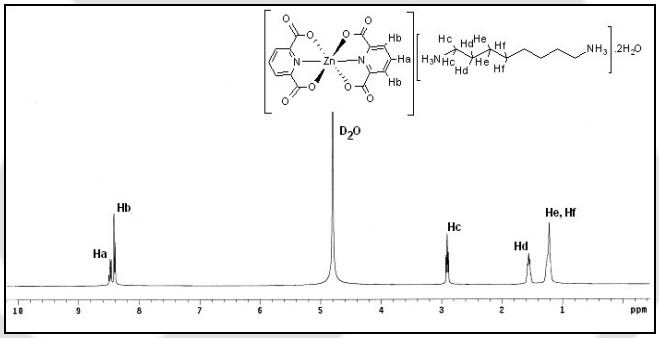

Fig. 2.8.4: ^{1}HNMR (D_2O) spectra of complex **2.9**

2.8.4: Complex $[bamH]_2[NiL_2]\cdot 5H_2O$ (2.10), $[bamH]_2[CuL_2]\cdot 5H_2O$ (2.11) and $[bamH]_2[ZnL_2]\cdot 3H_2O$ (2.12)

These complexes were synthesized through a similar method as discussed earlier; only difference being the use of 4-aminobenzylamine (226.0 µL, 2.0 mmol) as organic amine.

Complex **2.10:** Isolated yield: 76%. Elemental anal calcd for $C_{28}H_{38}N_6NiO_{13}$, C, 46.32; N, 11.58; H, 5.24%; found C, 46.17; N, 11.45; H, 5.13%. IR (KBr, cm^{-1}): 3381 (b), 3302 (w), 3038 (m), 1633 (s), 1621 (s), 1590 (m), 1590 (w), 1519 (s), 1424 (m), 1374 (s), 1279 (m), 1185 (m), 1081 (w). Molar conductance: 229.8 S cm^2 mol^{-1} in water. Vis. (H_2O) λ_{max}: 609.0

nm; ε = 10.50 M^{-1} cm^{-1}. μ_{eff} at 298 K: 2.91 BM. Thermal analysis: ~ 70-105 ºC (loss of five water molecules of crystallization).

Complex **2.11**: Isolated yield: 75%. Elemental anal calcd for $C_{28}H_{38}N_6CuO_{13,}$ C, 46.01; N, 11.50; H, 5.20%; found C, 45.93; N, 11.36; H, 5.12%. IR (KBr, cm^{-1}): 3410 (b), 3380 (b), 3041 (w), 2956 (w), 2597 (w), 1633 (s), 1620 (s), 1590 (s), 1518 (m), 1421 (m), 1374 (s), 1359 (m), 1273 (m), 1186 (w), 1085 (w). Molar conductance: 233.7 S cm^2 mol^{-1} in water. Vis. (H_2O) λ_{max}: 773.0 nm; ε = 67.30 $M^{-1}cm^{-1}$. $\mu_{eff.}$ at 298 K: 1.56 BM. Thermal analysis: ~70-105 ºC (loss of five water molecules of crystallization).

Complex **2.12**: Isolated yield: 79%. Elemental anal calcd for $C_{28}H_{34}N_6ZnO_{11,}$ C, 48.28; N, 12.07; H, 4.89%; found C, 48.25; N, 11.93; H, 4.80%. IR (KBr, cm^{-1}): 3388 (b), 3300 (w), 3220 (w), 3037 (b), 2956 (w), 2655 (w), 2611 (w), 1633 (s), 1621 (b), 1574 (w), 1519 (m), 1428 (s), 1374 (s), 1281 (s), 1186 (m), 1079 (m). ^{1}HNMR (D_2O, 400 MHz, ppm): 8.3 (6H, m), 7.2 (4H, d, J = 8.0 Hz), 6.8 (4H, d, J = 8.0 Hz), 4.0 (4H, s). Molar conductance: 232.8 S cm^2 mol^{-1} in water. Thermal analysis: ~ 70-105 ºC (evaporation of three lattice water molecules).

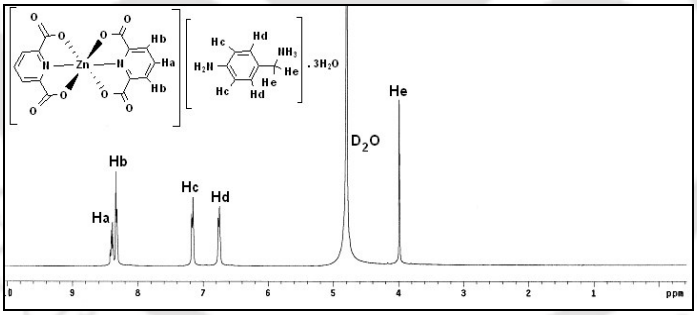

Fig. 2.8.5: ^{1}HNMR (D_2O) spectra of complex **2.12**

2.8.5. Complex $\{[Na(H_2O)_2]_2[CuL_2]\cdot 2H_2O\}_n$ (2.13), $\{[K_2(H_2O)_7][CuL_2]\}_n$ (2.14), $[Mg(H_2O)_5]$ $[CuL_2]\cdot 2H_2O$ (2.15) and $\{[Ca(H_2O)_4][CuL_2]\cdot 2H_2O\}_n$ (2.16)

These complexes were synthesized by mixing either of the complex $[penH_2][CuL_2]\cdot 5H_2O$ (**2.5**), (0.588 g, 1.0 mmol), $[docH_2][CuL_2]\cdot 2H_2O$ (**2.8**) (0.573 g, 1.0 mmol) or $[bamH]_2[CuL_2]\cdot 5H_2O$ (**2.11**), (0.730 g, 1.0 mmol) with sodium chloride (0.117 g, 2.0 mmol), potassium chloride (0.149 g, 2.0 mmol), magnesium chloride hexahydrate (0.203 g, 1.0 mmol) or fused calcium chloride (0.111 g, 1.0 mmol) respectively in 10 ml water with

continuous stirring for 2 hour at room temperature. The complexes **2.13** and **2.14** were obtained upon slow evaporation of reaction mixtures at ambient temperature. However, the light blue precipitates of complexes **2.15** and **2.16** were recrystallised from water / pyridine (10:1) mixture.

Complex **2.13**: Isolated yield: 80%. Elemental anal calcd for $C_{14}H_{18}N_2CuNa_2O_{14,}$ C, 30.67; N, 5.11; H, 3.29%; found C, 30.56; N, 5.03; H, 3.24%. IR (KBr, cm^{-1}): 3412 (b), 3108 (w), 2931 (w), 2135 (w), 1644 (w), 1622 (s, b), 1592 (m), 1421 (s), 1374 (s), 1363 (m), 1279 (m), 1185 (w), 1081 (m). Molar conductance: 275.5 S cm^2 mol^{-1} in water. Vis. (H_2O) λ_{max}: 773.0 nm; ε = 67.50 M^{-1} cm^{-1}. μ_{eff}. at 298 K: 1.63 BM. Thermal analysis: ~ 65-130 ºC (evaporation of coordinated water molecules).

Complex **2.14**: Isolated yield: 78%. Elemental anal calcd for $C_{14}H_{20}CuK_2N_2O_{15,}$ C, 28.09; N, 4.68; H, 3.34%; found C, 27.97; N, 4.57; H, 3.27%. IR (KBr, cm^{-1}): 3401 (s), 3072 (m), 2932 (s), 2855 (w), 2134 (w), 1621 (s), 1586 (s), 1424 (m), 1363 (s), 1278 (m), 1186 (w), 1082 (m). Molar conductance: 426.2 S cm^2 mol^{-1} in water. Vis. (H_2O) λ_{max}: 774.0 nm; ε = 35.00 M^{-1} cm^{-1}. μ_{eff}. at 298 K: 1.58 BM. Thermal analysis: ~ 65-135 ºC (evaporation of coordinated water molecules).

Complex **2.15**: Isolated yield: 70%. Elemental anal calcd for $C_{14}H_{20}CuN_2MgO_{15,}$ C, 30.87; N, 5.15; H, 3.68%; found C, 30.81; N, 5.09; H, 3.60%. IR (KBr, cm^{-1}): 3502 (m), 3204 (s), 1686 (w), 1621 (s), 1587 (m), 1433 (s), 1386 (s), 1282 (s), 1185 (m), 1084 (m). Molar conductance: 255.8 S cm^2 mol^{-1} in water. Vis. (H_2O) λ_{max}: 777.0 nm; ε = 60.10 $M^{-1}cm^{-1}$. μ_{eff}. at 298 K: 1.57 BM. Thermal analysis: ~ 65-165 ºC (evaporation of crystallized and coordinated water molecules).

Complex **2.16**: Isolated yield: 72%. Elemental anal calcd for $C_{14}H_{18}CaCuN_2O_{14,}$ C, 31.00; N, 5.17; H, 3.32%; found C, 30.96; N, 5.11; H, 3.26%. IR (KBr, cm^{-1}): 3396 (s), 3092 (w), 1615 (s), 1584 (s), 1427 (m), 1392 (s), 1367 (m), 1284 (m), 1086 (w). Molar conductance: 263.5 S cm^2 mol^{-1} in water. Vis. (H_2O) λ_{max}: 772.0 nm; ε = 67.10 M^{-1} cm^{-1}. μ_{eff}. at 298 K: 1.68 BM. Thermal analysis: ~ 60-145 ºC (evaporation of crystallized and coordinated water molecules).

2.9: Crystallographic data and refinement parameters for the complexes 2.1-2.16

Compound No.	**2.1**	**2.2**	**2.3**	**2.4**
Formula	$C_{16}H_{22}N_4NiO_{11}$	$C_{34}H_{46}Cu_3N_{10}O_{20}$	$C_{16}H_{20}N_4O_{10}Zn$	$C_{19}H_{32}N_4NiO_{13}$
Formula wt.	505.04	1105.43	493.70	583.20
Crystal system	Monoclinic	Monoclinic	Monoclinic	Monoclinic
Space group	*C2/c*	*C2/m*	*P2/c*	$P2_1/c$
a (Å)	16.7653(15)	14.1801(19)	8.3194(2)	12.4366(2)
b (Å)	16.3274(15)	19.234(2)	8.2588(2)	9.4435(2)
c (Å)	15.3524(18)	8.1810(11)	15.4667(5)	22.1352(5)
α (deg)	90.00	90.00	90.00	90.00
β (deg)	110.554(5)	107.272(11)	110.122(2)	91.5750(10)
γ (deg)	90.00	90.00	90.00	90.00
V (Å^3)	3934.9(7)	2130.7(5)	997.83(5)	2598.69(9)
Z	8	2	2	4
D_{calc} (gcm^{-3})	1.685	1.723	1.630	1.491
μ (mm^{-1})	1.057	1.578	1.294	0.817
F(000)	2048	1134	500	1224
Total no. of reflns	25928	9276	6907	31246
Independent reflns.	4682	2708	2349	6520
$\theta_{max.}$	2.56 - 28.04	2.61 - 28.42	2.44 - 28.19	1.64 - 28.42
Ranges (h, k, l)	$-22 \le h \le 22$ $-21 \le k \le 21$ $-20 \le l \le 20$	$-18 \le h \le 18$ $-25 \le k \le 23$ $-10 \le l \le 10$	$-11 \le h \le 11$ $-10 \le k \le 7$ $-20 \le l \le 20$	$-16 \le h \le 16$ $-10 \le k \le 12$ $-29 \le l \le 29$
Completeness to 2θ (%)	98.1	98.5	95.5	99.7
Data / restraints / parameters	4682 / 0 / 294	2708 / 0 / 180	2349 / 0/ 143	6520 / 0 / 346
GOF (F^2)	1.019	1.060	1.020	1.095
R_1, wR_2 [$I > 2\sigma(I)$]	0.0390, 0.1186	0.0362, 0.1010	0.0554, 0.1756	0.0500, 0.1506
R_1, wR_2 (all data)	0.0460, 0.1240	0.0417, 0.1036	0.0650, 0.1836	0.0656, 0.1584
Largest diff peak/hole (e Å^{-3})	0.540 / -0.731	0.754 / -0.533	0.706 / -0.686	0.980 / -0.749

Continued……..

Compound No.	**2.5**	**2.6**	**2.7**	**2.8**
Formula	$C_{19}H_{32}CuN_4O_{13}$	$C_{19}H_{32}N_4O_{13}Zn$	$C_{22}H_{32}N_4NiO_{10}$	$C_{22}H_{32}CuN_4O_{10}$
Formula wt.	588.03	589.86	571.23	576.06
Crystal system	Monoclinic	Monoclinic	Monoclinic	Monoclinic
Space group	$P2_1/c$	$P2_1/c$	$P2_1/n$	$P2_1/n$
a (Å)	12.4252(3)	12.5043(4)	14.5289(7)	14.4738(11)
b (Å)	9.4178(2)	9.4148(3)	11.1186(6)	11.0442(8)
c (Å)	22.3633(6)	22.2135(7)	16.1188(9)	16.1347(12)
α (deg)	90.00	90.00	90.00	90.00
β (deg)	92.0430(10)	91.754(2)	100.754(3)	99.147(4)
γ (deg)	90.00	90.00	90.00	90.00
V (Å^3)	2615.25(11)	2613.87(14)	2558.1(2)	2546.4(3)
Z	4	4	4	4
D_{calc} (gcm^{-3})	1.493	1.499	1.483	1.503
μ (mm^{-1})	0.905	1.010	0.820	0.920
F(000)	1228	1232	1200	1204
Total no. of reflections	40258	40060	30470	30231
Independent reflections	6475	6483	6299	6316
$\theta_{max.}$	1.64 - 28.30	1.63 - 28.39	1.73 - 28.41	1.76 - 28.42
Ranges (h, k, l)	-16 ≤ h ≤ 15 -12 ≤ k ≤ 12 -29 ≤ l ≤ 29	-16 ≤ h ≤ 16 -12 ≤ k ≤ 12 -29 ≤ k ≤ 29	-17 ≤ h ≤ 19 -14 ≤ k ≤ 14 -20 ≤ l ≤ 21	-19 ≤ h ≤ 19 -14 ≤ k ≤ 14 -21 ≤ l ≤ 21
Completeness to 2θ (%)	99.5	99.0	97.9	98.4
Data / restraints / parameters	6475 / 0 / 341	6483 / 0 / 346	6299 / 0 / 337	6316 / 0 / 337
GOF (F^2)	1.023	1.020	1.011	1.023
R_1, wR_2 [$I > 2\sigma(I)$]	0.0530, 0.1711	0.0483, 0.1542	0.0335, 0.1042	0.0513, 0.1608
R_1, wR_2 (all data)	0.0627, 0.1802	0.0601, 0.1620	0.0456, 0.1097	0.0683, 0.1701
Largest diff peak / hole (e Å^{-3})	1.105 / -0.873	1.054 / -0.878	0.511 / -0.293	0.781 / -0.656

Continued……..

Compound No.	**2.9**	**2.10**	**2.11**	**2.12**
Formula	$C_{22}H_{32}N_4O_{10}Zn$	$C_{28}H_{38}N_6NiO_{13}$	$C_{28}H_{38}CuN_6O_{13}$	$C_{28}H_{34}N_6O_{11}Zn$
Formula wt.	577.89	725.35	730.18	695.98
Crystal system	Monoclinic	Triclinic	Triclinic	Triclinic
Space group	*P2₁/n*	*P-1*	*P-1*	*P-1*
a (Å)	14.5130(4)	8.8199(2)	8.7564(2)	11.3924(2)
b (Å)	11.0085(3)	13.4278(3)	13.4398(3)	12.2040(2)
c (Å)	16.1696(5)	14.6945(3)	14.8013(3)	12.7638(2)
α (deg)	90.00	71.4380(10)	71.5160(10)	65.5000(10)
β (deg)	98.9380(10)	73.9150(10)	74.2570(10)	72.9250(10)
γ (deg)	90.00	81.4020(10)	81.5040(10)	76.9260(10)
V (Å^3)	2551.99(13	1581.59(6)	1586.41(6)	1532.46(4)
Z	4	2	2	2
D_{calc} (gcm^{-3})	1.504	1.523	1.529	1.508
μ (mm^{-1})	1.025	0.690	0.765	0.872
F(000)	1208	760	762	724
Total no. of reflections	31348	14822	10866	19118
Independent reflections	6392	5017	4998	4954
$\theta_{max.}$	1.76 - 28.39	1.51 - 24.50	2.28 - 24.50	1.80 - 24.50
Ranges (h, k, l)	$-16 \le h \le 19$ $-14 \le k \le 14$ $-21 \le k \le 21$	$-10 \le h \le 10$ $-15 \le k \le 15$ $-17 \le l \le 16$	$-10 \le h \le 8$ $-15 \le k \le 15$ $-17 \le l \le 17$	$-13 \le h \le 12$ $-14 \le k \le 14$ $-14 \le k \le 14$
Completeness to 2θ (%)	99.6	95.3	94.6	97.3
Data / restraints / parameters	6392 / 0 / 336	5017 / 8 / 529	4998 / 0 / 452	4954 / 0 / 426
GOF (F^2)	1.061	1.130	1.008	1.107
R_1, wR_2 [$I > 2\sigma(I)$]	0.0453, 0.1351	0.0359, 0.0957	0.0386, 0.1077	0.0606, 0.1928
R_1, wR_2 (all data)	0.0602, 0.1419	0.0393, 0.0977	0.0426, 0.1105	0.0656, 0.1984
Largest diff peak / hole (e Å^{-3})	0.668 / -0.721	0.303 / -0.809	0.431 / -0.414	0.980 / -0.683

Continued……..

Compound No.	**2.13**	**2.14**	**2.15**	**2.16**
Formula	$C_{14}H_{18}CuN_2Na_2O_{14}$	$C_{14}H_{20}CuK_2N_2O_{15}$	$C_{14}H_{20}CuMgN_2O_{15}$	$C_{14}H_{18}CaCuN_2O_{14}$
Formula wt.	547.82	598.06	544.17	541.92
Crystal system	Monoclinic	Orthorhombic	Triclinic	Triclinic
Space group	*P2/c*	*Pnna*	*P-1*	*P-1*
a (Å)	9.7737(5)	20.8272(5)	8.4012(16)	8.6483(3)
b (Å)	7.9812(4)	13.4041(3)	9.7039(19)	8.8062(3)
c (Å)	12.9258(6)	8.1916(2)	13.965(3)	13.9356(4)
α (deg)	90.00	90.00	101.426(9)	80.8320(10)
β (deg)	90.0211(4)	90.00	102.165(9)	73.2140(10)
γ (deg)	90.00	90.00	97.580(8)	89.5940(10)
V (Å^3)	1008.29(9)	2286.85(9)	1072.8(4)	1002.26(6)
Z	2	4	2	2
D_{calc} (gcm^{-3})	1.804	1.737	1.685	1.796
μ (mm^{-1})	1.206	1.396	1.127	1.424
F(000)	558	1220	558	554
Total no. of reflections	8744	15353	10254	14299
Independent reflections	1751	2843	3453	4851
$\theta_{max.}$	1.58 - 25.00	1.96 - 28.36	1.53 - 24.50	2.34 - 28.09
Ranges (h, k, l)	$-11 \le h \le 11$ $-9 \le k \le 9$ $-13 \le l \le 15$	$-27 \le h \le 24$ $-17 \le k \le 17$ $-10 \le l \le 10$	$-7 \le h \le 9$ $-11 \le k \le 11$ $-16 \le l \le 16$	$-11 \le h \le 11$ $-11 \le k \le 11$ $-18 \le l \le 18$
Completeness to 2θ (%)	98.3	99.5	96.9	99.0
Data / restraints / parameters	1751 / 6 / 177	2843 / 6 / 178	3453 / 11 / 347	4851 / 12 / 338
GOF (F^2)	1.050	1.028	1.055	1.072
R_1, wR_2 [$I > 2\sigma(I)$]	0.0337, 0.0836	0.0345, 0.0950	0.0396, 0.1257	0.0271, 0.0759
R_1, wR_2 (all data)	0.0341, 0.0838	0.0413, 0.0986	0.0414, 0.1272	0.0291, 0.0770
Largest diff peak / hole (e Å^{-3})	0.407 / -0.871	0.438 / -0.490	0.573 / -0.496	0.434 / -0.545

2.10: Selected bond lengths (Å) and bond angles (°) of some selected metal dipicolinate complexes

Table 2.4: The bond lengths (Å) and bond angles (°) in $[ML_2]^{2-}$ core of complex **2.4 - 2.6**

	2.5		**2.4**		**2.6**
Cu1–N1	1.940(2)	Ni1–N1	1.9712(19)	Zn1–N1	2.022(2)
Cu1–N2	1.950(2)	Ni1–N2	1.9736(19)	Zn1–N2	2.0189(19)
Cu1–O1	2.1419(19)	Ni1–O1	2.1275(18)	Zn1–O1	2.1969(17)
Cu1–O3	2.1844(19)	Ni1–O3	2.1349(18)	Zn1–O3	2.1612(18)
Cu1–O5	2.225(2)	Ni1–O5	2.1057(18)	Zn1–O5	2.2029(18)
Cu1–O7	2.2157(19)	Ni1–O7	2.1403(18)	Zn1–O7	2.1825(18)
N1–Cu1–N2	176.06(8)	N1–Ni1–N2	176.22(8)	N1–Zn1–N2	175.36(7)
N1–Cu1–O1	78.80(8)	N1–Ni1–O1	78.01(7)	N1–Zn1–O1	75.76(7)
N2–Cu1–O1	98.82(8)	N2–Ni1–O1	99.15(7)	N2–Zn1–O1	106.63(7)
N1–Cu1–O3	77.57(8)	N1–Ni1–O3	77.75(8)	N1–Zn1–O3	76.53(7)
N2–Cu1–O3	104.93(8)	N2–Ni1–O3	105.17(8)	N2–Zn1–O3	101.21(7)
O1–Cu1–O3	156.21(7)	O1–Ni1–O3	155.64(7)	O3–Zn1–O1	152.16(7)
N1–Cu1–O7	99.27(8)	N1–Ni1–O7	105.10(7)	N1–Zn1–O7	107.67(7)
N2–Cu1–O7	77.63(7)	N2–Ni1–O7	77.43(7)	N2–Zn1–O7	76.45(7)
O1–Cu1–O7	92.74(8)	O1–Ni1–O7	93.29(8)	O1–Zn1–O7	90.69(8)
O3–Cu1–O7	93.69(9)	O3–Ni1–O7	90.68(8)	O3–Zn1–O7	95.08(8)
N1–Cu1–O5	105.77(8)	N1–Ni1–O5	99.19(7)	N1–Zn1–O5	100.07(7)
N2–Cu1–O5	77.45(8)	N2–Ni1–O5	78.34(7)	N2–Zn1–O5	75.91(7)
O1–Cu1–O5	94.36(9)	O1–Ni1–O5	92.19(7)	O1–Zn1–O5	94.15(8)
O3–Cu1–O5	89.45(8)	O3–Ni1–O5	94.01(8)	O3–Zn1–O5	93.32(7)
O7–Cu1–O5	154.85(7)	O7–Ni1–O5	155.71(7)	O7–Zn1–O5	152.18(7)

Table 2.5: The bond lengths (Å) and bond angles (°) in $[ML_2]^{2-}$ core of complex **2.7 - 2.9**

	2.8		**2.7**		**2.9**
Cu1–O1	2.271(2)	Ni1–O1	2.1268(14)	Zn1–O1	2.1778(18)
Cu1–O3	2.257(2)	Ni1–O3	2.1262(13)	Zn1–O3	2.1794(17)
Cu1–O5	2.125(2)	Ni1–O5	2.1335(13)	Zn1–O5	2.262(2)
Cu1–O7	2.143(2)	Ni1–O7	2.1354(14)	Zn1–O7	2.1634(17)
Cu1–N1	1.954(2)	Ni1–N1	1.9675(15)	Zn1–N1	2.0241(18)
Cu1–N2	1.933(2)	Ni1–N2	1.9659(14)	Zn1–N2	2.0154(16)
N2–Cu1–N1	175.72(8)	N2–Ni1–N1	176.21(5)	N2–Zn1–N1	172.25(7)
N2–Cu1–O5	78.75(8)	N2–Ni1–O5	77.63(5)	N2–Zn1–O5	75.10(6)
N1–Cu1–O5	99.87(8)	N1–Ni1–O5	106.15(5)	N1–Zn1–O5	110.68(7)
N2–Cu1–O7	78.52(8)	N2–Ni1–O7	78.05(5)	N2–Zn1–O7	76.97(7)
N1–Cu1–O7	103.03(8)	N1–Ni1–O7	98.16(5)	N1–Zn1–O7	97.34(7)
O1–Cu1–O3	153.65(7)	O1–Ni1–O3	155.76(6)	O1–Zn1–O3	152.26(7)
N2–Cu1–O3	107.19(8)	N2–Ni1–O3	101.89(5)	N2–Zn1–O3	105.27(6)
N1–Cu1–O3	76.89(8)	N1–Ni1–O3	78.11(6)	N1–Zn1 O3	76.38(7)
O5–Cu1–O3	94.20(8)	O3–Ni1–O5	90.06(5)	O3–Zn1–O5	92.52(6)
O7–Cu1–O3	89.37(8)	O7–Ni1–O3	92.64(5)	O7–Zn1–O3	91.22(7)

N2–Cu1–O1	98.92(8)	N2–Ni1–O1	102.33(5)	N2–Zn1–O1	102.46(7)
N1–Cu1–O1	77.09(7)	N1–Ni1–O1	77.76(6)	N1–Zn1–O1	76.11(7)
O1–Cu1–O5	94.31(7)	O1–Ni1–O5	94.47(5)	O1–Zn1–O5	94.42(7)
O7–Cu1–O1	92.41(7)	O7–Ni1–O1	92.95(5)	O7–Zn1–O1	95.15(7)
O5–Cu1–O7	157.03(8)	O5–Ni1–O7	155.57(5)	O5–Zn1–O7	151.82(6)

Table 2.6: The bond lengths (Å) and bond angles (°) in $[ML_2]^{2-}$ core of complex **2.10 - 2.12**

	2.11		**2.10**		**2.12**
Cu1–N1	1.9592(19)	Ni1–N1	1.9677(16)	Zn1–N1	2.013(3)
Cu1–N2	1.918(2)	Ni1–N2	1.9618(16)	Zn1–N2	2.019(3)
Cu1–O1	2.3090(19)	Ni1–O1	2.1448(13)	Zn1–O1	2.224(3)
Cu1–O3	2.279(2)	Ni1–O3	2.1612(13)	Zn1–O3	2.166(3)
Cu1–O5	2.117(2)	Ni1–O5	2.1268(13)	Zn1–O5	2.122(3)
Cu1–O7	2.1175(19)	Ni1–O7	2.1331(13)	Zn1–O7	2.277(3)
N1–Cu1–N2	179.20(8)	N1–Ni1–N2	178.66(6)	N1–Zn1–N2	163.87(12)
N2–Cu1–O7	79.07(8)	N2–Ni1–O7	77.84(6)	N2–Zn1–O7	73.80(11)
N1–Cu1–O7	101.30(7)	N1–Ni1–O7	102.81(6)	N1–Zn1–O7	90.99(11)
N2–Cu1–O5	79.07(8)	N2–Ni1–O5	78.17(6)	N2–Zn1–O5	78.08(12)
N1–Cu1–O5	100.58(8)	N1–Ni1–O5	101.20(6)	N1–Zn1–O5	117.20(12)
O7–Cu1–O5	158.03(7)	O5–Ni1–O7	155.97(6)	O5–Zn1–O7	151.80(11)
N2–Cu1–O3	102.29(7)	N2–Ni1–O3	103.49(6)	N2–Zn1–O3	107.97(12)
N1–Cu1–O3	76.97(7)	N1–Ni1–O3	77.73(6)	N1–Zn1–O3	76.67(12)
O7–Cu1–O3	98.47(7)	O7–Ni1–O3	88.49(5)	O3–Zn1–O7	89.84(12)
O5–Cu1–O3	88.32(8)	O5–Ni1–O3	95.70(5)	O5–Zn1–O3	96.92(15)
N2–Cu1–O1	104.13(8)	N2–Ni1–O1	101.05(6)	N2–Zn1–O1	100.90(12)
N1–Cu1–O1	76.61(7)	N1–Ni1–O1	77.74(6)	N1–Zn1–O1	75.31(12)
O7–Cu1–O1	87.70(7)	O7–Ni1–O1	96.80(5)	O7–Zn1–O1	97.47(13)
O5–Cu1–O1	95.50(8)	O5–Ni1–O1	89.16(5)	O5–Zn1–O1	89.74(16)
O3–Cu1–O1	153.56(6)	O3–Ni1–O1	155.46(5)	O3–Zn1–O1	151.12(12)

References:

[1] C. Sanchez (ed.), J. Mat. Chem. 15 (2005) 3541.

[2] P. Gomez-Romero / C. Sanchez (eds.), Functional hybrid materials, Wiley-VCH, 2003.

[3] G. Kickelbick (ed.), Hybrid materials, Wiley-VCH, 2006.

[4] MRS Symposium Proceedings-Organic / Inorganic hybrid materials, volumes 435, 519, 576, 628, 726, 847.

[5] L. Thylen, M. Qiu, S. Anand, ChemPhysChem 5 (2004) 1268.

[6] S.R. Batten, K.S. Murray, Coord. Chem. Rev. 246 (2003) 103.

[7] D.M. Shin, I.S. Lee, Y.K. Chung, Eur. J. Inorg. Chem. (2003) 2311.

[8] R.W. Grimshaw, The Chemistry and Physics of Clays, 4th ed.; Wiley: New York, 1971.

[9] L.R. Nassimbeni, Acc. Chem. Res. 36 (2003) 631.

[10] J.A. Swift, M.D. Ward, Chem. Mater. 12 (2000) 1501.

[11] A.M. Pivovar, K.T. Holman, M.D. Ward, Chem. Mater. 13 (2001) 3018.

[12] K.T. Holman, A.M. Pivovar, M.D. Ward, Science 294 (2001) 1907.

[13] S.M. Martin, J. Yonezawa, M.J. Horner; C.W. Macosko, M.D. Ward, Chem. Mater. 16 (2004) 3045.

[14] R.E. Melendez, M.J. Zaworotko, Supramol. Chem. 8 (1997) 157.

[15] K. Biradha, D. Dennis, V.A. MacKinnon, C.V.K. Sharma, M.J. Zaworotko, J. Am. Chem. Soc. 120 (1998) 11894.

[16] R.S. Armstrong, I.M. Atkinson, E. Carter, M.S. Mahinay, B.W. Skelton, P. Turner, G. Wei, A.H. White, L.F. Lindoy, Proc. Natl. Acad. Sci. U.S.A. 99 (2002) 4987.

[17] T. Kurc, J. Janczak, J. Hoffmann, V. Videnova-Adrabinska, Cryst. Growth Des. 12 (2012) 2613.

[18] A.M. Beatty, B.A. Helfrich, G.A. Hogan, B.A. Reed, Cryst. Growth Des. 6 (2006) 122.

[19] T.D. Keene, I. Zimmermann, A. Neels, O. Sereda, J. Hauser, S.-X. Liu, S. Decurtins, Cryst. Growth Des. 10 (2010) 1854.

[20] A.M. Beatty, K.E. Granger, A.E. Simpson, Chem.-Eur. J. 8 (2002) 3254.

[21] A.M. Beatty, C.M. Schneider, A.E. Simpson, J. L. Zaher, CrystEngComm. 4 (2002) 282.

[22] T. Yuge, M. Miyata, N. Tohnai, Cryst. Growth Des. 6 (2006) 1271.

[23] H.M. State, Inorganic Syntheses VI (1960) 198.

[24] S.A. Patil, V.H. Kulkarni, Inorg. Chim. Acta 73 (1983) 125.

[25] R. Griesser, H. Sigel, Inorg. Chem. 10 (1971) 2229.

[26] P. Ayyappan, M. Asnani, A. Ramanan, Y. Piffard, Proc. Indian Acad. Sci. (Chem. Sci.), 115 (2003) 33.

[27] M. Nayak, R. Koner, H.-H. Lin, U. Florke, H.-H. Wei, S. Mohanta, Inorg. Chem. 45 (2006) 10764.

[28] M. Nayak, A. Jana, M. Fleck, S. Hazraa, S. Mohanta, CrystEngComm. 12 (2010) 1416.

[29] C.-C. Chou, C.-C. Su, H.-L. Tsai, K.-H. Lii, Inorg. Chem. 44 (2005) 628.

[30] S. Hazra, R. Koner, M. Nayak, H.A. Sparkes, J.A.K. Howard, S. Mohanta, Cryst. Growth Des. 9 (2009) 3603.

[31] C.B. Aakeroy, J. Desper, M.M. Smith, Chem. Commun. (2007) 3936

[32] M. Nayak, S. Hazra, P. Lemoine, R. Koner, C. R. Lucas, S. Mohanta, Polyhedron, 27 (2008) 1201.

[33] C. De Stefano, A. Gianguzza, R. Maniaci, D. Piazzese, S. Sammartano, Talanta, 46 (1998) 1079.

[34] C. Ma, C. Chen, F. Chen, X. Xhang, H. Zhu, Q. Liu, D. Liao, L. Li, Bull. Chem. Soc. Jpn (2003) 301.

Chapter 3

Intercalation of protonated amino acids in layers of cobalt(II) or copper(II) dipicolinates

Intercalation of amino acids by artificial host molecules is of special interest [1-4]. Layered double hydroxides (LDH) have been investigated as a host material for intercalation of amino acids [5-8]. For example, the intercalation of amino acids and some peptides into Mg-Al layered double hydroxide (also known as hydrotalcite) was examined by reconstruction method [9]. Intercalation of basic amino acids into layers of zirconium proline-N-methylphosphonate (α-ZPMP) is known [10]. Artificial receptors such as the phophonate containing compounds intercalate basic amino acids such as lysine, arginine and histidine [11-12]. Ferrocene carboxylic acids are used for recognition of α-amino acids [13]. Similarly, zinc complexes of guanidine derivatives act as color sensor for aspartic acid [14]. Color change from colorless to red occurs when a mixture of spiropyran and histidine in water is kept in dark [15].

We have mentioned in the chapter 2 that the metal dipicolinate complexes intercalate varieties of ammonium cations leading to layered inorganic-organic hybrid materials. We have extended our study to amino acids, which are equivalent to diamino compounds bearing extra carboxylate functionality. Intercalation of amino acids is expected to be difficult due their ability to exist in zwitterionic form. Since the metal containing dipicolinate complexes are acidic in nature, advantage has been taken to synthesize supramolecular complexes with basic amino acids such as L-histidine and L-ornithine. The X-ray diffraction study shows that the amino acids are in the dicationic form and lie in the anionic layers of these metal dipicolinate complexes. This chapter therefore deals with the intercalation of dications of two optically active amino acids namely L-histidine and L-ornithine into layers of cobalt(II) or copper(II) dipicolinates. The interlayer separations generated by these protonated amino acids are presented. Further, the changes in optical activity and related properties of the amino acids upon interaction with metal dipicolinates are also discussed.

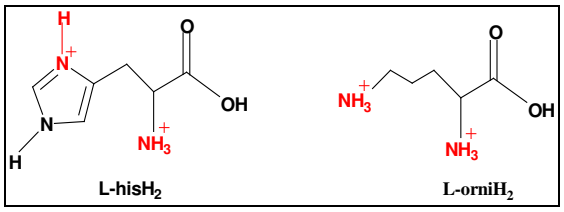

Fig. 3.1: Dications of amino acids used

The complexes are synthesized from the reaction of Co(II) or Cu(II) dipicolinate with L-histidine or L-ornithine as basic amino acid (scheme 3.1). L-histidine is a α–amino acid with an imidazole functional group. It is an essential amino acid in humans and other mammals due to various functions in metallo-proteins and catalytic sites in certain enzymes [16]. The other amino acid studied is L-ornithine that plays role in the urea cycle. The side chains of basic amino acids contain nitrogen and resembles with ammonia. Their pKa's are high enough to abstract proton from the metal dipicolinate complex, $H_2[ML_2]$ to form supramolecular host-guest complexes. In the complex the zwitterionic form of the parent amino acid changes to dicationic form by protonation at the nitrogen atoms of imidazole ring or the amine group of the amino acids. The carboxylate group of amino acid changes to carboxylic acid group. It may be noted that copper(II) amino acid complexes are easily formed from the reaction of amino acids with copper(II) acetate under ambient condition [17-18]. Such neutral complexes however, on dissolution in water followed by treatment with dipicolinic acid do not exchange ligands.

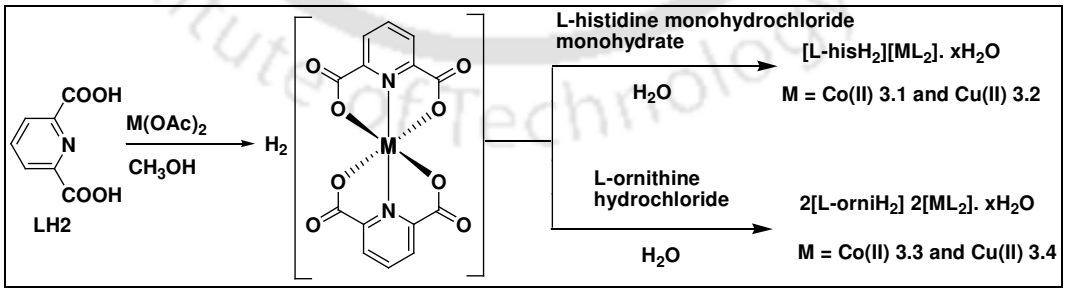

Scheme 3.1: Synthesis of Co(II) or Cu(II) dipicolinate amino acid complexes

3.1: Synthesis, characterization and intercalation of dication of L-histidine in layers of Co(II) or Cu(II) dipicolinate complexes

The complexes $[L\text{-}hisH_2][CoL_2]\cdot 3H_2O$ (**3.1**) and $[L\text{-}hisH_2][CuL_2]\cdot 5H_2O$ (**3.2**) are synthesized from the reaction of Co(II) or Cu(II) dipicolinate treating with L-histidine independently. Each of them constitutes of a complex anion, a protonated L-histidine and lattice hydrates in the crystal structure. It has been reported that Co(II) forms tetrahedral bis complexes with L-histidine in highly alkaline aqueous solution [19]. Formations of such complexes are dependent on the deprotonation of the imidazole ring of the amino acid. Cu(II)-histidine complexes with proposed structures and stability of the complexes have been investigated [20-25]. The most possible structures of $Cu(his)_2$ complex predicted in these investigations are shown in Fig. 3.1.1. In the tetrahedral complex, the amino acid may coordinate with the Cu(II) either through α-NH_2 and carboxyate group or *via* imidazole nitrogen and α-NH_2 group. In the Cu(II) dipicolinate complex, two dipicolinate ligands is meridionally coordinated to Cu(II) ion *via* tridentate chelating mode. Thus, it is unlikely for L-histidine, being in zwitterionic form, to replace the dipicolinate ligand to form Cu(II)-histidine complex.

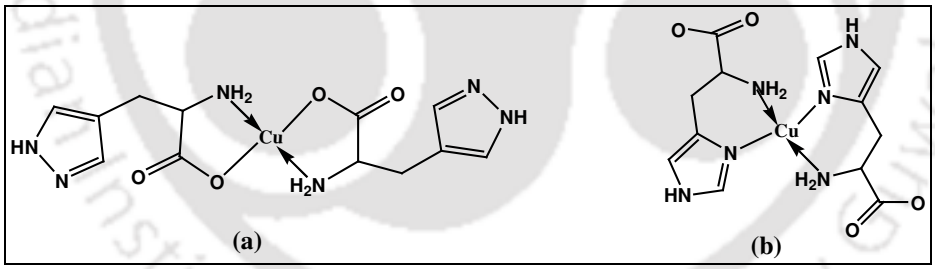

Fig. 3.1.1: Schematic representations of Cu(II)-histidine complex

FTIR spectra of the complexes provide information about the binding sites of the ligands [26]. Each of the complexes shows stretching frequencies for carboxylic acid group, coordinated carboxylates and NH_3^+ groups. The dications of amino acids show the C=O stretching frequency for the acid groups in the range of 1735-1731 cm^{-1}. For NH_3^+ groups, a broad and strong stretching band appears in the region 3108-2617 cm^{-1} followed by a fairly

strong symmetrical bending band in the range of 1496-1481 cm^{-1}. The asymmetric deformation band of $-NH_3^+$ overlap with the C=O stretching band and the deformation band of water molecules. Further, the complex exhibits IR stretching frequencies in the range of 1634-1590 cm^{-1} and 1380-1365 cm^{-1} due to the asymmetric and symmetric carboxylate stretching respectively. As a representative case the FTIR spectra of complex **3.2** is shown in Fig. 3.1.2. The complexes show low molar conductance values, 162.0 and 177.0 S cm^2 mol^{-1} respectively corresponding to 2:2 electrolytes in water. This is attributed to the presence of relatively large sized ions in the complex.

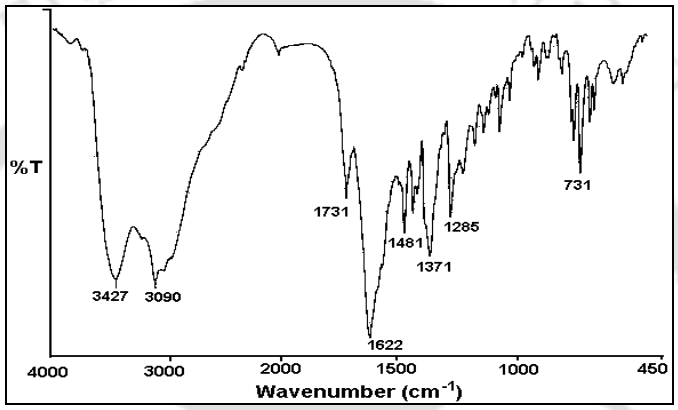

Fig. 3.1.2: FTIR spectra of complex **3.2**

The complex $[L\text{-}hisH_2][CoL_2]\cdot 3H_2O$ (**3.1**) is composed of a distorted octahedral $[CoL_2]^{2-}$ complex anion, a dication of L-histidine and three lattice water molecules (Fig. 3.1.3a). The complex anion $[CoL_2]^{2-}$ holds dication of L-histidine in 1:1 ratio similar to diamine complexes. The complex anion interacts with each dication through ammonium-carboxylate ion pairing and carboxylic acid-carboxylate interactions. Fig. 3.1.3c shows that the dication forms three ion pairing with the carboxylate of $[CoL_2]^{2-}$ and one carboxylic acid-carboxylate interaction between the two oppositely charged species. Some of the interactions are N(3)-H(3A)···O(4) [($d_{D}\ldots_{H}$, 1.99 Å, $d_{D\cdots A}$, 2.76 Å; < D-H····A, 145º], N(5)-H(5A)···O(6) [($d_{D}\ldots_{H}$, 2.02 Å, $d_{D\cdots A}$, 2.79 Å; < D-H····A, 148º], N(3)-H(3B)···O(7) [($d_{D}\ldots_{H}$, 1.94 Å, $d_{D\cdots A}$, 2.78 Å; < D-H····A, 164º], O(10)-H(10A)···O(2) [($d_{D}\ldots_{H}$, 1.73 Å, $d_{D\cdots A}$, 2.58 Å; < D-H····A, 166º]. The hydrogen bond parameters are listed in table 3.1.

The non-covalent interactions play major role in the formation of host guest supramolecular complexes. In the L-histidinium dinitrate, the cations and anions are linked to each other *via*

–N^+-H and NO_3^- interactions [27]. Binding of dicationic L-histidine ester with a macrocyclic host having tetra phophonate anionic unit *via* cation - phosphonate interactions have been reported by Schrader and coworkers [28]. In that case, the dication interacts with four strategically placed phophonate anions of macrocyclic host *via* ammonium as well as imidazolium proton. In contrast, the additional carboxylic acid-carboxylate interaction along with ammonium-carboxylate interactions available in our complexes may contribute further stability to these complexes.

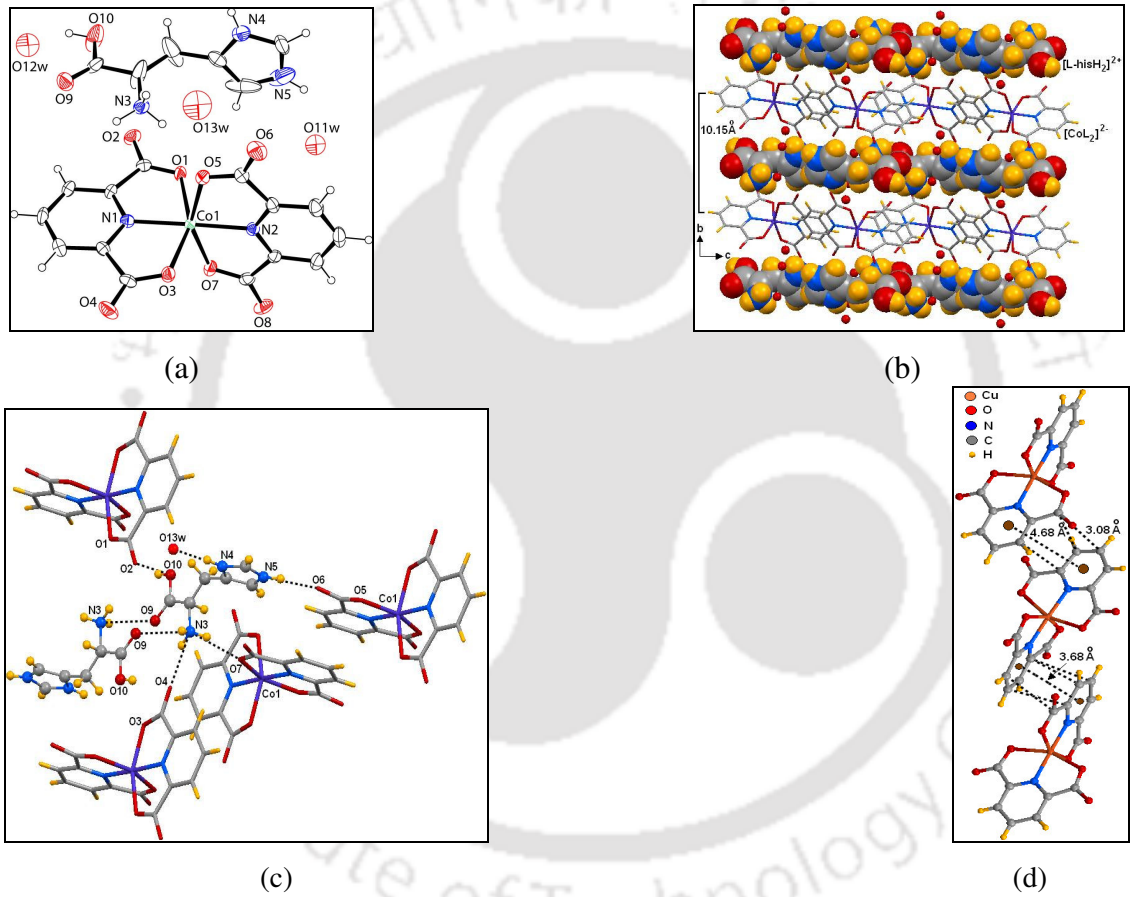

Fig. 3.1.3: (a) ORTEP of complex [L-hisH_2][CoL_2]·3H_2O (**3.1**) (30% thermal ellipsoids), (b) Layered packing arrangement, (c) Hydrogen bond interactions, and (d) Anion-π and π-π interactions of **3.1.**

From crystal engineering point of view, the complex anion and dication form inorganic-organic layer, as was the case with diamines in chapter 2. The distance between two adjacent $[CoL_2]^{2-}$ complex that sandwiches the L-histidine dicationic layer is ~ 10.15 Å (Fig. 3.1.3b).

The anionic layers is stabilized by π-π stacking (centroid to centroid distance ~ 4.14 Å) between adjacent $[CoL_2]^{2-}$ (Fig. 3.1.3d), whereas ammonium-carboxylic acid interactions between the adjacent L-histidine dication further stabilizes the cationic layer. Extensive hydrogen bonds by lattice water molecules also contribute to the stability of the complexes. The complexes become amorphous once the lattice water molecules are removed by heating.

Table 3.1: Selected hydrogen bond parameters for the complex **3.1** and **3.2**

Complex	Bond (symmetry)	$d_{D\cdots H}$(Å)	$d_{H\cdots A}$(Å)	$d_{D\cdots A}$(Å)	< D-H····A (º)
3.1	N(3)--H(3A)···O(9) [x, y, z]	0.88	2.26	2.682(9)	109
	N(3)--H(3A)···O(4) [1-x,-y,-z]	0.88	1.99	2.761(9)	145
	N(3)--H(3B)···O(7) [x, y, z]	0.86	1.94	2.778(8)	164
	N(3)--H(3C)···O(11) [x, y, z]	0.86	2.34	3.041(11)	139
	N(3)--H(3C)···O(9) [1-x,1-y,-z]	0.86	2.34	2.972(10)	131
	N(4)--H(4A)···O(13) [x, y, z]	0.86	1.82	2.682(10)	174
	N(5)--H(5A)···O(6) [2-x,-y,1-z]	0.86	2.02	2.789(16)	148
	O(10)--H(10A)···O(2) [2-x,1-y,-z]	0.87	1.73	2.577(10)	166
3.2	N(3)--H(3A)···O(15) [x,y,1+z]	0.89	1.96	2.840(6)	172
	N(3)--H(3B)···O(12) [x,y,1+z]	0.89	2.43	2.833(6)	108
	N(3)--H(3B)···O(14) [1/2-x,1/2+y,1-z]	0.89	2.09	2.885(6)	148
	N(3)--H(3C)···O(2) [1/2+x,1/2-y,1-z]	0.89	1.88	2.773(5)	176
	N(4)--H(4N)···O(11) [x, y, z]	0.86	1.94	2.761(6)	160
	N(5)--H(5N)···O(5) [1/2-x,-1/2+y,1-z]	0.86	2.49	3.177(6)	137
	N(5)--H(5N)···O(6) [1/2-x,-1/2+y,1-z]	0.86	2.13	2.959(6)	162
	O(10)--H(10A)···O(7) [-x,1-y,1+z]	0.82	1.83	2.608(5)	157

The Cu(II) dipicolinate L-histidine complex $[L\text{-}hisH_2][CuL_2]\cdot 5H_2O$ (**3.2**) is not isostructural with the Co(II) complex (**3.1**). It crystallizes in orthorhombic $P2_12_12_1$ space group with two symmetry non-equivalent $0.5[CuL_2]^{2-}$ anions, one L-histidine dication and five lattice water molecules in the asymmetric unit. The complex **3.2** exhibits identical supramolecular interactions with the previous Co(II) complex. The dication interacts with the complex anion *via* -COOH, $-NH_3^+$ and imidazolium part of L-histidine dication (Fig. 3.1.4a). Selected hydrogen bond interactions are N(3)-H(3C)···O(2) [($d_{D\ldots H}$, 1.88 Å, $d_{D\cdots A}$, 2.77 Å; < D-H····A, 176º], N(5)-H(5N)···O(6) [($d_{D\ldots H}$, 2.13 Å, $d_{D\cdots A}$, 2.96 Å; < D-H····A, 162º], O(10)-

H(10A)···O(7) [($d_{D}\ldots_{H}$, 1.83 Å, $d_{D\cdots A}$, 2.61 Å; < D-H····A, 157º]. In the complex **3.1**, the L-histidine dications form a hydrogen bonded dimer in the lattice; however, no such interaction is available in complex **3.2**. Another weak interaction that contributes to stabilize the complex is the face to face π-π stacking interactions. The π-π stacking distance between two neighboring $[CuL_2]^{2-}$ units is ~ 3.68 Å, which is much stronger than observed in the layers of $[CoL_2]^{2-}$ (~ 4.14 Å) of **3.1**.

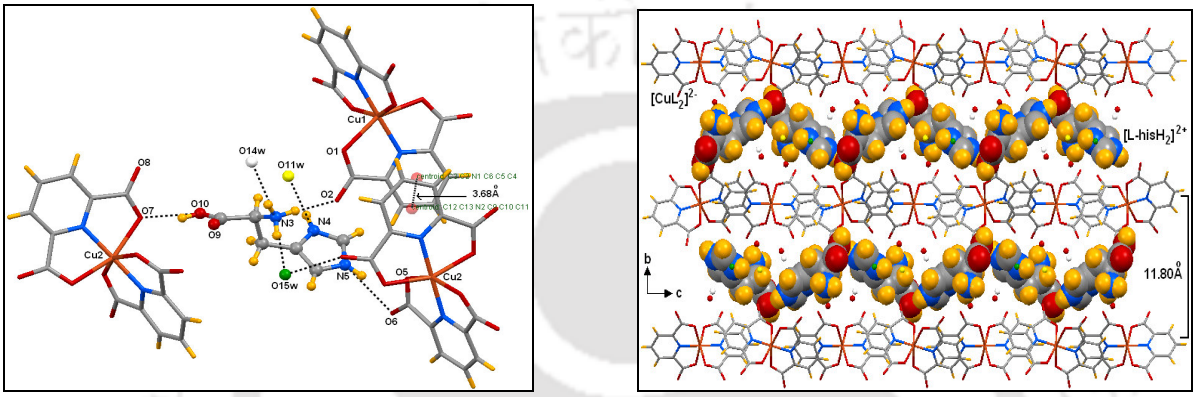

(a) (b)

Fig. 3.1.4: (a) Hydrogen bond interactions of L-histidine dication with $[CuL_2]^{2-}$ in complex **3.2**, (b) Layered packing diagram of complex **3.2** viewed along *a* axis.

In association with these supramolecular interactions, the complex anion $[CuL_2]^{2-}$ and L-histidine dication generate inorganic-organic layered structure in the crystal lattice. The minimum inter-metal distance between two adjacent $[CuL_2]^{2-}$ complex that sandwiches the L-histidine dicationic layer is ~ 11.80 Å (Fig. 3.1.4b). This distance is slightly longer than observed in previous Co(II) complex (~ 10.15 Å). Although both the complexes **3.1** and **3.2** form layered structures, the arrangement of the dication in the lattice is different. A linear chain of L-histidine dication is observed in Co(II) complex (**3.1**), whereas the dications form a wave pattern in Cu(II) complex (**3.2**) extending along crystallographic *a* axis. This difference in packing arrangement arises due to difference in size and John Teller distortion experienced by the metal ions.

The diffraction pattern of the complexes $[L\text{-}hisH_2][CoL_2]\cdot 3H_2O$ (**3.1**) and $[L\text{-}hisH_2][CuL_2]\cdot 5H_2O$ (**3.2**) tallies well with those simulated from the single crystal structures (Fig. 3.1.5). It exhibits intense peaks and the (h, k, l)s could be indexed properly and are in

proper agreement with the simulated pattern. Agreement of the major peaks, which are indexed based on the simulated ones, indicates the bulk purity of the samples.

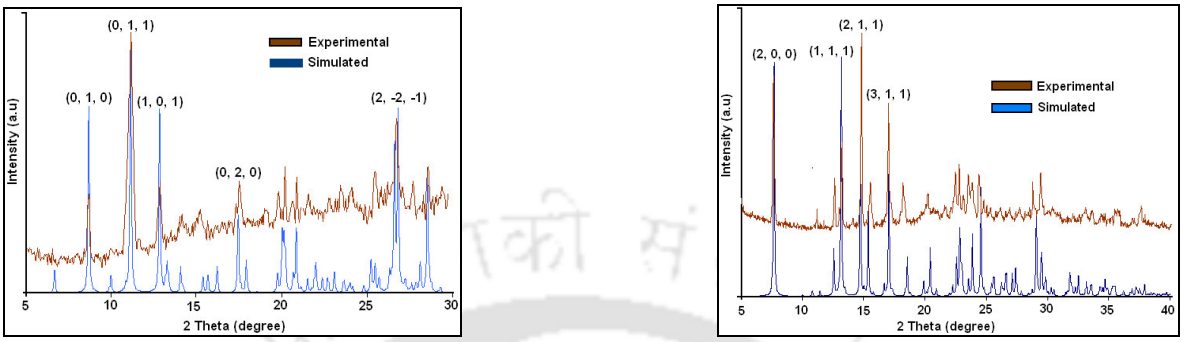

(a) (b)

Fig. 3.1.5: Simulated and experimental PXRD pattern of (a) complex **3.1**, (b) complex **3.2**

3.2: Synthesis, characterization and intercalation of dication of L-ornithine in layers of Co(II) or Cu(II) dipicolinate complexes

The complexes $[L\text{-orni}H_2]_2[CoL_2]_2{\cdot}9H_2O$ (**3.3**) and $[L\text{-orni}H_2]_2[CuL_2]_2{\cdot}5H_2O$ (**3.4**) are synthesized using basic amino acid L-ornithine as dication (scheme 3.1). The recurring units in the self-assembly of the complexes have the cations and anions in the 2:2 ratio. It has been mentioned that formation of mononuclear Cu(II) complex with L-ornithine was carried out by potentiomery, calorimetry, UV-Vis and ESR studies [29]. In this complex, the amino acid coordinates with the Cu(II) through ω-NH_2 terminal group and carboxylate group.

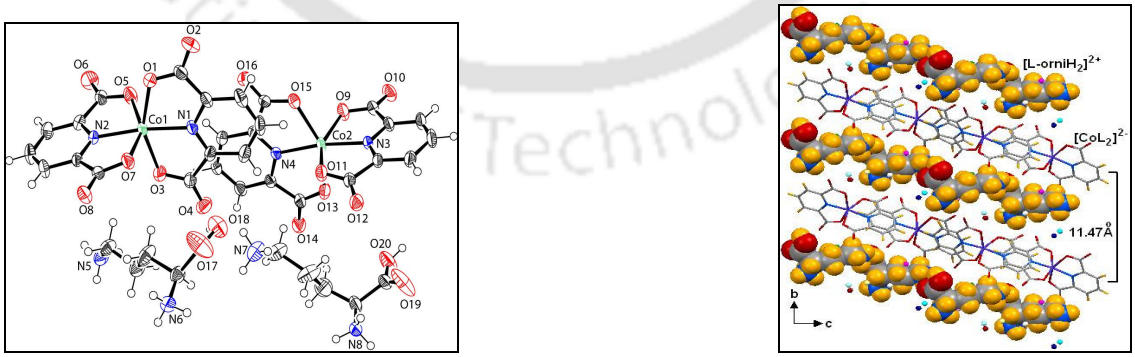

(a) (b)

Fig. 3.2.1: (a) ORTEP complex **3.3** (drawn with 30% thermal ellipsoids), and (b) Layered packing diagram of complex **3.3.**viewed along *a* axis.

The crystal structure of complex **3.3** contains two crystallographically nonequivalent dianions $[CoL_2]^{2-}$ and two L-ornithine dications with nine water molecules of crystallization (Fig. 3.2.1a). Similarly, the complex **3.4** comprise of four unsymmetrical units, two complex anions, and two dications of L-ornithine stabilized *via* electrostatic and hydrogen bond interactions. Fourier analysis shows that both the amine group (α-NH_2 and ω-NH_2) of L-ornithine is protonated. The two crystallographically independent dications of L-ornithine adopt different conformer than the unprotonated form. The flexible nature of the L-ornithine allows the dication to act differently in terms of weak interactions resulting in the higher cation to anion ratio in the complexes. This is expected for a positively charged ammonium species having a flexible alkyl chain backbone in the vicinity of a negatively charged dipicolinate complex.

Similar to L-histidine, the dication of L-ornithine involves in extensive charge-assisted -NH_3^+-COO^- hydrogen bond with the complex anion. Further, the carboxylic acid group of the amino acid form strong hydrogen bond with the carboxylate group of adjacent $[ML_2]^{2-}$ unit ([(d_D…$_H$, 1.81Å, $d_{D\cdots A}$, 2.63 Å; < D-H···A, 172° in **3.3**; [(d_D…$_H$, 1.72Å, $d_{D\cdots A}$, 2.53 Å; < D-H···A, 170° in **3.4**]). The lattice water molecules complete the remaining donor-acceptor hydrogen bonds with both the –COO^- of metal dipicolinates and with the ammonium cations of amino acid. Details of hydrogen bond parameters are listed in table 3.2. In the 2:1 complex of L-ornithine with macrocyclic host, the dication interacts with the similar ammonium-phosphate interactions available for L-histidine complex [28]. The exception being the imidazole ring of L-histidine that acts as hydrogen bond donor to one of the phophonate moiety.

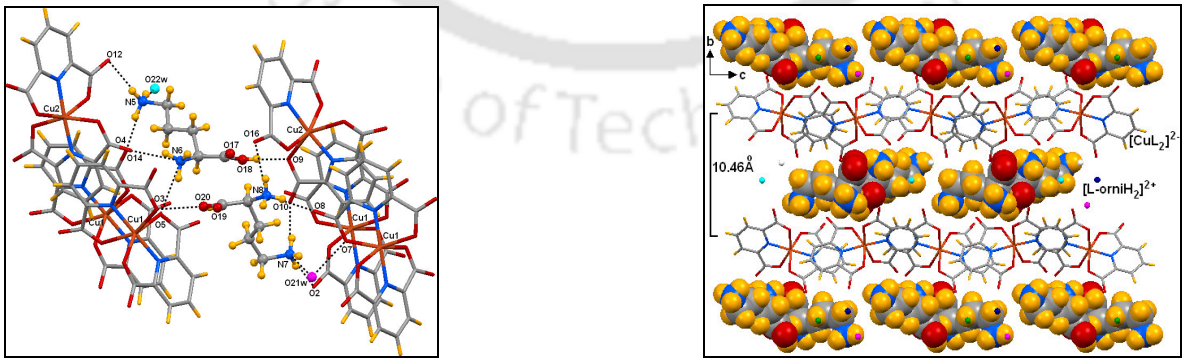

(a) (b)

Fig. 3.2.2: (a) Hydrogen bond interactions of complex **3.4**, (b) Layered structure of **3.4** viewed along *a* axis.

The packing of both the complexes reflect lamellar structures built up of $[ML_2]^{2-}$ as inorganic layer and corresponding dications as organic layer in the lattice. In addition to ion pairing and hydrogen bond, the π-π interactions also guide the crystal packing of these complexes. The L-ornithine complexes **3.3** and **3.4** exhibit weak π-π stacking interactions (~ 4.25 and 4.60 Å) than the L-histidine complexes (~ 3.68 and 4.14 Å). The inter layer separation in the complexes **3.3** and **3.4** are ~ 10.46 and 11.47 Å respectively. The water molecules present as solvent of crystallization play important role to hold the dications of the amino acid and complex anions in the layered structures. Thus, the lattice molecules play interesting role as space fillers as well as responsible for high crystallinity / stability of the complexes by participating in extensive hydrogen bond with the host / guest molecule as a donor / acceptor.

Table 3.2: Selected hydrogen bond parameters for the complex **3.3** and **3.4**

Complex	Bond (symmetry)	$d_{D\cdots H}$(Å)	$d_{H\cdots A}$(Å)	$d_{D\cdots A}$(Å)	< D-H····A(°)
3.3	N(5)--H(5A)···O(21W) [x, y, z]	0.89	2.02	2.901(5)	169
	N(5)--H(5B)···O(12) [x,y,1+z]	0.89	1.94	2.826(5)	171
	N(5)--H(5C)···O(19) [x,y,1+z]	0.89	2.48	2.838(7)	105
	N(5)--H(5C)···O(22W) [x, y, z]	0.89	1.92	2.797(6)	168
	N(6)--H(6A)···O(26W) [1+x,y,z]	0.89	1.95	2.799(9)	160
	N(6)--H(6A)···O(29W) [x, y, z]	0.89	2.47	3.027(12)	121
	N(6)--H(6B)···O(16) [x,-1+y,z]	0.89	1.86	2.747(5)	175
	N(6)--H(6C)···O(23W) [1+x,y,z]	0.89	1.98	2.842(6)	164
	N(7)--H(7A)···O(27W) [x, y, z]	0.89	1.97	2.852(8)	169
	N(7)--H(7B)···O(4) [x, y, z]	0.89	2.04	2.887(6)	158
	N(7)--H(7C)···O(24W) [x, y, z]	0.89	2.05	2.919(6)	164
	N(8)--H(8A)···O(22W) [x,y,-1+z]	0.89	2.18	2.939(6)	143
	N(8)--H(8B)···O(1) [-1+x,-1+y,-1+z]	0.89	2.01	2.844(5)	156
	N(8)--H(8C)···O(10) [x,-1+y,z]	0.89	1.89	2.775(5)	177
	O(20)--H(20)···O(8) [-1+x,y,-1+z]	0.82	1.81	2.623(6)	172
	N(5)--H(5B)···O(22W) [-1+x,y,-1+z]	0.89	1.96	2.823(11)	164
	N(5)--H(5C)···O(11) [1-x,1/2+y,-z]	0.89	2.44	3.080(10)	130
	N(5)--H(5C)···O(12) [1-x,1/2+y,-z]	0.89	2.07	2.928(9)	162

3.4	N(6)--H(6A)···O(5) [1-x,1/2+y,1-z]	0.89	2.09	2.925(10)	157
	N(6) --H(6B)···O(14) [1-x,1/2+y,-z]	0.89	1.86	2.690(12)	155
	N(6)--H(6C)···O(17) [x, y, z]	0.89	2.23	2.657(12)	109
	N(6)--H(6C)···O(22W) [x,y,-1+z]	0.89	2.52	3.112(10)	125
	N(7)--H(7A)···O(10) [x, y, z]	0.89	2.01	2.889(9)	171
	N(7)--H(7B)···O(2) [x, y, z]	0.89	1.96	2.836(10)	169
	N(7)--H(7C)···O(21W) [1+x, y, z]	0.89	2.06	2.885(10)	153
	N(8)--H(8A)···O(15) [x, y, z]	0.89	2.44	2.920(9)	114
	N(8)--H(8A)···O(16) [x, y, z]	0.89	1.98	2.822(8)	157
	N(8)--H(8B)···O(8) [1+x, y, z]	0.89	1.90	2.785(10)	173
	N(8)--H(8C)···O(19) [x, y, z]	0.89	2.38	2.712(9)	102
	N(8)--H(8C)···O(24W) [1+x, y, z]	0.89	2.13	2.945(9)	151
	O(18)--H(18A)···O(9) [x, y, z]	0.82	1.72	2.534(9)	170

The complexes exhibit characteristic IR absorptions for $–N^{+}$-H, -COOH and $–COO^{-}$ groups in the similar absorption ranges observed with L-histidine complex earlier [26]. TG analysis was carried out to see the weight loss of the components obtained in the crystallographic study. An illustrative thermogram of complex **3.3** is shown in Fig. 3.2.3a. It involves three major steps of weight loss. The weight loss of 11.5% (calcd. 13.4%) in the range of 50-110 ºC corresponds to the loss of nine lattice water molecules. Loss of amino acid occurs in the temperature range of 200-290 ºC (obsd. 21.1%, calcd. 22.0%), followed by continuous decomposition of the Co(II) dipicolinate complex.

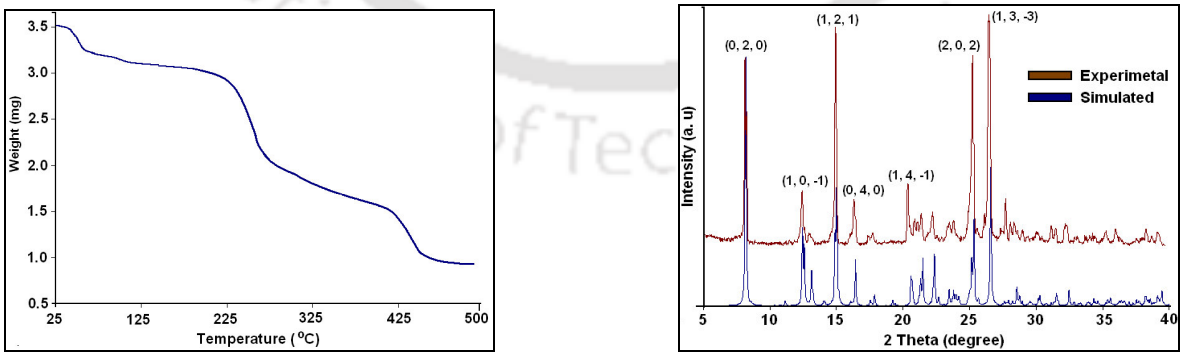

(a) (b)

Fig. 3.2.3: (a) TG of complex **3.3**, (b) Simulated and experimental powder pattern of complex **3.4**.

The X-ray powder diffraction pattern of the complexes show agreement with those simulated from the single crystal structures. For example, the powder diffraction data of simulated and experimental pattern of complex **3.4** is overlaid in the same plot showing the lattice plane against each indexed intense peak (Fig. 3.2.3b). This indicates the bulk purity of the samples.

It is to be mentioned that we could not crystallize the metal dipicolinate complexes with other basic amino acids such as L-arginine and L-lysine, although several attempt has been made. These give sticky solid materials instead of a crystal. However, we were successful to synthesize cerium dipicolinate complexes with L-arginine as dication along with the other two amino acids reported in this chapter [30].

3.3: Optical activity of the complexes

The parent amino acids used in this study are optically active. Thus, it is likely that the optical activity of these parent amino acids will be carried over to the complexes also. Accordingly, the specific rotations were determined for the parent amino acids as well as the complexes. The values of the specific rotations are listed in table 3.3. From the table it is clear that the specific rotations are lower in the complexes than the parent amino acids.

Table 3.3: Specific Rotation (º) of the complexes **3.1-3.4** (in H_2O)

Amino acids / Complexes	**Specific rotation $[\alpha]_D^{25}$ (º)**
L-histidine	+ 8.6
L-ornithine	+ 23.2
[L-hisH_2][CoL_2]·3H_2O (**3.1**)	+ 4.3
[L-hisH_2][CuL_2]·5H_2O (**3.2**)	+ 4.5
[L-orniH_2]$_2$ [CoL_2] $_2$·9H_2O (**3.3**)	+ 11.5
[L-orniH_2]$_2$ [CuL_2]$_2$·5H_2O (**3.4**)	+ 12.2

The advantage of these amino acid containing complexes is that they undergo selective exchange of amino acids with alkali or alkaline earth metal ions without exchanging the

ligand/s similar to diamines discussed in chapter 2. While doing so the parent optically active amino acids can be recovered.

3.4: Conclusion

This chapter demonstrates a simple one-pot procedure for synthesizing optically active water-soluble amino acid containing complexes. The amino acid dications namely L-histidine and L-ornithine are intercalated in layers of Co(II) or Cu(II) dipicolinates by a combination of ammonium-carboxylate and carboxylic acid-carboxylate hydrogen bond interactions. The protonated amino acids maintain identical packing arrangement irrespective of the amino acids. Despite differences in the structure of L-ornithine from L-histidine (alkyl to imidazole substituents), the inter layer separations created by the amino acid dications are not significant. This is attributed to the flexible nature of the amino acids resulted from the ammonium-carboxylate electrostatic interactions in the crystal lattice. Further, the advantage of these complexes is that the dications can be de-intercalated *via* ion exchange with alkali or alkaline earth metal ions.

3.5: Experimental section

3.5.1: Synthesis and characterization of $[L\text{-}hisH_2][CoL_2]\cdot 3H_2O$ (3.1) and $[L\text{-}hisH_2][CuL_2]\cdot 5H_2O$ (3.2)

To a solution of dipicolinic acid (0.334 g, 2.0 mmol) dissolved in methanol (20 ml) a solution of cobalt (II) acetate tetrahydrate (0.249 g, 1.0 mmol) and copper(II) acetate monohydrate (0.199 g, 1.0 mmol) was added respectively. Depending on the metal ions, pink or blue colored precipitates were obtained. The reaction mixture was stirred for half an hour; 10 ml of pre-dissolved L-histidine mono hydrochloride (0.21 g, 1.0 mmol) solution in water was added in small portions to the respective precipitate and stirred. The solution was left overnight at room temperature. A pink (for cobalt) or blue (for copper) precipitate obtained from the reaction mixtures were filtered, dried and crystallized from ultra pure water.

Complex **3.1:** Isolated yield, 78%. Elemental anal calcd for $C_{20}H_{23}CoN_5O_{13}$, C, 39.98; N, 11.66; H, 3.83%; found C, 39.76; N, 11.57; H, 3.67%. IR (KBr, cm^{-1}): 3410 (bs), 3108 (s), 3022 (w), 1622 (bs), 1496 (m), 1380 (m), 1336 (m), 1285 (m), 1078 (w). $[\alpha]_D^{25}$ = + 4.3. Molar conductance: 162.0 S cm^2 mol^{-1} in water. μ_{eff}. at 298 K: 4.32 BM. Thermal analysis: ~ 70-135 ºC (evaporation of three water molecules of crystallization).

Complex **3.2**: Isolated yield: 76%. Elemental anal calcd for $C_{20}H_{27}CuN_5O_{15}$, C, 37.45; N, 10.92; H, 4.21%; found C, 37.28; N, 10.85; H, 4.11%. IR (KBr, cm^{-1}): 3443 (b, s), 3108 (s), 3022 (m), 1634 (bs), 1601 (w), 1495 (m), 1337 (s), 1276 (m), 1182 (w), 1085 (w). $[\alpha]_D^{25}$ = + 4.5. Molar conductance: 166.0 S cm^2 mol^{-1} in water. μ_{eff}. at 298 K: 1.68 BM. Vis (H_2O) λ_{max}: 776.0 nm; ε = 87.5 M^{-1} cm^{-1}. Thermal analysis: ~ 70-200 ºC (loss of five water molecules of crystallization).

3.5.2: $[L\text{-}orniH_2]_2[CoL_2]_2 \cdot 9H_2O$ (3.3) and $[L\text{-}orniH_2]_2[CuL_2]_2 \cdot 5H_2O$ (3.4)

These complexes were prepared following the similar procedure described for **3.1** and **3.2** using 10 ml of L-ornithine hydrochloride (0.17 g, 1.0 mmol) adding in the cobalt(II) pink and copper(II) blue precipitates respectively, obtained after mixing corresponding metal acetates with dipicolinic acid.

Complex **3.3:** Isolated yield, 75%. Elemental anal calcd for $C_{38}H_{58}Co_2N_8O_{29}$, C, 37.72; N, 9.27; H, 4.80%; found C, 37.44; N, 9.20; H, 4.57%. IR (KBr, cm^{-1}): 3427 (b, s), 3090 (b, s), 1731 (w), 1622 (b, s), 1481 (m), 1447 (w), 1371 (s), 1285 (m), 1078 (w). $[\alpha]_D^{25}$ = + 11.5. Molar conductance: 174.0 S cm^2 mol^{-1} in water. μ_{eff}. at 298 K: 4.28 BM. Thermal analysis: ~ 45-130 ºC (evaporation of nine water molecules of crystallization).

Complex **3.4**: Isolated yield: 79%. Elemental anal calcd for $C_{38}H_{50}Cu_2N_8O_{25}$, C, 39.80; N, 9.77; H, 4.36%; found C, 39.49; N, 9.70; H, 4.19%. IR (KBr, cm^{-1}): 3422 (b, s), 3092 (m), 2927 (m) 1633 (s), 1591 (w), 1481 (w), 1365 (s), 1276 (w), 1083 (w). $[\alpha]_D^{25}$ = +12.2. Molar conductance: 177.0 S cm^2 mol^{-1} in water. μ_{eff}. at 298 K: 1.64 BM. Vis (H_2O) λ_{max}: 775.0 nm; ε = 78.0 M^{-1} cm^{-1}. Thermal analysis: ~ 55-110 ºC (evaporation of five water molecules of crystallization).

3.6: Crystallographic data and refinement parameters for the complexes 3.1-3.4

Compound No.	**3.1**	**3.2**	**3.3**	**3.4**
Formula	$C_{20}H_{23}CoN_5O_{13}$	$C_{20}H_{27}CuN_5O_{15}$	$C_{38}H_{58}Co_2N_8O_{29}$	$C_{38}H_{50}Cu_2N_8O_{25}$
Formula wt.	600.36	640.93	1208.78	1145.86
Crystal system	Triclinic	Orthorhombic	Triclinic	Monoclinic
Space group	*P-1*	$P2_12_12$	*P-1*	*P2(1)*
a (Å)	8.9548(3)	23.0775(16)	8.8851(4)	8.5427(18)
b (Å)	10.1494(3)	13.7009(9)	11.9990(5)	21.598(5)
c (Å)	13.3597(4)	8.2049(6)	12.8666(5)	12.601(2)
α (deg)	91.545(2)	90.00	107.303(2)	90.00
β (deg)	98.698(2)	90.00	92.059(2)	90.757(13)
γ (deg)	90.232(2)	90.00	103.324(2)	90.00
V (Å^3)	1199.77(6)	2594.2(3)	1266.32(9)	2324.6(8)
Z	2	4	1	2
D_{calc} (gcm^{-3})	1.662	1.615	1.585	1.623
μ (mm^{-1})	0.796	0.926	0.758	1.014
F(000)	618	1284	628	1164
Total no. of reflns	13934	38176	16420	11689
Independent reflns.	3826	6464	9846	7376
$\theta_{max.}$	1.54 – 24.50	1.73 – 28.48	1.67 – 28.40	1.62 – 24.50
Ranges (h, k, l)	$-10 \le h \le 10$	$-30 \le h \le 30$	$-11 \le h \le 11$	$-8 \le h \le 9$
	$-11 \le k \le 11$	$-18 \le k \le 18$	$-16 \le k \le 15$	$-22 \le k \le 23$
	$-15 \le l \le 14$	$-10 \le l \le 10$	$-16 \le l \le 17$	$-14 \le l \le 14$
Completeness to 2θ (%)	95.8	98.8	98.1	95.0
Data / restraints / parameters	3826 / 0 / 337	6464 / 0 / 348	9846 / 0 / 655	7376 / 0 / 639
GOF (F^2)	1.099	1.071	0.991	1.075
R_1, wR_2 [$I > 2\sigma(I)$]	0.0667, 0.2122	0.0740, 0.1782	0.0521, 0.1359	0.0631, 0.1559
R_1, wR_2 (all data)	0.0814, 0.2342	0.0976, 0.1885	0.0558, 0.1393	0.0746, 0.1632
Largest diff peak/hole (e Å^{-3})	0.844 / -0.729	1.302 / -1.256	0.945 / -0.583	0.717 / -0.652

References:

[1] J.-M. Lehn, P. Vierling, R.C. Hayward, J. Chem. Soc. Chem. Commun. (1979) 296.

[2] A.V. Eliseev, M.I. Nelen, J. Am. Chem. Soc. 119 (1997) 1147.

[3] J. Chin, S.S. Lee, K.J. Lee, S. Park, D.H. Kim, Nature 401 (1999) 254.

[4] T.W. Bell, A.B. Khasanov, M.G.B. Drew, J. Am. Chem. Soc. 124 (2002) 14092.

[5] H. Nakayama, N. Wada, M. Tsuhako, Inter. J. of Pharma. 269 (2004) 469.

[6] J. Tronto, L. Patricio Cardoso, J. Barros Valim, J. Maldonado Marchetti, M.V.B. Bentley, Mol. Crystals Liq. Crystals 390 (2002) 79.

[7] A. Sumio, N. Eiichi, Zeolite News Letter 17 (2000) 101.

[8] A.I. Khan, A. Ragavan, B. Fong, C. Markland, M. O'Brien, T.G. Dunbar, G.R. Williams, D. O'Hare, Ind. Eng. Chem. Res. 48 (2009) 10196.

[9] M.X. Reinholdt, R.J. Kirkpatrick, Chem. Mater. 18 (2006) 2567.

[10] R.-Q. Zeng, X.-K. Fu, X.-B. Yang, Chemical Papers 65 (2011) 676.

[11] T. Schrader, Angew. Chem. Int. Ed. 35 (1996) 2649.

[12] T. Schrader, J. Am. Chem. Soc. 120 (1998) 11816.

[13] P. Debroy, M. Banerjee, M. Prasad, S.P. Moulik, S. Roy, Org. Lett. 7 (2005) 403.

[14] H. Imai, H. Munakata, Y. Uemori, N. Sakura, Inorg. Chem. 43 (2004) 1211.

[15] Y. Liu, M. Fan, S. Zhang, X. Sheng, J. Yao, New J. Chem., 31 (2007) 1878.

[16] J.D. Kopple, M.E. Swendseid, J Clin Invest. 55 (1975) 881.

[17] J.J. Farrell, J. Chem. Educ. 54 (1977) 445.

[18] P. O'Brien, J. Chem. Educ. 59 (1982) 1052.

[19] P.J. Morris, R.B. Martin J. Am. Chem. Soc. 92 (1970) 1543.

[20] I. Jakab, K. Hernad, D. Mehn, T. Kollar, I. Palinko, J. Mol. Struct. 651 (2003) 109.

[21] V. Patel, P. Bhattacharya, Inorg. Chim. Acta 92 (1982) 199.

[22] M. Linder, Biochemistry of Copper, Plenum Press, New York 1991.

[23] P. Manikandan, B. Epel, D. Goldfarb Inorg. Chem. 40 (2001) 781.

[24] T. Venelinov, S. Arpadjan, I. Karadjova, J. Beattie, Acta Pharm. 56 (2006) 105.

[25] K. Osz, K. Varnagy, H. Suli-Vargha, A. Csampay, D. Sanna, G. Micera, I. Sovago, J. Inorg. Biochem. 98 (2004) 24.

[26] R.M. Silverstein, F.X. Webster, D.J. Kiemle, Spectrometric identification of organic compounds, pp 72-126, John Wiley & Sons, Inc.: New York, 7th ed. 2005.

[27] N. Benali-Cherif, L. Benguedouar, A. Cherouana, L. Bendjeddou, H. Merazig, Acta Cryst. E58 (2002) o822.

[28] T. Grawe, T. Schrader, P. Finocchiaro, G. Consiglio, S. Failla, Org. Lett. 3 (2001) 1597.

[29] C. Conato, A. Contino, G. Maccarrone, A. Magri, M. Remelli, G. Tabbi, Thermochimica Acta 362 (2000) 13.

[30] B. Das, K. Ghosh, J.B. Baruah, Metal-Org. nano-Met. Chem. xx (2013) xx.

Chapter 4

Intercalation of nucleobases by metal dipicolinates

Intercalation of neutral or protonated nucleobases by various artificial receptor molecules has been a subject of numerous theoretical and experimental investigations [1-4]. Nucleobases such as adenine (6-aminopurine) plays important role in biochemistry such as in ATP, NAD^+ and nucleic acids [5]. Cytosine act in many biochemical processes such as enzymatic reactions, stabilization of triplex structures and also plays key role in acid-base catalysis [6-9]. Hydrogen bonded self-assemblies of nucleobases has been used to design and construct highly ordered supramolecular nanostructures that find applications in molecular devices [10-12]. Influence of metal ions on the behaviour of nucleobases has attracted growing attention in recent years [13,14]. The studies on metal–nucleobase bindings provide understanding on the role of metal ions in the function of nucleic acids especially in genetic information transfer [15-17]. Studies concerning these nucleobases are carried out in gas phase or aqueous media [18-20]. Some studies on nucleobases are directed towards pharmaceuticals; construction of ligands; stabilization of noncanonical tautomers through interactions with metallic ions; development of artificial receptors for specific DNA/RNA base recognition and for determination of therapeutic agents [21-24]. Molecular recognition of adeninium and cytosinium cation by artificial receptors such as oxalate and malonate complexes has been reported in literature [25-28]. Hexachlorostannate anions stabilise cytosinium and adeninium cation in hydrogen bond networks [29,30]. The multiple hydrogen bonding sites allow the nucleobases to form various self-assemblies. Adenine shows formation of infinite assemblies *via* 9H-adenine, 1H,9H-adeninium or through 3H,7H-adeninium cation. Cytosine has a single tautomer in the form of 1H,3H-cytosinium cation. Despite the single protonated form, its special geometry allows it to form discrete, dimeric, trimeric, tetrameric or infinite assemblies. Crystal structure database showed that neutral cytosine and/or its 1H,3H-cytosinium exhibits five different 1D nucleobase patterns [31]. Some of such assemblies formed by adenine and cytosine in their neutral or protonated form are shown in Fig. 4.1.

In this chapter, metal dipicolinate complexes are used to intercalate these nucleobases. A systematic attempt has been made to intercalate these nucleobases by varying the central metal ion of dipicolinate complex and also the flexibility of the receptor molecule. Since the nucleobases undergo self-association through intermolecular hydrogen bonding, it would be interesting to study the self-assembly processes of these nucleobases in the interstices of relatively bulky metal dipicolinate complex anion or similar dicarboxylate complexes. Further, the supramolecular nucleobase architectures may further contribute to understand the tautomeric and protonation equilibria of these nucleobases.

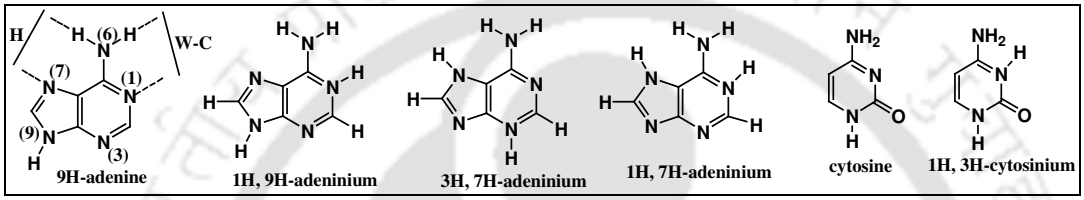

(a)

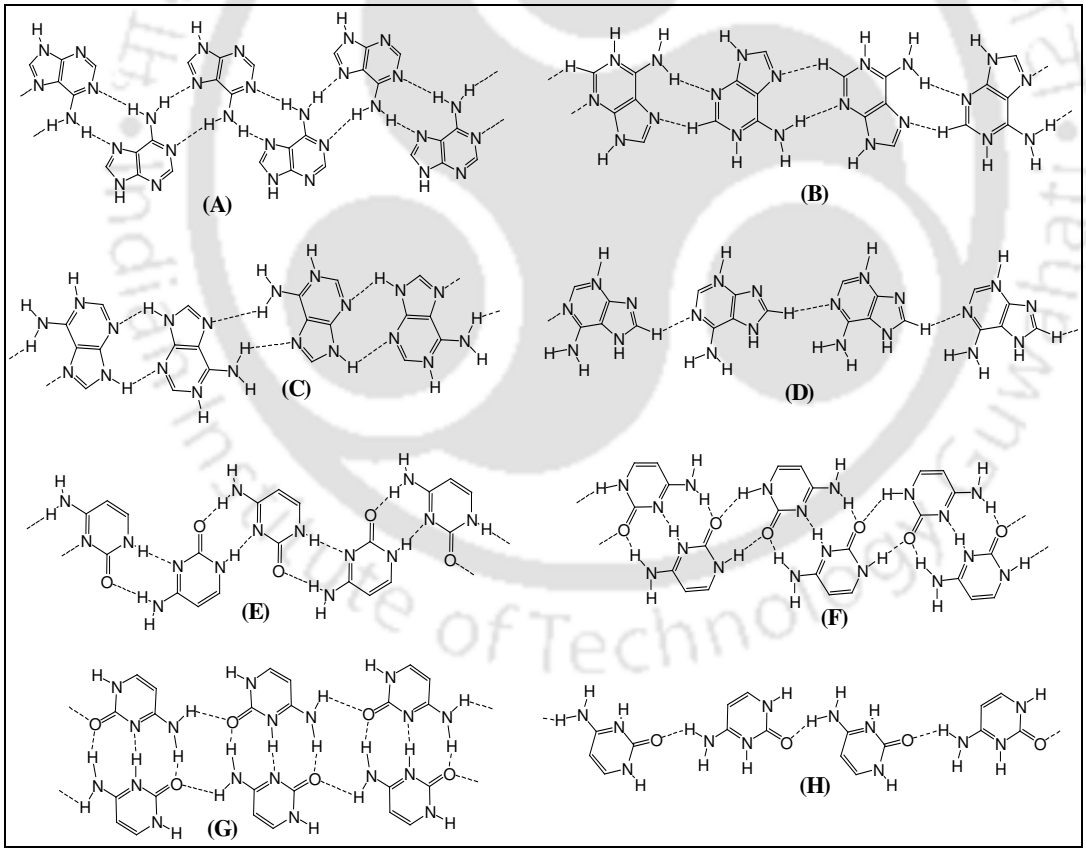

(b)

Fig. 4.1: (a) Neutral and protonated form of adenine and cytosine, and (b) Hydrogen bonded assemblies of (A) neutral adenine, (B-C) 1H,9H-adeninium, (D) 3H,7H-adeninium, (E) neutral cytosine, (F-G) cytosine-cytosinium, (H) cytosinium assembly.

With this background, a series of metal dipicolinate complexes with adenine and cytosine base as depicted in scheme **4.1** are synthesized and characterized. The intercalated adenine and cytosine assemblies formed in the layers of metal dipicolinates are further compared with those obtained in the rigid polymeric metal quinolinate frameworks and also in flexible polycarboxylic acids. The flexibility or the rigidity of the receptor molecule and the role of central metal ion that govern the nature of the nucleobase assemblies is also discussed.

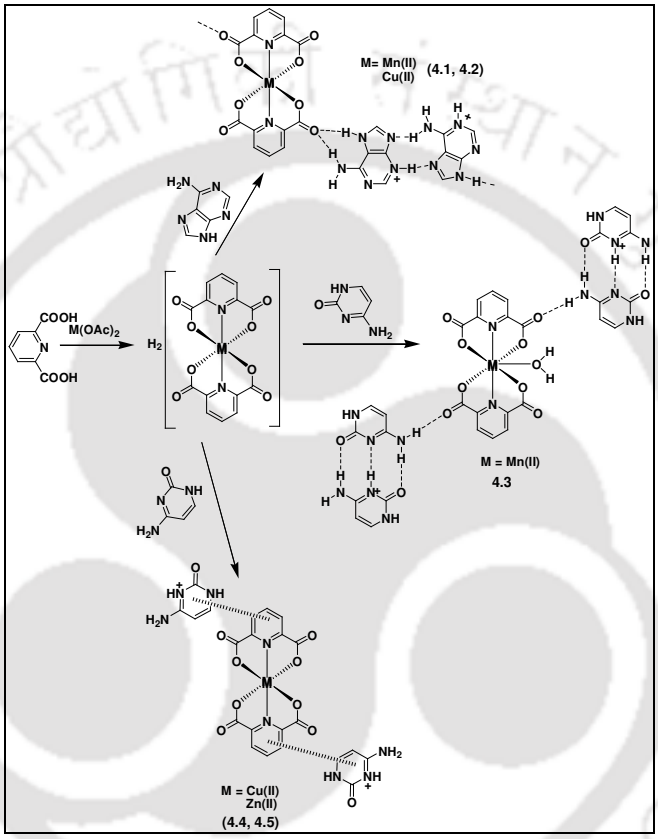

Scheme 4.1: Synthesis of the complexes with cations of adenine and cytosine

4.1: Synthesis, characterization and intercalation of protonated adenine by Mn(II) / Cu(II) dipicolinates

Reactions of adenine with water soluble metal dipicolinates at acidic pH give the compounds [1H,9H-ade][3H,7H-ade][ML_2]·$3H_2O$ (where ade = adeninium cation, L = dipicolinate, M(II) = Mn (**4.1**) / Cu (**4.2**)). The complexes exhibit strong IR absorptions in the range of 1699-1584 cm^{-1} and 1372-1369 cm^{-1} due to the carboxylate stretching; the –N-H stretching appears in the range 3078-2968 cm^{-1}. The FTIR spectra of complex **4.1** is shown

in Fig. 4.1.1 as a representative case. The molar conductance values are found to be 201.0 and 205.0 S cm^2 mol^{-1} respectively in water, which reflects the ionic nature of the complexes.

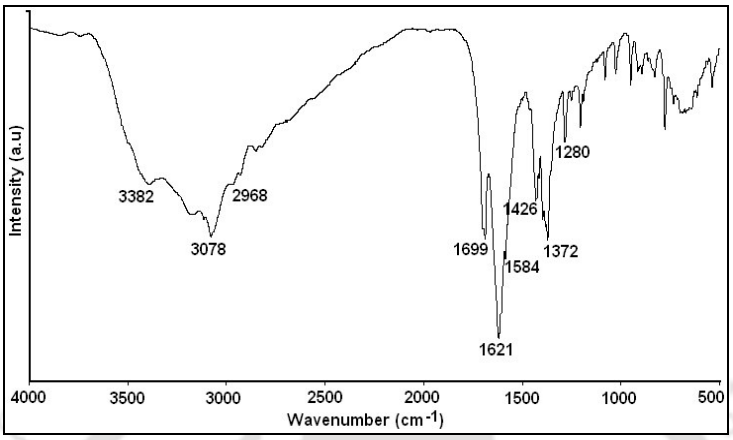

Fig. 4.1.1: FTIR of complex **4.1**

Since the complexes **4.1** and **4.2** have similar structural features, only the perspective view of complex [1H,9H-ade][3H,7H-ade][CuL_2]·3H_2O (**4.2**) is shown in Fig. 4.1.2a. The crystal structures reveal the presence of complex anion $[CuL_2]^{2-}$, two adeninium cations and three lattice water molecules in the asymmetric unit. The coordination polyhedron and structure of $[CuL_2]^{2-}$ has already been discussed in previous chapters. The protonation of the two adeninium cation in these complexes is different. Difference Fourier synthesis map showed that the representative compound consists of one 1H,9H-adeninium cation and another adeninium cation having hydrogen atoms at N3 and N7; thus showing the presence of two differently protonated state of adenine in the molecule. This is observed as unprecedented in the adenine solid-state chemistry. These two non-equivalent adeninium cation aggregates *via* hydrogen bond leading to a 1D zigzag ribbon intercalated in the Cu(II) dipicolinate anionic frameworks (Fig. 4.1.2b). It is to be noted that density functional theory calculations shows that 1H,9H-adeninium cation is the most stable form followed by 3H,7H-adeninium cation by an energy difference of 0.46 kcal/mol [32]. Recently, stabilizations of 1H,9H-adeninium cation has been observed in Cu(II) oxalate complexes with adenine, (1H,9H-ade)$_2$ [$Cu(ox)_2(H_2O)$] [where ox = oxalate] [26]. The isostructural complexes with other metal ion such as Co(II) and Zn(II) showed formation of 3H,7H-adeninium cation in the complex. Both the 1H,9H-adeninium and 3H,7H-adeninium cation showed formation of 1D self-

assemblies independently in layers of these metal oxalate complexes stabilized by hydrogen bond and π-π stacking interactions. Similarly, 1D assemblies of 1H,9H-adeninium cation in the form of cationic ribbon were established in Cu(II) malonate complexes by the same group of coworkers [28]. The other complexes with Co(II) or Ni(II) showed coordinated as well as adeninium cation outside the coordination sphere. Self-assemblies of neutral adenine in the form of 'double-sided adhesive tape' were reported in $[M(quin\text{-}2\text{-}c)_2(H_2O)_2]\cdot(9H\text{-}ade)_2$ (where quin-2-c = quionoline-2-carboxylate ion, M = Mn, Fe or Co at +2 oxidation state) [33]. The adenine tape was stabilized by extensive hydrogen bond and π-π interactions. Further, there are examples of adeninium-water supramolecular assemblies stabilized by polyiodide frameworks [34,35].

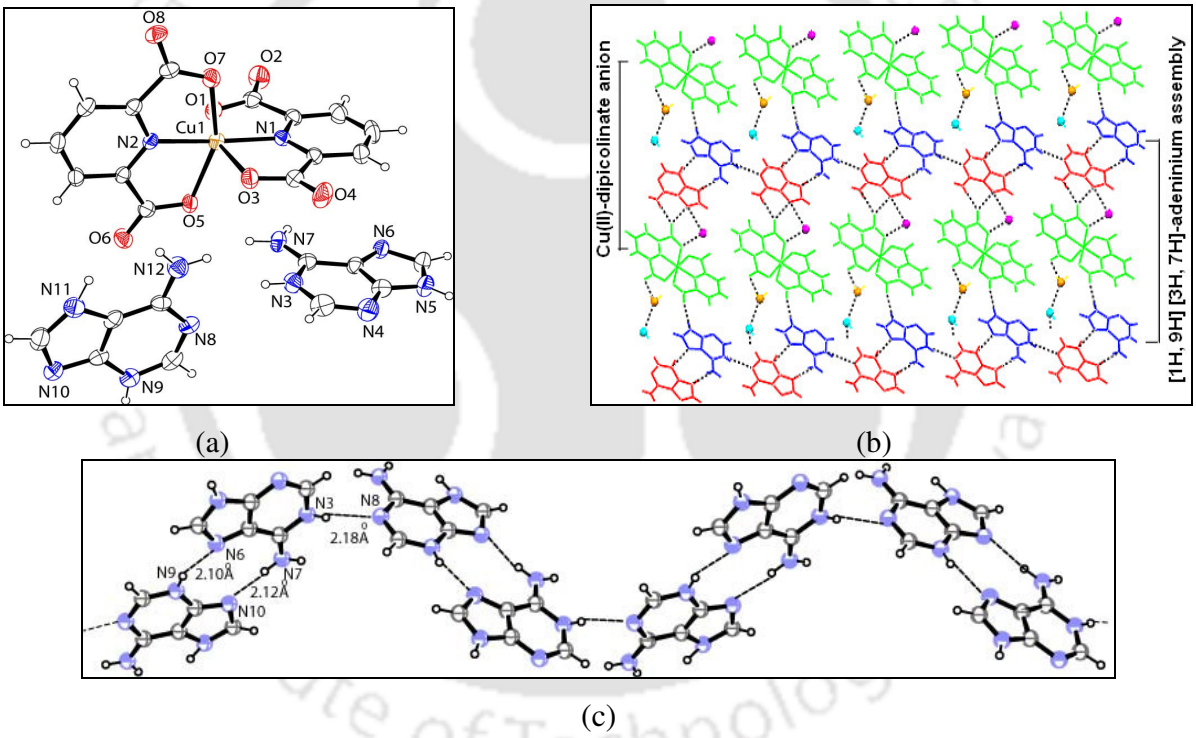

Fig. 4.1.2: (a) ORTEP of complex **4.2** (drawn with 50% thermal ellipsoid), (b) Hydrogen bonds of adeninium ribbon with $[CuL_2]^{2-}$ and lattice water molecules in **4.2** viewed along *c* axis, (c) [1H,9H] and [3H,7H] adeninium ribbon with hydrogen bond distances.

The 1D cationic ribbon observed in the complex **4.2** propagates along the crystallographic *c* axis between the Hoogsteen face of a 1H, 9H-adeninium cation and the protonated N3 and unprotonated N9 atoms of an adjacent 3H,7H-adeninium cation. This is followed by a

hydrogen bond between the protonated N1 site of 1H,9H-adeninium nucleobase and the unprotonated N1 site of the other nucleobase (Fig. 4.1.2c). These planar protonated dimers are perpendicularly accommodated in the ribbon with one another. The ribbon is further stabilized by π-π stacking with the dipicolinate unit of the complex anion. It is to be mentioned that although several self-assemblies adenine are reported in literature, the ribbon consisting of two differently protonated cations, discussed in this chapter, have not been observed earlier.

Table 4.1: Hydrogen bond parameters of 1D adeninium and cytosine-cytosinium assembly

	Bond (symmetry)	$d_{D\text{-}H}$(Å)	$d_{H\cdots A}$(Å)	$d_{D\cdots A}$(Å)	< D-H···A(°)
1D adenine ribbon in **4.1**	N(9)--H(9N)···N(6) [1+x,1/2-y,1/2+z]	0.84(4)	2.10(4)	2.899(5)	160(3)
	N(7)--H(7B)···N(10) [-1+x,1/2-y,-1/2+z]	0.86	2.12	2.959(4)	165
	N(3)--H(3N)···N(8) [x, y, z]	0.81(3)	2.18(3)	2.971(4)	163(4)
Tetrameric cytosine – cytosinium assembly in **4.3**	N(3)--H(3A)···O(13) [-1+x,y,1+z]	0.86	2.00	2.847(7)	167
	N(4)--H(4N)···N(12) [-1+x,y,1+z]	0.97(5)	1.87(6)	2.814(7)	165(5)
	N(14)--H(14A)···O(10) [1+x,y,-1+z]	0.86	1.99	2.842(7)	175
	N(8)--H(8A)···O(12) [1-x,1-y,-z]	0.86	1.94	2.795(7)	178
	N(6)--H(6N)···N(9) [1-x,1-y,-z]	0.99(7)	1.89(7)	2.850(7)	164(6)
	N(11)--H(11A)···O(11) [1-x,1-y,-z]	0.86	2.08	2.938(7)	171
	N(5)--H(5N)···O(10) [1-x,-y,2-z]	0.86	1.95	2.805(7)	170
	N(10)--H(10N)···O(13) [1-x,1-y,-z]	0.86	2.03	2.869(7)	166
	N(13)--H(13N)···O(12) [1-x,1-y,-z]	0.86	1.92	2.774(7)	171

4.2: Synthesis, characterization and intercalation of cytosine assemblies by metal dipicolinates

Reactions of cytosine with Mn(II), Cu(II) or Zn(II) dipicolinates afforded two different types of complexes under the same reaction condition (scheme 4.1). Mn(II) dipicolinate cytosine complex [1H,3H-cyt]$_2$ [$MnL_2(H_2O)$]·$(cyt)_2$·$6H_2O$ (**4.3**) represent the type I complex. The asymmetric unit of **4.3** showed the presence of both neutral and protonated cytosine molecule. In type II, Cu(II) or Zn(II) form isostructural complexes with cytosine nucleobase with general composition of [1H,3H-cyt]$_2$[ML_2]·$5H_2O$ (**4.4, 4.5**). The complexes exhibit –

N^+-H stretching frequencies in the range of 3370-2808 cm^{-1}. The complex **4.3** shows intense –N^+-H stretching frequencies spreading over a broad range than **4.4** or **4.5,** because of different N^+-H stretching available in the cytosine assemblies. The comparative overlay FTIR spectra of complex **4.3** and **4.4** are shown in Fig. 4.2.1a. The other interesting feature is that the complex **4.4** shows intense C=O stretching frequency at 1729 cm^{-1}, whereas in **4.3**, this stretching frequency appears at 1661 cm^{-1}. This is attributed to the hydrogen bond interactions in cytosine assemblies between the carbonyl and the amine group.

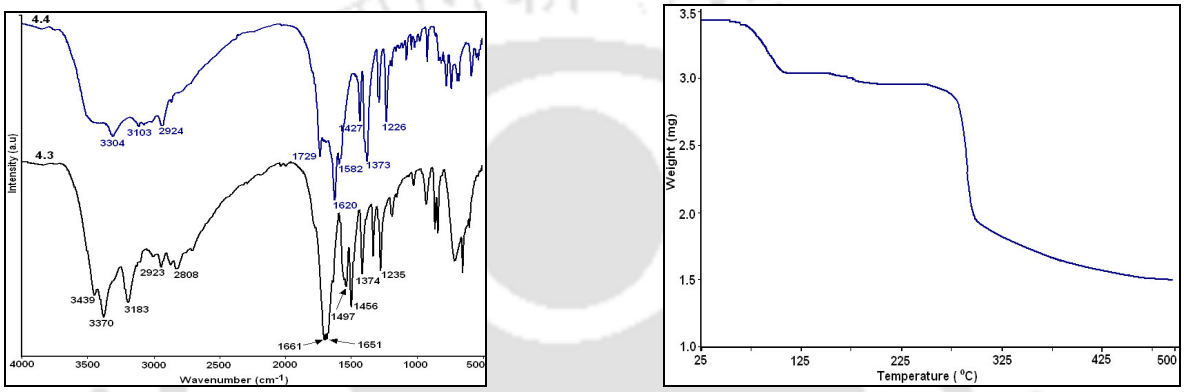

(a) (b)

Fig. 4.2.1: (a) Overlay FTIR spectra of complex **4.3** and **4.4,** (b) Thermogram of complex **4.3.**

The thermogravimetric analysis of each compound shows loss of water molecules and nucleobases on heating. The thermogram of complex **4.3** reveals that the weight loss occurs in four steps (Fig. 4.2.1b). The first two step is the loss of crystallized and coordinated water molecules that takes place in the range of 60-115 ºC (obsd. 8.8%, calcd. 9.4%) and 166-175 ºC respectively. The major weight change takes place in the third step where loss of the cytosine nucleobase occurs in the range of 275-320 ºC (obsd. 38.6%, calcd. 42.0%). Fourth step is not sharp but spreads over a temperature range 350-450 ºC which is ascribed due to decomposition of Mn(II) dipicolinate complex. It is to be mentioned that the loss of adenine nucleobase takes place at a lower temperature (170-270 ºC in complex **4.1**) than the cytosine nucleobase (275-320 ºC). These differences in weight loss spreading over the temperature range occur due to the differences in the packing pattern and variation of electrostatic interactions upon change of cations (metal or nucleobase). A low molar conductance value of 30.0 S cm^2 mol^{-1} is observed for complex **4.3**, whereas the complexes **4.1** and **4.2** exhibit

the molar conductance values of 205.0 and 201.0 S cm^2 mol^{-1} respectively in water. The later two values are slightly on the higher side for 1:2 electrolytes. The low conductance value for the complex **4.3** is attributed to the stability of the nucleobase assemblies in solution. Formation of such assemblies could reduce the ionic mobility of the charged species.

The crystal structure of *bis*-dipicolinate Mn(II) complex $(1H,3H\text{-cyt})_2[MnL_2(H_2O)]\cdot(cyt)_2\cdot 6H_2O$ (**4.3**) consists of two crystallographically independent cytosinium cations and two neutral cytosine molecules along with six water molecules (Fig. 4.2.2a). Besides two tridentate dipicolinate ligands coordinated with Mn(II), there is an aqua-ligand that occupies the seventh coordination site. This makes pentagonal bipyramidal geometry around the metal ion. The dihedral angle is 75.7º between the dipicolinates. In the complex, the neutral and protonated cytosines self-assemble to form dimer by three hydrogen bonds, two of which involve the N4 hydrogen bond donors and O2 hydrogen bond acceptors, while the third one is formed between the protonated N3 atom of one base and the unprotonated N3 site of the other base. Furthermore, the adjacent $CytHcyt^+$ pairs are held together by double N1-H···O=C hydrogen bonds leading to two different types of 1D planar supramolecular tetrameric ribbons with alternating neutral and protonated cytosine entities. The hydrogen bond parameters for this tetrameric cytosine ribbon are summarized in table 4.1. It is to be stressed that this self-assembled tetrameric ribbon with a dimension of 33.45 Å finally gets terminated *via* hydrogen bond interactions (N1-H···O=C; $d_{H\cdots A}$, 1.91 Å, $d_{D\cdots A}$, 2.77 Å; < D-H···A, 175°) with the complex anion (Fig. 4.2.2c). A similar complex that consists of both neutral and protonated cytosine was reported in $[Ni(nta)(H_2O)_2]\cdot(cytosinium)\cdot(cytosine)\cdot 2H_2O$ (where nta = nitrilotriacetate) [36]. The neutral and protonated cytosine form complementary base-pair through three hydrogen bonds as discussed above. The base-pair thus formed are linked through other adjacent similar pair resulting in an infinite hydrogen bonded tape-like molecular sheet passing through the layers of $[Ni(nta)(H_2O)_2]^-$. In contrast, we have observed two neutral and two protonated cytosine molecules in the Mn(II) dipicolinate complex, that formed tetrameric assembly. The metal oxalate complexes, $(1H,3H\text{-cyt})_2\,[M(ox)_2(H_2O)_2]$ [where M(II) = Mn, Co, Cu, Zn at +2 oxidation state] exhibits ribbon-like 1D supramolecular cytosinium aggregation stabilized by hydrogen bond between the –C=O and the amine group of adjacent cytosinium cations [25].

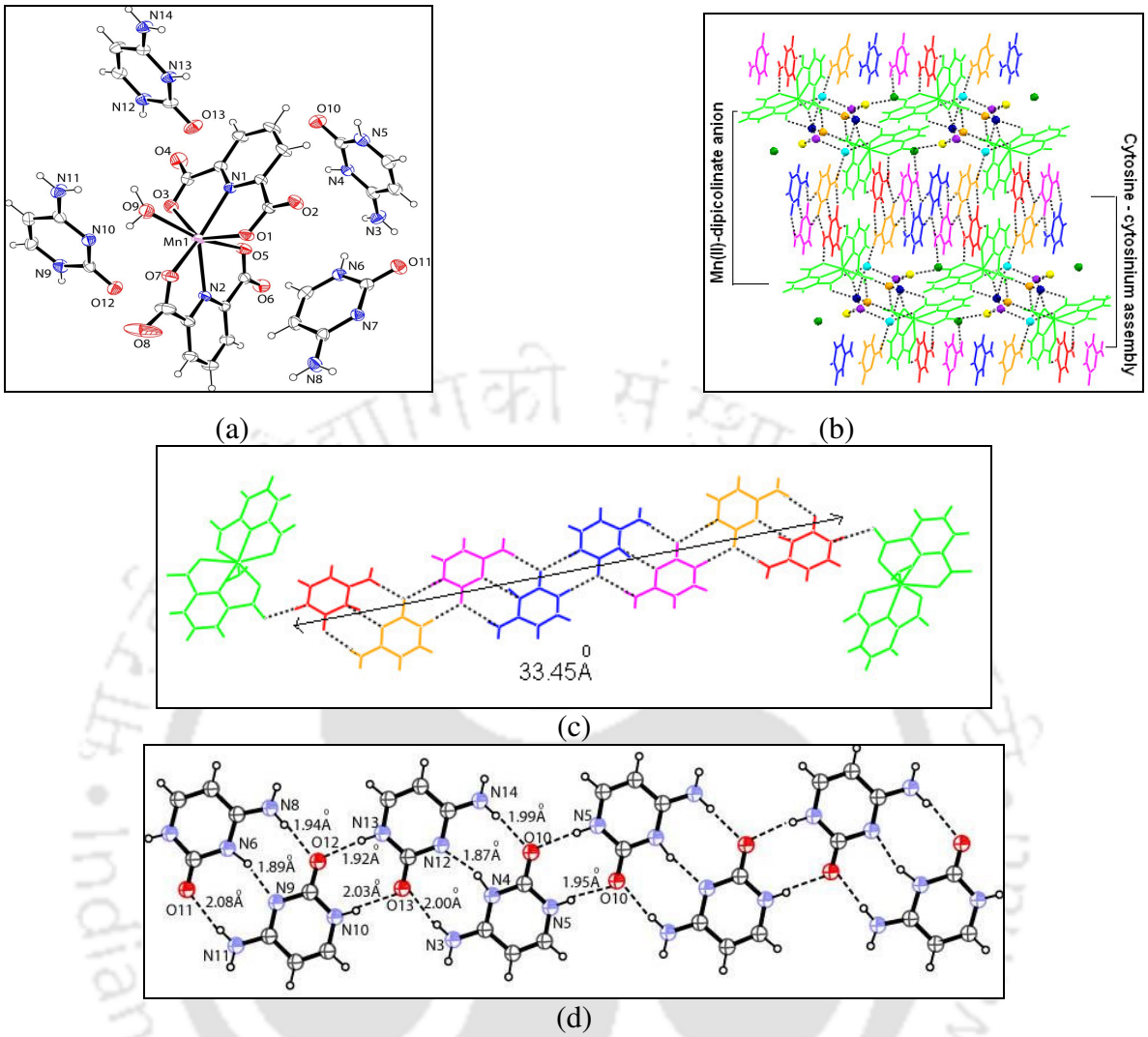

Fig. 4.2.2: (a) ORTEP of **4.3** (drawn with 50% thermal ellipsoids), (b) Hydrogen bond interactions in **4.3** along *a* axis, (c) Tetrameric cytosine - cytosinium ribbon terminated by Mn(II) dipicolinate anion, (d) Close view of tetrameric cytosine - cytosinium assembly.

In lattice, the complex **4.3** displays a supramolecular three-dimensional lamellar structure built up of Mn(II) dipicolinate anion and planar hydrogen bonded tetrameric 1D ribbon intercalated among them. The complex is further stabilized by face to face π-π interactions among the planar nucleobases and/or with the planar dipicolinate unit. The centroid to centroid distances of the aromatic rings of dipicolinate ligand with the neutral and protonated cytosine entities are 3.99 and 4.30 Å respectively. On the other hand, the π - π stacking distances (centroid to centroid) between the neutral and protonated cytosine

molecules are 3.60, 3.63 and 3.75 Å respectively. The crystallized water molecules exhibit hydrogen contact to both the metal dipicolinate anion as well as with tetrameric cytosine ribbon. The locations of the hydrogen atoms in the protonated cytosine are justified by difference Fourier synthesis map. It is also determined by complementary hydrogen bonding interactions between the cationic and neutral cytosine molecule in the crystal structure. As the neutral and protonated cytosine molecules form a dimer, it is likely that these protons are disordered over two different nitrogen atoms. This is also evident from the relatively longer $–N^{+}$-H bond distances, 0.97 and 0.99 Å respectively observed in the two symmetrically independent protonated cytosine molecules (Table 4.1).

The *bis*-dipicolinate complexes of Cu(II) or Zn(II) with 1H,3H-cytosinium cation namely $[1H, 3H\text{-cyt}]_2[CuL_2]\cdot 5H_2O$ **(4.4)** and $[1H, 3H\text{-cyt}]_2[ZnL_2]\cdot 5H_2O$ **(4.5)** has two cytosinium cations per $[ML_2]^{2-}$ complex anion along with five lattice water molecules. Apart from electrostatic and hydrogen bond, face to face π-π interactions between the planar protonated cytosinium cation and the aromatic ring of dipicolinate complex also contribute to the stability of these complexes. The two cytosinium cations are stacked parallel to the aromatic ring of dipicolinate counterpart of the $[ML_2]^{2-}$. The stacks are comprised of partially slipped aromatic rings with centroid to centroid π-π distances measured as 3.98 and 4.06 Å respectively. Since the complexes **4.4** and **4.5** have similar structural features only the structure of complex **4.5** is shown in Fig. 4.2.3a. The crystal packing of the complexes exhibit lamellar inorganic-organic hybrid network built up of anionic sheets of Zn(II) dipicolinates and hydrogen bonded cationic cytosines intercalated among them. In the lattice, the cytosinium cation interacts with the adjacent crystallographically non-equivalent cation through $–NH_2$ and –C=O hydrogen bonds. This leads to a tetramer when lattice water molecules are considered as part of the assembly (Fig. 4.2.3b). The cation further interacts with the complex anion either through the $–N^{+}$-H or through the $–NH_2$ group. The crystallized water molecules complete the remaining donor / acceptor functionality bridging the anion / cation or the cation / cation entity. In a similar supramolecular complex, $[cytH+]_2(I_5^-)_2(H_2O)_3$, the hydrogen bonded cytosinium-water ribbons and combined polyiodide chains built a sheet-like structure [34]. In an another example, the cytosinium cation of complex $[Ni(nta)(H_2O)_2]\cdot(cytosinium)\cdot 2H_2O$, is anchored to the $[Ni(nta)(H_2O)_2]$ by

triple hydrogen bonds. In that complex, the cytosinium cation form a hydrogen bonded cyclic tetramer in association with the complex anion [36].

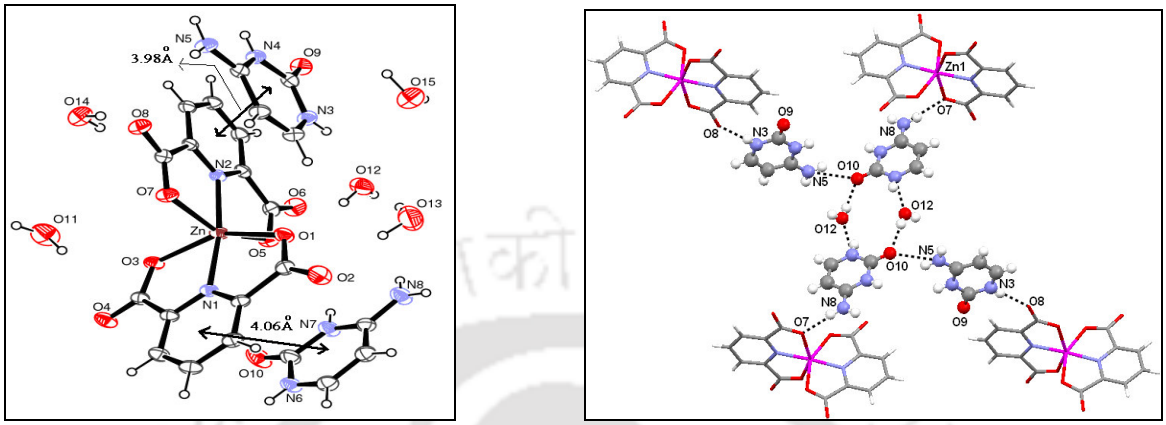

(a) (b)

Fig. 4.2.3: (a) ORTEP of **4.5** (drawn with 50% thermal ellipsoids), (b) View showing hydrogen bond interactions of cytosinium cation with Zn(II) dipicolinates and lattice water molecules in **4.5**.

4.3: Intercalation of discrete adeninium or cytosinium cations in layers of polymeric metal quinolinates

Quinolinic acid or 2,3-pyridinedicarboxylic acid, one of the isomer of dipicolinic acid, is widely used to construct large number of coordination complexes [37,38]. It generally forms relatively rigid polymeric frameworks with metal ions such as Mn(II) and Cu(II). In this section, the intercalations of the protonated nucleobases in layers of these polymeric frameworks are studied. The crystal structure of these complexes consists of a cationic nucleobase, metal quinolinate polymeric complex along with crystallized water molecules. In the complex $\{[1H, 9H\text{-ade}]_2[MnL_2]\cdot 4H_2O\}_n$, (**4.6**) (where L = 2,3-pyridinedicarboxylate), the 1H,9H-adeninium cation is intercalated by polymeric Mn(II) quinolinates. The cation interacts through hydrogen bonding with the carboxylate atoms ($d_{D\ldots H}$, 1.65 Å, $d_{D\cdots A}$, 2.59 Å; < D-H$\cdots$A, 161º) of the polymeric complex anion. The nucleobase is further stabilized by strong π-π stacking interactions among them. The centroid to centroid stacking distances between two such rings are observed as 3.34 Å and 3.89 Å respectively (Fig. 4.3.1a). Thus, it can be regarded as 1D adeninium assembly formed *via* face to face stacking interactions.

The crystallized water molecules further contribute to the stability of these complexes bridging the oppositely charged species through hydrogen bond.

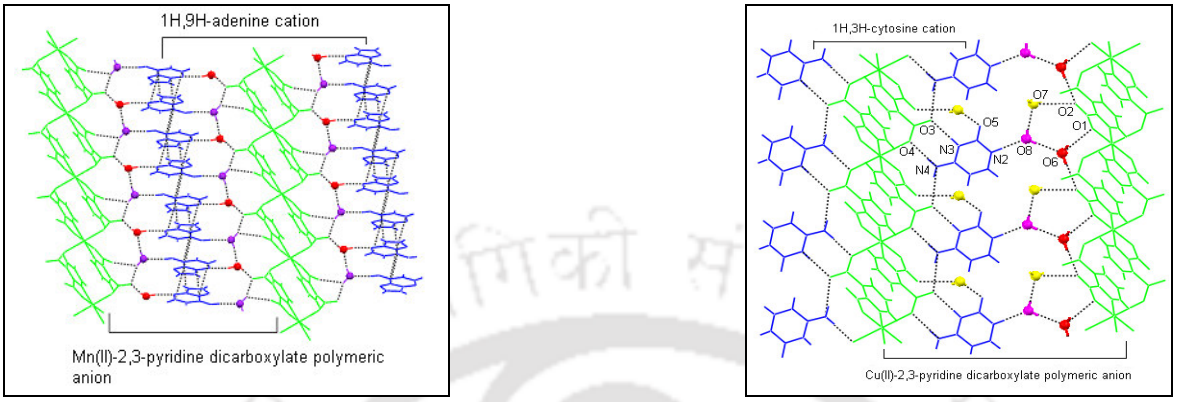

(a) (b)

Fig. 4.3.1: (a) Hydrogen bond and π-stacked adeninium cations in layers of Mn(II) quinolinates, (b) Hydrogen bonded cytosinium cations in layers of Cu(II) quinolinates.

The complex $\{[1H,3H\text{-cyt}]_2[CuL_2]\cdot 6H_2O\}_n$ (**4.7**) intercalates 1H,3H-cytosinium cation in polymeric layers of Cu(II) quinolinates by electrostatic and hydrogen bond interactions. The amine group and N3H atom of cytosine interacts with carboxylate group of polymeric complex but no π-π stacking interactions exist among the nucleobases. The C=O group and N1H atom of cytosinium cation interacts with crystallized water molecules. The rigid polymeric complexes irrespective of metal ions show the intercalation of the stable tautomeric form of the nucleobase in the cationic layers of the complexes.

4.4: Intercalation of cytosinium assemblies in layers of adipic acid, citric acid

Several attempts have been made to synthesize supramolecular complexes in the analogues organic systems, using pyridinedicarboxylic acids and nucleobases, but the crystallization was not successful as these complexes led to microcrystalline solids. However, we succeed to synthesize cytosine complexes with flexible organic molecules such as adipic acid and citric acid. Both the adipic acid and citric acid (Fig. 4.4.1a) are considered as safe excipients and therefore widely used to synthesize multi-component crystals with large number of active pharmaceutical ingredients (API) [39-41]. In this study, the adipic acid-cytosine (1:2) supramolecular complex (**4.8**) shows partial proton transfer from the acid to the cytosine

base. The partially protonated cytosines form a dimeric or duplex hydrogen bonded assembly *via* triple hydrogen bonds. The dimeric assembly is intercalated in layers of adipic acid infinite chain (Fig. 4.4.1a-b). The hydrogen bonded interactions of the cytosine duplex assembly have already been discussed in section **4.2**. The H-atom attached to N3 atom of cytosinium cation is disordered over two positions. A similar disordered situation of cytosine assembly has been elaborated in the cocrystal with decavanadate anion, $Na_3[V_{10}O_{28}][cytH]_3$ $[cyt]_3 \cdot 10H_2O$ based on charge density analysis and topological analysis [42]. It has been stated that the H-atom is statistically distributed between the two cytosine molecules at high temperature.

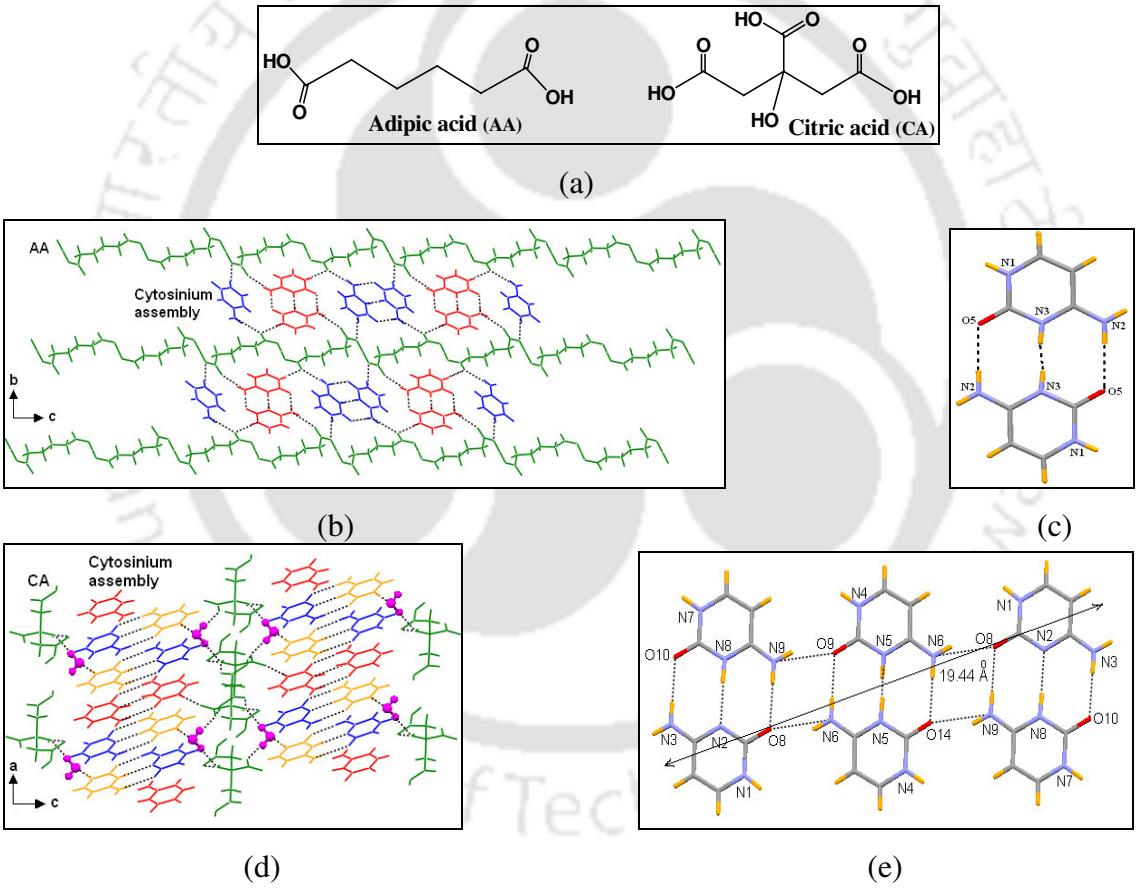

Fig. 4.4.1: (a) Organic host molecules studied, (b) Hydrogen bond interactions of cytosinium assembly with adipic acid viewed along *a* axis, (c) Close view of duplex assembly of cytosinium**,** (d) Hydrogen bond interactions of trimeric cytosine-cytosinium assembly in layers of citric acid viewed along *b* axis, (e) Close view of trimeric cytosine-cytosinium assembly.

In the complex described in this chapter, adipic acid adopts a conformation different from its crystal structure in its unsolvated form. The acidic protons occupy an inversion center leading to a polymeric 1D chain of adipic acid. The interaction of cytosine with adipic acid takes place through amine group and N1H protons. The cytosine assemblies are further stabilized by face to face π-π interactions (centroid to centroid distance ~ 3.65 Å).

Citric acid-cytosine complex (1:3) (**4.9**) shows the presence of partially ionized citric acid and protonated and neutral cytosine molecules in the crystal structure. These protonated and neutral cytosine molecules form two different triple hydrogen bonded self-assemblies. These cytosine-cytosinium assemblies are further held together by double N1H···O=C or N4H···O=C hydrogen bonds leading to a planar trimeric motif with a length of 19.44 Å intercalated between layers of citric acid (Fig. 4.4.1c). The crystallized water molecule is encapsulated within the parallel layers of partially ionized citric acid and cytosinium assemblies. They are hydrogen bonded to the N1H proton of cytosine, oxygen atoms of 3-carboxy group and hydroxyl group of two adjacent citric acid molecules. It is to be mentioned that the crystal structures consists of equal numbers of cytosine molecules corresponding to the acid groups irrespective of their neutral or protonated form. Flexible nature of the organic acids allow cytosine molecules not only to interact with the acids but also among themselves to form duplex assemblies *via* triple hydrogen bond. In a study by Pedireddi and coworkers showed formation of 3D assemblies of molecular adducts of cytosine with benzoic acid, phthalic acid and isophthalic acid [43]. A tetrameric assembly based on cytosine duplex was observed in 1:1 cytosine-benzoic acid adduct, whereas the phthalic acid and isophthalic acid stabilized the infinite cytosine assembles based on similar hydrogen bonded duplex assembly. Thus by correlating the patterns obtained with adipic acid and citric acid in this study with other assemblies available in literature, it appears that cytosine prefer dimeric triple hydrogen bonded assembly in the dicarboxylic acid complexes.

We also anticipated similar intercalation chemistry with other two nucleobases, guanine and thymine but unfortunately, we were not successful. It has been seen that compared to adenine and cytosine, supramolecular complexes with guanine and thymine are less [44-46]. This may be due to insoluble nature of guanine and weak basicity of thymine nucleobase [47]. Attempts to synthesize complexes with guanine, dissolving in dilute hydrochloric acid,

followed by treatment with metal dipicolinate complexes led to crystallize them independently. Thymine also did not bind with the metal containing dicarboxylic acid starting materials. We are interested on other host molecules with different functional moieties that could interact with guanine and thymine as a future prospectus.

4.5: Conclusion

We have demonstrated the intercalation of hydrogen bonded infinite chain of adeninium cations having two non-equivalent 1H,9H and 3H,7H-adeninium cations at alternating positions in layers of Mn(II)/Cu(II) dipicolinates. This is the first solid-state characterized 1H,9H and 3H,7H-adeninium tautomer in relatively rigid dipicolinate frameworks. We have also established the stabilization of adeninium cation in rigid 1D coordination polymer of Mn(II) quinolinates. The other interesting finding of this chapter was the intercalation of different types of hydrogen bonded cytosine assemblies such as discrete, dimeric, trimeric and tetrameric assemblies in layers of various host molecules. The discrete cations of cytosine are stabilized by electrostatic, hydrogen bond and stacking interactions within the polymeric inorganic layers of Cu(II) quinolinates. Intercalations of dimeric and trimeric assemblies were observed in flexible organic host molecules such as adipic acid and citric acid respectively. Intercalation of tetrameric planar 1D ribbon formed by neutral and 1H,3H-cytosinium cation was established in a seven-coordinated Mn(II) dipicolinate complex. Thus, it appears difficult to understand the nature of assembly formation in a particular metal complex or in an analogues organic system. However, it can be predicted that the assemblies are dependent on the central metal ions and the nature of host molecules. Further, crystal packing and hydrogen bonding functionality also plays key role in the formation of different types of nucleobase assemblies. This chapter therefore demonstrates generation of different types of nucleobase assemblies with definite dimension and shape in confined environment. It may further contribute to the molecular recognition processes of the cations of adenine or cytosine by these different artificial host molecules.

4.6: Experimental section

Detailed synthetic methodologies for the synthesized complexes are given below. Analytical as well as spectroscopic data are also listed along with each of the complexes.

4.6.1: [1H, 9H-ade][3H, 7H-ade][MnL_2]·$3H_2O$ (4.1) and [1H, 9H-ade][3H, 7H-ade] [CuL_2]·$3H_2O$ (4.2)

To a solution of dipicolinic acid (0.334 g, 2.0 mmol) dissolved in methanol (20 ml) a solution of manganese(II) acetate tetrahydrate (0.245 g, 1.0 mmol) or copper(II) acetate monohydrate (0.199 g, 1.0 mmol) was added. Depending upon the metal ion, different coloured solids were obtained; for example, white or blue precipitate for manganese(II) or copper(II) respectively. The reaction mixture was stirred for half an hour; 10ml of solution of adenine (0.27 g, 2.0 mmol dissolved in 50% methanol) was added in small portions to the respective precipitate and stirred. The solution was left overnight at room temperature. A pale yellow (for manganese) or blue (for copper) precipitate obtained from the reaction mixture were filtered, dried and crystallized from Milli Q water.

Complex **4.1:** Isolated yield: 45%. Elemental anal calcd for $C_{24}H_{24}MnN_{12}O_{11}$, C, 40.47; N, 23.61; H, 3.37%; found C, 40.50; N, 23.48; H, 3.34%. IR (KBr, cm^{-1}): 3410 (b, s), 1621 (s), 1590 (w), 1424 (w), 1374 (s), 1277 (w), 1085 (w). Molar conductance: 205.0 S cm^2 mol^{-1} in water. μ_{eff}. at 298 K: 5.42 BM. Thermal analysis: decomposition range: ~ 60-139 ºC (evaporation of three water molecules of crystallization).

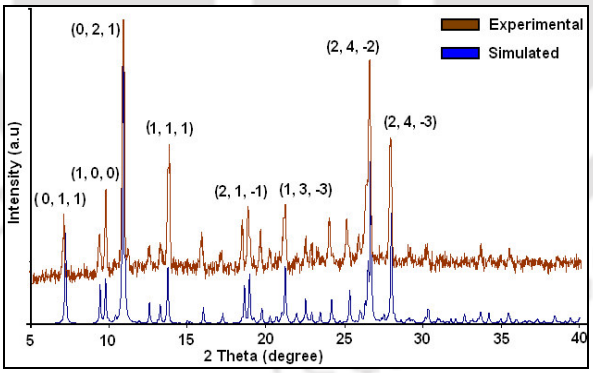

Fig. 4.6.1: PXRD pattern of complex **4.1**

Complex **4.2**: Isolated yield: 48%. Elemental anal calcd for $C_{24}H_{24}CuN_{12}O_{11}$, C, 40.00; N, 23.33; H, 3.33%; found C, 39.78; N, 23.21; H, 3.24%. IR (KBr, cm^{-1}): 3413 (b, s), 1624 (s), 1591 (w), 1426 (w), 1377 (s), 1279 (w), 1088 (w). Molar conductance: 201.0 S cm^2 mol^{-1} in water. μ_{eff}. at 298 K: 1.65 BM. Vis (H_2O) λ_{max}: 772.0 nm; ε = 57.5 M^{-1} cm^{-1}. Thermal

analysis: decomposition range: ~ 50-136 ºC (loss of three water molecules of crystallization).

4.6.2: [1H,3H-cyt]$_2$[MnL$_2$(H$_2$O)]·(cyt)$_2$·6H$_2$O (4.3), [1H,3H-cyt]$_2$[CuL$_2$]·5H$_2$O (4.4) and [1H,3H-cyt]$_2$[ZnL$_2$]·5H$_2$O (4.5)

The dipicolinic acid (0.334 g, 2.0 mmol), manganese(II) acetate tetrahydrate (0.245 g, 1.0 mmol) or copper(II) acetate monohydrate (0.199 g, 1.0 mmol) or zinc(II) acetate dihydrate (0.219 g, 1.0 mmol) were reacted in 20 ml methanol for half an hour. To the precipitate obtained in each case, 10ml of cytosine (0.22 g, 2.0 mmol dissolved in 20% methanol) solution was added in small portion. The reaction was left overnight at room temperature. The white, blue and white precipitates obtained were filtered, dried and kept for crystallization in Milli Q water. White, blue and colourless crystals of manganese, copper and zinc complexes respectively were formed in 2-3 days.

Complex **4.3**: Isolated yield: 42%. Elemental anal calcd for $C_{30}H_{42}MnN_{14}O_{19}$, C, 37.59; N, 20.47; H, 4.38%; found C, 37.54; N, 20.40; H, 4.40%. IR (KBr, cm^{-1}): 3370 (s), 3183 (s), 2923 (w), 2808 (w), 1661 (b, s), 1651 (b, s), 1497 (m), 1456 (s), 1374 (m), 1290 (m), 1235 (m), 791 (m). μ_{eff}. at 298 K: 5.38 BM. Molar conductance: 30.0 S cm^2 mol^{-1} in water. Thermal analysis: decomposition range: ~ 65-130 ºC (loss of six water molecules of crystallization), further decomposition occurs at ~ 166 ºC (loss of coordinated water molecule).

Complex **4.4**: Isolated yield: 74%. Elemental anal calcd for $C_{22}H_{28}CuN_8O_{15}$, C, 37.29; N, 15.82; H, 3.95%; found C, 37.22; N, 15.74; H, 3.84%. IR (KBr, cm^{-1}): 3306 (b), 3102 (w), 2930 (w), 1729 (m), 1614 (s), 1581 (m), 1422 (m), 1370 (s), 1279 (w), 1228 (m), 774 (w). Molar conductance: 185.0 Scm^2mol^{-1} in water. μ_{eff}. at 298 K: 1.60 BM. Vis (H_2O) λ_{max} 774.0 nm; ε = 70.0 M^{-1} cm^{-1}. Thermal analysis: decomposition range: ~ 66-115 ºC (loss of five water molecules of crystallization).

Complex **4.5**: Isolated yield: 72%. Elemental anal calcd for $C_{22}H_{28}Zn\ N_8O_{15}$, C, 37.18; N, 15.78; H, 3.94%; found C, 37.07; N, 15.67; H, 3.79%. IR (KBr, cm^{-1}): 3304 (b), 3103 (w), 2924 (w), 1729 (m), 1620 (s), 1582 (w), 1427 (m), 1373 (s), 1284 (m), 1226 (m), 733 (w). ^{1}HNMR (D_2O, 400 MHz, ppm): 8.4 (2H, t, J = 6.8 Hz), 8.35 (4H, d, J = 7.2 Hz), 7.6 (2H, d, J = 7.6 Hz), 6.0 (2H, d, J = 7.2 Hz). Molar conductance: 181.0 S cm^2 mol^{-1} in water.

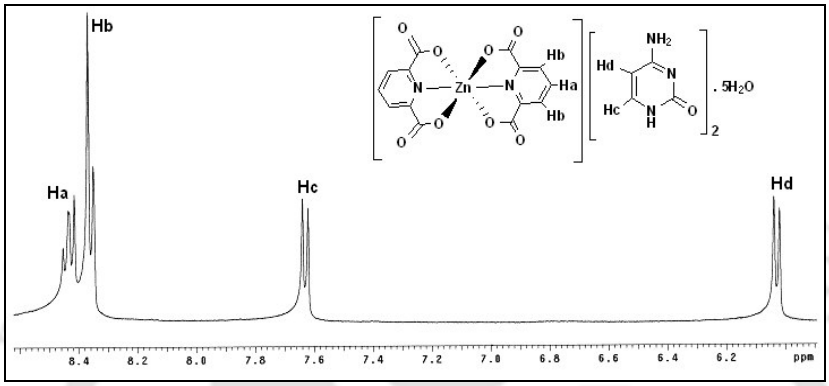

Fig. 4.6.2: ^{1}HNMR (in D_2O) spectra of complex **4.5**

4.6.3: {[1*H*, 9*H*-ade]$_2$[MnL_2].4H_2O}$_n$ (4.6) and {[1*H*, 3*H*-cyt]$_2$[CuL_2].6H_2O}$_n$ (4.7)

To a solution of quinolinic acid (0.334 g, 2.0 mmol) dissolved in methanol (20 ml), a solution of copper(II) acetate monohydrate (0.199 g, 1.0 mmol) and manganese(II) acetate tetrahydrate (0.245 g, 1.0 mmol)) was added respectively. Depending upon the metal ion, different coloured precipitates were obtained; for example, pale yellow for manganese(II) and blue precipitate for copper (II). The reaction mixture was stirred for half an hour. 10ml of adenine (0.27 g, 2.0 mmol dissolved in 50% methanol) and cytosine (0.22 g, 2.0 mmol dissolved in 50% methanol) was added in small portions to the respective precipitates and stirred. The solutions were left overnight at room temperature. Pale yellow precipitate for manganese and blue precipitate for copper obtained were filtered, dried and crystallized from Milli Q water.

Complex **4.6**: Isolated yield: 68%. Elemental anal calcd for $C_{24}H_{26}MnN_{12}O_{12}$, C, 39.48; N, 23.03; H, 3.56%; found C, 38.86; N, 22.67; H, 3.51%. IR (KBr, cm^{-1}): 3355 (m), 3190 (s), 2990 (s), 1670 (s), 1617 (m), 1586 (w), 1548 (w), 1464 (m), 1409 (w), 1382 (m), 1245 (m),

1170 (m), 1039 (w), 875 (m), 808 (s). Molar conductance: 101.0 S cm^2 mol^{-1} in water. Thermal analysis: ~ 55-90 ºC (loss of crystallization water molecules).

Complex **4.7**: Isolated yield: 65%. Elemental anal calcd for $C_{22}H_{30}CuN_8O_{16}$, C, 52.90; N, 15.43; H, 4.13%; found C, 52.58; N, 15.24; H, 4.09%. IR (KBr, cm^{-1}): 3501 (w), 3335 (b, s), 3199 (m), 3094 (w), 1646 (b, s), 1591 (w), 1517 (m), 1459 (m), 1365 (s), 1236 (m), 1117 (m), 831 (w). Molar conductance: 105.0 S cm^2 mol^{-1} in water. Vis (H_2O) λ_{max}: 772.0 nm; ε = 77.5 M^{-1} cm^{-1}. Thermal analysis: ~ 60-105 ºC (loss of crystallization water molecules).

4.7: Crystallographic data and refinement parameters for the complexes 4.1-4.5

Compound No.	**4.1**	**4.2**	**4.3**	**4.4**	**4.5**
Formula	$C_{24}H_{24}MnN_{12}O_{11}$	$C_{24}H_{24}CuN_{12}O_{11}$	$C_{30}H_{42}MnN_{14}O_{19}$	$C_{22}H_{28}CuN_8O_{15}$	$C_{22}H_{28}N_8O_{15}Zn$
Formula wt.	711.49	720.09	957.62	708.06	709.89
Crystal system	Monoclinic	Monoclinic	Triclinic	Triclinic	Triclinic
Space group	*P2₁/c*	*P2₁/c*	*P-1*	*P-1*	*P-1*
a (Å)	9.707(2)	9.6497(4)	10.5913(4)	9.4706(4)	9.4076(3)
b (Å)	18.695(3)	18.7034(7)	13.0090(4)	11.8131(4)	11.8945(5)
c (Å)	17.370(3)	17.8872(6)	16.5020(5)	13.4429(5)	13.4682(5)
α (deg)	90.00	90.00	73.770(2)	77.635(2)	77.712(2)
β (deg)	112.008(14)	116.027(2)	79.787(2)	84.664(2)	84.142(2)
γ (deg)	90.00	90.00	73.752(2)	82.454(2)	82.466(2)
V (Å^3)	2922.5(9)	2900.93(19)	2083.73(12)	1453.07(10)	1455.55(9)
Z	4	4	2	2	2
D_{calc} (gcm^{-3})	1.617	1.649	1.507	1.618	1.620
μ (mm^{-1})	0.534	0.836	0.410	0.839	0.931
F(000)	1460	1476	970	730	732
Total no. of reflns	21547	19237	23178	19655	9965
Independent reflns.	5030	5112	7043	7125	4926
$\theta_{max.}$	1.67 - 25.00	1.67 - 25.00	1.29 - 25.00	1.55 - 28.35	2.13 - 25.00
Ranges (h, k, l)	-11 ≤ h ≤ 11 -21 ≤ k ≤ 22 -14 ≤ l ≤ 20	-11 ≤ h ≤ 11 -22 ≤ k ≤ 21 -21 ≤ l ≤ 21	-12 ≤ h ≤ 12 -15 ≤ k ≤ 15 -19 ≤ l ≤ 19	-12 ≤ h ≤ 12 -15 ≤ k ≤ 15 -17 ≤ l ≤ 17	-11 ≤ h ≤ 11 -14 ≤ k ≤ 14 -15 ≤ l ≤ 15
Complete-ness to 2θ (%)	97.6	99.9	95.8	98.2	96.2
Data / restraints / parameters	5030 / 0 / 434	5112 / 2 / 466	7043 / 0 / 590	7125 / 4 / 495	4926 / 4 / 467
GOF (F^2)	0.988	0.992	1.007	0.993	1.013
R_1, wR_2 [$I > 2\sigma(I)$]	0.0774, 0.1803	0.0384, 0.0829	0.0606, 0.2155	0.0321, 0.0890	0.0335, 0.0923
R_1, wR_2 (all data)	0.1029, 0.2491	0.0637, 0.0937	0.0892, 0.2399	0.0372, 0.0916	0.0376, 0.0950
Largest diff peak/hole (e Å^{-3})	0.405 / -0.573	0.356 / -0.200	0.967 / -0.881	0.407 / -0.405	0.431 / -0.390

Continued….

Compound No.	**4.6**	**4.7**	**4.8**	**4.9**
Formula	$C_{24}H_{26}MnN_{12}O_{12}$	$C_{22}H_{30}CuN_8O_{16}$	$C_{14}H_{21}N_6O_6$	$C_{18}H_{26}N_9O_{11}$
Formula wt.	729.51	726.08	369.37	544.48
Crystal system	Triclinic	Triclinic	Triclinic	Triclinic
Space group	*P-1*	*P-1*	*P-1*	*P-1*
a (Å)	6.6148(7)	6.5329(3)	5.31190(10)	8.1285(8)
b (Å)	8.9184(13)	8.1345(3)	10.0939(3)	9.7220(9)
c (Å)	13.4019(13)	14.0855(5)	16.3001(4)	15.3195(15)
α (deg)	77.094(8)	90.364(2)	74.5220(10)	98.673(6)
β (deg)	80.684(8)	92.104(2)	84.0300(10)	98.892(6)
γ (deg)	75.215(8)	92.058(2)	81.0100(10)	101.946(6)
V (Å^3)	740.51(15)	747.52(5)	830.15(4)	1149.06(19)
Z	1	1	2	2
D_{calc} (gcm^{-3})	1.636	1.613	1.478	1.574
μ (mm^{-1})	0.532	0.820	0.117	0.132
F(000)	375	375	390	570
Total no. of reflns	8023	7905	9898	13704
Independent reflns.	2517	2528	2720	3774
$\theta_{max.}$	1.57 - 24.99	1.45-25.00	1.30 - 24.50	1.37 - 24.50
Ranges (h, k, l)	$-7 \le h \le 7$ $-10 \le k \le 10$ $-15 \le l \le 12$	$-7 \le h \le 7$ $-9 \le k \le 9$ $-16 \le l \le 15$	$-6 \le h \le 6$ $-11 \le k \le 11$ $-18 \le l \le 18$	$-9 \le h \le 9$ $-11 \le k \le 11$ $-17 \le l \le 17$
Completeness to 2θ (%)	96.4	95.9	98.4	98.7
Data /restraints/ parameters	2517 / 4 / 267	2528 / 0 / 247	2720 / 0 / 253	3774 / 0 / 380
GOF (F^2)	1.049	1.069	1.178	0.964
R_1, wR_2 [$I > 2\sigma(I)$]	0.0697, 0.2153	0.0403, 0.1125	0.0388, 0.0998	0.0518, 0.1394
R_1, wR_2 (all data)	0.0851, 0.2433	0.0428, 0.1157	0.0403, 0.1008	0.0879, 0.1664
Largest diff peak/hole (e Å^{-3})	0.888 / -0.522	0.557 / -0.683	0.186 / -0.286	0.243 / -0.252

4.8: Comparative bond distances (Å) and bond angles (º) of the complexes 4.1 - 4.5

Bond parameters	For **4.1**; M = Mn	For **4.2**; M = Cu	Bond parameters	For **4.1**; M = Mn	For **4.2**; M = Cu
M(1)-N(1)	2.144(9)	1.939(2)	<O(1)-M(1)-O(7)	93.5(3)	93.93(8)
M(1)-N(2)	2.142(9)	1.950(2)	<O(5)-M(1)-O(7)	144.6(3)	154.72(7)
M(1)-O(5)	2.159(8)	2.213(2)	<N(1)-M(1)-O(7)	102.4(3)	98.10(9)
M(1)-O(1)	2.179(7)	2.109(2)	<N(2)-M(1)-O(7)	71.4(4)	77.74(9)
M(1)-O(3)	2.232(7)	2.175(2)	<O(1)-M(1)-O(3)	145.7(3)	156.10(8)
M(1)-O(7)	2.253(8)	2.184(2)	<O(5)-M(1)-O(3)	95.6(3)	90.88(8)
<N(2)-M(1)-N(1)	166.1(4)	175.64(11)	<N(1)-M(1)-O(3)	72.1(3)	77.33(10)
<N(2)-M(1)-O(5)	74.2(4)	76.97(9)	<N(2)-M(1)-O(3)	95.9(3)	101.52(8)
<N(1)-M(1)-O(5)	113.0(3)	107.18(9)	<O(5)-M(1)-O(1)	95.4(3)	91.25(8)
<N(2)-M(1)-O(1)	118.4(3)	102.15(9)	<N(1)-M(1)-O(1)	73.8(3)	79.30(10)

Bond parameters	For **4.3**	Bond parameters	For **4.3**
Mn(1)-N(1)	2.234(4)	<O(1)-Mn(1)-O(7)	78.33(15)
Mn(1)-N(2)	2.271(4	<O(5)-Mn(1)-O(7)	134.68(14)
Mn(1)-O(5)	2.456(4)	<N(1)-Mn(1)-O(7)	139.25(16)
Mn(1)-O(1)	2.214(4)	<N(2)-Mn(1)-O(7)	69.34(15)
Mn(1)-O(3)	2.395(4)	<O(1)-Mn(1)-O(3)	140.89(14)
Mn(1)-O(7)	2.419(4)	<O(5)-Mn(1)-O(3)	76.38(15)
Mn(1)-O(9)	2.221(5)	<O(1)-Mn(1)-O(9)	102.88(18)
<N(2)-Mn(1)-N(1)	141.10(17)	<N(1)-Mn(1)-O(3)	69.38(15)
<N(2)-Mn(1)-O(5)	67.33(15)	<N(2)-Mn(1)-O(3)	112.37(16)
<N(1)-Mn(1)-O(5)	76.06(15)	<O(5)-Mn(1)-O(1)	95.59(16)
<N(2)-Mn(1)-O(1)	98.76(15)	<N(1)-Mn(1)-O(1)	71.52(14)
<O(9)-Mn(1)-N(1)	90.45(16)	<O(9)-Mn(1)-N(2)	128.52(14)
<O(9)-Mn(1)-O(3)	76.36(16)	<O(9)-Mn(1)-O(7)	70.02(15)

Bond parameters	For **4.4;** M = Cu	For **4.5**; M= Zn	Bond parameters	For **4.4**; M=Cu	For **4.5**; M= Zn
M(1)-N(1)	1.9580(12)	2.0168(19)	<O(1)-M(1)-O(7)	91.06(5)	92.72(6)
M(1)-N(2)	1.9279(12)	2.0199(19)	<O(5)-M(1)-O(7)	157.70(5)	151.87(7)
M(1)-O(5)	2.1215(12)	2.1478(15)	<N(1)-M(1)-O(7)	104.37(5)	100.53(6)
M(1)-O(1)	2.2819(12)	2.1292(14)	<N(2)-M(1)-O(7)	79.05(5)	75.20(6)
M(1)-O(3)	2.2227(12)	2.2109(15)	<O(1)-M(1)-O(3)	153.38(4)	152.72(7)
M(1)-O(7)	2.1275(12)	2.2487(14)	<O(5)-M(1)-O(3)	93.87(5)	94.06(6)
<N(2)-M(1)-N(1)	175.78(5)	171.16(6)	<N(1)-M(1)-O(3)	77.40(5)	75.23(6)
<N(2)-M(1)-O(5)	78.71(5)	77.14(7)	<N(2)-M(1)-O(3)	105.24(5)	97.19(6)
<N(1)-M(1)-O(5)	94.86(5)	107.56(6)	<O(5)-M(1)-O(1)	97.92(5)	91.98(6)
<N(2)-M(1)-O(1)	101.11(5)	110.09(7)	<N(1)-M(1)-O(1)	76.52(5)	77.58(7)

References:

[1] J. Sponer, J. Leszczynski, P. Hobza, Biopolymers 61 (2002) 2002.

[2] F. Turecek, X. Chen, J. Am. Soc. Mass Spectrom. 16 (2005) 1713.

[3] C.E. Crespo-Hernandez, B. Cohen, P.M. Hare, B. Kohler, Chem. Rev. 104 (2004) 1977.

[4] H. Chen, L. Shuhua, J. Phys. Chem. A 109 (2005) 8443.

[5] V.A. Bloomfield, D.M. Crothers, I. Tinoco, Jr., Nucleic Acids: Structures, Properties, and Functions, University Science Books, Sausalito, CA, 2000.

[6] Y. Boulard, J.A. Cognet, G.V. Fazakerly, J. Mol. Biol. 268 (1997) 331.

[7] D. Vlieghe, L.V. Meervalt, A. Dautant, B. Gallois, C. Precigoux, O. Kennard, Science 273 (1996) 1702.

[8] M. Wu, J.A. McDowell, D.H. Turner, Biochemistry 34 (1995) 3204.

[9] K. Gehring, J.L. Leroy, M. Gueron, Nature 363 (1993) 561.

[10] J.M. Lehn, Supramolecular Chemistry, VCH, Weinheim, p. 121, 1995.

[11] G. Gottarelli, S. Masiero, E. Mezzina, S. Pieraccini, J.P. Rabe, P. Samori, G.P. Spada, Chem. Eur. J. 6 (2000) 3242.

[12] S.J. Sowerby, M. Edelwirth, W.M. Keck, J. Phys. Chem. B. 102 (1998) 5914.

[13] B. Lippert, Progress in Inorganic Chemistry; K.D. Karlin (ed.); John Wiley and Sons: New York, Vol. 54, pp 385-447, 2005.

[14] H. Sigel, Pure Appl. Chem. 76 (2004) 1869.

[15] A.D. Richards, A. Rodger, Chem. Soc. Rev. 36 (2007) 471.

[16] H.T. Chifotides, K.R.Dunbar, Acc. Chem. Res. 38 (2005) 146.

[17] J.A.R. Navarro, B. Lippert, Coord. Chem. Rev. 222 (2001) 219.

[18] C. Fonseca-Guerra, F.M. Bickelhaupt, S. Saha, F.J. Wang, Phys. Chem. A 110 (2006) 4012.

[19] A.K. Vrkic, T. Taverner, P.F. James, A.J. O'Hair, Dalton Trans. (2004) 197.

[20] M. Hanus, M. Kabelac, J. Rejnek, F. Ryjacek, P. Hobza, J. Phys. Chem. B 108 (2004) 2087.

[21] M. Legraverend, D.S. Grierson, Bioorg. Med. Chem. 14 (2006) 3987.

[22] C.S. Purohit, S. Verma, J. Am. Chem. Soc. 128 (2006) 400.

[23] J.P. García-Teran, O. Castillo, A. Luque, U. García-Couceiro, P. Roman, F. Lloret, Inorg. Chem. 43 (2004) 5761.

[24] D. Olea, S.S. Alexandre, P. Amo-Ochoa, A. Guijarro, F. de Jesus, J.M. Soler, P.J. de Pablo, F. Zamora, J. Gomez-Herrero, Adv. Mater. 17 (2005) 1761.

[25] J.P. García-Teran, O. Castillo, A. Luque, U. García-Couceiro, G. Beobide, P. Román, Cryst. Growth Des. 7 (2007) 2594.

[26] J.P. García-Teran, O. Castillo, A. Luque, U. García-Couceiro, G. Beobide, P. Román, Inorg. Chem. 46 (2007) 3593.

[27] J.P. García-Teran, O. Castillo, A. Luque, U. García-Couceiro, G. Beobide, P. Román, Dalton Trans. (2006) 902.

[28] S. Pérez-Yáñez, O. Castillo, J. Cepeda, J.P. García-Terán, A. Luque, P. Román, Eur. J. Inorg. Chem. (2009) 3889.

[29] S. Bouacida, H. Merazig, A. Beghidja, C. Beghidja, Acta Cryst. E61 (2005) m2072.

[30] S. Bouacida, H. Merazig, A. Beghidja, C. Beghidja, Acta Cryst. E61 (2005) m1153.

[31] F. H. Allen, Acta Crystallogr. B58 (2002) 380.

[32] C. Marian, D. Nolting, R. Weinkauf, PhysChem ChemPhys. 7 (2005) 3306.

[33] D. Dobrzynska, L.B. Jerzykiewicz, J. Am. Chem. Soc. 126 (2004) 11118.

[34] Z. Wang, Y. Cheng, C. Liao, C. Yan, CrystEngComm, 50 (2001) 1.

[35] Y. Cheng, Z. Wang, C. Liao, C. Yan, New. J. Chem. 26 (2002) 1360.

[36] M.A. Salam, K. Aoki, Inorg. Chim. Acta 311 (2000) 15.

[37] B.O. Patrick, C.L. Stevens, A. Storr, R.C. Thomson, Polyhedron 22 (2003) 3025.

[38] G.-H. Wang, Z.-G. Li, H.-Q. Jia, N.-H, Hu, J.-W, Xu, CrystEngComm. 11 (2009) 292.

[39] D.-K. Bucar, R.F. Henry, X. Lou, T.B. Borchardt, G.G.Z. Zhang, Chem. Commun. (2007) 525.

[40] S. Karki, T. Friscic, W. Jones, W.D.S. Motherwell, Mol. Pharm. 4 (2007) 347.

[41] A. Lemmerer, J. Bernstein, CrystEngComm. 12 (2010) 2029.

[42] N. Bosnjakovic-Pavlovic, A. Spasojevic-de Bire, J. Phys. Chem. A 114 (2010) 10664.

[43] S.R. Perumalla, E. Suresh, V.R. Pedireddi, Angew. Chem. Int. Ed. 44 (2005) 7752.

[44] C.J. Burrows, S.E. Rokita, Acc. Chem. Res. 27 (1994) 295.

[45] D.S. Lawrence, T. Jiang, M. Levett, Chem. Rev. 95 (1995) 2229.

[46] G. Paragi, Z. Kupihár, C.F. Guerra, F.M. Bickelhaupt, L. Kovács, Molecules 18 (2013) 225.

[47] K. Rajabi, K. Theel, E.A.L. Gillis, G. Beran, T.D. Fridgen, J. Phys. Chem. A 113 (2009) 8099.

Chapter 5

Intercalation of drug related molecules, thiamine and quinolines

Intercalations of drug molecules have been directed for safe, therapeutically effective and patient-compliant drug delivery systems in recent years. It can also protect them from decomposition or denaturization. Intercalation of drugs or biomolecules into inorganic layers of LDH has been extensively studied [1-4]. Vitamin B_1 alternately known as thiamine, plays important role in human life [5,6]. It undergoes decomposition easily by light, heat or change of pH [7]. When vitamin B_1 is used as a medicine, its delivery in a protective form with formation of harmless materials to animal bodies is desirable [8]. One way to deliver vitamin B_1 to animals could be *via* preformed metal complexes, which would dissociate and release it in *vivo* at ambient condition. Thus, synthesis of metal complexes having vitamin B_1 as ligand could release thiamine without degrading to multiple products or to toxic substances and will also help in storage and delivery of vitamin B_1. Thus, it should be possible to use such dication with complex metal anion and intercalate them *via* weak interactions. It would be possible to control the release of vitamin B_1 from such metal complexes by adjusting hydrogen ion concentrations. For such study, prior knowledge of the structures of different types of metal complexes of vitamin B_1 is essential. Several metal complexes of vitamin B_1, such as that of tin [9], cadmium [10], platinum [11-14] are reported in literature. It has also been observed that the poisoning effects that can be caused by metal ions such as manganese and cadmium on biological systems can be controlled by vitamin B_1 [15-17]. Thus, metal complexes [18,19] of vitamin B_1 are important in biology. Further to this, such metal complexes act as mimic of enzymes having potential utility in bio catalysis [20-22]. Similar to thiamine, quinolinum cations also find special attention due to their π-stacking ability that guides the packing pattern and also from biological point of view [23-25].

This chapter deals with formation of inorganic/organic hybrid complexes that are comprised of thiamine and quinolinium cations intercalated by metal dipicolinate complex anion. It has been already discussed in chapter 1 that the cobalt(II) dipicolinate complex anion is known to have insulin mimic activity (Ch. 1, [40]). Thus, by forming adduct with thiamine, it is

expected to add further medicinal value to these complexes. It has also been reported that 8-hydroxyquinolinium cations intercalated in nickel dipicolinate complexes exhibit antimicrobial activity against gram-positive bacteria and yeast [26]. Based on these available literatures and the potentiality of these complexes, we have studied the intercalation chemistry of thiamine, quinoline and 5-aminoquinoline bases in layers of metal dipicolinate complexes *via* proton transfer reactions. It is to be mentioned that in biological systems proton transfer reactions play key role since they can lead to mutations [27]. Thus, it is important to investigate the changes in properties of the base molecules due to protonation. It would also be interesting to study the de-intercalation process of these drug molecules from the complex with variation of pH and their chemical integrity. The drug related molecules studied are shown in Fig. 5.1.

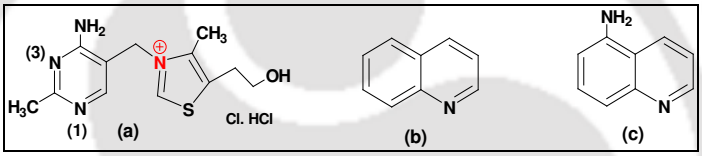

Fig. 5.1: Organic molecules studied, (a) Thiamine, (b) Quinoline, (c) 5-Aminoquinoline

5.1: Metal dipicolinate complexes with thiamine as dication

The complexes are synthesized by reacting dipicolinic acid with hydrated metal acetates followed by treatment with thiamine chloride hydrochloride by employing similar synthetic procedure described in previous chapters (Scheme 5.1.1). The complexes **5.1**-**5.3** consist of a metal complex anion, a dication of thiamine and lattice water molecules. They are represented by the general composition, $[HT][ML_2]\cdot 5H_2O$ [where T = thiamine, L = dipicolinate, M = Co(II), Cu(II) or Zn(II) at +2 oxidation state].

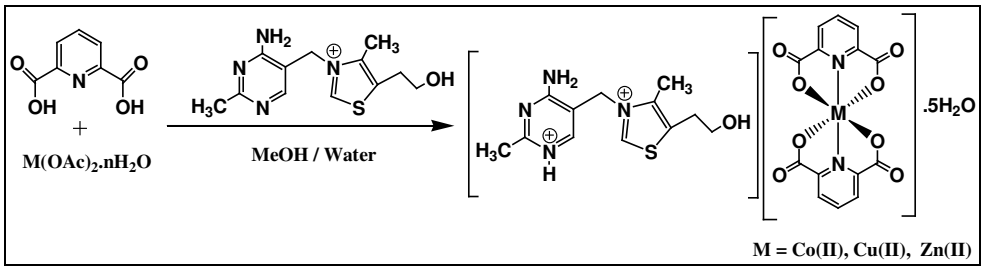

Scheme 5.1.1: Synthesis of the complexes **5.1**-**5.3**

The complexes show broad and sharp IR absorptions around 3440 cm^{-1} due to O–H stretching. The N–H stretching appears in the range of 3108-2925 cm^{-1}. They also exhibit intense IR frequencies in the range of 1659-1591 cm^{-1} and 1380-1378 cm^{-1} due to the asymmetric and symmetric carboxylate stretching. The molar conductance values are observed in the range of 327.0-333.0 S cm^2 mol^{-1}. These values are high for 2:2 electrolytes, which suggest that each complex possess some amount of proton conductivities in addition to the contributions from the simple dissociation in aqueous solution.

All the three complexes are isostructural. The structure of the cobalt(II) complex $[HT][CoL_2]\cdot 5H_2O$ (**5.1**) is discussed in details. The structure consists of thiamine dication, $[CoL_2]^{2-}$ and five solvent water molecules. Thiamine, which is obtained in the mono protonated salt, gets converted to a dicationic form in the complex *via* protonation at the less sterically crowded nitrogen atom (N1 atom) of the pyrimidine ring. Such cation was also observed earlier from vitamin B_1 [28]. Thiamine monophosphate cations with different anions were studied [14]; in those cases also similar protonations were observed. It is to be mentioned that binding of thiamine to the metal ion takes place through N1 atom of pyrimidine ring [29]. This is observed as difficult due to the net positive charge of thiamine. It is thus observed that protonation is easy for N1 atom of pyrimidine ring than to coordinate with metal ion. As a consequence, it forms large number of salt-type complexes than the coordinated complexes. In such a situation, it is unlikely to expect thiamine metal coordination complexes replacing the dipicolinate ligand in our study. Nevertheless, a few metal complexes of thiamine with Mn, Zn, Cd, Pt etc.,(at +2 oxidation state) containing mainly a M-N1 direct bonding were reported in literature [30,31]. In an another complex, $Zn(thiamine)Cl_3\cdot 0.4H_2O$, Zn(II) is coordinated to the N1 atom of the pyrimidine ring (Fig. 5.1.1) [32]. Such is case in the complexes of Zn(II), Cd(II) and Hg(II) with 2-(hydroxybenzyl) thiamine and 2-(hydroxycyclohexylmethyl) thiamine [29,33]. Further, Pt(II) and Pd(II) metal complexes through M-S linkage of the thiazolium ring of thiamine are also reported [34].

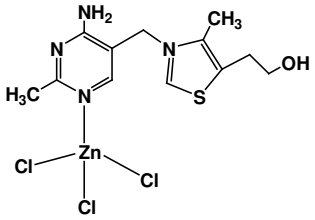

Fig. 5.1.1: Zn(thiamine)Cl_3 complex (*Bencini et al*)

In the crystal lattice of **5.1**, the Co(II) dipicolinate complex anion and thiamine dication appear as pairs. They exhibit wide range of supramolecular interactions. Thiamine dication interacts with the $–COO^-$ unit of $[CoL_2]^{2-}$ anion *via* $–N^+$-H and $–NH_2$ group of pyrimidine ring . The hydroxyl group of the thiamine is also involved in hydrogen bond with an oxygen atom of the coordinated carboxylate group of the complex anion. The remaining $–COO^-$ unit of $[CoL_2]^{2-}$ anion shows hydrogen contact with the solvent water molecules. In addition to these hydrogen bonds, the complexes further exhibit anion-π and π-π interactions (Fig. 5.1.2a). For example, the centroid to centroid distance between the thiazole and pyridine ring of $[CoL_2]^{2-}$ is ~ 3.80 Å, whereas such distance between the pyrimidine ring and $–COO^-$ group of complex anion is ~ 3.23 Å. This type of stacking interactions led to non layered packing arrangement in the lattice (Fig. 5.1.2b). Selected hydrogen bond parameters for the representative complex are listed in table 5.1. In solid state structure, we could not locate the hydrogen atoms of water molecules, it is therefore selected hydrogen bond parameters of the representative complex are provided in table 5.1. The water molecules form hydrogen bond among themselves and also with the anionic and cationic parts.

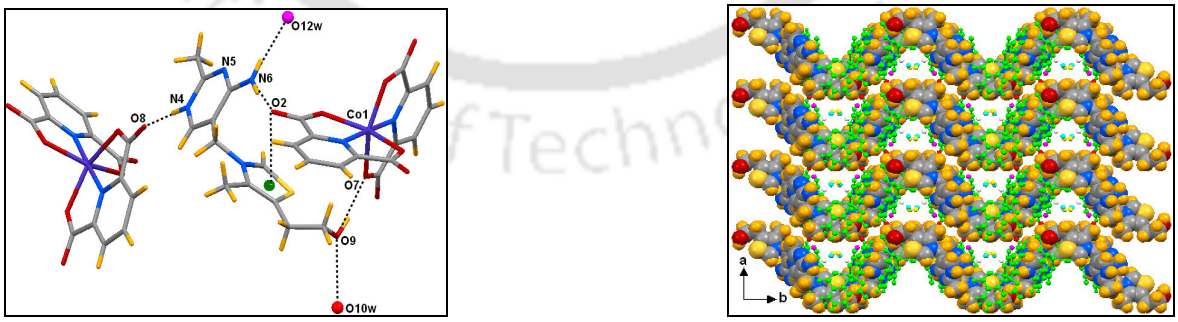

(a) (b)

Fig. 5.1.2: (a) Weak interactions, (b) Packing diagram of complex **5.1** viewed along crystallographic *c* axis (thiamine dication in space filled mode, $[CoL_2]^{2-}$ in ball and stick mode).

Table 5.1: Hydrogen bond parameters for the complex **5.1**

Complex	Bond (symmetry)	$d_{D...H}$(Å)	$d_{H\cdots A}$(Å)	$d_{D\cdots A}$(Å)	< D-H···A(º)
5.1	N6--H6NA···O2 [x, 1/2-y, 1/2+z]	0.89(5)	1.95(5)	2.834(5)	169(4)
	N6--H6NB···O12w [1+x, 1/2-y, 1/2+z]	0.84(6)	2.14(6)	2.971(8)	171(6)
	N4--H4N···O8 [2-x, 1-y, -z]	0.84(3)	1.85(3)	2.696(5)	175(3)
	O9--H9O···O7 [x, 1/2-y, 1/2+z]	0.91(4)	1.90(5)	2.770(5)	159(5)

In thermogravimetry, three prominent steps of weight loss are observed. An illustrative thermogram of complex **5.3** is shown in Fig. 5.1.3a. The weight loss of 10.8% (calcd. 12.0%) in the range of 55-100 ºC corresponds to the loss of five crystallized water molecules. The complexes become amorphous after the loss of solvent water molecules. The major weight change occurs in the temperature range of 220-370 ºC due to loss of thiamines (obsd. 36.7%, calcd. 38.9%). The last step is the continuous decomposition of the Zn(II) dipicolinate complex that occurs above 400 ºC.

The powder X-ray diffraction (PXRD) data of each compound is recorded to ascertain phase purity and the experimental PXRD patterns are compared with the simulated patterns obtained from the crystallographic information files. As a representative case, the PXRD pattern of complex [HT][ZnL_2]·5H_2O (**5.3**) is shown in Fig. 5.1.3b indexing the intense peaks.

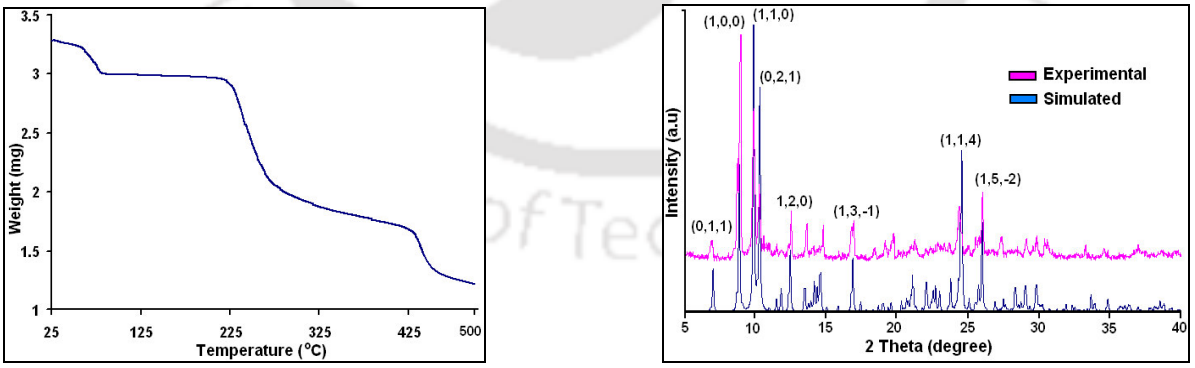

(a) (b)

Fig. 5.1.3: (a) TG of **5.3** and (b) Simulated and experimental PXRD pattern of complex **5.3**

These complexes are stable in solution. This is revealed by ^{1}HNMR and UV-spectroscopic studies. The ^{1}HNMR spectra of the zinc complex display the peaks from thiamine showing its existence in the complex (Fig. 5.1.4a). The signals from dipicolinate part appear at 8.40(d) and 8.48(t) for the two different sets of protons. These chemical shift positions reflect deshielding to a large extent from the parent uncoordinated dipicolinic acid. The intensity of the C-2 proton of thiazole ring of thiamine dication that appears at δ 9.6 ppm decreased considerably in the complex. A 2D (^{1}H-COSY) spectrum was recorded to see the coupling of the proton (Fig. 5.1.4b), but it shows no coupling with the other available protons in the complex. But it is available in literature that the C-2 proton of thiazole ring may be transferred or abstracted by an external base [35]. This process is facilitated by inductive electron withdrawal into the substituent bonded to the quaternary nitrogen atom. In the complex studied in this chapter, Zn(II) dipicolinates act as a base which abstracts the C-2 proton of thiazolium ring. Thus reducing the intensity of the proton in ^{1}HNMR spectra. This proton abstraction process also led to high molar conductivity of the complexes. Earlier cobalt(II) dipicolinate complexes were reported as insulin mimic and it was found to dissociate easily in solution to give multiple species (Ch. 1, [40]). Such dissociation processes were reported to be highly hydrogen ion dependent. In that study it was also shown that the cobalt(II) ions being labile it could lead to multinuclear species. The cobalt(II) complex reported here has two medicinal parts which are in the form of thiamine dication and cobalt(II) dipicolinate anion. Both parts are proven medicine, that makes this complex more attractive. The UV-spectra of thiamine displays two characteristic bands at 239.0 and 261.0 nm respectively (Fig. 5.1.4c). In aqueous medium the complexes **5.1** and **5.2** exhibit absorption peak at 261 nm, which is similar to the parent thiamine molecule. These absorptions of the metal complexes do not change with time or when exposed to ordinary light for at least a week. This shows that the complexes are stable under ordinary thermal and photochemical condition.

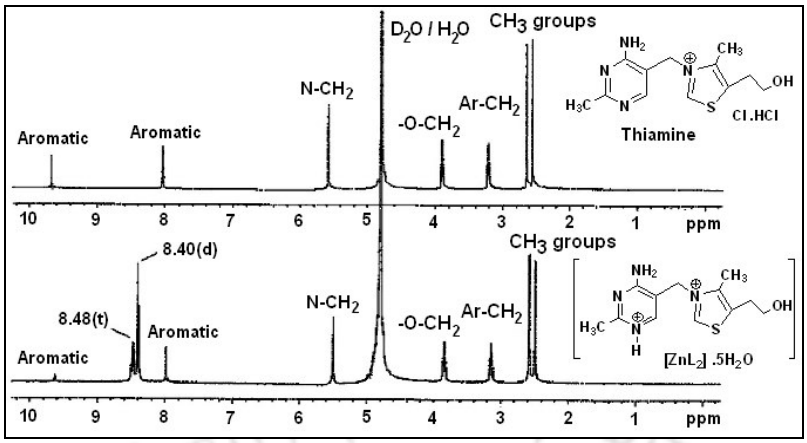

(a)

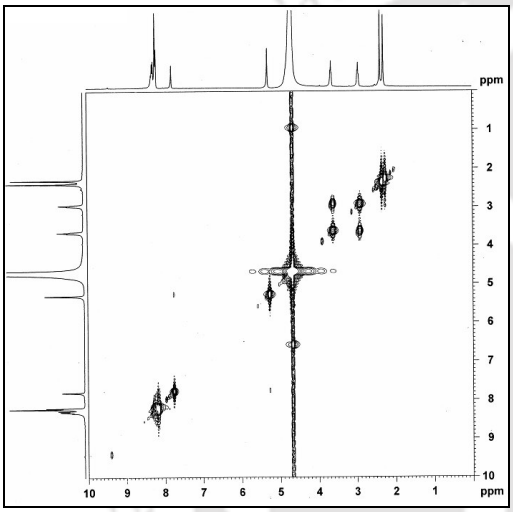

(b)

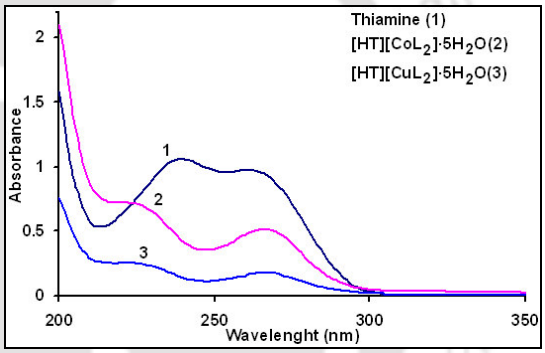

(c)

Fig. 5.1.4: (a) 400 MHz ^{1}HNMR spectra of thiamine hydrochloride and $[HT][ZnL_2]\cdot 5H_2O$ in D_2O, (b) 300 MHz 2D (^{1}H-COSY) spectra of $[HT][ZnL_2]\cdot 5H_2O$ in D_2O (c) UV-spectra of thiamine (**1**), $[HT][CoL_2]\cdot 5H_2O$ (**2**) and $[HT][CuL_2]\cdot 5H_2O$ (**3**) in water (10^{-5} M).

5.2: Solvent-free synthesis of Ni(II) and Cu(II) dipicolinate complexes with protonated quinolines

The Ni(II) and Cu(II) dipicolinate complexes with quinoline bases were synthesized by reacting with $H_2[NiL_2]\cdot nH_2O$ / $H_2[CuL_2]\cdot nH_2O$ (where x = 3 for Ni, x = 1 for Cu) and quinoline or 5-aminoquinoline respectively through reactions in solution and also through solvent free cation exchange reactions (Scheme 5.2.1). The complexes $[HQ]_2$ $[NiL_2]\cdot 5H_2O$ (**5.4**), $[HQ]_2[CuL_2]\cdot 5H_2O$ (**5.5**), $[H5AQ]_2[NiL_2]\cdot 4H_2O$ (**5.6**), $[H5AQ]_2[CuL_2]\cdot 2H_2O$ (**5.7**)

(where L = dipicolinate, Q = quinoline, 5AQ = 5-aminoquinoline) are characterized by FTIR, solid state visible spectroscopy and X-ray single crystal study. In these complexes, protonation takes place at the quinoline nitrogen atom of the corresponding bases. The complexes are in the hydrated form. Depending on the cation used, they have different amounts of water of crystallization.

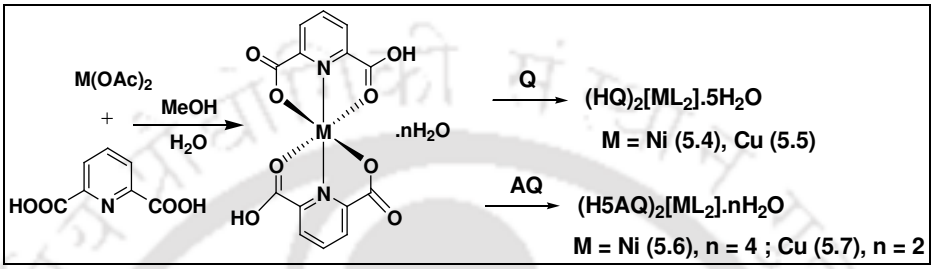

(a)

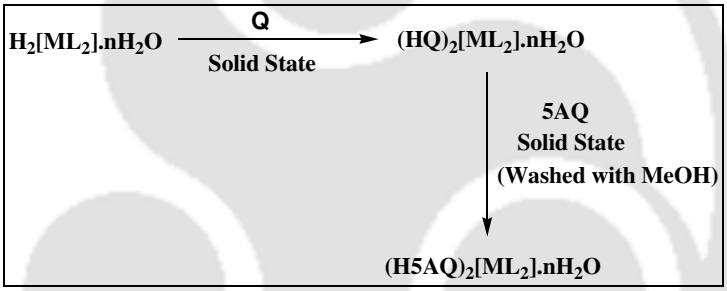

(b)

Scheme 5.2.1: Synthesis of the complexes, (a) In solution, (b) Solid state cation exchange reactions

The most significant IR absorptions in these complexes are observed for –OH, -N^+-H and –COO^- groups. The strong and broad absorption bands in the range of 3413-3408 cm^{-1} are attributed to the ν(OH) vibrations of water of crystallization. The absorption bands appeared in the range of 3318-2913 cm^{-1} are related to ν(-N^+-H) vibrations of protonated quinoline bases. The stretching frequencies of the -COO^- groups of the complex anion appeared in the range of 1627-1615 cm^{-1} and 1593-1586 cm^{-1} for asymmetric (ν_{as}) and symmetric (ν_s) vibrations respectively. Solid-state electronic absorption spectrums of the complexes are recorded. The visible spectrum of starting Ni(II) dipicolinate complex $H_2[NiL_2]\cdot 3H_2O$ and its complexes with quinoline bases are shown in Fig. 5.2.1a. The λ_{max} value for $H_2[NiL_2]\cdot 3H_2O$ appears at 637.0 nm, whereas the corresponding value for quinoline

complex **5.4** is 610.0 nm showing shift toward shorter wavelength. These values are assigned for d-d transitions ($^3A_{2g} \rightarrow {}^3T_{2g}$), which is in conformity with octahedral geometry. The dark red complex $[H5AQ]_2[NiL_2]\cdot 4H_2O$ (**5.6**) exhibits maximum absorption band at 460.0 nm.

The complexes exhibit similar trend of thermal behaviour. The thermal decomposition profile of complex **5.6** is discussed in details (Fig. 5.2.1b). In the 1st step, the 9.2% (calcd. 9.6%) weight loss in the range of 65-135 ºC implying removal of four lattice water molecules. The 2nd weight loss of 39.0% in the temperature range 230-300 ºC is consistent with the departure of two 5-aminoquinoline molecules (calcd. 38.5%). The 3rd step is the usual decomposition of Ni(II) dipicolinates that occurs above 400 ºC.

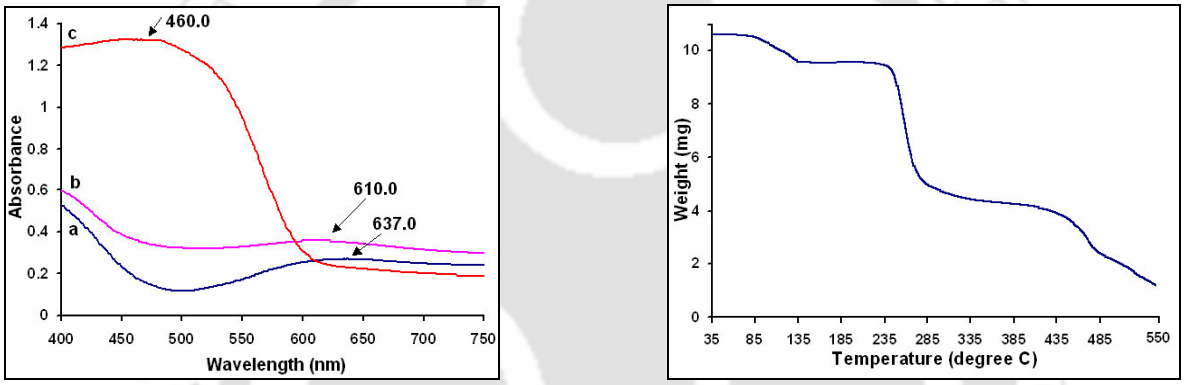

Fig. 5.2.1: Solid state visible spectra (left) of (a) $H_2[NiL_2]\cdot 3H_2O$, (b) [HQ] $[NiL_2]\cdot 5H_2O$ (**5.4**), (c) [H5AQ] $[NiL_2]\cdot xH_2O$ (**5.6**); TG of complex **5.6** (right).

Since the quinolinium complexes of Ni(II) and Cu(II) are isostructural, the structural aspects of $[HQ]_2$ $[NiL_2]\cdot 5H_2O$ (**5.4**) are discussed in details. The structure of complex **5.4** is made up of Ni(II) dipicolinate complex anion, quinolinium cations and crystallization water molecules held together by electrostatic and hydrogen bond interactions. There are two symmetry independent quinolinium cations per molecule since the metal complex is a dianion. Out of four, two $-COO^-$ groups of complex anion form charge assisted hydrogen bond with $-N^+$-H of quinolinium cation. The remaining carboxylate groups complete hydrogen bond functionality with the lattice water molecules. Another weak interaction stabilizing the complex is the face to face π-π interactions between the quinolinium cations. The centroid to centroid distance between two adjacent cations is ~ 3.69 Å. It has also been

observed that the five lattice water molecules available in the crystal structure form a discrete hydrogen bonded pentamer in the lattice (Fig. 5.2.2a). The O···O distance between the oxygen atoms of the pentamer lie in the range of 2.81-2.83 Å.

The complexes $[H5AQ]_2[NiL_2]\cdot 4H_2O$ **(5.6)** and $[H5AQ]_2[CuL_2]\cdot 2H_2O$ (**5.7**) are not isostructural and crystallizes in *P2₁/c* and *P-1* respectively. They differ by the number of lattice water molecules. The complex $[H5AQ]_2[NiL_2]\cdot 4H_2O$ (**5.6**) consists of two symmetry independent 5-aminoquinolinium cation and $[NiL_2]^{2-}$ complex anion along with four lattice water molecules. In addition to electrostatic interactions, the complex exhibits wide range of supramolecular interactions. Both the $-N^+$-H and $-NH_2$ group of the cation involves in hydrogen bond with the carboxylate group of complex anion. The cation exhibits stacking interactions with the complex anion and also among themselves. Detail geometrical parameters of the hydrogen bonds are given in table 5.2.

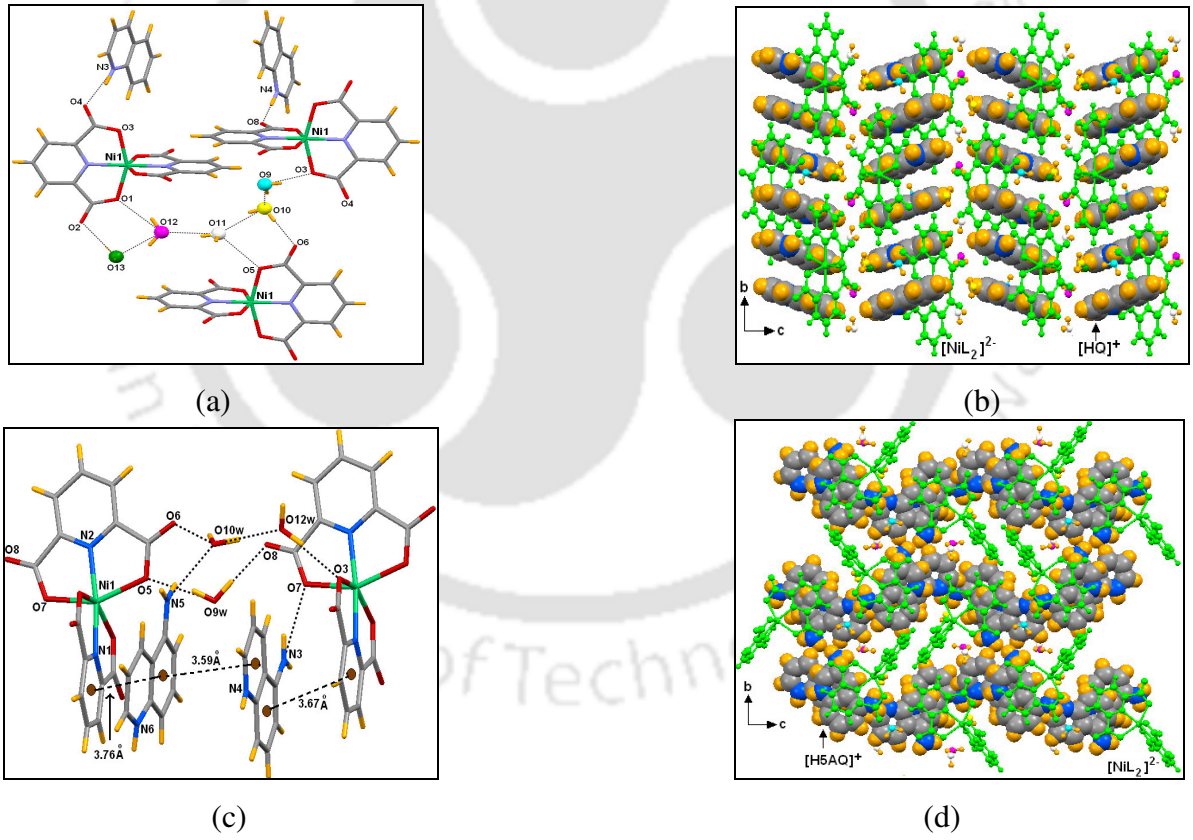

Fig. 5.2.2: (a) Hydrogen bond interactions in complex **5.4**, (b) Packing diagram of **5.4** ($[NiL_2]^{2-}$ in ball and stick mode, quinolinium cation in space filled mode) viewed along crystallographic *a* axis, (c) Selected hydrogen bond and π-π interactions in **5.6**, (d) Packing diagram of **5.6** ($[NiL_2]^{2-}$ in ball and stick mode, 5AQ cation in space filled mode) viewed along crystallographic *a* axis.

Due to π stacking capability, the cation exhibits extensive face to face π-π interactions in the crystal lattice. The centroid to centroid distance between two adjacent cations is ~ 3.59 Å, whereas such distances between the cation and the complex anion are ~ 3.67 and 3.76 Å respectively (Fig. 5.2.2c). In addition, the lattice water molecules act as hydrogen-bonded bridge between the charged species.

Both Ni(II) and Cu(II) form chelate complexes with these quinoline bases [36-38]. In this study, no ligand exchange reactions are preceded even in the presence of relatively strong chelating ligands. Mn(II), Ni(II), Co(II) and Zn(II) dipicolinate complexes with 8-hydroxyquinoline have been reported recently [26,39]. Ni(II) dipicolinate complexes with 8-hydroxy-2-methylquinolinium cation are also known [40,41]. These complexes exhibit similar structural features with the quinoline and 5-aminoquinoline bases discussed in this chapter. All of them consists of two 8-hydroxyquinolinium cations, one bis(dipicolinate) M(II) anion (M = Mn(II), Ni(II) and Zn(II)) and lattice water molecules. The packing of these complexes also exhibits similar supramolecular interactions in their crystal lattice.

In the representative examples, both the complexes having Ni(II) as central metal ion exhibit differences in their crystal-packing pattern. Complex **5.4** shows that the anionic and cationic units lie perpendicular to each other (Fig. 5.2.2b). The quinolinium cations exhibit π-π stacking among themselves, but no such interactions with $[NiL_2]^{2-}$ units. In the lattice of complex **5.6**, the 5AQ cations lies between two $[NiL_2]^{2-}$ units in such a way that it simultaneously stacks with adjacent symmetry independent cationic units as well as with the complex anion. The 8-hydroxyquinolinium cation also exhibits weak π-π stacking interaction with the pyridine ring of $[NiL_2]^{2-}$ in the crystal lattice [26]. Due to planar geometry of the cations, they can easily be intercalated in the empty space created by the bulky complex anion *via* stacking interactions. This extensive stacking interaction led to non-lamellar structures in the lattice, an exception with the diamines or amino acids.

Table 5.2: Geometrical parameters for the hydrogen bonds in **5.4** and **5.6**

Complex	**Bond (symmetry)**	$d_{D\text{-}H}$(Å)	$d_{H\cdots A}$(Å)	$d_{D\cdots A}$(Å)	**< D-H···A(°)**
	N(3)-H(3N)···O(4) [2-x, 1/2+y, 1/2-z]	0.95(5)	1.71(5)	2.635(5)	164(3)
	N(4)-H(4N)···O(8) [x, y, z]	0.98(5)	1.68(5)	2.661(5)	177(4)
	O(9)-H(9A)···O(3) [1-x, 1/2+y, 1/2-z]	0.84(3)	2.03(3)	2.851(3)	167(3)

5.4	O(9)-H(9B)···O(10) [x, y, z]	0.84(2)	1.99(2)	2.806(4)	165(5)
	O(10)-H(10A)···O(6) [-1+x, y, z]	0.84(5)	1.88(5)	2.722(4)	178(7)
	O(10)-H(10B)···O(11) [-1+x, 1/2-y, -1/2+z]	0.76(5)	2.12(5)	2.831(6)	156(5)
	O(11)-H(11A)···O(12) [x, y, z]	0.84(5)	2.05(4)	2.826(5)	153(5)
	O(12)-H(12A)···O(1) [x, y, z]	0.92(6)	2.09(5)	2.947(4)	155(5)
	O(12)-H(12B)···O(13) [x, y, z]	0.94(5)	2.00(5)	2.825(7)	146(4)
	O(13)-H(13B)···O(2) [x, y, z]	0.85(7)	1.93(7)	2.772(6)	175(8)
5.6	N(3)-H(3A)···O(11) [x, y, z]	0.86	2.10	2.948(3)	171
	N(3)-H(3B)···O(7) [-1+x, y, z]	0.86	2.09	2.892(3)	155
	N(4)-H(4N)···O(1) [1-x, -1/2+y, 1/2-z]	0.81(3)	2.00(3)	2.792(3)	163(3)
	N(4)-H(4N)···O(2) [1-x, -1/2+y, 1/2-z]	0.81(3)	2.52(3)	3.141(3)	135(3)
	N(5)-H(5A)···O(10) [1-x, 1/2+y, 1/2-z]	0.86	2.26	3.048(4)	152
	N(5)-H(5B)···O(4) [x, 1/2-y, 1/2+z]	0.86	2.19	2.994(3)	156
	N(6)-H(6N)···O(9) [x, y, z]	0.91(4)	1.78(4)	2.689(3)	176(3)
	O(9)-H(9A)···O(8) [-1+x, y, z]	0.93(3)	1.92(3)	2.849(3)	176(2)
	O(9)-H(9B)···O(5) [x, y, z]	0.88(4)	1.93(4)	2.802(3)	171(4)
	O(9)-H(9B)···O(6) [x, y, z]	0.88(4)	2.60(4)	3.258(3)	133(3)
	O(10)-H(10A)···O(6) [x, y, z]	0.91(3)	2.02(4)	2.822(3)	146(3)
	O(10)-H(10B)···O(12) [-1+x, 1/2-y, -1/2+z]	0.94(2)	1.90(2)	2.785(4)	156(3)
	O(11)-H(11A)···O(10) [x, 1/2-y, 1/2+z]	0.92(3)	1.94(3)	2.855(3)	174(4)
	O(11)-H(11B)···O(4) [1-x, 1/2+y, 1/2-z]	0.90(3)	1.90(2)	2.797(3)	174(3)
	O(12)-H(12A)···O(2) [x, y, z]	0.93(3)	1.90(2)	2.808(3)	169(3)
	O(12)-H(12B)···O(3) [x, 1/2-y, 1/2+z]	0.93(3)	1.95(3)	2.855(3)	164(3)

5.3: Nature of the complex with change of pH

The formation of the complexes is largely affected by pH of the medium. The starting material of these complexes have the general composition, $H_2[ML_2]\cdot xH_2O$ (where M = Co, Ni, Cu or Zn at +2 oxidation state, x = 1-3). The aqueous solutions (0.05M) of these complexes have a pH in the range of ~ 1.5 to 1.7. The aqueous solutions of the reported complexes derived from thiamine or quinoline exhibit pH in the range ~ 4.0 to 4.2. An increase of pH of such solution by adding base from an external source, these complexes release the cationic part. Such release generally starts at pH ~ 6.0 and completes at pH ~ 8.0, which is confirmed by measuring the pH of such solution during the course of precipitation.

The complete release of the cationic molecules from the metal dipicolinate complex takes place at pH ~ 8.0. Above this pH, polymeric sodium or potassium salts of metal dipicolinates crystallize, depending on whether the sodium hydroxide or the potassium hydroxide is used to make the medium basic. Thus, it is possible to release the thiamine cations from these metal complexes just by changing the pH. Further, the chemical composition of the released molecule is monitored by comparing FTIR spectra with the thiamine molecule and found intake.

For example, when pH of aqueous solution of the Co(II) dipicolinate thiamine complex (**5.1**) is raised by adding sodium hydroxide; in basic medium (pH > 8) thiamine part gets dislodged from the metal complex and led to the formation of a mixed metal complex with a composition $\{[Na(H_2O)_2]_2[CoL_2]\cdot 2H_2O\}_n$. This complex is a cation coordinated complex similar to analogous Cu(II) dipicolinate complex described in chapter 2. The crystal structure of the complex is depicted in Fig. 5.3.1a.

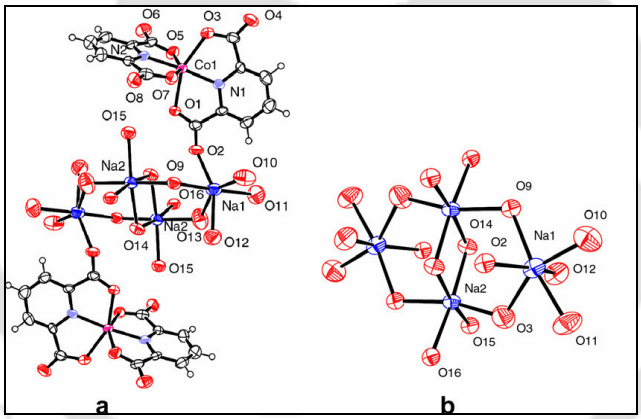

Fig. 5.3.1: (a) The crystal structure of $\{[Na(H_2O)_2]_2[CoL_2]\cdot 2H_2O\}_n$ (the hydrogen atoms of water molecules are not located), (b) The tetra-nuclear coordinated cation of the complex (water molecules of crystallization are omitted).

The complex may be described as an aquated tetranuclear sodium complex cation coordinated to two Co(II) dipicolinate anions. The cationic part is coordinated to the dipicolinate unit through carbonyl oxygen of the anionic part as shown in Fig. 5.3.1b. There are two types of sodium environments in the tetranuclear aquated sodium complex cation. Two sodium ions (Na1) have biprismatic environments, whereas the other two sodium ions

(Na2) have distorted octahedral environments. Overall the hetero-metallic polynuclear complex is symmetric with respect to a mirror plane passing through two sodium ions (Na2) and O13 atoms bisecting the molecules into equal halves.

5.4: Conclusion

We have synthesized and characterized three water-soluble vitamin B_1 containing first row transition metal complexes. In these complexes, the thiamine does not coordinate with the metal ion and remain as a dicationic form outside the coordination sphere. The complexes are stabilized by wide range of supramolecular interactions. We have also synthesized Ni(II) and Cu(II) dipicolinate complexes with quinoline or 5-aminoquinoline base that also does not go inside the coordination sphere and form analogous inorganic-organic hybrid complexes. Due to extensive stacking interactions among the quinolinium cations or with the complex anion, the intercalated complexes do not form well-defined layered structures. This is being an exception with the aliphatic diamines or the amino acids discussed earlier. These complexes are able to release thiamine or quinolines upon variation of pH. The resultant sodium containing Co(II) dipicolinate complex formed after the release of thiamine in basic medium is structurally characterized. Thus, the unique ability of the metal dipicolinate complex to associate with different cations in a wide pH range is established. The reported complexes are stable in aqueous solution. This study further provides a way to synthesize a new class of complexes where a medicinally active inorganic anionic site is attached to cation derived from medicine.

5.5: Experimental section

Detailed synthetic methodologies for synthesized complexes are given below. Analytical as well as spectroscopic data are also listed along with each of these complexes.

5.5.1: $[HT][CoL_2]\cdot 5H_2O$ (5.1), $[HT][CuL_2]\cdot 5H_2O$ (5.2) and $[HT][ZnL_2]\cdot 5H_2O$ (5.3)

A solution of $Co(OAc)_2\cdot 4H_2O$ (0.249 g, 1.0 mmol), $Cu(OAc)_2\cdot H_2O$ (0.199 g, 1.0 mmol) and $Zn(OAc)_2\cdot 2H_2O$ (0.219 g, 1.0 mmol) in water (2.0 ml) was carefully added respectively to a 20 ml methanolic solution of dipicolinic (0.334 g, 2.0 mmol), followed by drop wise

addition of a solution of thiamine chloride (0.337 g, 1.0 mmol) in water (2.0 ml). The resulting reaction mixtures were left overnight at ambient temperature. Upon slow evaporation of direct Q Millipore water dark red (cobalt), blue (copper) and colorless (zinc) single crystals suitable for X-ray analysis were obtained after a period of 3-4 days.

Complex **5.1:** Isolated yield: 64%. Elemental anal calcd for $C_{26}H_{44}CoN_6O_{14}S$, C, 41.29; N, 11.11; H, 5.82%; found C, 40.94; N, 10.96; H, 5.67%. IR (KBr, cm^{-1}): 3442 (b, s), 3239 (m), 3103 (m), 2969 (w), 1659 (m), 1615 (s), 1590 (s), 1421 (m), 1376 (s), 1357 (m), 1278 (m). Molar conductance: 333.0 S cm^2 mol^{-1} in water. μ_{eff}. at 298 K: 4.36 BM. Vis (H_2O) λ_{max}: 580.0 nm; ε = 52.1 M^{-1} cm^{-1} and 502.0 nm; ε = 79.3 M^{-1} cm^{-1}. Thermal analysis: decomposition range: ~ 45-90 ºC (evaporation of five water molecules of crystallization); further decomposition occurs at ~ 188 ºC.

Complex **5.2**: Isolated yield: 66%. Elemental anal calcd for $C_{26}H_{44}CuN_6O_{14}S$, C, 41.04; N, 11.05; H, 5.79%; found C, 40.88; N, 10.90; H, 5.64%. IR (KBr, cm^{-1}): 3441 (b, s), 2925 (w), 1622 (bs), 1591 (m), 1380 (s), 1274 (m). Molar conductance: 328.0 S cm^2 mol^{-1} in water. μ_{eff}. at 298 K: 1.67 BM. Vis (H_2O) λ_{max}: 773.0 nm; ε = 73.6 M^{-1} cm^{-1}. Thermal analysis: decomposition range: ~ 45-110 ºC (loss of crystallization water molecules).

Complex **5.3**: Isolated yield: 65%. Elemental anal calcd for $C_{26}H_{44}N_6O_{14}SZn$, C, 40.94; N, 11.02; H, 5.77%; found C, 40.75; N, 10.91; H, 5.60%. IR (KBr, cm^{-1}): 3442 (b, s), 3108 (w), 2926 (w), 1659 (m), 1622 (s), 1591 (m), 1379 (s), 1279 (m). Molar conductance: 327.0 S cm^2 mol^{-1} in water. ^{1}HNMR (D_2O, 400 MHz, ppm): 8.4 (6H, m), 8.0 (1H, s), 5.5 (2H, s), 3.8 (2H, t, J = 8.0 Hz), 3.1 (2H, t, J = 8.0 Hz), 2.6 (3H, s), 2.5 (3H, s). Thermal analysis: decomposition range: ~ 55-100 ºC (loss of five crystallization water molecules).

5.5.2: $[HQ]_2$ $[NiL_2]\cdot 5H_2O$ (5.4), $[HQ]_2$ $[CuL_2]\cdot 5H_2O$ (5.5), $[H5AQ]_2[NiL_2]\cdot 4H_2O$ (5.6), and $[H5AQ]_2[CuL_2]\cdot 2H_2O$ (5.7)

The Ni(II)/Cu(II) containing dicarboxylic acid complexes $H_2[NiL_2]\cdot 3H_2O$ or $H_2[CuL_2]\cdot H_2O$ (0.5 mmol each) are mixed with quinoline and 5-aminoquinoline bases (1.0 mmol each) in

independent experiments in a mortar for half an hour. The resultant precipitates are kept at 80 ºC in an oven for one hour. The green, blue or red precipitates obtained *via* solid-state reaction are dissolved in Milli Q water and left for crystallization in a beaker. Single crystals suitable for X-ray diffraction quality were obtained after one week.

Complex **5.4:** Isolated yield: 65%. Elemental anal calcd for $C_{32}H_{32}N_4NiO_{13}$, C, 51.92; N, 7.57; H, 4.33%; found C, 51.78; N, 7.45; H, 4.28%. IR (KBr, cm^{-1}): 3410 (b, s), 1621 (s), 1590 (w), 1424 (w), 1374 (s), 1277 (w), 1085 (w). Molar conductance: 215.0 S cm^2 mol^{-1} in water. μ_{eff}. at 298 K: 2.88 BM. Thermal analysis: decomposition range: ~ 65-125 °C (loss of three crystallization water molecules).

Complex **5.5:** Isolated yield: 76%. Elemental anal calcd for $C_{32}H_{32}CuN_4O_{13}$, C, 51.60; N, 7.52; H, 4.30%; found C, 51.36; N, 7.51; H, 4.15%. IR (KBr, cm^{-1}): 3408 (b, s), 1620(s), 1588(w), 1422 (w), 1373 (s), 1275 (w), 1085 (w). Molar conductance: 212.5 S cm^2 mol^{-1} in water. μ_{eff}. at 298 K: 1.62 BM. Thermal analysis: decomposition range: ~ 60-110 °C (loss of three crystallization water molecules).

Complex **5.6**: Isolated yield: 70%. Elemental anal calcd for $C_{32}H_{32}N_6NiO_{12}$, C, 51.11; N, 11.18; H, 4.26%; found C, 50.94; N, 11.05; H, 4.20%. IR (KBr, cm^{-1}): 3413 (b, s), 1624 (s), 1591 (w), 1426 (w), 1377 (s), 1279 (w), 1088 (w). Molar conductance: 206.0 S cm^2 mol^{-1} in water. μ_{eff}. at 298 K: 2.85 BM. Thermal analysis: decomposition range: ~ 65-135 °C (loss of crystallization water molecules).

Complex **5.7**: Isolated yield: 68%. Elemental anal calcd for $C_{32}H_{28}CuN_6O_{10}$, C, 53.33; N, 11.66; H, 3.89%; found C, 53.13; N, 11.44; H, 3.74%. IR (KBr, cm^{-1}): 3409 (b, s), 1621 (s), 1587 (w), 1424 (w), 1377 (s), 1277 (w), 1086 (w). Molar conductance: 200.0 S cm^2 mol^{-1} in water. μ_{eff}. at 298 K: 1.70 BM. Thermal analysis: decomposition range: ~ 75-100 °C (loss of crystallization water molecules).

5.6: Crystallographic data and refinement parameters for the complexes 5.1 - 5.3

Compound No.	**5.1**	**5.2**	**5.3**
Formula	$C_{26}H_{44}CoN_6O_{14}S$	$C_{26}H_{44}CuN_6O_{14}S$	$C_{26}H_{44}N_6O_{14}SZn$
Formula wt.	755.58	760.27	762.02
Crystal system	Monoclinic	Monoclinic	Monoclinic
Space group	*P2(1)/c*	*P2(1)/c*	*P2(1)/c*
a (Å)	9.9242(3)	9.8547(2)	9.9414(7)
b (Å)	20.3418(7)	20.3946(4)	20.3201(13)
c (Å)	16.0738(5)	16.0644(3)	16.0927(11)
α (deg)	90.00	90.00	90.00
β (deg)	92.040(2)	92.050(10)	91.980(4)
γ (deg)	90.00	90.00	90.00
V (Å^3)	3242.86(18)	3226.69(11)	3248.9(4)
Z	4	4	4
D_{calc} (gcm^{-3})	1.527	1.565	1.537
μ (mm^{-1})	0.670	0.820	0.897
F(000)	1548	1596	1560
Total no. of reflns	47065	39073	37936
Independent reflns.	7127	7986	7837
$\theta_{max.}$	1.26 - 27.29	1.61 - 28.31	1.61 - 28.29
Ranges	$-12 \le h \le 12$	$-11 \le h \le 13$	$-13 \le h \le 12$
(h, k, l)	$-25 \le k \le 26$	$-27 \le k \le 27$	$-25 \le k \le 27$
	$-20 \le l \le 20$	$-21 \le l \le 21$	$-21 \le l \le 19$
Completeness to 2θ (%)	97.6	99.5	97.0
Data /restraints/ parameters	7127 / 2 / 459	7986 / 2 / 452	7837 / 1 / 440
GOF (F^2)	1.020	1.047	0.988
R_1, wR_2 [$I > 2\sigma(I)$]	0.0561, 0.1498	0.0404, 0.1228	0.0475, 0.1403
R_1, wR_2 (all data)	0.0877, 0.1827	0.0603, 0.1297	0.0791, 0.1513
Largest diff peak/hole (e Å^{-3})	0.849 / -0.628	0.509 / -0.357	0.971 / -0.547

Continued…

Compound No.	**5.4**	**5.5**	**5.6**	**5.7**
Formula	$C_{32}H_{32}N_4NiO_{13}$	$C_{32}H_{32}CuN_4O_{13}$	$C_{32}H_{32}N_6NiO_{12}$	$C_{32}H_{28}CuN_6O_{10}$
Formula wt.	739.33	744.16	751.35	720.14
Crystal system	Monoclinic	Monoclinic	Monoclinic	Triclinic
Space group	*P21/c*	*P21/c*	*P21/c*	*P-1*
a (Å)	12.3307(3)	12.3500(5)	10.2129(3)	8.5658(6)
b (Å)	18.3048(4)	18.2719(7)	16.3019(4)	13.7408(10)
c (Å)	18.2981(3)	18.2835(6)	20.3817(6)	13.9704(10)
α (deg)	90.00	90.00	90.00	68.141(4)
β (deg)	126.6710(10)	126.630(2)	103.7910(10)	84.376(5)
γ (deg)	90.00	90.00	90.00	80.899(4)
V (Å^3)	3312.65(12)	3311.0(2)	3295.52(16)	1505.52(19)
Z	4	4	4	2
D_{calc} (gcm^{-3})	1.482	1.493	1.514	1.589
μ (mm^{-1})	0.659	0.733	0.663	0.798
F(000)	1536	1540	1560	742
Total no. of reflns	33609	49534	33623	20852
Independent reflns.	5836	8356	5768	6751
$\theta_{max.}$	1.78 - 25.00	1.78 - 28.58	1.62 - 25.00	1.61 - 27.55
Ranges	$-14 \le h \le 14$	$-16 \le h \le 16$	$-12 \le h \le 11$	$-11 \le h \le 11$
(h, k, l)	$-21 \le k \le 21$	$-24 \le k \le 24$	$-19 \le k \le 19$	$-17 \le k \le 17$
	$-21 \le l \le 21$	$-24 \le l \le 24$	$-24 \le l \le 23$	$-17 \le l \le 18$
Completeness to 2θ (%)	100.0	98.5	99.6	97.1
Data /restraints/ parameters	5836 / 6 / 499	8356 / 2 / 491	5768 / 4 /500	6751 / 2 / 458
GOF (F^2)	1.108	1.076	0.989	1.010
R_1, wR_2 [$I > 2\sigma(I)$]	0.0389, 0.1029	0.0457, 0.0867	0.0391, 0.1241	0.0644, 0.1657
R_1, wR_2 (all data)	0.0497, 0.1102	0.0686, 0.0888	0.0495, 0.1352	0.0845, 0.1826
Largest diff peak/hole (e Å^{-3})	1.074 / -0.482	0.810 / -0.554	0.400 / -0.534	1.083 / -1.086

5.7: Selected bond distances (Å) and bond angles (°) in 5.1, 5.2 and 5.3

Bond parameters	**(M = Co)**	**(M = Cu)**	**(M = Zn)**
Metal–ligand bond distances			
M(1)–N(1)	2.023(3)	1.959(16)	2.019(2)
M(1)–N(2)	2.024(3)	1.928(17)	2.013(2)
M(1)–O(1)	2.176(3)	2.259(16)	2.203(19)
M(1)–O(3)	2.159(3)	2.267(17)	2.195(19)
M(1)–O(5)	2.116(3)	2.137(16)	2.120(2)
M(1)–O(7)	2.195(3)	2.089(17)	2.257(2)
Ligand–metal–ligand bond angles			
<N(1)–M(1)–N(2)	177.97(12)	179.31(7)	176.21(9)
<N(1)–M(1)–O(5)	105.24(10)	100.86(6)	106.26(8)
<N(2)–M(1)–O(5)	76.79(11)	78.60(7)	77.53(9)
<N(1)–M(1)–O(3)	76.56(10)	76.46(6)	76.41(7)
<N(2)–M(1)–O(3)	103.70(11)	103.12(7)	103.81(8)
<O(5)–M(1)–O(3)	91.23(11)	93.51(7)	92.48(8)
<N(1)–M(1)–O(1)	75.70(11)	77.23(6)	75.74(8)
<N(2)–M(1)–O(1)	104.13(11)	103.21(6)	104.09(8)
<O(5)–M(1)–O(1)	93.39(12)	92.83(6)	93.77(9)
<O(3)–M(1)–O(1)	152.11(10)	153.65(6)	152.11(8)
<N(1)–M(1)–O(7)	102.24(11)	101.29(7)	101.01(8)
<N(2)–M(1)–O(7)	75.74(12)	79.25(7)	75.21(9)
<O(5)–M(1)–O(7)	152.45(11)	157.84(6)	152.70(8)
<O(3)–M(1)–O(7)	93.22(11)	92.09(7)	92.57(8)
<O(1)–M(1)–O(7)	95.25(12)	91.60(6)	94.21(8)

References:

[1] J.H. Choy, S.Y. Kwak, J.S. Park, Y.J. Jeong, J. Portier, J. Am Chem. Soc. 121 (1999) 1399.

[2] J.H. Choy, S.Y. Kwak, Y.J. Jeong, J.S. Park, Angew Chem. Int. Ed. 39 (2000) 4042.

[3] J.H. Choy, S.Y. Kwak, J.S. Park, Y.J. Jeong, J. Mater. Chem. 11 (2001) 1671.

[4] S.Y. Kwak, W.M. Kriven, M.A. Wallig, J.H. Choy, Biomaterials 25 (2004) 5995.

[5] R.E. Davis, G.C. Icke, Adv. Clin. Chem. 23 (1983) 93.

[6] F.L. Iber, J.P. Blass, M. Brin, C.M. Leevy, Am. J. Clin. Nutr. (1982) 1067.

[7] F. Juana, V.-V. Concepción, J. Agric. Food. Chem. 49 (2001) 2313.

[8] R. Zhao, F. Gao, I.D. Goldman, Am. J. Physiol. Cell Physiol. 282 (2002) C1512.

[9] J.S. Casas, A. Castineiras, M.D. Couce, G. Martinez, J. Sordo, J.M. Varela, J. Orgnanomet. Chem. 517 (1996) 165.

[10] N.-H. Hu, W. Liu, K. Aoki, Bull. Chem. Soc. Jpn. 73 (2000) 1043.

[11] N. Hadjiliadis, J. Markopoulos, G. Pneumatikakis, D. Katakis, N. Theophanides, Inorg. Chim. Acta 25 (1977) 21.

[12] N. Hadjiliadis, J. Markopoulos, J. Chem. Soc., Dalton Trans. (1981) 1635.

[13] N. Hadjiliadis, J. Markopoulos, G. Pneumatikakis, D. Katakis, J. Clin. Hematal. Oncol. 7 (1977) 289.

[14] N.-H. Hu, K. Aoki, A.O. Adeyemo, G.N. Williams, Inorg. Chim. Acta 321 (2001) 9.

[15] M.F. Richardson, K. Franklin, D.M. Thompson, J. Am. Chem. Soc. 97 (1975) 3204.

[16] K. Dodi, M. Louloudi, G. Malandrinos, N. Hadjiliadis, J. Inorg. Biochem. 73 (1999) 41.

[17] K. Dodi, I.P. Gerothanasis, N. Hadjiliadis, A. Schreiber, R. Bau, I.S. Butler, P.J. Barrie, Inorg. Chem. 35 (1996) 6513.

[18] S.Y. Reddy, R. Pullakhandam, B.D. Kumar, Biometals 23 (2010) 247.

[19] N.-H. Hu, T. Norifusa, K. Aoki, Polyhedron 18 (1999) 2987.

[20] K. Dodi, I.P. Gerothanassis, N. Hadjiliadis, A. Schreiber, R. Bau, I.S. Butler, P.J. Barrie, Inorg. Chem. 35 (1996) 6513.

[21] G. Malandrinos, M. Louloudi, A.I. Koukkou, I. Sovago, C. Drainas, N. Hadjiliadis, J. Biol. Inorg. Chem. 5 (2000) 218.

[22] M. Louloudi, N. Hadjiliadis, Coord. Chem. Rev. 429 (1994) 135.

[23] R.F. Semeniuc, T.J. Reamer, M.D. Smith, New J. Chem**.** 34 (2010) 439.

[24] J.A Obaleye, A.C. Tella, R.O. Arise, Adv. Nat. Appl. Sci., 3 (2009) 43.

[25] P. Srivani, G.N. Sastry, J. Mol. Graphics and Modelling 27 (2009) 676.

[26] A.T. Colak, F. Colak, O.Z. Yesilel, O. Buyukgungor, J. Mol. Struct. 936 (2009) 67.

[27] P.O. Lowdin, Adv. Quantum Chem. 2 (1965) 213.

[28] J.S. Casas, A. Castineiras, M.D. Couce, G. Martinez, J. Sordo, J.M. Varela, J. Organomet. Chem. 517 (1996) 165.

[29] M. Louloudi, N Hadjiliadis, J.A Feng, S. Sukumar, R. Bau. J. Am. Chem. Soc. 112 (1990) 7233.

[30] J. Gary, A. Adeyemo, Inorg. Chim. Acta 55 (1981) 93.

[31] A. Adeyemo, F. Akinwumi, J. Coord. Chem. 14 (1986) 231.

[32] A. Bencini, E. Borghi, Inorg. Chim. Acta 135 (1987) 85.

[33] N. Hadjiliadis, M. Louloudi, I.S. Butler. Spectrochim. Acta Part A: Mol. Spectros. 47 (1991) 445.

[34] A. Adeyemo, R. Oderinde, A. Turner, A. Shamim, Bulletin des Sociétés Chimiques Belges, 96 (1987) 15.

[35] J. Crosby, R. Stone, G.E. Lienhard, J. Am Chem. Soc. 92 (1970) 2891.

[36] B. Maciasa, I. Garcia, M.V. Villa, J. Borras, A. Castineiras, F. Sanz, Polyhedron 21 (2002) 1229.

[37] J. Casabo, M. Izquierdo, J. Ribas, C. Diaz, Transition Met. Chem. 8 (1983) 110.

[38] L. Morales, M.I. Toral, M.J. Alvarez, Talanta 74 (2007) 110.

[39] A.T. Colak, F. Colak, O.Z. Yesilel, O. Buyukgungor, J. Coord. Chem. 62 (2009) 1650.

[40] H. Aghabozorg, A. Gholizadeh, M. Mirzaei, B. Notash, N. Moshki, Acta Cryst. E67 (2011) m891.

[41] H. Aghabozorg, A. Gholizadeh, M. Mirzaei, B. Notash, Acta Cryst. E6**7** (2011) m379.

Chapter 6

Mono or polynuclear copper(II) dipicolinate complexes

Coordination complexes of Cu(II) dipicolinates and nitrogenous bases play active role in chemical biology [1-4]. Nucleobase incorporated Cu(II) dipicolinate complexes are found to act as artificial nucleobases [5]. Both dipicolinic acid and chelidonic acid are incorporated into the skeletons of molecules that inhibit β-site amyloid precursor protein cleaving enzyme, which are used in therapeutics for Alzheimer's disease [6]. Copper(II) dipicolinate peptidomimetic conjugates are used as potential inhibitors of the Src homology 2 domain of the Src tyrosine kinase [7]. Further, mixed ligand complexes are also important in biology because in biological fluids the different ligands are likely to compete for metal ions *in vivo* [8]. Beyond the chemical biology, due to multiple coordination modes of dipicolinates to metal ions, and the ability to form extensive arrays of hydrogen bonding, the ligand is available in many metal-organic frameworks discussed in the previous chapters. It adopts diverse binding modes such as monodentate, bidentate or tridentate chelating as discussed in chapter 1. The chelation and sidewise coordination of carboxylate oxygen of dipicolinate ligand leads to formation of self-assembly. Such assemblies may be in the form of mixed metal complexes or coordination polymers. The structural varieties are encountered in structures of dipicolinate complexes with nitrogen containing ligands as well as in stabilization of interesting water clusters [9-13]. Since the side on binding mode needs approach of a bulky ligand to another metal ion, such coordination mode will be guided by steric factor. Despite of large numbers of structural studies on the intercalation of cations in the layered structures of dipicolinate complexes, there is limited study on the structural aspects about the role of ancillary ligands on the structure of dipicolinate complexes. Thus, there is further scope to use this metal dipicolinate complex anion as a ligand to make multinuclear species.

We have extended the research in this area by synthesizing mono or polynuclear Cu(II) dipicolinate complexes with nitrogen containing ancillary ligands. The role of the ancillary ligands such as imidazole (im), pyridine (py), 2,2′-bipyridine (bpy) and 1,10-phenanthroline (phen) in the assembly of Cu(II) dipicolinate complexes are presented. Effect of

monodentate and bidentate chelating ligands on the structural variations of Cu(II) dipicolinate complexes are discussed. In addition, the nature of the ligand and competition between ligand exchange versus aquation by the metal ion is also presented. The poly-nuclear complexes are prepared by taking advantage of different binding modes of dipicolinate ligands. Reactions of copper (II) acetate monohydrate with dipicolinate ligand (L) and ancillary ligands such as imidazole, pyridine, 2,2′-bipyridine and 1,10-phenanathroline led to the formation of the complexes (Scheme 6.1). The crystal morphologies of the complexes are shown in Fig. 6.1.

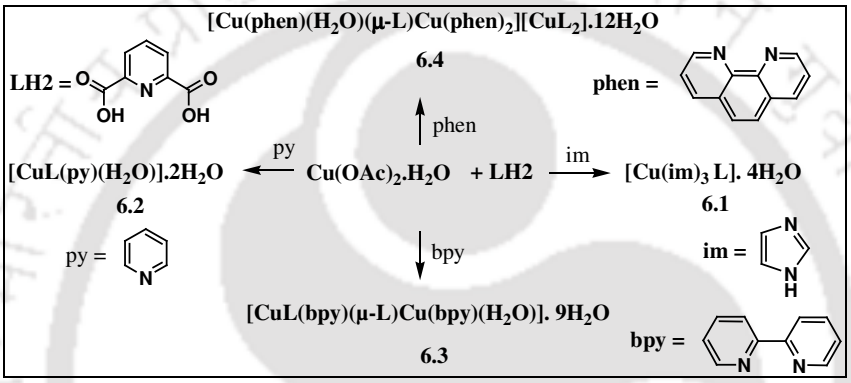

Scheme 6.1: Synthesis of the complexes

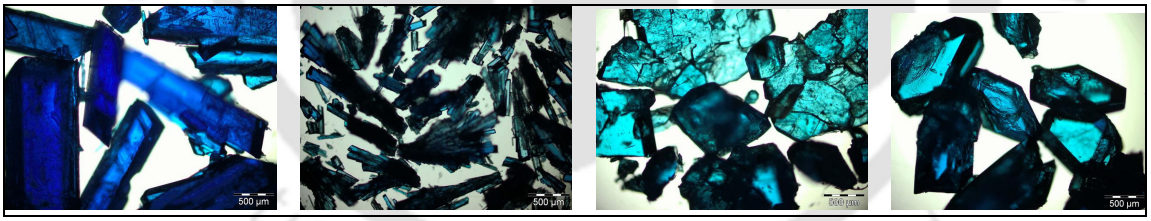

6.1 **6.2** **6.3** **6.4**

Fig. 6.1: Optical micrograph of the complexes **6.1 - 6.4**

6.1: Cu(II) dipicolinate complex with imidazole as ancillary ligand

The coordination complex $[CuL(im)_3]\cdot 4H_2O$ (**6.1**) was synthesized from the reaction of dipicolinic acid and imidazole ligand by treating with Cu(II) acetate monohydrate in methanol/water mixture under ambient condition. Complex **6.1** has distorted octahedral environment around the copper ion. The ligands around the copper ion comprise one tris chelate dipicolinate ligand and three imidazole ligands. The complex has four water molecules of crystallization. The asymmetric unit of complex $[CuL(im)_3]\cdot 4H_2O$, as shown in

Fig. 6.1.1a, has two crystallographically independent mononuclear complex molecules (Z′ = 2). There are two different [CuL(im)$_3$] units organized in staggered fashion in each asymmetric unit, so that a tight packed structure is obtained by filling the interstitial spaces with water molecules of crystallization. These symmetry non-equivalent molecules interact with each other through hydrogen bond interactions. Such interactions arise from the N-H bond of the imidazole moiety with the carboxylate oxygen of two neighboring units of dipicolinate, as well as from the water molecules in the interstices. These complimentary interactions contribute to cause symmetry non-equivalence among the complex molecules by carrying the signature of an orientation required to make the two molecules to be non-equivalent in terms of the symmetry relationship. Some prominent hydrogen bonds involved are N5-H5···O5 ($d_{D\cdots H}$, 1.84(2) Å, $d_{D\cdots A}$, 2.70(4) Å; ∠D-H···A, 176(23)°) and N12-H5···O4 ($d_{D\cdots H}$, 1.92(3) Å, $d_{D\cdots A}$, 2.77(4) Å; ∠D-H···A, 170.5(24)°) (Fig. 6.1.1b).

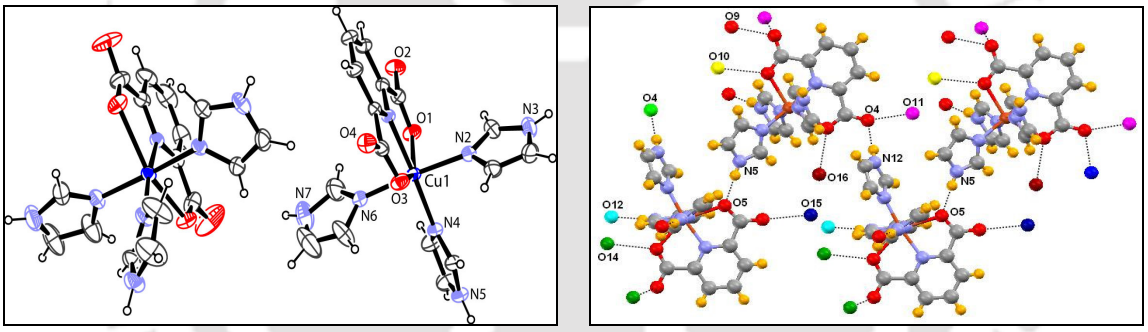

(a) (b)

Fig. 6.1.1: (a) ORTEP of complex **6.1** (drawn with 30% thermal ellipsoids; crystallized water molecules are omitted for clarity), (b) H-bond interactions between the symmetry independent units of **6.1** along with crystallized water molecules.

The phenomenon of symmetry non-equivalence (high Z′) in inorganic molecules is less studied [14-18]. Generally, Z′ denotes the number of molecules in asymmetric unit in a single component system. It is believed that symmetry non-equivalence arises due (i) irregular and non-self complimentary molecular shape, (ii) relatively less number of interacting functional groups, (iii) competition between the close packing and strong directional interactions, mismatched length between the molecules etc. [16]. Weak interactions are directional, thus, they play a major role in the phenomenon, which is related to the symmetry of packing the molecules in the crystal lattice.

The stability of the crystal lattice of complex **6.1** is further enhanced by various hydrogen bond interactions between the crystallized water molecules, either through the oxygen atom of the dipicolinates or nitrogen atom of imidazole. The hydrogen atoms of the water molecules of crystallization in this complex could not be located in the X-ray crystal structure. Copper complexes $[CuL(LH_2)]\cdot xH_2O$ (where x is an integer) that are devoid of ancillary ligands are reported in literature [19]. These complexes have self-assembled structures through hydrogen bonds. On the other hand, imidazole and benzimidazole have similar structural features in terms of ligating sites; the difference is that the later has an extra aromatic ring. The crystal structure of a penta-coordinated mono-aqua, mono-benzimidazole copper dipicolinate complex is known [20], in which one benzimidazole and an aqua ligand are present. Thus it may be concluded that the ligating ability along with the supramolecular feature with the ancillary ligands are important in deciding the composition of imidazole complexes.

6.2: Cu(II) dipicolinate complex with pyridine as ancillary ligand

Crystals of the complex $[CuL(py)(H_2O)]\cdot 2H_2O$ (**6.2**) were obtained in the $P2_1/c$ space group. It is a penta-coordinated complex with a square pyramidal geometry (Fig. 6.2.1a). The base of each square pyramid is constituted by one tridentate ligand L and a monodentate py ligand. One aqua ligand is coordinated with the Cu(II) ion in the axial position to complete the square pyramid. In this complex, the aromatic plane of the py molecule is not collinear to the plane of the aromatic ring of the dipicolinate unit. There are intermolecular hydrogen bonds between the coordinated water molecules that connect to the oxygen atoms of the carboxylate units, as illustrated in Fig. 6.2.1b. This makes a layered structure in which the interstitial water molecules are trapped. The formation of the five coordinate copper complex **6.2** is attributed to the extensive hydrogen bonding among the molecules. A careful look at the packing of the molecules in the crystal lattice of this penta-coordinate complex suggests that for an external ligand to occupy the sixth position, it would have to overcome the repulsive forces offered by the O4 atom. It would also have to force the pyridine ring to rotate, so as to bring it in line with the plane of the dipicolinate ligand. In this complex the plane of pyridine ligand is slightly oblique. This plane has a dihedral angle of 36.9º with the plane of the dipicolinate ligand.

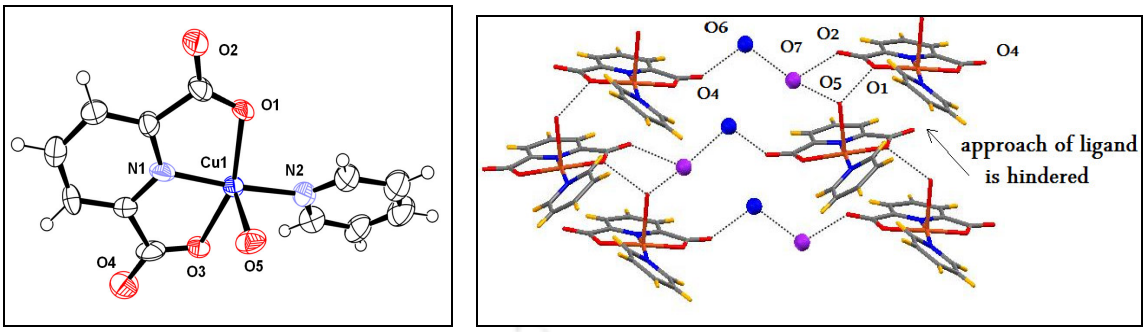

(a) (b)

Figure 6.2.1: (a) ORTEP of complex **6.2** (drawn with 50% thermal ellipsoids; water of crystallization are not drawn for clarity), (b) Hydrogen bond interactions.

A Cu(II) dipicolinate complex with 2-(2-hydroxyethyl)pyridine, [Cu(hepy)(L)H_2O] (where hepy = 2-(2-hydroxyethyl)pyridine) was reported recently [21]. In this complex Cu(II) is in a distorted octahedral environment, coordinating with one L, an aqua ligand and with 2-(2-hydroxyethyl)pyridine which acts as a chelating ligand. With 2-aminopyridine, a four coordinated Cu(II) complex is observed where one L and one 2-aminopyridine ligand is attached [22]. It is also reported that Cu(II) dipicolinate form adducts with 2-aminopyridine, where it remains as a cation in the outside of the coordination sphere (Ch. 1, [85]). It can also be mentioned that pyridine may remain in the outside the coordination sphere as pyridinium ion instead of coordinating with metal ion. This study therefore shows that coordination and protonation ability of the ancillary ligand may play important role to decide the nature of the complexes.

6.3: Synthesis, characterization and structural features of Cu(II) dipicolinate complex with 2,2′-bipyridine as ancillary ligand

A dinuclear complex [CuL(bpy)(μ-L)Cu(bpy)H_2O]·9H_2O (**6.3**), was obtained from the reaction of copper(II) acetate monohydrate with LH_2 and bpy. In the complex, the two copper ions are in different environments. Each copper has a distorted octahedral geometry. Both the copper centers are meridional, having L in a tridentate fashion, whereas the bpy ligands bind to the metal centers through nitrogen atoms in a bidentate fashion (Fig. 6.3.1a). For Cu1, the sixth coordination site is occupied by a water molecule whereas in the case of

Cu2 the sixth position is occupied by a carboxylate oxygen atom of a bridging L ligand. The two copper centers are separated by a distance of ~ 5.56 Å. The dihedral angle between the L and bpy plane at the Cu1 site 78.13º, whereas the same angle at the Cu2 site is observed to be 83.55º. Carbonyl groups of dipicolinate complexes are generally involved in coordinating to alkali and alkaline earth metals as discussed in chapter 1. Further such binding to carbonyl complexes leads to coordination polymers that are useful in making metal-organic hybrid materials. In the case of complex **6.3**, it is observed that the Cu1-O9 bond distance [2.02(9) Å] is shorter than the Cu1-O1 [2.25(9) Å] or Cu1-O3 [2.38(10) Å]. This suggests that the elongation of the bonds in the distorted octahedron is in the O1-Cu1-O3 direction in one part of the complex. In the other part of the complex, Cu2-O4 is 2.02(7) Å, whereas the bond distances of Cu2-O7 and Cu2-O5 are 2.27(11) and 2.39(11) Å respectively, suggesting elongation along the O5-Cu2-O7 direction. The crystal structure of **6.3** possesses nine water molecules as solvent of crystallization occupying the interstitial spaces of the complex. Each of these water molecules involve in extensive and complicated network of hydrogen bonding with coordinated water molecules as well as with carboxylate oxygen atoms (Fig. 6.3.1b).

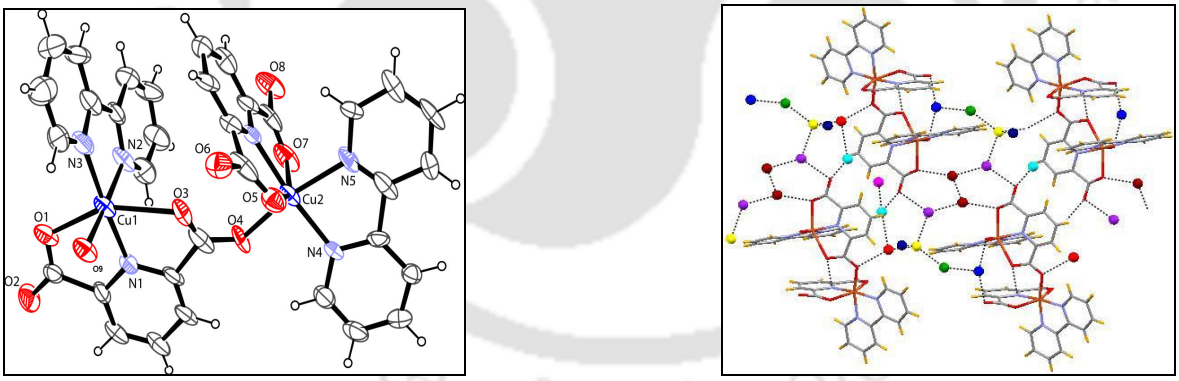

(a) (b)

Fig. 6.3.1: (a) ORTEP of complex **6.3** (drawn with 50% thermal ellipsoids; water of crystallization are omitted for clarity), (b) Hydrogen bond interactions with the crystallized water molecules.

In contrast to our dinuclear complex **6.3**, it was shown earlier that the reaction between LH_2 and $[Cu(bpy)Cl_2]$ led to the formation of the ionic complex $[Cu(LH_2](bpy)H_2O]$ $[CuL_2]\cdot 3H_2O$ that consists of two distinct cationic and anionic species (Ch. 1, [54]). Thus,

the method of preparation is an important factor in obtaining different compositions and coordination modes.

6.4: Synthesis, characterization and structural features of Cu(II) dipicolinate 1,10-phenanthroline complex

The complex $[Cu(phen)(H_2O)(\mu\text{-}L)Cu(phen)_2][CuL_2]\cdot 12H_2O$ **(6.4)** crystallizes as a pair of complex ions (Fig. 6.4.1a). The cation $[Cu(phen)(H_2O)(\mu\text{-}L)Cu(phen)_2]^{2+}$ consists of a dinuclear copper unit derived from L and phen ligands and the anion is $[CuL_2]^{2-}$. The dipicolinate ligand is coordinated to the Cu1 center and a phen ligand along with an aqua ligand, resulting in the formation of a distorted octahedral environment. The Cu2 ion of the dinuclear cation is bridged by the carboxylate oxygen atoms of L and it has two phen ligands attached through nitrogen donors, and it has a similar environment to Cu1. It may be mentioned that ligand scrambling is not a common feature in dipicolinate complexes, as in our earlier study we observed positive cooperativity of the dipicolinate ligands (Ch. 2). Presumably, the scrambling of a ligand in the present case occurs to minimize the repulsive effect between the coordinated ligands and to maximize the stability in this system by stacking the phen rings in near parallel layers. The complex has an unusual carboxylate bridge. In general, the carbonyl oxygen of carboxylate coordinates to metal cations to form dinuclear or polynuclear complexes, but in this complex the coordination takes place by the oxygen atom, which is already coordinated with Cu1 (Fig 6.4.1b). This is reflected in the bond distances; the Cu2-O1 distance is 2.01 Å whereas the Cu2-O2 distance is 2.74 Å, and the latter interaction may be considered to be a weak interaction. This effect may be due to the stacking of the phen ligands in the crystal packing, which forces the O1 atom to project away by virtue of stack formations between phen rings attached to two independent metal sites. The situation can be explained as coordination of a neutral molecule [CuL(phen)] to the complex cation $[Cu(phen)_2]^{2+}$ through chelate formation, as illustrated in Fig. 6.4.1b. The nearly parallel phen ligands in cationic part $[Cu(phen)_2]^{2+}$ shows face to face π-π stacking interactions. The minimum (centroid to centroid) distance between two such rings of phen ligands is ~ 3.71 Å. A similar π-π stacking interaction between the phen ligands was reported by Goldberg and coworkers in the complex $[CoCl_2(phen)_2][CoCl(phen)_2(H_2O)]\cdot Cl\cdot 6H_2O$ [23]. The phen ligands of the cationic part $[CoCl(phen)_2(H_2O)]^{+}$ of this

complex shows face to face π-π (centroid to centroid) distance of ~ 3.73 Å, similar to the complex **6.4** described here. Thus, π-stacking interaction is an important and reliable motif among planar aromatic ligands widely used in supramolecular chemistry [24].

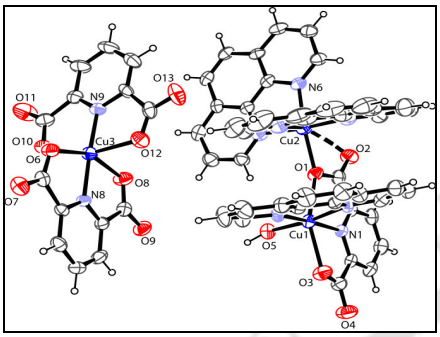

(a)

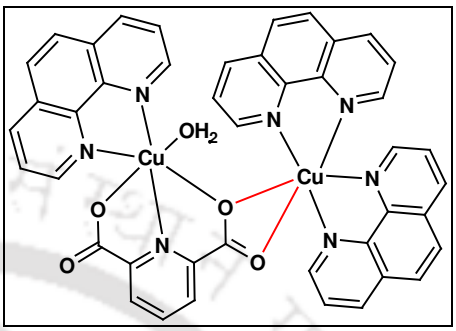

(b)

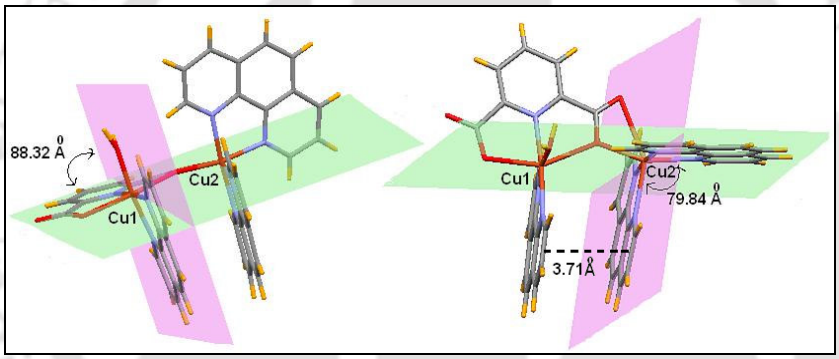

(c)

Fig. 6.4.1: ORTEP of complex **6.4** (drawn with 30% thermal ellipsoids), (b) Cationic part showing chelation to a neutral complex, (c) View from two directions of the Cu(II) ions in the cationic part of complex **6.4** to show the π-π interaction and the dihedral angles between the ligands attached to $[CuL_2]^{2-}$ (the anion $[CuL_2]^{2-}$ is omitted in both views).

The dihedral angle between the dipicolinate and phen plane at the Cu1 site is 88.32º, whereas the same angle between the two phen planes at the Cu2 site is observed to be 79.84º (Fig. 6.4.1c). In addition to electrostatic interactions, the complex is also stabilized by extensive hydrogen bond interactions. Such interactions arise from the twelve crystallized water molecules present in the asymmetric unit. The only H-bond interaction between the coordinated water of the cationic part and the carboxylate oxygen atom of anionic part takes place through O5-H5A···O7 [d = 1.78(3) Å, D = 2.71(3) Å, θ = 166.4(4)º]. Since the hydrogen atoms in most of the water molecules could not be located, a complete hydrogen-

bonding table is not presented. The reaction between dipicolinic acid and [Cu(phen)Cl_2] was reported to form a neutral copper(II) dinuclear complex [$Cu_2(LH_2)$(dipic)(phen)]·5.5H_2O (Ch. 1, [54]). In contrast to this we have observed an ionic complex **6.4**, which has different environments for the two different copper ions. It is to be noted that a mononuclear five coordinate distorted square pyramidal Cu(II) complex having bidentate 2,9-dimethyl- 1,10-phenanthroline (dmphen) and tridentate L ligands is reported in literature [25]. This complex shows face-to-face and slipped π-π interactions between dmphen rings of neighboring molecules. Thus, our results suggest that the formation of different products is guided by the steric factors associated with the ligands and the method of preparation.

In thermogravimetry, the complex shows loss of crystallized water molecules in the range of 50-100 ºC (obsd. 14.1%, calcd. 14.8%). This is followed by sharp loss of 1,1-phenenthroline ligands in narrow temperature range 240-270 ºC (obsd. 35.5%, calcd. 37.0%). The 3rd step is the usual continuous decomposition of Cu(II) dipicolinates that begins at ~ 300 ºC. The powder pattern of the bulk samples shows agreement with those simulated from the single crystal data, depicting the pure phase of the complex **6.4** (Fig. 6.4.2b).

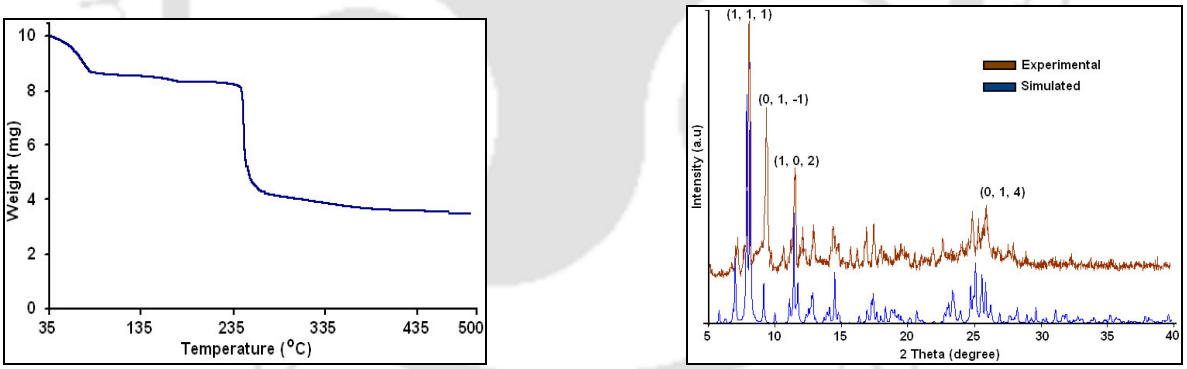

(a) (b)

Fig. 6.4.2: (a) Thermogram of complex **6.4** and (b) Simulated and experimental PXRD pattern of complex of **6.4**.

6.5: Conclusion

In this chapter, we have synthesized and characterized four Cu(II) dipicolinate complexes in association with nitrogen containing ancillary ligands. Although similar stoichiometries are

taken, the composition and structural features of the complexes are found to be different in each case. In the case of imidazole there is three imidazole ligand per copper(II) ion; whereas in case of pyridine there is only one pyridine per copper(II) ion. Among pyridine and imidazole, both being monodentate ligand have different skeleton of heterocyclic ring that has differences in terms of ability to coordinate with metal ions. The presence of a single pyridine ligand per copper ion in complex **6.2** is attributed to self-association assisted by water of crystallization among the molecules, inhibiting the approach of additional ligands to the metal site. Thus, it can be imagined that such processes are guided by two major factors; nature of the ligand and competition between ligand exchange versus aquation in the complexes. The formation of assemblies guided by bidentate ligands such as 2,2′-bipyridine and 1,10-phenanthroline in copper dipicolinate complexes are also studied. The dinuclear assemblies in complexes **6.3** and **6.4** differ due to the nature of the two different aromatic ligands. We found that with 2,2′-bipyridine dinuclear Cu(II) dipicolinate complex is formed, whereas in the case of 1,10-phenthroline, the cationic dimer formed have scrambled ligand among two copper ions making a complex dication, whose charges are neutralized by $[CuL_2]^{2-}$. In complex **6.4**, the stacking effect of the phen ligand decides the non-uniform distribution of ligands amongst the two copper ions. These compounds are synthesized under thermodynamic conditions, so the self-assembling process in the solid state may be taken as the signature carried from the structures in solution.

6.6: Experimental section

Detailed synthetic methodologies for the described complexes are given below. Analytical as well as spectroscopic data are also listed along with each of the complexes.

6.6.1: $[CuL(im)_3]\cdot 4H_2O$ (6.1), $[CuL(py)(H_2O)]\cdot 2H_2O$ (6.2), $[CuL(bpy)(\mu\text{-}L)Cu(bpy)(H_2O)]\cdot 9H_2O$ (6.3) and $[Cu(phen)(H_2O)(\mu\text{-}L)Cu(phen)_2][CuL_2]\cdot 12H_2O$ (6.4)

To a methanolic solution (20 ml) of dipicolinic acid (0.334 g, 2.0 mmol), an aqueous solution of copper(II) acetate monohydrate (0.199 g, 1.0 mmol) was added and stirred for half an hour. A blue precipitate was obtained. The precipitate obtained was further reacted with heterocyclic compounds namely imidazole, pyridine, 2,2'-bipyridine and 1,10-

phenanthroline (1.0 mmol each) in independent experiments to obtain homogeneous solutions in each case. The solutions on standing at room temperature resulted in the formation of crystals after 3-4 days.

Complex **6.1:** Isolated yield: 64%. Elemental anal calcd for $C_{16}H_{23}CuN_7O_8$; C, 38.02; N, 19.41; H, 4.55%; found C, 38.23; N, 19.23; H, 4.71%. IR (KBr, cm^{-1}): 3437 (b, s), 3129 (m), 1699 (w), 1616 (s), 1597 (w), 1429 (m), 1371 (s), 1076 (s). Vis (H_2O) λ_{max}: 773.0 nm; ε = 92.0 M^{-1} cm^{-1}. μ_{eff}. at 298 K: 1.68 BM. Thermal analysis: decomposition range: ~ 65-115 ºC (evaporation of four water molecules of crystallization); further decomposition occurs at ~ 252 ºC.

Complex **6.2:** Isolated yield: 61%. Elemental anal calcd for $C_{12}H_{12}CuN_2O_7$; C, 39.80; N, 7.73; H, 3.86%; found C, 39.93; N, 7.70; H, 3.97%. IR (KBr, cm^{-1}): 3429 (b, s), 3089 (m), 1661 (w), 1633 (s), 1596 (w), 1366 (m), 1180 (s), 1085 (s). Vis (H_2O) λ_{max}: 777.0 nm; ε = 88.0 M^{-1} cm^{-1}. μ_{eff}. at 298 K: 1.72 BM. Thermal analysis: decomposition range: ~ 60-120 ºC (evaporation of coordinated and crystallized water molecules); further decomposition occurs at ~ 278 ºC.

Complex **6.3:** Isolated yield: 54%. Elemental anal calcd for $C_{34}H_{40}Cu_2N_6O_{18}$; C, 43.04; N, 8.86; H, 4.22%; found C, 42.84; N, 8.67; H, 4.04%. IR (KBr, cm^{-1}): 3443 (b, s), 1645 (s), 1588 (w), 1475 (m), 1427 (m), 1363 (s), 1278 (m), 1031 (m). Vis (H_2O) λ_{max}: 772.0 nm; ε = 82.0 M^{-1} cm^{-1}. μ_{eff}. at 298 K: 1.69 BM. Thermal analysis: decomposition range: ~ 50-110 ºC (evaporation of crystallized water molecules); further decomposition occurs at ~ 232 ºC.

Complex **6.4:** Isolated yield: 52%. Elemental anal calcd for $C_{57}H_{59}Cu_3N_9O_{25}$; C, 46.82; N, 8.62; H, 4.04%; found C, 46.51; N, 8.50; H, 3.87%. IR (KBr, cm^{-1}): 3410 (b, s), 3061 (w), 1627 (w), 1587 (s), 1516 (m), 1427 (m), 1369 (s), 1275 (m). Vis (H_2O) λ_{max}: 778.0 nm; ε = 96.0 M^{-1} cm^{-1}. μ_{eff}. at 298K: 1.75 BM. Thermal analysis: decomposition range: ~ 50-125 ºC (evaporation of crystallized water molecules); further decomposition occurs at ~ 248 ºC.

6.7: Crystal structure and refinement parameters of the complexes 6.1-6.4

Compound No.	**6.1**	**6.2**	**6.3**	**6.4**
Formula	$C_{16}H_{23}CuN_7O_8$	$C_{12}H_{12}CuN_2O_7$	$C_{34}H_{40}Cu_2N_6O_{18}$	$C_{57}H_{59}Cu_3N_9O_{25}$
Formula wt.	504.95	361.79	947.80	1460.75
Crystal system	Triclinic	Monoclinic	Triclinic	Triclinic
Space group	*P-1*	*P2₁/c*	*P-1*	*P-1*
a (Å)	11.6309(19)	14.8001(8)	10.3205(12)	14.4488(8)
b (Å)	14.833(4)	13.4613(7)	13.3677(17)	15.5726(9)
c (Å)	15.572(3)	7.1451(4)	16.1299(19)	15.9094(9)
α (deg)	109.406(12)	90.00	85.115(7)	78.386(2)
β (deg)	108.450(9)	90.344(3)	75.815(7)	63.553(2)
γ (deg)	100.940(13)	90.00	67.397(6)	81.014(2)
V (Å^3)	2269.3(8)	1423.48(13)	1991.6(4)	3130.4(3)
Z	4	2	2	2
D_{calc} (gcm^{-3})	1.478	1.688	1.580	1.550
μ (mm^{-1})	1.018	1.572	1.153	1.100
F(000)	1044	740	976	1502
Total no. of reflns	27259	7509	23511	29108
Independent reflns.	7451	2492	6461	9869
$\theta_{max.}$	1.52 – 24.50	1.38 – 25.00	1.30 – 24.50	1.45 – 24.5
Ranges	$-13 \le h \le 13$	$-8 \le h \le 8$	$-12 \le h \le 12$	$-16 \le h \le 15$
(h, k, l)	$-17 \le k \le 17$	$-15 \le k \le 16$	$-15 \le k \le 14$	$-18 \le k \le 15$
	$-17 \le l \le 18$	$-17 \le l \le 17$	$-18 \le l \le 18$	$-18 \le l \le 18$
Completeness to 2θ (%)	98.8	99.0	97.4	94.7
Data / restraints / parameters	7451 / 0 / 577	2492 / 0 / 199	6461 / 0 / 541	9869 / 2 / 795
GOF (F^2)	0.933	1.036	1.177	1.175
R_1, wR_2 [$I > 2\sigma(I)$]	0.0439, 0.1313	0.0672, 0.2179	0.0720, 0.2077	0.0749, 0.2292
R_1, wR_2 (all data)	0.0579, 0.1405	0.0902, 0.2492	0.1030, 0.2403	0.1037, 0.2403
Largest diff peak/hole (e Å^{-3})	0.502 / -0.399	1.070 / -1.156	1.046 / -1.156	1.082 / -0.582

References:

[1] X. Wu, P.G. Schultz, J. Am. Chem. Soc. 131 (2009) 12497.

[2] L.A. Levine, M.E. Williams, Curr. Opin. Chem. Biol. 13 (2009) 669.

[3] C. Liu, L. Wang, Dalton Trans. (2009) 227.

[4] M.M. Rodriguez-Ramos, J.J. Wilker, J. Biol. Inorg. Chem. 15 (2010) 629.

[5] E. Meggers, P.L. Holland, W.B. Tolman, F.E. Romesberg, P.G. Schultz, J. Am. Chem. Soc. 122 (2000) 10714.

[6] Y. Hamada, H. Ohta, N. Miyamoto, R. Yamaguchi, A. Yamani, K. Hidaka, T. Kimura, K. Saito, Y. Hayashi, S. Ishiura, Y. Kiso, Bioorg. Med. Chem. Lett. 18 (2008) 1654.

[7] B. Schmidt, J. Jiricek, A. Titz, G. Ye, K. Parang, Bioorg. Med. Chem. Lett. 14 (2004) 4203.

[8] M. Koman, J. Moncol, D. Hudecova, B. Dudova, M. Melnik, M. Korabik, J. Mrozinski, Pol. J. Chem. 75 (2001) 957.

[9] A.J. Blake, M. Felloni, P. Hubberstey, C. Wilson, M. Schroder, Acta Cryst. E58 (2002) m43.

[10] L. Mao, Y. Wang, Y. Qi, M. Cao, C. Hu, J. Mol. Struct. 688 (2004) 197.

[11] M.P. Brandi-Blanco, D. Choquesillo-Lazarte, C.G. Garcıa-Collado, J.M. Gonza´lez-Pe´rez, A. Castineiras, J. Niclo´s-Gutie´rrez, Inorg. Chem. Commun. 8 (2005) 231.

[12] S. Cui, Y. Zhao, J. Zhang, Q. Liu, and Y. Zhang, Cryst. Growth Des. 8 (2003) 3803.

[13] A.A. El-Sherif, B.J.A. Jeragh, Spectrochim. Acta A68 (2007) 877.

[14] K.M. Anderson, A.E. Goeta, J.W. Steed, Cryst. Growth Des. 8 (2008) 2517.

[15] G.R. Desiraju, CrystEngComm 9 (2007) 91.

[16] J.W. Steed, CrystEngComm 5 (2003) 169.

[17] T. Steiner, Acta Cryst. 56B (2000) 673.

[18] A. Gavezzotti, CrystEngComm 10 (2008) 389.

[19] E.E. Sileo, M.A. Blesa, G. Rigotti, B.E. Rivero, E.E. Castellano, Polyhedron 15 (1996) 4531.

[20] G.-Y. Dong, L.-H. Fan, L.-X. Yang, I.U. Khan, Acta Cryst. 66E (2010) m532.

[21] O. Tamer, B. Sariboga, I. Ucar, Struct Chem. 23 (2012) 659.

[22] E. Altin, R. Kirchmaier, A. Lentz, Z. Kristallogr. NCS 219 (2004) 35.

[23] J.M. Rubin-Preminger, L, Kozlov, I. Goldberg, Acta Cryst. C64 (2008) m83.

[24] E.R.T. Tiekink, J. Zukerman-Schpector (eds.), The Importance of Pi-Interactions in Crystal Engineering: Frontiers in Crystal Engineering, John Wiley and Sons, UK, 2012.

[25] I. Ucar, A. Bulut, O. Buyukgungor, Acta Cryst. C61 (2005) m479.

Chapter 7

Metal dipicolinates stabilized hydrogen bonded water clusters

Water plays an important in biological self-assembly processes such as in protein-DNA binding, native conformation of biopolymers etc. [1-4]. They are relevant to crystal engineering, because of their versatile hydrogen bonding capabilities in crystalline solids [5-6]. In pharmaceutical science, a large number of API molecules prefer the hydrated form than the anhydrous one [7-8]. Encapsulation of water clusters in the metal-organic frameworks has been widely studied. Due to relatively small size and diverse hydrogen bonding interactions, water molecules can readily be incorporated into crystal lattice to stabilize the crystal packing [9-10]. The stabilization of different types of water clusters, $(H_2O)_n$ (n = 2-20), infinite 1D or 2D water chain is of considerable interest among crystal engineers and theoretical scientist. One-dimensional water chains play key role in the transport of water, protons, and ions in biological processes [11-17]. The decameric cluster $(H_2O)_{10}$ stabilized by dimeric Cu(II) complex reported by Atwood and coworkers shows resemblance with ice-like molecular arrangement [18]. Hexameric clusters are the building blocks of ice I_h and have relevance to structure of liquid water [19-21]. Some of interesting water clusters available in literature are shown in Fig. 7.1.

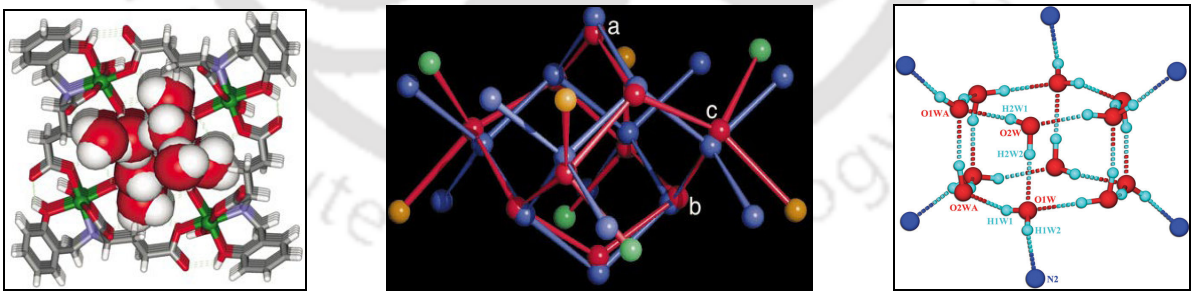

(a) (b) (c)

Fig. 7.1: (a) 1D helical water chain (top view) in cavities of $[(H_2O)_2\{Ni(Hsglu)(H_2O)_2\}]\cdot H_2O$ (H_3sglu = N-(2-hydroxybenzyl)-l-glutamic acid) reported by Vittal and coworkers [12], (b) Atwood's decameric cluster $(H_2O)_{10}$ stabilized by dimeric Cu(II) complex [18], (c) Hexagonal prismatic dodecameric water cluster encapsulated in supramolecular network of $[(Bmib)_3\ (H_2O)_{12}]_n$ (where Bmib = 1,4-bis(2-methylimidazol-1´-yl)butane (Li and coworkers) [20].

Because of hydrophilic nature, metal dipicolinate complexes are known to form different types of water clusters. Whether small water clusters are very common, some higher ordered water clusters are also discussed in chapter 1. Though large number water clusters have been reported in literature relevant to biological and chemical importance, formation of different types of water clusters by varying the composition of a metal organic framework in a single component system are not yet established. We have synthesized relatively large sized ionic complexes with metal dipicolinate complex as anion and bulky cationic complex derived from transition metals and 1,10-phenanthroline ligand or in association with 2,2′-bipyridine or aqua ligand. Change in ligand composition of the cationic part showed creation of both hydrophilic and hydrophobic environment in the complex. An attempt has been made to encapsulate new types of water clusters by varying the central metal ion or the local cationic or anionic environment of the complex. Thus, this chapter deals with stabilization five different types of hydrogen bonded water clusters in the interstices of the supramolecular ionic complexes, namely $[Co(phen)_2(H_2O)_2][ZnL_2]\cdot 7H_2O$ (**7.1**), $[Ni(phen)_2(bpy)][CoL_2]\cdot 8H_2O$ (**7.2**) and $[Co(phen)_3][MnL_2]\cdot 12H_2O$ (**7.3**), $[Ni(phen)_3][CoL_2]\cdot 9H_2O$ (**7.4**), $[Ni(phen)_3]_2\,[ZnL_2]_2\cdot 20H_2O$ (**7.5**) (where phen = 1,10-phenanthroline, bpy = 2,2′-bipyridine, L = dipicolinate). The complexes are synthesized by mixing their preformed cationic and anionic parts together (Chart 7.1).

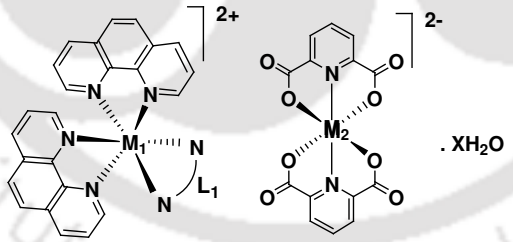

$[M_1(phen)_2L_1][M_2L_2].xH_2O$

Complex 7.1: $M_1 = Co^{2+}$, $M_2 = Zn^{2+}$, $L_1 = 2H_2O$, X = 7

7.2: $M_1 = Ni^{2+}$, $M_2 = Co^{2+}$, L_1 = bpy, X = 8

7.3: $M_1 = Co^{2+}$, $M_2 = Mn^{2+}$, L_1 = phen, X = 12

7.4: $M_1 = Ni^{2+}$, $M_2 = Co^{2+}$, L_1 = phen, X = 9

7.5: $M_1 = Ni^{2+}$, $M_2 = Zn^{2+}$, L_1 = phen, X = 10

Chart 7.1: Synthesized complexes

Selection of metal ions in these complexes are based on the differences in CFSE of first row transition metal ions towards 1,10-phenanthroline or 2,2′-bipyridine (strong-field) and dipicolinate (weak-field) ligands. Mn(II), being a hard acid prefers to bind with dipicolinate ligand, whereas Ni(II)/Co(II) (borderline acid) coordinates with 1,10-phenanthroline in an octahedral environment. Zn(II) also prefers dipicolinate anion in these mixed ionic complexes because of zero CFSE in an octahedral environment [22].

The complexes are characterized by various spectroscopic, thermal and X-ray diffraction techniques. The complexes exhibit intense IR absorptions in the range of 3415-3399 cm^{-1} for O-H absorptions. The carboxylate groups exhibit similar stretching frequencies in the range of 1626-1585 cm^{-1} and 1378-1374 cm^{-1} as observed earlier, due to asymmetric and symmetric stretching respectively. Due to larger size of the charged species, the complexes show low molar conductance values in the range of 109.0-121.0 S cm^2 mol^{-1} in water. X-ray powder pattern were recorded to confirm the bulk purity of the complexes. TG analyses were carried out to see the thermal stability of the water clusters.

7.1: Infinite cyclic decameric water cluster in mixed ionic complex, $[Co(phen)_2(H_2O)_2][ZnL_2]\cdot 7H_2O$

Two separate coordination complexes, Co(II) phenanthroline and Zn(II) dipicolinates, were synthesized independently and mixed them in one-pot to form the complex $[Co(phen)_2(H_2O)_2][ZnL_2]\cdot 7H_2O$ (**7.1**). The complex **7.1** consists of two distinct cationic and anionic complexes along with seven lattice water molecules. The anionic unit $[ZnL_2]^{2-}$ has an octahedral Zn(II) center with two meridionally coordinated dipicolinate ligands. The cationic unit comprised of a Co(II) center coordinating with two bidentate 1,10-phenanthroline ligands and two aqua ligands to provide a composition $[Co(phen)_2(H_2O)_2]^{2+}$ with an octahedral geometry. The key feature of the complex is that out of seven water molecules of crystallization, the group of five (O12w, O13w, O14w, O15w and O17w) and their symmetry related partners assemble in formation of hydrogen-bonded centrosymmetric cyclic decamer $(H_2O)_{10}$ with chair conformation (Fig. 7.1.1a). The cyclic decamer, thus formed further propagates through both O16w and disordered O17w molecule, resulting in an infinite two-dimensional cyclic decameric chain. Aggregation of 10-water molecules

entangled in 2D infinite chain in metal-organic framework is obtained as rare case, however discrete decameric units are commonly observed [23-26]. In the crystal lattice, the infinite 2D decameric cluster is stabilized by four identical $[ZnL_2]^{2-}$ units *via* hydrogen bonding to the carboxylate O atoms leading to a complicated 3D network structure (Fig. 7.1.1b). The prominent H-bond interactions are O15w--H(15A)···O2 ($d_{D\ldots H}$, 1.820(2) Å, $d_{D\cdots A}$, 2.749(2) Å; ∠D-H···A, 176(3)°), O12w--H(12A)···O6 ($d_{D\ldots H}$, 1.780(2) Å, $d_{D\cdots A}$, 2.725(2) Å; ∠D-H···A, 177(3)°) and O13w--H(13A)···O5 ($d_{D\ldots H}$, 2.020(2) Å, $d_{D\cdots A}$, 2.870(2) Å; ∠D-H···A, 154(4)°). The coordinated water molecule O9w, of the cationic unit $[Co(phen)_2(H_2O)_2]^{2+}$, exhibits hydrogen contact with the carboxylate O atoms (O3) and the seventh lattice water molecule (O11w), whereas O10w interacts with O4 and O7 carboxylate atoms of the anionic unit as a donor.

A view of the uniform decameric cluster in 2D infinite chain in chair conformation is shown in Fig. 7.1.1c. The donor-acceptor (O···O) distances for the H-bonds between the water molecules in these decameric cluster typically in the range of 2.707(2)-2.899(2) Å, whereas the corresponding distances between the cluster and the complex anions are in the range of 2.723(2)-2.870(2) Å. Important bond distances and angles related to the infinite $(H_2O)_{10}$ cluster are listed in Table 7.1. The average (O···O) distances between the oxygen atoms is 2.787(2) Å, which is nearly identical to the oxygen distances (2.80(5) Å) in the 10-membered 3D cluster observed by Atwood and coworkers [18]. A discrete cyclic decameric cluster with similar morphology stabilized by Cu(II) cyano complex also appears as a quasiplanar single ring of 10 waters [27]. Other cyclic decameric cluster was trapped in erbium fumarate $[Er_2(fum)_3(H_2O)_4]\cdot 8H_2O$ frameworks with boat-chair-boat conformation [28].

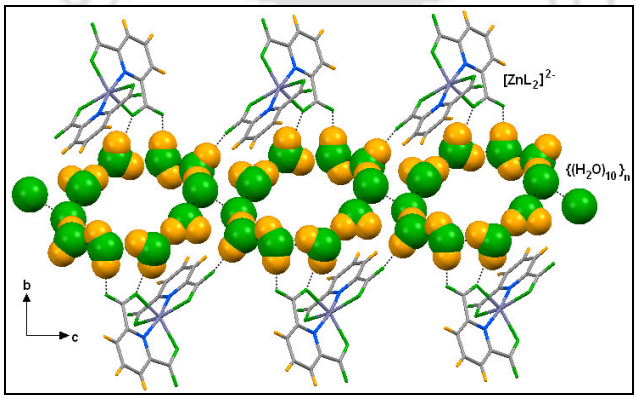

(a)

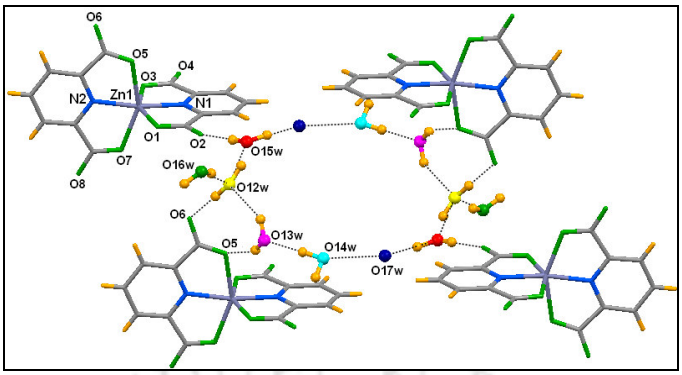

(b)

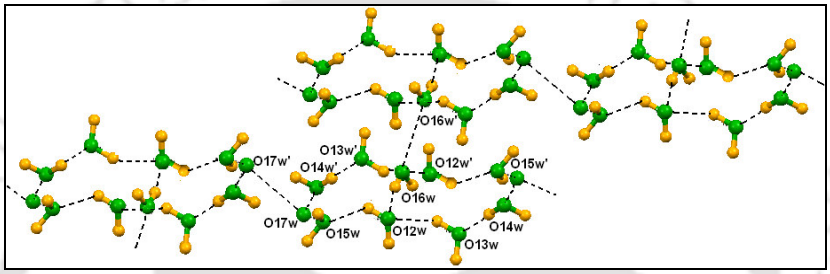

(c)

Fig. 7.1.1: (a) A view showing the 2D $(H_2O)_{10}$ cluster passing through $[ZnL_2]^{2-}$ unit, (b) Perspective view of the cluster showing the H-bond interactions with the anionic units, (c) Close view of the cluster with chair conformation.

X-ray powder diffraction pattern was recorded to confirm the bulk purity of the complex. The diffraction pattern of the complex $[Co(phen)_2\ (H_2O)_2][ZnL_2]\cdot 7H_2O$ (**7.1**) tallies well with the simulated from the single crystal structure (Fig. 7.1.2). The (h, k, l)s could be indexed and shown in Fig. 7.1.2.

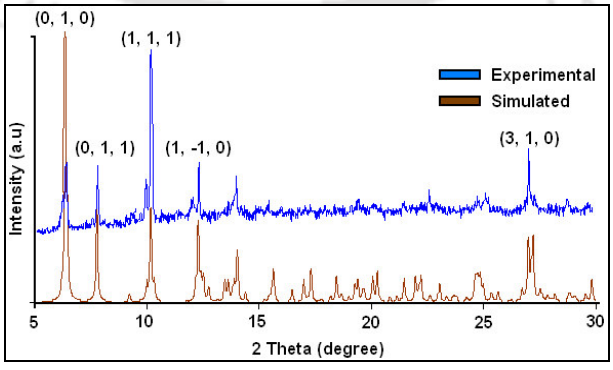

Fig. 7.1.2: Simulated and experimental PXRD pattern of complex **7.1**

7.2: Hexadecameric water cluster $(H_2O)_{16}$ in complex, $[Ni(phen)_2(bpy)][CoL_2]\cdot 8H_2O$

Complex $[Ni(phen)_2(bpy)][CoL_2]\cdot 8H_2O$ (**7.2**), also a mixed metal ionic complex, where the anionic moiety is Co(II) dipicolinate complex and the cationic unit is made up of two 1,10-phenanthroline and one 2,2′-bipyridine ligands coordinating to Ni(II) center in an octahedral fashion. Except the metal center, the core of the anionic unit is isostructural with **7.1**, whereas the cationic unit's aqua ligands are replaced by 2,2′-bipyridine ligand. This creates both hydrophilic and hydrophobic environment in the crystal structure. Formation of hydrophobic environment leaves the lattice water molecules in the surrounding of the hydrophilic Co(II) dipicolinate anion, thus, changing the overall MOF structure in **7.2**. The eight lattice water molecules and their symmetric equivalents aggregate to form a discrete hexadecamric cluster, $(H_2O)_{16}$ surrounded by $[CoL_2]^{2-}$ in the hydrophilic cavities (Fig. 7.2.1a). The water cluster is encapsulated by eight Co(II) dipicolinate anion *via* hydrogen bonding with all the carboxylate O atoms of the anionic unit in a spirocyclic fashion (Fig. 7.2.2b).

The perspective view of supramolecular discrete $(H_2O)_{16}$ cluster is shown in Fig. 7.2.3c. The hexadecameric cluster has its two tetrameric core, based on a zigzag heptameric chain, generated by O13w, O14w, O15w and O17w. The dihedral angle between the two tetrameric core centered at O15 site is 85º. The inversion center located at O15w with half occupancy shows five hydrogen bonding interaction with nearby O atoms. Selected hydrogen bonds involved are O10w--H(10A)···O2 ($d_{D\ldots H}$, 1.893(2) Å, $d_{D\cdots A}$, 2.801(2) Å; ∠D-H···A, 159.7(3)°), O9w--H(10A)···O8 ($d_{D\ldots H}$, 1.896(2) Å, $d_{D\cdots A}$, 2.800(2) Å; ∠D-H···A, 157.0 (3)°), O9w--H(10A)···O6 ($d_{D\ldots H}$, 2.170(2) Å, $d_{D\cdots A}$, 2.772(2) Å; ∠D-H···A, 119 (4)°). The water molecules O14w and O17w of the tetrameric core make further hydrogen contact with O11w and O16w respectively to complete the cluster.

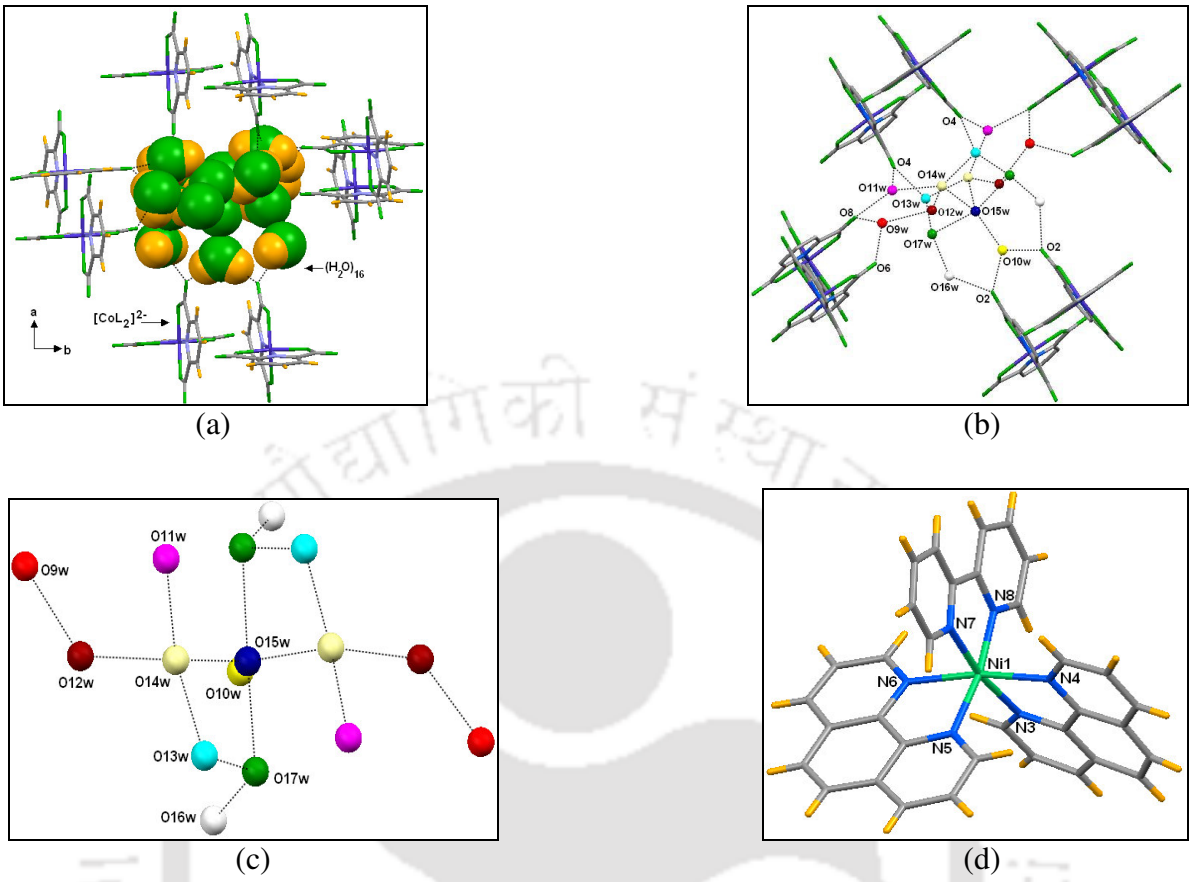

Fig. 7.2.1: (a) A view showing the encapsulation of $(H_2O)_{16}$ cluster (in space filled mode) in the hydrophilic cavity of $[CoL_2]^{2-}$, (b) A view illustrating the binding of water molecules to the complex anions, (c) H-bonded discrete $(H_2O)_{16}$ cluster, (d) Hydrophobic cationic species $[Ni(phen)_2(bipy)]^{2+}$.

The first discrete hexadecameric cluster stabilized by polymeric $\{Cu_{2.5}(pytc)(py)_8(NO_3)\cdot 10H_2O\}_n$ (where pytc = 2,3,5,6-pyrazinetetracarboxylate, py = pyridine) contains both five and six-membered ring along with fused cubes of $(H_2O)_8$ [29]. Other reported $(H_2O)_{16}$ cluster constitutes of two tetramer and one hexamer stabilized in polymeric Co(II) complex of 3,5-dinitrobenzoic acid [30]. The $(H_2O)_{16}$ cluster generated in the complex $[In_2SO_4L_2(phen)_2(H_2O)_2]\cdot 5.5H_2O$ (where L = dipicolinate, phen = 1,10-phenanthroline) is a finite branched chain cluster of 10-water molecules on the main chain (Ch. 1, [70]). In contrast, the cluster reported in this study forms a pentameric or hexameric cluster when carboxylate O atoms of anionic unit are taken into account. Such a supramolecular arrangement of $(H_2O)_{16}$ that basically aggregates due to imbalance of donor-acceptors functionality of the anionic unit is observed as a rare case. The distances between the

oxygen atoms in the cluster 2.525(2)-2.955(2) Å, whereas the corresponding distances with carboxylate O atoms are in the range of 2.696(2)-2.871(2) Å. In every cluster, the average O···O distance is 2.755(2) Å, which is interestingly, identical with the ice phase (2.759 Å) and compared to 2.85 Å in liquid water [31-32].

7.3: Encapsulation of infinite water cluster $(H_2O)_n$ in complex $[Co(phen)_3][MnL_2]\cdot 12H_2O$

The crystal structure of complex $[Co(phen)_3][MnL_2]\cdot 12H_2O$ **(7.3)**, shows the presence of both hydrophilic $[MnL_2]^{2-}$ and hydrophobic $[Co(phen)_3]^{2+}$ unit along with twelve solvent water molecules (Fig. 7.3.2a). The anionic unit is Mn(II) dipicolinate complex; whereas in the cationic part $[Co(phen)_3]^{2+}$, Co(II) is coordinated with three 1,10-phenanthroline ligand in an distorted octahedral polyhedron. Electrospray mass spectrometry is often used to investigate the existence of cationic or anionic species in solution [33]. In ESI + ve mode, the mass ion peak (m/z value) at 299.57 represent the cationic species $[Co(phen)_3]^{2+}$ of complex **7.3**, which also showed that cationic species are consistent and validate the crystal structure.

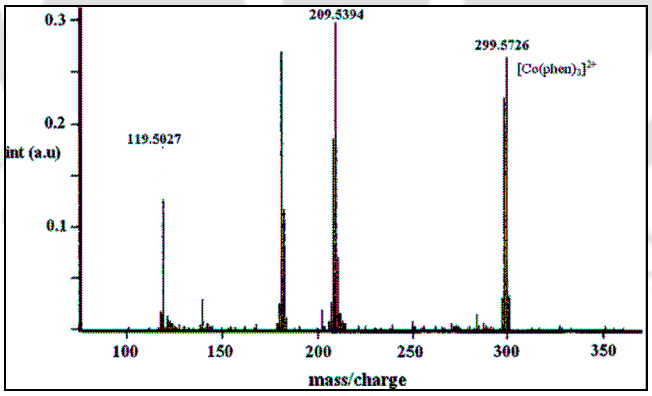

Fig. 7.3.1: ESI-MS spectra of complex 7.**3.**

The water molecules fill the voids created during packing of the bulky complex ions in the crystal lattice. Interestingly, they aggregate to form a wavelike hydrogen bonded infinite water chain (Fig. 7.3.2b). Out of twelve, the group of ten water molecules aggregate (O10w–

O19w) to constitute the part of the infinite chain. The remaining two water molecules (O9w, O20w) form a dimer and shows hydrogen contact with $[MnL_2]^{2-}$. Each of the water molecules in the chain form three hydrogen bonds, one as an acceptor and two as a donor, although each oxygen atom in the assembly tends to achieve four-coordination. Exception being the O18w, that forms an additional hydrogen bond with carboxylate O atoms of the complex anion as a donor. The chain is thus, stabilized by Mn(II) dipicolinate frameworks forming hydrogen bonds with the available nearby carboxylate O atoms. In the chain like structure, the oxygen atoms are not coplanar but rather involves in formation of a side arm wave pattern extending along crystallographic *c* axis (Fig. 7.3.2c). Thus, it adopts a flexible conformation to act as hydrogen bond donor to the nearby carboxylate oxygen atoms of the dianion. An infinite $(H_2O)_\infty$ chain with similar cluster shape have been reported in the proton transfer complex $[InL(LH)(H_2O)_2]\cdot 5H_2O$ (where L = dipicolinate) (Ch. 1, [69]). It has less branched water molecule in the infinite chain and also varies in terms of arrangement of the cluster observed in complex **7.3**. The O···O distances (2.754(2)- 2.936(2) Å) resembles with the reported 1D water chain stabilized by various organic/inorganic hosts [15-17]. The average distance between the oxygen atoms 2.827(2) Å, is in the range observed for the ice phase (2.77-2.84 Å), and comparable to those in liquid water (2.85 Å). The wide variation in O···O distances and ∠O···O···O angles (84.8(3)-133.5(3)^o) may be attributed due to the flexibility of the chain.

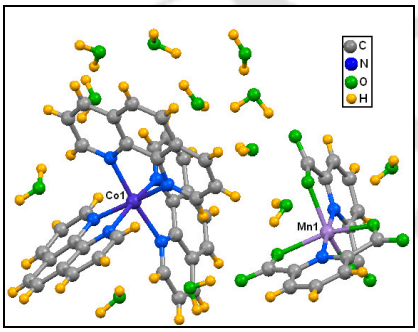

(a)

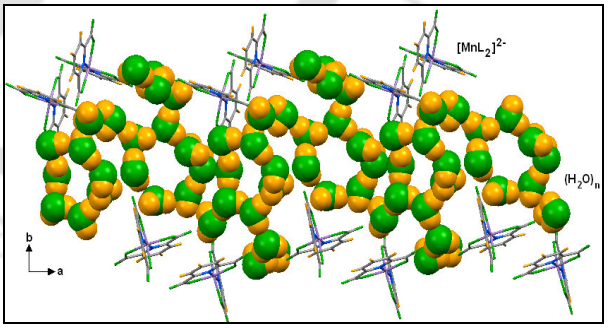

(b)

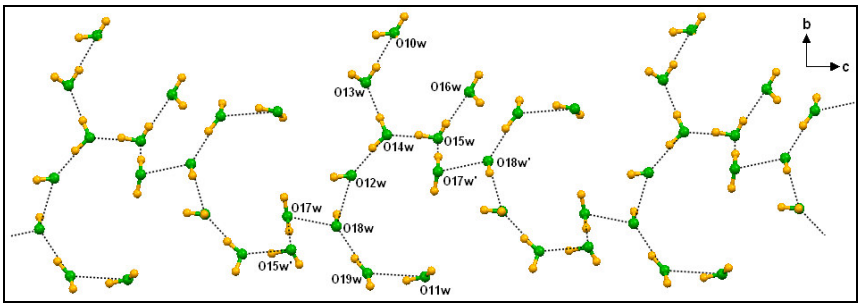

(c)

Fig. 7.3.2: (a) Crystal structure of complex **7.3**, (b) Wave like infinite water cluster stabilized by $[MnL_2]^{2-}$, (c) An perspective view of the cluster showing the hydrogen bond interaction.

7.4: Infinite water cluster with cyclic tetrameric core in $[Ni(phen)_3][CoL_2]\cdot 9H_2O$ and $[Ni(phen)_3]_2[ZnL_2]_2\cdot 20H_2O$

The complexes $[Ni(phen)_3][CoL_2]\cdot 9H_2O$ (**7.4**) and $[Ni(phen)_3]_2[ZnL_2]_2\cdot 20H_2O$ (**7.5**), are derived from the same set of ligands but with different metal ions. Both the complexes contain same cationic complex $[Ni(phen)_3]^{2+}$, but the anionic units are derived from Co(II) and Zn(II) ions respectively. They have different number of lattice water molecules in the crystal structure. Both the complexes crystallize in the triclinic space group *P-1*, but the later comprises two crystallographically non-equivalent molecules. Interestingly, both the complexes encapsulate similar type of hydrogen bonded infinite water cluster having a cyclic tetrameric core in the chain. The infinite chains are stabilized by Co(II) and Zn(II) dipicolinates in the respective crystal lattice (Fig. 7.4.1a). A close view of the infinite water cluster encapsulated in complex **7.4** is shown in Fig. 7.4.1b. The geometry of cluster is different from the infinite cluster obtained in complex **7.3**. It is non-planar branched chain cluster with cyclic tetrameric core. The O···O distances between the oxygen atoms in the cluster are in the range of 2.667(2)-2.906(2). The average distance between the oxygen atoms 2.790(2) Å, is in the range of ice phase (2.77-2.84 Å), and comparable to those in liquid water (2.85 Å) [31-32].

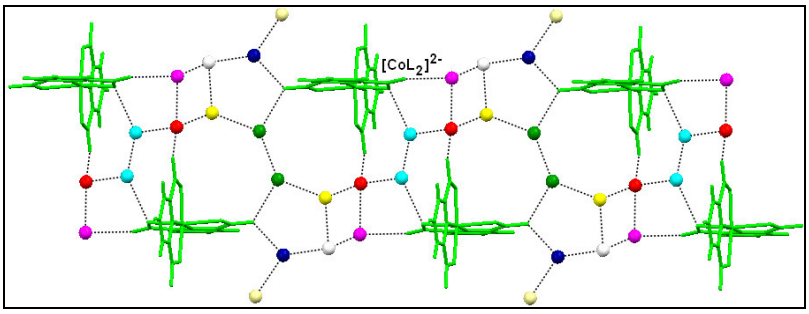

(a)

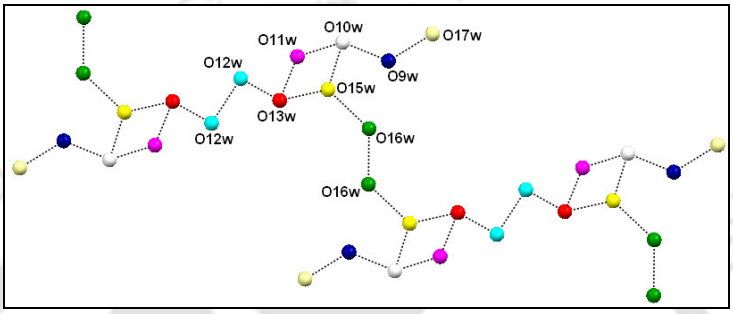

(b)

Fig. 7.4.1: (a) Hydrogen bond interactions of Co(II) dipicolinates with infinite water chain in **7.4**, (b) Part of infinite water chain of complex **7.4**.

7.5: Thermogravimetric analysis

Thermal stability of the water clusters stabilized in these complexes were studied. The thermograms of each of the complexes showed three prominent steps of weight loss. In the 1st step, water evolution begins in the range of 30-40 ºC and removal of all the lattice water molecules occurs in the range of 100-125 ºC with a distinct plateau in the curve. The 2nd step involves the weight loss of 1,10-phenanthroline or 2,2′-bipyridine ligand and the 3rd step is the continuous decomposition of metal dipicolinate complex. Complex **7.1** loses 15.6% of its total weight in the temperature range 40-125 °C, which corresponds to the removal of the lattice and coordinated water molecules (calcd. 16.5%). Loss of 1,10-phenanthroline takes place in the temperature range 220-400 °C, followed by continuous decomposition of Co(II) dipicolinate complex that starts at 420 °C. Complex 7.**2** and 7.**3** displays similar behavior, losing 12.1% and 15.8% of the total weight in the range 40-120 °C corresponding to the lattice water molecules (calcd. 13.0% and 17.3%). As a representative case, the thermogram of complex **7.2** is shown in Fig. 7.5.1. The 29.3% weight loss in the temperature region of 260-400 °C was due to the loss of two 1,10-phenanthroline and one 2,2′-bipyridine ligand

(calc. 31.3%). The third step is the decomposition of Co(II) dipicolinate complex that begins at 460 °C. Complex **7.4** and **7.5** follows similar trend of thermal behavior about the loss of water molecules and other components of the complex. The thermal analysis thus, shows the loss of lattice water molecules at relatively low temperature. This indicates that the water clusters are hydrogen bonded in a similar fashion and exhibits weak interaction between the complexes and the water cluster. Lattice water molecules thus, not only act as space fillers, but also act as supramolecular glue responsible for holding the cations and anions together to provide high crystalline properties to these complexes.

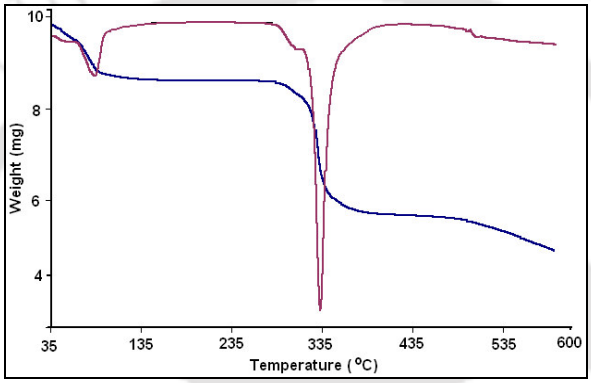

Fig. 7.5.1: Thermogram of complex **7.2**

In FTIR, the O–H stretching frequencies were observed spreading over a narrow range of 3415- 3399 cm^{-1}. The same stretching vibration for ice appears at 3220 cm^{-1}, whereas in liquid water, it appears at 3490 and 3280 cm^{-1}, showing a more resemblance of these clusters to liquid water [34]. It should be noted that some other reported water clusters also show O–H stretching vibrations in the same range [27-28]. The broad band centered at 3400 cm^{-1}, for the clusters disappears when heated at 120 ℃ for 2 hours and it did not reappear upon deliberate exposure to moisture, which proves that water loss is irreversible in nature.

7.6: Conclusion

In this chapter, we have synthesized and characterized few ionic complexes consisting of bulky cationic and anionic complex ions. The cationic complexes are derived from 1st row transition metals and 1,10-phenanthroline ligands or in association with 2,2′-bipyridine or

aqua ligands. Metal dipicolinates represent the anionic complex in each case. Each of the complexes contains relatively large number of lattice water molecules in the crystal structure. Depending on the cationic environment, the number of lattice water molecules varies in the molecule. Except the complex **7.1**, the cations are hydrophobic in nature. Since the cations are hydrophobic in nature, the anion needs to reorganize the water molecules limiting the exposure to the hydrophilic environment. Thus, in a system that possess both hydrophilic and hydrophobic environment, metal dipicolinate interacts with the lattice water molecules to stabilize the structure. The seven lattice water molecules in complex **7.1** aggregates to form 2D infinite cyclic decameric cluster. Changing the cationic unit to completely hydrophobic environment (in **7.2)** showed the formation of discrete 16-water cluster. The complexes **7.3**-**7.5** have similar ligand composition with **7.2** but with different central metal ion. Complex **7.3** shows stabilization of branched chain non-planar 1D chain, whereas complex **7.4** and **7.5** encapsulates 1D infinite chain having a cyclic tetrameric core in the chain. The central metal ions therefore play key role to govern the water cluster by accommodating different number of lattice water molecules in the complex. The differences with central metal ions arise due to their different size and John Teller distortion experienced by the metal ion in that particular complex. Thus, this chapter shows the stabilization of some higher ordered water clusters trapped in the interstices of metal dipicolinate complexes by modulating the complex cation and the central metal ions.

7.7: Experimental section

Detailed synthetic methodologies for the synthesized complexes are given below. Analytical as well as spectroscopic data are also listed along with each of the complexes.

7.6.1: $[Co(phen)_2(H_2O)_2][ZnL_2]\cdot 7H_2O$ (7.1), $[Ni(phen)_2(bpy)][CoL_2]\cdot 8H_2O$ (7.2) and $[Co(phen)_3][MnL_2]\cdot 12H_2O$ (7.3), $[Ni(phen)_3][CoL_2]\cdot 9H_2O$ (7.4) and $[Ni(phen)_3]_2[ZnL_2]_2\cdot 20H_2O$ (7.5)

To a methanolic solution (20 mL) of dipicolinic acid (0.167 g, 1.0 mmol), an aqueous solution of hydrated Zn(II)/Co(II)/Mn(II)/Co(II)/Zn(II) acetates (0.5 mmol) were added and stirred for half an hour that led to different coloured precipitates based on metal ions.

Similarly, 1,10-phenanthroline (0.20 g, 1.0 mmol) or mixture of 1,10-phenanthroline (0.20 g, 1.0 mmol) and 2,2′-bipyridine (0.08 g, 0.5 mmol) or 1,10-phenanthroline (0.30 g, 1.5 mmol) in 20 mL of water were reacted with hydrated Co(II)/Ni(II) acetates in another round bottom flask which resulted in pink / dark pink complexes. On subsequent addition of these phen / bpy complexes to the preformed precipitates led to the homogenous solutions in independent experiment. The solutions on standing at room temperature resulted in the formation of the crystals suitable for X-ray diffraction after 3-4 days. Few drops of pyridine were also used for recrystallization of the complexes.

Complex **7.1**: Isolated yield: 74%. Elemental anal calcd for $C_{38}H_{40}N_6O_{17}CoZn$, C, 46.67; N, 8.60; H, 4.09%; found C, 46.54; N, 8.53; H, 4.03%. IR (KBr, cm^{-1}): 3412 (b, s), 2924 (m), 1622 (s), 1590 (m), 1516 (m), 1424 (s), 1378 (s), 1278 (w). Molar conductance: 117.0 S cm^2 mol^{-1} in water. Vis (H_2O) λ_{max}: 572.0 nm; ε = 27.5 M^{-1} $cm^{-1.}$ μ_{eff}. at 298 K: 4.35 BM. Thermal analysis: decomposition range: ~ 40-120 ºC (loss of lattice and coordinated water molecules).

Complex **7.2**: Isolated yield: 68%. Elemental anal calcd for $C_{48}H_{46}CoN_8NiO_{16}$, C, 52.96; N, 10.10; H, 4.15%; found C, 52.82; N, 9.99; H, 4.07%. IR (KBr, cm^{-1}): 3408 (b, s), 1624 (s), 1588 (m), 1514 (m), 1423 (s), 1373 (s), 1276 (w). Molar conductance: 121.0 S cm^2 mol^{-1} in water. Vis (H_2O) λ_{max}: 521.0 nm; ε = 38.6 M^{-1} cm^{-1} and λ_{max}: 574.0 nm; ε = 29.8 M^{-1} $cm^{-1.}$ μ_{eff}. at 298 K: 3.78 BM. Thermal analysis: decomposition range: ~35-110 ºC (loss of lattice water molecules).

Complex **7.3:** Isolated yield: 72%. Elemental anal calcd for $C_{100}H_{106}N_{16}O_{39}CoMn$, C, 50.34; N, 9.40; H, 4.45%; found C, 50.22; N, 9.38; H, 4.41%. IR (KBr, cm^{-1}): 3415 (b, s), 1626 (s), 1587 (m), 1516 (m), 1424 (s), 1376 (s), 1276 (w). Molar conductance: 109.0 S cm^2 mol^{-1} in water. Vis (H_2O) λ_{max}: 574.0 nm; ε = 36.2 M^{-1} cm^{-1}. μ_{eff}. at 298 K: 5.14 BM. Thermal analysis: decomposition range: ~ 35-100 ºC (loss of lattice water molecules).

Complex **7.4:** Isolated yield: 66%. Elemental anal calcd for $C_{50}H_{48}CoN_8NiO_{17}$, C, 52.15; N, 9.73; H, 4.17%; found C, 52.04; N, 9.51; H, 4.13%. IR (KBr, cm^{-1}): 3418 (b, s), 1626 (s),

1586 (m), 1516 (m), 1425 (s), 1376 (s), 1276 (w). Molar conductance: 112.0 S cm^2 mol^{-1} in water. Vis (H_2O) λ_{max}: 524.0 nm; ε = 25.2 M^{-1} cm^{-1} and λ_{max}: 576.0 nm; ε = 27.5 M^{-1} cm^{-1}. μ_{eff}. at 298 K: 4.40 BM. Thermal analysis: decomposition range: ~ 45-115 ºC (loss of lattice water molecules).

Complex **7.5:** Isolated yield: 65%. Elemental anal calcd for $C_{100}H_{100}N_{16}Ni_2O_{36}Zn_2$, C, 51.06; N, 9.53; H, 4.25%; found C, 50.87; N, 9.47; H, 4.20%. IR (KBr, cm^{-1}): 3409 (b, s), 1622 (s), 1587 (m), 1517 (m), 1425 (s), 1378 (s), 1279 (w). Molar conductance: 110.0 S cm^2 mol^{-1} in water. Vis (H_2O) λ_{max}: 528.0 nm; ε = 42.4 $M^{-1}cm^{-1}$. μ_{eff}. at 298 K: 2.84 BM. Thermal analysis: decomposition range: ~ 40-110 ºC (loss of lattice water molecules).

7.8: Crystallographic data and refinement parameters for the complexes 7.1 - 7.5

Compound No.	**7.1**	**7.2**	**7.3**	**7.4**	**7.5**
Formula	$C_{38}H_{40}CoN_6O_{17}Zn$	$C_{48}H_{46}CoN_8NiO_{16}$	$C_{100}H_{106}Co_2Mn_2N_{16}O_{39}$	$C_{50}H_{48}CoN_8NiO_{17}$	$C_{100}H_{100}N_{16}Ni_2O_{36}Zn_2$
Formula wt.	977.06	1108.57	2383.75	1150.60	2350.12
Crystal system	Triclinic	Monoclinic	Monoclinic	Triclinic	Triclinic
Space group	*P-1*	*C2/c*	*C2/c*	*P-1*	*P-1*
a (Å)	10.0385(7)	28.6537(9)	29.9475(15)	13.6914(5)	14.4598(4)
b (Å)	14.7747(11)	15.6732(4)	15.0062(6)	14.4828(3)	15.6973(4)
c (Å)	14.9628(10)	22.9430(5)	24.7702(11)	15.6309(3)	25.1903(6)
α (deg)	73.937(3)	90.00	90.00	115.4610(10)	92.9330(10)
β (deg)	78.512(3)	106.690(2)	104.623(4)	107.761(2)	99.0890(10)
γ (deg)	74.992(3)	90.00	90.00	97.995(2)	115.4300(10)
V (Å^3)	2040.3(2)	9869.5(5)	10771.1(8)	2530.01(12)	5053.3(2)
Z	2	8	4	2	2
D_{calc} (gcm^{-3})	1.590	1.492	1.470	1.510	1.545
μ (mm^{-1})	1.078	0.797	0.626	0.782	0.932
F(000)	1006	4584	4936	1190	2432
Total no. of reflns	25290	35374	39996	28335	72640
Independent reflns.	6975	8687	9481	8824	17273
$\theta_{max.}$	1.43 – 25.00	1.48 – 25.00	1.41 – 25.00	1.61 – 25.00	0.83 – 25.00
Ranges (h, k, l)	-11 ≤ h ≤ 11 -17 ≤ k ≤ 17 -17 ≤ l ≤ 17	-34 ≤ h ≤ 33 -17 ≤ k ≤ 18 -27 ≤ l ≤ 27	-35 ≤ h ≤ 34 -17 ≤ k ≤ 17 -29 ≤ l ≤ 29	-16 ≤ h ≤ 16 -17 ≤ k ≤ 17 -18 ≤ l ≤ 18	-17 ≤ h ≤ 17 -18 ≤ k ≤ 18 -29 ≤ l ≤ 29
Completeness to 2θ (%)	97.1	99.8	100.0	99.1	97.1
Data /restraints/ parameters	6475 / 10 / 632	8687 / 10 / 712	9481 / 12 / 805	8824 / 0 / 682	17273 / 0/ 1405
GOF (F^2)	0.990	1.042	1.024	0.995	1.171
R_1, wR_2 [$I > 2\sigma(I)$]	0.0339, 0.1168	0.0651, 0.1957	0.0429, 0.1338	0.0784, 0.2528	0.0795, 0.2262
R_1, wR_2 (all data)	0.0380, 0.1223	0.0929, 0.2140	0.0568, 0.1423	0.1040, 0.2691	0.1039, 0.2479
Largest diff peak/hole (e Å^{-3})	1.055 / -0.817	0.857 / -0.512	0.760 / -0.435	1.021 / -1.072	0.981 / -1.032

7.9: Table 7.1: Some (O-O) distances (Å) and (O-O-O) angles (º) for the infinite decameric water cluster in **7.1**

O12w – O13w	2.900(2)	O12w – O13w – O14w	139.2(3)
O13w – O14w	2.780(2)	O13w – O14w – O17w	153.5(3)
O14w – O17w	2.707(2)	O14w – O17w – O15w	150.6(3)
O12w – O15w	2.792(2)	O12w – O15w – O17w	137.5(2)
O15w – O17w	2.758(2)	O13w – O12w – O15w	120.3(2)
O12w – O16w	2.801(2)	O13w – O12w – O16w	106.1(2)
O16w – O16w′	2.749(2)	O15w – O12w – O16w	127.4(3)
O17w – O17w′	2.780(2)	O12w – O16w – O16w′	128.2(3)
O14w – O17w – O17w′	95.2(3)	O15w – O17w – O17w′	93.4(3)

Table 7.2: Some (O-O) distances (Å) and (O-O-O) angles (º) for $(H_2O)_{16}$ water cluster in 7.**2**

O9w – O12w	2.871(2)	O14w – O15w	2.955(2)
O12w – O14w	2.798(2)	O15w – O17w	2.880(2)
O14w – O11w	2.845(2)	O13w – O17w	2.525(2)
O14w – O13w	2.614(2)	O16w – O17w	2.698(2)
O15w – O10w	2.613(2)		
O9w – O12w – O14w	117.2(3)	O14w – O13w – O17w	98.0(3)
O12w – O14w – O11w	90.4(3)	O14w – O15w – O10w	132.4(3)
O12w – O14w – O13w	113.0(3)	O14w – O15w – O14w′	95.2(3)
O11w – O14w – O13w	139.8(3)	O15w – O17w – O16w	102.7(2)
O11w – O14w – O15w	113.0(3)	O13w – O17w – O16w	117.0(3)
O14w – O15w – O17w	84.6(3)	O10w – O15w – O17w	99.0(3)

Table **7.**3: Selected (O-O) distances (Å) and (O-O-O) angles (º) for the infinite water chain in **7.3**

O10w – O13w	2.904(2)	O14w – O15w	2.826(2)
O11w – O19w	2.936(2)	O15w – O16w	2.807(2)
O12w – O18w	2.857(2)	O15w – O17w	2.783(2)
O13w – O14w	2.860(2)	O17w – O18w	2.765(2)
O14w – O12w	2.754(2)	O18w – O19w	2.779(2)
O10w – O13w – O14w	119.4(3)	O18w – O19w – O11w	127.7(3)
O13w – O14w – O12w	117.6(3)	O14w – O12w – O18w	133.5(3)
O13w – O14w – O15w	120.1(4)	O14w – O12w – O16w	122.2(4)
O14w – O15w – O17w	111.7(4)	O12w – O18w – O19w	122.5(3)
O12w – O18w – O17w	84.8(3)	O17w – O18w – O19w	127.9(4)
O15w – O17w – O18w	100.2(4)		

References:

[1] B. Jayaram, T. Jain, Annu. Rev. Biophys. Biomol. Struct. 33 (2004) 343.

[2] C. Migchelsen, H.J.C. Berendsen, A. Rupprecht, J. Mol. Biol. 37 (1968) 235.

[3] K. Mitsuoka, K. Murata, T. Walz, T. Hirai, P. Agre, J. B. Heymann, A. Engel, Y. Fujiyoshi, J. Struct. Biol. 128 (1999) 34.

[4] W.E. Royer, A. Pardanani, Q.H. Gibson, E.S. Peterson, J.M. Feldman, Proc. Natl. Acad. Sci. U.S.A. 93 (1996) 14526.

[5] G.R. Desiraju, "Crystal engineering: The design of organic solids", Elsevier, Amsterdam, 1989.

[6] G.R. Desiraju, Angew. Chem. Int. Ed. Eng. 34 (1995) 2311.

[7] D.C. Apperly, P.A. Basford, C.I. Dallman, R.K. Harris, M. Kinns, P.V. Marshall, A. G. Swanson, J. Pharm. Sci. 94 (2005) 516.

[8] G.A. Stephenson, E.G. Groleau, R.L. Kleeman, W. Xu, D.R. Rigsbee, J. Pharm. Sci. 87 (1998) 536.

[9] G.R. Desiraju, J. Chem. Soc., Chem. Commun. (1991) 426.

[10] H.D. Clarke, K.K. Arora, H. Bass, P. Kavuru, T.T. Ong, T. Pujari, L. Wojtas, M.J. Zaworotko, Cryst. Growth Des. 10 (2010) 2152.

[11] L.E. Cheruzel, M.S. Pometun, M.R. Cecil, M.S. Mashuta, R.J. Wittebort, R.M. Buchanan, Angew. Chem., Int. Ed. 42 (2003) 5452.

[12] B. Sreenivasulu, J.J. Vittal, Angew. Chem., Int. Ed. 43 (2004) 5769.

[13] A. Mukherjee, M.K. Saha, M. Nethaji, A.R. Chakravarty, Chem. Commun. (2004) 716.

[14] M. Mascal, L. Infantes, J. Chisholm, Angew. Chem. Int. Ed. 45 (2006) 32.

[15] U.S. Raghavender, Kantharaju, S. Aravinda, N. Shamala, P. Balaram, J. Am. Chem. Soc. 132 (2010) 1075.

[16] R. Natarajan, J.P.H. Charmant, A.G. Orpen, A.P. Davis, Angew. Chem., Int. Ed. 49 (2010) 5125.

[17] B.K. Saha, A. Nangia, Chem. Commun. (2005) 3024.

[18] L.J. Barbour, G.W. Orr, J.L. Atwood, Nature 393 (1998) 671.

[19] J.N. Moorthy, R. Natarajan, P. Venugopalan, Angew. Chem. Int. Ed. 41 (2002) 3417.

[20] X.-M. Zhang, R.-Q. Fang, H.-S. Wu, Cryst. Growth Des. 5 (2005) 1335.

[21] B-Q. Ma, H.-L. Sun, S. Gao, Chem. Commun. (2005) 2336.

[22] D.F. Shriver, P.W. Atkins, Inorganic Chemistry; Oxford University Press: Oxford, U.K. 2001.

[23] M. Yoshizawa, T. Kusukawa, M. Kawano, T. Ohhara, I. Tanaka, K. Kurihara, N. Niimura, M. Fujita, J. Am. Chem. Soc. 127 (2005) 2798.

[24] R.D. Bergougnant, A.Y. Robin, K.M. Fromm, Cryst. Growth Des. 5 (2005) 1691.

[25] L.J. Barbour, G.W. Orr, J.L. Atwood, Chem. Commun. (2000) 859.

[26] L. Wang, J. Wang, C. Xie, J. Coord. Chem. 61 (2008) 3401.

[27] U. Mukhopadhyay, I. Bernal, Cryst. Growth Des. 6 (2006) 363.

[28] A. Michaelides, S. Skoulika, E.G. Bakalbassis, J. Mrozinski, Cryst. Growth Des. 3 (2003) 487.

[29] S.K. Ghosh, P.K. Bharadwaj, Inorg. Chem. 43 (2004) 6887.

[30] Y. Jin, Y.X. Che, J.M. Zheng, Inorg. Chim. Acta. 361 (2008) 2799.

[31] G.A. Jeffrey, An Introduction to Hydrogen Bonding; Oxford University Press: Oxford, U.K. 1997.

[32] J. Lu, J.H. Yu, X.Y. Chen, P. Cheng, X. Zhang, J.Q. Xu, Inorg. Chem. 44 (2005) 5978.

[33] R.B. Core, Electrospray ionization mass spectrometry-Fundamentals, instrumentation, and applications; VCH: Weinheim, 1997.

[34] D. Eisenberg, W. Kauzmann, The Structure and Properties of Water; Oxford University Press: Oxford, U.K. 1969.